Modelling interactions between quay walls and utility lines

In the inner-city of Amsterdam

O.A. Ophof

TU Delft Delft University of Technology

TAUW

Modelling interactions between quay walls and utility lines

In the inner-city of Amsterdam

by

O.A. Ophof

to obtain the degree of Master of Science
at the Delft University of Technology,
to be defended publicly on July 30, 2021.

Student number:	4289250	
Project duration:	November, 2020 – July, 2021	
Thesis committee:	Dr. ir. W. Broere (Chair of Committee)	TU Delft
	Ir. M.J. Hemel	TU Delft
	Prof. dr. ir. S.N. Jonkman	TU Delft
	Dr. ir. D.J. Peters	TU Delft
	Ir. T. Feenstra	Tauw

This thesis is confidential and cannot be made public until January 30, 2022.

TU Delft Delft University of Technology

TAUW

Preface

This thesis concludes my master program Hydraulic Engineering at the Delft University of Technology. As my specialization is into Hydraulic Structures, it was a great opportunity to study the inner-city quay walls designed by my engineering predecessors, and to see how structures interact with their environment. I am proud to hereby present the final version of my thesis.

I want to thank the people at TAUW for facilitating my research. Although my physical presence at their office was limited due to the COVID-19 pandemic, they offered me great support. Additionally, I would like to express my gratitude to the Kadaster and Waternet for their data and help. I also want to thank my supervisors for their guidance and for providing me with the necessary feedback. Many thanks to Ernst Oosterveld for giving me the opportunity to carry out my research at TAUW, and a special thanks to Theo Feenstra of TAUW for his support, insights, and guidance during my thesis.

Finally, I want to thank my friends and family during my thesis and my academic studies as a whole. Your support and motivation have, as always, served me very well. My time in Delft has been amazing, and I can only hope the future will be as exiting as the past 8 years.

Oscar Ophof
Rotterdam, 23rd July 2021

Figure on front page: collapsed road in subsidence pit behind a quay wall,
at the Marnixstraat in Amsterdam (Waternet, 2017).

Samenvatting

De historische binnensteden van Nederland staan bekend om hun iconische grachten en de kademuren die hierbij horen, waarvan het overgrote deel meer dan een eeuw geleden gebouwd zijn. Vanwege de beperkte beschikbare ruimte in de ondergrond van dit stedelijke gebied zijn een groot aantal leidingen (zowel waterleidingen als rioleringen) in de buurt van kademuren geplaatst. In de afgelopen jaren zijn er een aantal kademuurinstortingen voorgekomen, waarvan een deel zijn toegeschreven aan lekkages van nutsleidingen. Echter is er weinig onderzoek gedaan naar de interactie tussen binnenstedelijke kademuren en leidingen. Het doel van dit onderzoek is daarom ook om de volgende vraag te beantwoorden: "Hoe is lekkage van leidingen gerelateerd aan het vervormen en falen van de binnenstedelijke kademuren in Amsterdam en wanneer wordt deze interactie significant?" Het onderzoek ook opgesplitst in twee delen, aangezien de interactie tussen kademuren en nutsleidingen beide richtingen op werkt. Het effect van leiding lekkage op verplaatsingen- en falen van kademuren zijn op een kwalitatieve manier bestudeerd door middel van een literatuurstudie. Het effect van kademuurverplaatsing op leiding lekkage zijn op een kwantitatieve manier bestudeerd, door middel van een analytisch model. In dit model zijn de interacties tussen leidingen en de omringende grond weergegeven met behulp van een Winkler oplegging, oftewel een balk op een verdeelde veeroplegging. De veerstijfheid van deze oplegging is als bilineair aangenomen, gebaseerd op de evenwichtsdraagvermogen van de grond. Kademuurverplaatsing variërend van 20 tot 100 mm werden opgelegd op de meest voorkomende diameters en soorten leidingen in de buurt van kademuren. Het is aangenomen dat leidinglekkage optreed op het moment dat een van de leiding afhankelijke maximaal toegestane waarde van de hoekverdraaiing, buigend moment, of schuifkracht wordt overschreden. Al deze waardes zijn gebaseerd op de verplaatsing van de leiding. Alhoewel de scope van dit onderzoek zich beperkt tot de binnenstad van Amsterdam, is dit onderzoek ook toepasbaar in andere binnensteden met grachten onder dezelfde omstandigheden.

Uit de literatuurstudie volgde dat verplaatsing- falen van kademuren door leiding lekkage gerelateerd zijn aan interne erosie processen. Om interne erosie plaats te laten vinden zijn twee er twee vereisten: een lokaal verschil in waterstand tussen de waterstand in de gracht en het grondwater in het grondlichaam achter de kademuur en een open connectie in de kademuurconstructie in de buurt van de eerdergenoemde lokale verschil in waterstand, om de uitstroming van grond mogelijk te maken via de uitstroming van water. De lokale grondwaterstand verhoging kan het gevolg zijn van waterleiding lekkage maar kan ook door externe factoren worden veroorzaakt, zoals hevige regenval. Er zijn drie vormen van open connectie opgenomen in de studie. De eerste is lekkage van het ontgrondingsscherm, wat kan uitlopen tot erosie onder de constructie. De tweede is lekkage van de kademuurvloer, wat zowel kan uitlopen tot erosie onder de constructie als in het grondlichaam achter de kademuur. De derde is lekkage van een riolering, wat kan uitlopen tot erosie in het grondlichaam achter de kademuur. Het verschil in waterstand is niet nodig in het laatstgenoemde geval. In dit geval stroomt het grondwater niet richting het kanaal maar naar het lek in de riolering, mits de riolering onder het grondwaterniveau is gelegen. Erosie onder de kademuur kan leiden tot kademuurverplaatsing richting het kanaal, terwijl erosie in het grondlichaam achter de kademuur kan leiden tot de vorming van een ontgrondingskuil. Zie figuren 1 tot 3 voor schematisaties van de effecten van een verschil in waterstand in combinatie met de genoemde open connecties.

Het volgt uit de figuren dat zowel erosie onder- als achter de constructie kan leiden tot (verdere) deformaties van leidingen. In het eerstgenoemde geval is dit het gevolg van kademuurverplaatsing richting het kanaal, wat leidt tot lokale grondverplaatsing waar de leiding in is gelegen. In het laatstgenoemde geval is dit het gevolg van het lokale verlies van grond, wat leidt tot een afname van ondersteuning. Beide gevallen kunnen dus leiden tot relatieve verplaatsingen van leidingen, wat weer kan leiden tot lekkages. Dit proces kan worden omschreven als positieve terugkoppeling. Leidinglekkage is niet de enige reden voor kademuurverplaatsing. Dit kan ook het gevolg zijn van een toename in horizontale gronddruk door bijvoorbeeld zwaar verkeer. Het uiteindelijke falen van de kademuur kan komen in de vorm van instorting van de kademuur in de richting van het kanaal, of het instorten van de weg bovenop de kade in de gevormde ontgrondingskuil. Aangezien er een aantal externe factoren aanwezig moeten zijn voordat een kademuur faalt door leidinglekkage, kan deze vorm van falen worden omschreven als een tweede orde effect.

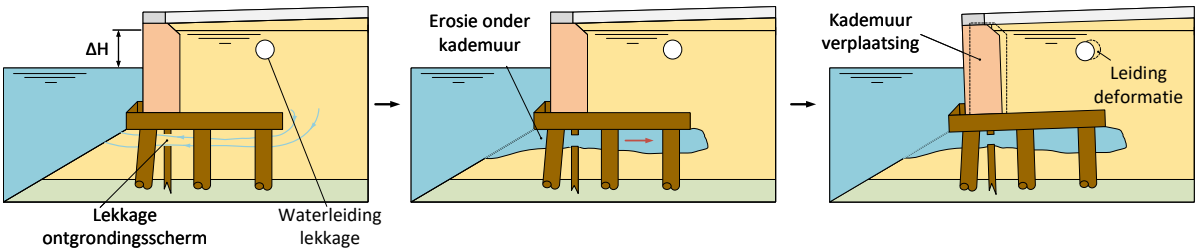

Figure 1: Doorsnede-aanzicht van de effecten van ontgrondingsscherm lekkage in combinatie met een verschil in waterstand (ΔH).

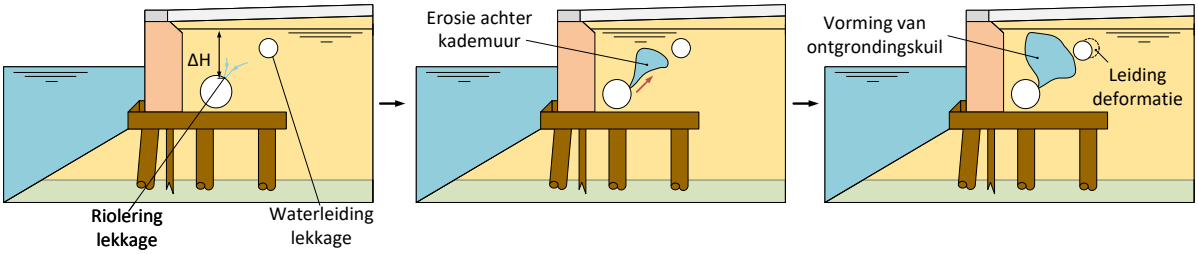

Figure 2: Doorsnede-aanzicht van de effecten van riolering lekkage in combinatie met een verschil in waterstand (ΔH).

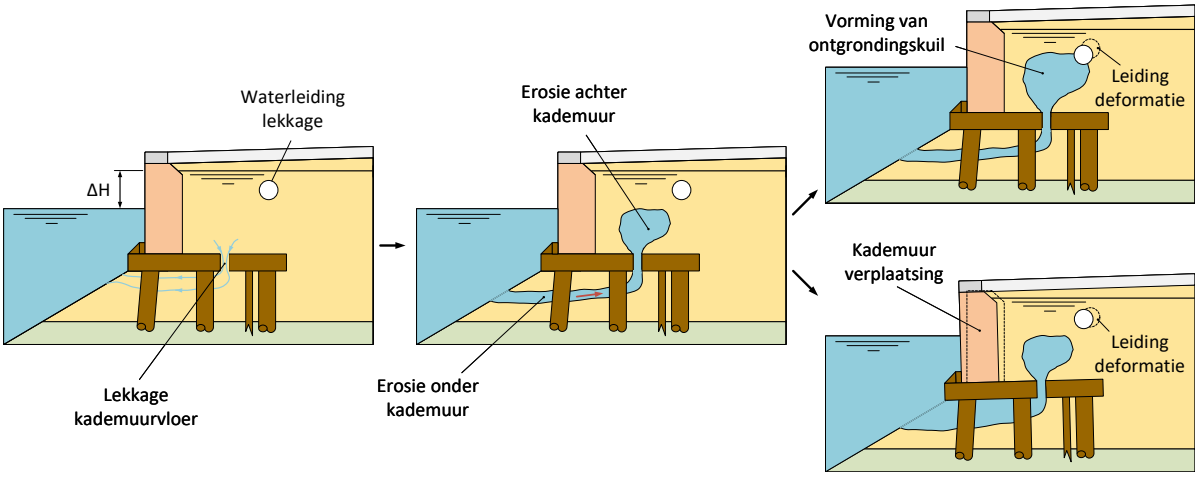

Figure 3: Doorsnede-aanzicht van de effecten van kademuurvloer lekkage in combinatie met een verschil in waterstand (ΔH).

Volgens het analytische model is het lekken van een leiding het meest waarschijnlijk doordat de maximale toelaatbare hoekverdraaiing van de leidingverbindingen wordt overschreden. Lekkage door overschrijding van het maximale toegestane buigend moment is minder waarschijnlijk maar nog steeds significant, terwijl lekkage door overschrijding van de maximale toegestane schuifkracht zeer onwaarschijnlijk is. Voor alle leidingen geld dat een hogere buigstijfheid (oftewel het product van de elasticiteitsmodulus en het oppervlaktetraagheidsmoment) leidt tot lagere gevoeligheid tot leidinglekkage. De lengte waarover kademuurvervorming optreed is ook relevant. Bij kademuurverplaatsingen over een lengte van 1 m wordt bij alle geteste leidingen geen enkel criteria voor leidinglekkage bereikt. Bij kademuurverplaatsingen over een lengte van 3 m gedragen leidingen met lagere buigstijfheden zich hetzelfde als bij kademuurverplaatsingen over grotere lengte, terwijl leidingen met hogere buigstijfheden zich hetzelfde gedragen als bij kademuurverplaatsingen over een lengte van 1 m. Bij kademuurverplaatsingen over een lengte van 7 m gedragen alle geteste leidingen zich hetzelfde als bij kademuurverplaatsingen over een grotere lengte.

Een overzicht van de resultaten is weergegeven in tabel 1. In deze tabel zijn de buitenste diameters gegeven voor de geteste leiding materialen waarbij geen lekkage was aangetroffen, bij de desbetreffende combinatie van horizontale kademuurverplaatsing en lengte waarover deze verplaatsing optreed. Als er leidingen worden aangetroffen

in de buurt van een kademuur van hetzelfde materiaal maar met een kleiner diameter, bij de desbetreffende combinatie van kademuurverplaatsing en lengte waarover deze verplaatsing optreed, wordt het aangeraden om dieper onderzoek te doen naar de desbetreffende leidingen. Hierbij moet de leiding gecheckt worden op lekkages, vervormingen en corrosie.

Table 1: Overzicht van de minimale buitenste diameters van leidingen die niet gevoelig zijn voor lekkage, voor alle geteste materialen, volgens het analytische model.

Grootte van horizontale kademuurverplaatsing (S_{max}) [mm]	Lengte waarover kademuurverplaatsing optreedt (L_s)			
	1 m	3 m	7 m	Grotere lengte
$0 < S_{max} \leq 20$	100 300	100 300	100 300	100 300
$20 < S_{max} \leq 40$	200 100 300	200 100 300	200 100 300	200 100 300
$40 < S_{max} \leq 60$	200 100 300	200 200 300	200 200 300	200 200 300
$60 < S_{max} \leq 80$	200 100 300	200 200 300	200 200 300	200 200 300
$80 < S_{max} \leq 100$	400 100 300	200 200 300	200 200 400	300 300 400

[value]	Buitenste diameter van grijs gietijzeren waterleiding in mm
[value]	Buitenste diameter van nodulair gietijzeren waterleiding in mm
[value]	Buitenste diameter van stalen waterleiding in mm
[value]	Buitenste diameter van betonnen riolering in mm

De aangegeven buitenste diameter in elke cel is een minimum waarde van de soort leiding die niet meer gevoelig is voor lekkage, onder de aangegeven omstandigheden. Leidingen van hetzelfde materiaal onder dezelfde omstandigheden met kleinere diameters kunnen wel gevoelig zijn voor lekkages.

Summary

The historic inner-cities in The Netherlands are largely known for their iconic channels and their accompanying quay walls, of which a significant number were constructed over 100 years ago. Due to the limited available space in the sub-surface of the urban environment, a high number of utility lines (i.e. potable water pipes and sewer systems) are situated in the vicinity of these quay walls. In recent years, a number of quay wall collapses have occured in the inner-city of Amsterdam, some of which have been attributed to utility line leakages. However, research into the interaction between inner-city quay walls and utility lines is lacking. Thus, the aim of this report is to answer the following question: "How does utility line leakage relate to deformation and failure of Amsterdam's inner-city quay walls and when does this interaction become significant?". The interaction between utility lines and inner-city quay walls works in both ways, thus the research is split up accordingly. The effects of utility line leakages on quay wall displacement and failure were qualitative studied using a literature study. The effects of quay wall displacement on utility line leakages were quantitatively studied using an analytical model. In this model, the interaction between utility line and surrounding soil was represented using a beam on a Winkler foundation, i.e. a beam supported by a distributed spring. The stiffness of the spring was represented as bi-linear, resulting from the equilibrium bearing capacity of the soil. Quay wall displacements ranging from 20 up to 100 mm were applied to the most common types and outer diameters of utility lines found in the vicinity of quay walls. Utility line leakage is deemed to occur if a predetermined threshold is passed of either maximum angular deflection, maximum allowable bending moment or maximum allowable shear force, each resulting from the utility line displacement. Although the scope of the study is the inner-city of Amsterdam, the study can be used in other cities with inner-city quay walls, given the circumstances are similar.

The literature study showed that quay wall displacement and failure due to utility line leakage follows from internal erosion processes. Two requirements have to be met for instigation of internal erosion: a local head difference between the water level in the channel and the groundwater level in the soil body behind the quay wall, and an open connection in the quay wall structure in the vicinity of the aforementioned local head difference, enabling the flow of soil via water. The rise of the groundwater level can be the result of a potable water pipe leakage, but can also follow from external factors like heavy rainfall. Three forms of open connections were appointed. The first is scour protection screen leakage, which can result in erosion underneath the structure. The second is quay wall floor leakage, which can result in both erosion underneath structure and erosion in the soil body behind the quay wall. The third is sewer leakage, which can result in erosion in the soil body behind the quay wall. In the latter, the aforementioned head difference is not required. This is because the direction of groundwater flow is not towards the channel, but towards the sewer leakage, given that the sewer pipe is located below the groundwater level. Erosion underneath the quay wall floor can result in quay wall displacement towards the channel, while erosion in the soil body behind the structure can result in the formation of a subsidence pit. See figures 4 to 6 for schematizations of the effects of a head difference in combination with the mentioned open connections.

As follows from the figures, both erosion underneath- as well as behind the structure can result in (further) deformations of utility lines. The former through quay wall displacement towards the channel, resulting in local soil displacement in which said utility line is embedded in. The latter trough local loss of soil, resulting in a local reduction of support. Both have the potential to result in relative utility line displacements, which can result in leakages. This process is can be denoted as a positive feedback loop. Actual failure of the quay wall due to utility line leakage can come in the form of collapse of the quay wall towards the channel or collapse of the road on top of the structure in the formed subsidence pit. Due to the dependence on external factors, quay wall failure resulting from utility line leakage can be described as a second order effect.

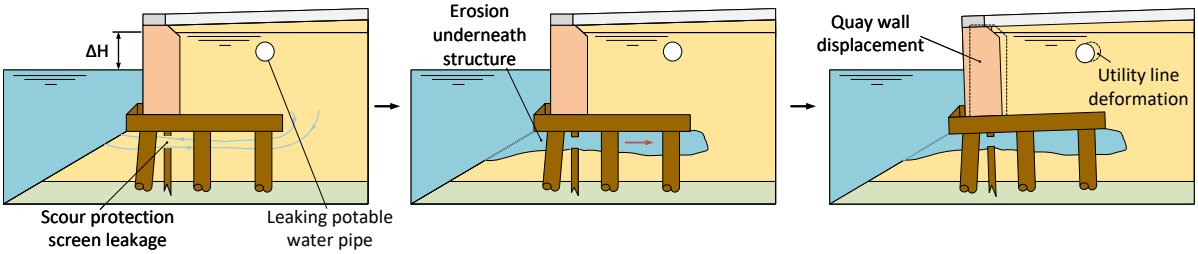

Figure 4: Cross-sectional view of the effects of scour protection screen leakage in combination with head difference (ΔH).

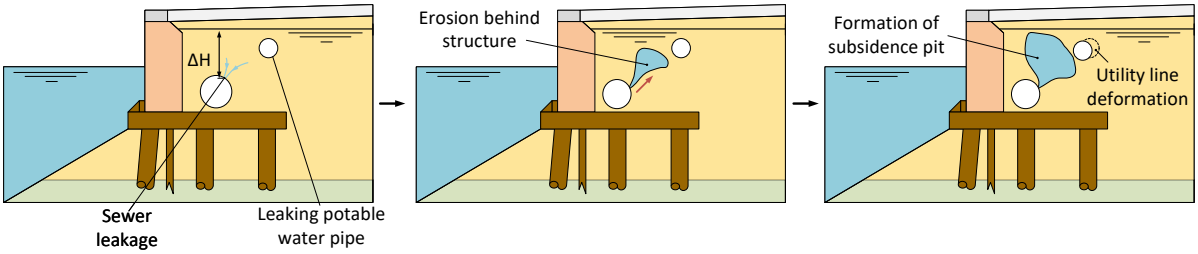

Figure 5: Cross-sectional view of the effects of sewer leakage in combination with head difference (ΔH).

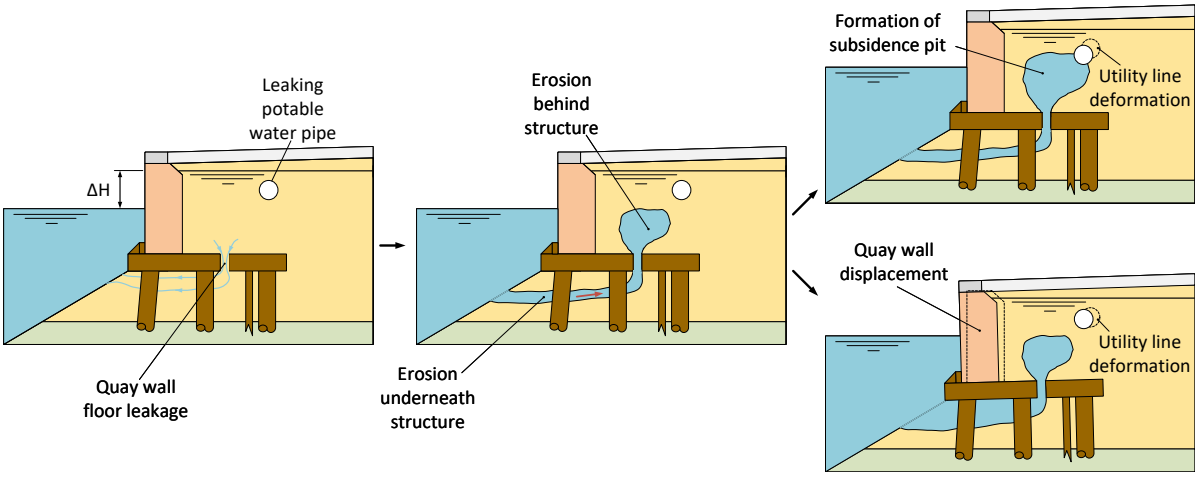

Figure 6: Cross-sectional view of the effects of quay wall floor leakage in combination with head difference (ΔH).

Using the analytical model, it was found that exceedance of the maximum allowable angular deflection of the utility line joints is most likely to result in leakages. Leakage due to exceedance of maximum allowable bending moment is relatively less likely but still significant, while leakage due to exceedance of maximum allowable shear force is unlikely. In all utility lines, a higher bending stiffness (i.e. the product of the modulus of elasticity and the cross-sectional moment of inertia) results in a lower susceptibility to leakage.The length over which quay wall displacement occurs is relevant as well. For quay wall displacements over a length of 1 m, none of the criteria for utility line leakage are met for any tested utility line. For quay wall displacements over a length of 3 m, utility lines of lower bending stiffness react similarly to quay wall displacement over greater length, while utility lines of higher bending stiffness react similarity to quay wall displacements over a length of 1 m. For quay wall displacements over a length of 7 m, all tested utility lines behaved similarly to the case of quay wall displacement over a greater length.

An overview of the results is provided in table 2. In this table, the outer diameters are provided of the tested utility line materials, for which no leakage was found for the corresponding combination of horizontal quay wall displacement and length over which said displacement occurs. If utility lines of the same material but smaller diameters are found in the vicinity of a quay wall, at the given combination of quay wall displacement and length over which said

displacement occurs, it is advised to carry out more in depth monitoring of these utility lines and check them for leakages, deformations and status of deterioration.

Table 2: Overview of minimum outer diameters of utility lines (D_o) which not are susceptible to leakage, for all tested materials, according to the analytical model.

		Length over which quay wall displacement occurs (L_s)			
		1 m	3 m	7 m	Greater length
Magnitude of horizontal quay wall displacement (S_{max}) [mm]	$0 < S_{max} \leq 20$	100 100 300	100 100 300	100 100 300	100 100 300
	$20 < S_{max} \leq 40$	100 100 300	200 100 300	200 100 300	200 100 300
	$40 < S_{max} \leq 60$	100 100 300	200 200 300	200 200 300	200 200 300
	$60 < S_{max} \leq 80$	100 100 300	200 200 300	200 200 300	200 200 300
	$80 < S_{max} \leq 100$	100 100 300	200 200 300	400 200 400	300 300 400

[value]	D_o [mm] of GCI potable water pipe
[value]	D_o [mm] of NCI potable water pipe
[value]	D_o [mm] of steel potable water pipe
[value]	D_o [mm] of concrete sewer pipe

The given outer diameter in each cell is a minimum value of the corresponding utility line for which it is not susceptible to leakage, under the corresponding circumstances. Utility lines of similar material under the same circumstances with smaller outer diameters may be susceptible to leakages.

Contents

Preface v

Samenvatting vi

Summary ix

List of Figures xvi

List of Tables xx

List of Symbols xxi

List of Abbreviations xxiii

Software used in study xxiii

1 Introduction 1

2 Analyis: Quay walls of Amsterdam 3
- 2.1 History . . . 3
- 2.2 Design of quay walls . . . 3
  - 2.2.1 Type of quay wall . . . 4
  - 2.2.2 Scour protection screen . . . 5
  - 2.2.3 Deterioration of wooden quay wall elements over time . . . 5
- 2.3 Loads acting on quay walls . . . 5
  - 2.3.1 Forces due to retaining of soil and head difference . . . 5
  - 2.3.2 Berthing- & direct impact forces . . . 5
  - 2.3.3 Vertical static- and dynamic loading . . . 6
  - 2.3.4 Propeller wash . . . 6
  - 2.3.5 Trees along the quay . . . 6
- 2.4 Surface-, water- & groundwater level . . . 6
- 2.5 Soil profile of inner-city of Amsterdam . . . 7
  - 2.5.1 Upper layers of soil profile . . . 7
  - 2.5.2 Lower layers of soil profile . . . 8
- 2.6 Observed displacements of quay walls . . . 8

3 Analysis: Utility lines 9
- 3.1 Definition of utility line . . . 9
- 3.2 Potable water pipes . . . 10
  - 3.2.1 Materials . . . 10
  - 3.2.2 Placement depth & foundation . . . 11
  - 3.2.3 Operating pressure . . . 11
  - 3.2.4 Joints . . . 11
  - 3.2.5 Emergency shutdown systems . . . 12
- 3.3 Sewer System . . . 12
  - 3.3.1 Materials . . . 13
  - 3.3.2 Placement depth, slope & foundation . . . 13
  - 3.3.3 Joints . . . 13
- 3.4 Factors contributing to utility line leakage . . . 13
  - 3.4.1 Corrosion and deterioration due to usage . . . 13
  - 3.4.2 Soil affecting deterioration of utility lines . . . 14
  - 3.4.3 Failure mechanisms of utility lines . . . 15
  - 3.4.4 Deterioration of joints . . . 16

3.5 Overview of utility lines further used in study . . . 16

4 Overview of the quay wall failure mechanisms caused by utility line leakage 17
4.1 Head difference between groundwater level and water level in channel . . . 18
4.2 Internal erosion in vicinity of quay wall . . . 19
4.2.1 Internal erosion due to scour protection screen leakage . . . 19
4.2.2 Internal erosion due to quay wall floor leakage . . . 20
4.2.3 Internal erosion due to sewer leakage . . . 21
4.3 Gaping leak resulting in erosion crater . . . 21
4.4 Actual failure of quay wall . . . 22

5 Effects of utility line leakage on soil medium 23
5.1 Types of utility line leakages . . . 23
5.1.1 Potable water pipe leakages . . . 23
5.1.2 Sewer system leakages . . . 24
5.2 Internal erosion . . . 24
5.2.1 Concentrated leak erosion . . . 24
5.2.2 Backward erosion . . . 25
5.2.3 Forward erosion . . . 25
5.3 Erosion craters due to gaping leaks . . . 25

6 Effect of utility line leakage in the vicinity of quay walls 27
6.1 Internal erosion in the vicinity of quay walls . . . 27
6.1.1 Susceptibility to backward erosion . . . 28
6.1.2 Possible open connections enabling internal erosion . . . 28
6.1.3 Pipe formation due to internal erosion . . . 29
6.1.4 Effects of erosion underneath structure . . . 31
6.1.5 Effect of erosion in soil body behind quay wall . . . 32
6.2 Gaping leaks in the vicinity of quay walls . . . 34

7 Analytical model of utility line deformation 35
7.1 Previously conducted research into quay wall-soil-utility line interaction . . . 35
7.2 Soil displacement due to quay wall displacement in 2D . . . 36
7.2.1 PLAXIS 2D model . . . 36
7.2.2 PLAXIS 2D result . . . 37
7.3 Relative soil displacement at location of quay wall displacement . . . 39
7.4 Analytical model for utility line deformation . . . 40
7.4.1 Horizontal distributed spring stiffness . . . 41
7.4.2 Equations of motion (EoM) . . . 42
7.4.3 Boundary- and interface conditions . . . 43
7.5 Applicability of the analytical model . . . 44
7.5.1 Representation of utility lines as continuous systems . . . 44
7.5.2 Applicability of Euler-Bernoulli beam model . . . 44
7.5.3 Applicability of the Winkler model . . . 45
7.5.4 Displacement over length of quay wall . . . 45
7.6 Input parameter values for analytical model . . . 47
7.7 Model output . . . 49
7.8 Formulation of criteria for utility line leakage . . . 49
7.8.1 Smaller utility lines . . . 49
7.8.2 Larger utility lines . . . 51
7.9 Case 1: quay wall displacement over greater length . . . 51
7.9.1 Quay wall displacement over greater length: utility line deformation larger than maximum allowable soil deformation . . . 52
7.9.2 Quay wall displacement over greater length: utility line displacement smaller than maximum allowable soil deformation . . . 52

7.10 Case 2: localised quay wall displacement . . . 53
7.10.1 Loc. quay wall displ: utility line displacement smaller than maximum allowable soil deformation over full length . . . 53
7.10.2 Loc. quay wall displ: utility line displacement only larger than maximum allowable quay wall displacement in displaced soil section . . . 54
7.10.3 Loc. quay wall displ: utility line displacement greater than maximum allowable soil deformation both in displaced soil section as right next to displacement . . . 55
7.10.4 Loc. quay wall displ: utility line displacement partially smaller than maximum allowable soil deformation in displaced soil section . . . 55
7.11 Overview of critical soil areas . . . 56

8 Results analytical model 58
8.1 Utility line leakage due to exceedance of allowable angular deflection . . . 58
8.1.1 Model results regarding angular deflection for quay wall deformation over greater length . . . 58
8.1.2 Model results regarding angular deflection for localized quay wall deformation . . . 59
8.2 Utility line leakage due to exceedance of maximum bending moment . . . 62
8.2.1 Model results regarding the maximum bending moment for quay wall deformation over greater length . . . 63
8.2.2 Model results regarding the maximum bending moment for localized quay wall deformation . . . 63
8.3 Utility line leakage due to exceedance of maximum shear force . . . 66
8.3.1 Model results regarding the maximum shear force for quay wall deformation over greater length . . . 66
8.3.2 Model results regarding the maximum shear force for localized quay wall deformation . . . 67
8.4 Influence of variation in horizontal distributed spring stiffness to analytical model . . . 69
8.5 Sensitivity analysis of analytical model input parameters . . . 70
8.6 Overview of results analytical model . . . 72
8.6.1 Overview of utility line leakage due to quay wall displacement . . . 72
8.6.2 Dimensionless parameter of utility line diameter and quay wall displacement in relation to leakage . . . 73

9 Discussion 75
9.1 Discussion of results of the analytical model . . . 75
9.1.1 Discussion of analytical model results: angular deflection . . . 75
9.1.2 Discussion of analytical model results: maximum bending moment . . . 76
9.1.3 Discussion of analytical model results: maximum shear force . . . 77
9.2 Relation between qualitative and quantitative studies . . . 77
9.2.1 Influence of utility line deterioration . . . 77
9.2.2 Relation between utility line leakage effects quay walls and analytical model . . . 78
9.3 Limitations of the study . . . 79

10 Conclusion 81

11 Recommendations 83

Bibliography 84

A Sloping revetment with sheetpiles 89

B Materials used for utility lines 90
B.1 Copper . . . 90
B.2 Polyethylene (PE) . . . 90
B.3 Asbestos cement . . . 90
B.4 Polyvinylchloride (PVC) . . . 90

C Inspection Haarlem 91

D Dike failure at Stein, Limburg 95

E Additional internal erosion mechanisms 97
E.1 Contact erosion . . . 97
E.2 Suffusion . . . 97

E.3 Dissolution . . . 97

F Study into erosion craters 98
F.1 Scaled down experiments . . . 98
F.2 On scale experiments . . . 99
F.3 Standard NEN 3651 . . . 99

G Adapted Sellmeijer model 102

H PLAXIS 2D model 105
H.1 Soil properties . . . 105
H.1.1 Assumption of sole presence of sand in model . . . 105
H.1.2 Material model . . . 105
H.1.3 Overview of soil parameters . . . 105
H.2 Quay wall structure . . . 106
H.3 Model composition and staged construction . . . 106

I Analytical model 108
I.1 Horizontal soil spring stiffness . . . 108
I.1.1 Soil spring stiffness: maximum allowable soil deformation . . . 108
I.1.2 Soil spring stiffness: horizontal equilibrium bearing capacity . . . 108
I.2 Vertical soil spring stiffness . . . 109
I.3 Cross-sectional moment of inertia for hollow circular cross-sections . . . 110
I.4 Relation influence length and utility line dimension . . . 111
I.5 Overview of case 1: utility line displacement larger than maximum allowable soil deformation . . . 111
I.6 Overview of case 1: utility line displacement smaller than maximum allowable soil deformation . . . 113
I.7 Overview of case 2 . . . 113
I.8 Overview of case 2 . . . 114
I.9 Overview of case 2 . . . 115
I.10 Overview of case 2 . . . 117
I.11 Normal forces in utility line . . . 118

J Continuous quay wall displacement 123
J.1 Discretization of quay wall displacement over its length . . . 123
J.2 oM, boundary- and interface conditions . . . 125
J.3 Validity of assumption of abrupt quay wall displacement . . . 126

K Graphs depicting relation between dimensionless ratio and angular deflection 128

List of Figures

1 Cross-sectional view of the effects of scour protection screen leakage in combination with head difference. . . . vii
2 Cross-sectional view of the effects of sewer leakage in combination with head difference. . . . vii
3 Cross-sectional view of the effects of quay wall floor leakage in combination with head difference. . . . vii
4 Cross-sectional view of the effects of scour protection screen leakage in combination with head difference. . . . x
5 Cross-sectional view of the effects of sewer leakage in combination with head difference. . . . x
6 Cross-sectional view of the effects of quay wall floor leakage in combination with head difference. . . . x

1.1 Map of the inner city of Amsterdam with locations of quay wall collapses. . . . 1

2.1 Typical cross-section of the quay wall design consisting of a gravity wall on piles. . . . 4
2.2 Overview of the soil profile in the inner-city of Amsterdam. . . . 7
2.3 Pictures of the inspection at both the water line and below the water line. . . . 8

3.1 Overview of the potable water pipe network of the inner-city of Amsterdam. . . . 10
3.2 Examples of both tensile- and non-tensile resistant pipe segment connections. . . . 11
3.3 Masonry pipe named the "Oude Spoye" being excavated, which mouthed in the "Rokin" channel. . . . 12
3.4 Overview of the failure modes of potable water pipes made of steel, NCI, and GCI (extreme cases). . . . 15
3.5 Schematization of the failure modes of concrete pipes (extreme cases). . . . 16

4.1 Flow chart relating utility line leakage to quay wall failure. . . . 17
4.2 Head difference between groundwater level and water level in channel. . . . 18
4.3 Possible effects of internal erosion due to scour protection screen leakage in combination with a head difference (exaggerated portrayal). . . . 19
4.4 Possible effects of internal erosion due to quay wall floor leakage in combination with a head difference (exaggerated portrayal). . . . 20
4.5 Possible effects of internal erosion due to sewer leakage in combination with a head difference (exaggerated portrayal). . . . 21
4.6 Gaping leak in the vicinity of a quay wall. . . . 22
4.7 Actual failure of quay wall due to utility line leakage. . . . 22

5.1 Phases of backward erosion. . . . 25
5.2 Overview of the definitions of erosion crater dimensions . . . 26
5.3 Graphs depicting the dimensions of erosion craters. . . . 26

6.1 Example of a leak in the scour protection screen as an open connection. . . . 28
6.2 Example of leak in the wooden floor as an open connection. . . . 29
6.3 Example of a leak in the sewer system as an open connection. . . . 29
6.4 Schematization of erosion underneath the structure due to scour protection screen leakage (exaggerated portrayal). . . . 30
6.5 Schematization of erosion underneath- as well as behind the structure due to quay wall floor leakage (exaggerated portrayal). . . . 30
6.6 Schematization of erosion underneath the structure due to sewer leakage (exaggerated portrayal). . . . 31
6.7 Effect of erosion underneath structure. . . . 32
6.8 Collapsed quay wall of the "Bemuurde Weerd Oost" in Utrecht. . . . 32
6.9 Effect of erosion behind structure. . . . 33
6.10 Subsidence pit as observed in the Marnixstraat, Amsterdam. . . . 33
6.11 Schematization of an erosion crater due to gaping leak. . . . 34

7.1 Overview of the PLAXIS 2D model. . . . 36
7.2 Soil displacements resulting from the PLAXIS 2D model with 20 mm horizontal quay wall displacement. 37
7.3 Soil displacements resulting from the PLAXIS 2D model with 40 mm horizontal quay wall displacement. 37
7.4 Soil displacements resulting from the PLAXIS 2D model with 60 mm horizontal quay wall displacement. 38
7.5 Soil displacements resulting from the PLAXIS 2D model with 80 mm horizontal quay wall displacement. 38
7.6 Soil displacements resulting from the PLAXIS 2D model with 100 mm horizontal quay wall displacement. . . . 38
7.7 Relative displacement of utility line at the location of abrupt quay wall displacement, top view. . . . 40
7.8 Relative displacement of utility line at the location of abrupt quay wall displacement, cross-sectional view. . . . 40
7.9 Left side: beam on a Winkler foundation. Right side: Euler-Bernoulli beam. . . . 41
7.10 Graph of the relation between horizontal soil deformation and -pressure. . . . 42
7.11 Relative displacement of utility line at the location of gentle quay wall displacement, top view. . . . 45
7.12 Relative displacement of utility line at the location of gentle quay wall displacement, cross-sectional view. . . . 46
7.13 Cross-section of a utility line, depicting its outer diameter and thickness. . . . 48
7.14 Model of the case: quay wall displacement over greater length, utility line displacement larger than maximum allowable soil deformation. . . . 52
7.15 Model of the case: quay wall displacement over greater length utility line displacement smaller than maximum allowable soil deformation. . . . 53
7.16 Model of the case: localized quay wall displacement, utility line displacement smaller than maximum allowable soil deformation over full length . . . 54
7.17 Model of the case: localized quay wall displacement, utility line displacement only larger than maximum allowable soil deformation in displaced soil section . . . 54
7.18 Model of the case: localized quay wall displacement, utility line displacement greater than maximum allowable soil deformation both in displaced soil section as right next to displacement . . . 55
7.19 Model of the case: localized quay wall displacement, utility line displacement partially smaller than maximum allowable soil deformation in displaced soil section . . . 56
7.20 Cross section of critical area's for both analytical models. . . . 56
7.21 Top view of critical areas for quay wall displacement over greater length. . . . 57
7.22 Top view of critical areas for localized quay wall displacement. . . . 57

8.1 Quay wall deformation plotted against the mean maximum angular deformation of multiple diameters of GCI and NCI utility lines, for quay wall deformation over greater length. . . . 59
8.2 Quay wall deformation plotted against the mean maximum angular deformation of multiple diameters of steel and concrete utility lines, for quay wall deformation over longer length. . . . 59
8.3 Quay wall deformation plotted against the mean maximum angular deformation of multiple diameters of GCI pipes, for localized quay wall displacement over a length of 1, 3 and 7 m. . . . 60
8.4 Quay wall deformation plotted against the mean maximum angular deformation of multiple diameters of NCI pipes, for localized quay wall displacement over a length of 1, 3 and 7 m. . . . 61
8.5 Quay wall deformation plotted against the mean maximum angular deformation of multiple diameters of steel pipes, for localized quay wall displacement over a length of 1, 3 and 7 m. . . . 61
8.6 Quay wall deformation plotted against the mean maximum angular deformation of multiple diameters of concrete pipes, for localized quay wall displacement over a length of 1, 3 and 7 m. . . . 62
8.7 Quay wall deformation plotted against the mean unity check regarding the maximum bending moment of multiple diameters of GCI pipes, for quay wall deformation over longer length. . . . 63
8.8 Quay wall deformation plotted against the mean, minimum, and maximum unity check regarding the maximum bending moment of NCI and steel pipes with outer diameters of 100 mm, for quay wall deformation over longer length. . . . 63
8.9 Quay wall displacement plotted against the mean unity check regarding the maximum bending moment of multiple diameters of GCI pipes, for localized quay wall deformation of 1, 3 and 7 m. . . . 64
8.10 Quay wall displacement plotted against the mean unity check regarding the maximum bending moment of 100 mm diameter NCI pipes, for localized quay wall deformation of 1, 3 and 7 m. . . . 65
8.11 Quay wall displacements plotted against the mean unity check regarding the maximum bending moment of 100 mm diameter steel pipes, for localized quay wall deformation of 1, 3 and 7 m. . . . 65

8.12 Quay wall deformation plotted against the mean unity check regarding the maximum shear force of multiple diameters of GCI pipes, for quay wall deformation over longer length. . . . 66
8.13 Quay wall deformation plotted against the mean, minimum, and maximum unity check regarding the maximum shear force of NCI and steel utility lines with outer diameters of 100 mm, for quay wall deformation over longer length. . . . 66
8.14 Quay wall deformation plotted against the mean unity check regarding the maximum shear force of multiple diameters of GCI pipes, for localized quay wall deformation of 1, 3 and 7 m. . . . 67
8.15 Quay wall deformation plotted against the mean unity check regarding the maximum shear force of 100 mm diameter NCI pipes, for localized quay wall deformation of 1, 3 and 7 m. . . . 68
8.16 Quay wall deformation plotted against the mean unity check regarding the maximum shear force of 100 mm diameter steel pipes, for localized quay wall deformation of 1, 3 and 7 m. . . . 68
8.17 Mean, maximum and minimum angular deflection plotted against the quay wall deformation for GCI and NCI utility lines . . . 69
8.18 Mean, maximum and minimum angular deflection plotted against the quay wall deformation for steel and concrete utility lines . . . 70
8.19 D_o/S_{max} plotted against the mean maximum angular deflection for all diameters of GCI utility lines, for quay wall displacement over greater length. . . . 74

A.1 Typical cross-section of a quay wall design consisting of a sheetpile with sloping gravity wall. . . . 89

C.1 Picture of settlements at top of quay wall as seen during quay wall inspection. . . . 91
C.2 Picture of wall inclination as seen during quay wall inspection. . . . 92
C.3 Picture of quay wall bulging towards channel as seen during quay wall inspection. . . . 92
C.4 Picture of masonry deterioration as seen during quay wall inspection. . . . 93
C.5 Picture of washed away masonry as seen during quay wall inspection. . . . 93
C.6 Picture of disconnected pile connection as seen during quay wall inspection. . . . 94

D.1 Resulting failure of the water pipe leakage at Stein. . . . 96

F.1 Pictures of the experiment set up after the generation of erosion pits due to gaping leaks. . . . 98
F.2 Overview of the definitions of erosion crater dimensions . . . 99
F.3 Width of erosion crater (R_W) plotted against the diameter of the gaping leak (d_h). . . . 100
F.4 Length of erosion crater (R_L) plotted against the diameter of the gaping leak (d_h). . . . 101
F.5 Height of erosion crater (D_c) plotted against the outer diameter of the potable water pipe (D_o). . . . 101

G.1 Graph of the critical hydraulic gradient for which backward erosion is an issue according to the adapted Sellmeijer model. . . . 104

H.1 Overview of the PLAXIS 2D model over full width. . . . 107
H.2 Detailed overview of the PLAXIS 2D model. . . . 107

I.1 Graph used to determine the loading coefficient K_q. . . . 109
I.2 Graph plotting the outer diameter of an utility line in relation to the magnitude of influence length. . . . 111
I.3 Model of the case: quay wall deformation over greater length, utility line displacement larger than maximum allowable soil deformation. . . . 112
I.4 Model of the case: quay wall displacement over greater length, utility line deformation smaller than maximum allowable soil deformation. . . . 113
I.5 Model of the case: Localized quay wall displacement, utility line displacement smaller than maximum allowable soil deformation over full length . . . 114
I.6 Model of the case: localized quay wall displacement, utility line displacement only greater than maximum allowable soil deformation in displaced soil section. . . . 115
I.7 Analytical model of the case: localised quay wall deformation, utility line displacement partially greater than maximum allowable soil deformation . . . 116
I.8 Model of the case: localised quay wall displacement, utility line displacement partially smaller than maximum allowable soil deformation in displaced soil section. . . . 117
I.9 Elongation of utility line due to displacement. . . . 119
I.10 Influence length L_{infl} plotted against the elongation ϵ. . . . 120

I.11 Additional length of utility line ΔL plotted against the influence length. 121

J.1 Abrupt displacement of quay wall as used in analytical model 123
J.2 Gentle displacement of quay wall, continuous displacement 124
J.3 Gentle displacement of quay wall, discretized displacement 125

K.1 D_o/S_{max} plotted against the mean maximum angular deflection for all diameters of NCI utility lines, for quay wall displacement over greater length. 128
K.2 D_o/S_{max} plotted against the mean maximum angular deflection for all diameters of steel utility lines, for quay wall displacement over greater length. 129
K.3 D_o/S_{max} plotted against the mean maximum angular deflection for all diameters of concrete utility lines, for quay wall displacement over greater length. 129

List of Tables

1 Overview of minimum outer diameters of utility lines which are not susceptible to leakage, for all tested materials. . . . viii
2 Overview of minimum outer diameters of utility lines which are not susceptible to leakage, for all tested materials. . . . xi

3.1 Overview of utility line parameters as used in study. . . . 16

7.1 Overview of the horizontal-, vertical- and total displacements of area B for the various quay wall displacements. . . . 38
7.2 Reduction of maximum angular deflection compared to assumption of abrupt quay wall displacement, for GCI pipes. . . . 46
7.3 Thickness of utility lines corresponding to the material type. . . . 48

8.1 Range of horizontal quay wall displacement in which maximum allowable angular deflection (1.5^o) is surpassed for quay wall displacement over greater length. . . . 59
8.2 Range of horizontal quay wall displacement in which maximum allowable deflection (1.5^o) is surpassed for quay wall displacement over greater length. . . . 62
8.3 Output parameters resulting from mean values for both model cases. . . . 71
8.4 Overview of sensitivity of the input parameters for model regarding quay wall displacement over greater length. . . . 71
8.5 Overview of sensitivity of the input parameters for localized quay wall displacement. . . . 71
8.6 Overview of minimum outer diameters of utility lines which are not susceptible to leakage, for all tested materials. . . . 73
8.7 Maximum value of D_o/S_{max} at which utility line is susceptible to leakage at quay wall displacement over greater length, for each tested material . . . 74

10.1 Overview of minimum outer diameters of utility lines which are not susceptible to leakage, for all tested materials. . . . 82

I.1 Horizontal- and vertical spring stiffness for typical utility line outer diameters at a coverage of 0.8 m. . . . 110
I.2 Horizontal- and vertical spring stiffness for typical utility line outer diameters at a coverage of 2.03 m. 110

J.1 Reduction of maximum angular deflection compared to assumption of abrupt quay wall displacement, for GCI pipes. . . . 127
J.2 Reduction of maximum moment compared to assumption of abrupt quay wall displacement, for GCI pipes. . . . 127
J.3 Reduction of maximum shear force compared to assumption of abrupt quay wall displacement, for GCI pipes. . . . 127

List of Symbols

General parameters

ρ_w	Density of water
g	Gravitational accelaration

General soil parameters

d_{10}	10^{th} percentile of the grain size distribution
d_{50}	50^{th} percentile of the grain size distribution
d_{60}	60^{th} percentile of the grain size distribution
d_{70}	70^{th} percentile of the grain size distribution
δ	Angle of external friction between utility line and soil
σ'_v	Effective vertical soil pressure
γ'	Effective weight of soil
K	Ratio of horizontal/vertical soil stresses, at neutral horizontal pressure
ϕ	Soil angle of internal friction
γ_p	Volumetric weight of particles
γ	Volumetric weight of soil
γ_w	Volumetric weight of water

Utility line parameters

H	Coverage of utility line
A	Cross-sectional area of utility line
I	Cross-sectional moment of inertia of utility line
z	Distance from neutral axis to the outer fibre of utility line
D_{in}	Internal diameter of utility line
$L_{segment}$	Length of utility line segment
$\tau_{max,mat}$	Maximum allowable shear stress of utility line material
$\sigma_{max,mat}$	Maximum allowable tensile stress of utility line material
E	Modulus of elasticity of utility line
D_o	Outer diameter of utility line
Z	Soil depth up to the utility line's longitudinal axis
t	Thickness of utility line

Analytical model parameters

ΔL	Additional length of utility line
ϵ	Elongation of utility line
α	Empirical stiffness constant
$K_{h,\%}$	Horizontal distributed spring stiffness corresponding to a predetermined percentage of equilibrium soil bearing capacity
Q_{he}	Horizontal equilibrium distributed soil load
L_{infl}	Influence length of boundary conditions
l	Length over which quay wall has displaced
L_{Smax}	Length over which continuous quay wall displacement occurs
$y_{s,max}$	Maximum allowable horizontal soil deformation
$y_{s,max,\%}$	Maximum allowable horizontal soil deformation corresponding to a predetermined percentage of equilibrium soil bearing capacity
σ_M	Maximum compression- and tension stress occurring in the utility line's cross-section due to maximum bending moment
σ_V	Maximum shear stress occurring in the utility line's cross-section due to maximum shear force
L'	New length of utility length

N	Normal force according to Hooke's law
σ	Normal stress according to Hooke's law
S_{max}	Quay wall displacement
$y(x)$	Utility line displacement

Parameters used for determination of horizontal distributed spring stiffness

K_h	Horizontal distributed spring stiffness
q_{he}	Horizontal equilibrium bearing capacity
y_s	Horizontal soil deformation
q_h	Horizontal soil pressure
K_q	Loading coefficient according to theory of Brinch-Hansen

Parameters used for determination of vertical distributed spring stiffness

d_q	Auxiliary factor
N_γ	Auxiliary factor
N_q	Auxiliary factor
S_q	Auxiliary factor
S_y	Auxiliary factor
γ'_{mean}	Mean effective volumetric weight
L_{sup}	Minimal support length
E_s	Modulus of elasticity of soil
q_n	Neutral soil pressure
P_{we}	Vertical equilibrium bearing capacity
K_v	Vertical distributed spring stiffness
$K_{v,2}$	Vertical distributed spring stiffness starting from 2/3 vertical equilibrium bearing capacity
$K_{v,1}$	Vertical distributed spring stiffness up to 2/3 vertical equilibrium bearing capacity

Erosion crater calculation parameters

A_h	Area of hole in pipe
d_h	Diameter of hole in pipe
μ	Discharge coefficient of hole
Q	Discharge through hole
P	Hydraulic power of outflow
R_L	Length of erosion crater
h	Pressure head at the location of the hole
R_W	Width of erosion crater

Parameters used in Adapted Sellmeijer check

D_{sand}	Characteristic thickness of sand layer
ΔH_c	Critical water gradient
κ	Intrinsic permeability of sand layer
d_{70m}	Mean value of the 70^{th} percentile of the grain size distribution
$F_{resistance}$	Parameter relating to equilibrium of sand particle on bottom of pipe formed by backward erosion
F_{scale}	Parameter relating to difference of scale between experiments and real life situation
$F_{geometry}$	Parameter relating to the geometry of the subsoil in regards to groundwater flow
k	Permeability of sand layer
θ_r	Rolling resistance of sand particles
γ_b	Safety factor due to schematization of the problem
γ_n	Safety factor relating to the allowed exceedance frequency
L_s	Seepage length
d_s	Thickness of impervious soil layer
ΔH	Water gradient present over structure
η	White's coefficient

List of Abbreviations

EoM	Equations of Motion
FEM	Finite Element Method
GCI	Grey cast iron
NEN	Nederlandse Norm
NCI	Nodular cast iron
NAP	Normaal Amsterdams Peil
PE	Polyethylene
PVC	Polyvinylchloride
VOC	Vereenigde Oostindische Compagnie

Software used in study

Autodesk AutoCAD Map 3D	Version 2021
Bentley PLAXIS 2D	Version 2017.01
Infracad MAP	Version 2012 v7.0.8814
Kadaster KLIC-viewer	Version 5.7.20
Maplesoft Maple	Version 2020
Microsoft Excel	Version Microsoft 365
Qgis	Version 3.12.3

1

Introduction

One of the biggest challenges in the coming years is the reassessment and renovation of the existing infrastructure in The Netherlands. Part of this infrastructure are the historic quay walls, iconic for a lot of inner-cities. Most of these were built over 100 years ago, without a clear definition of their projected lifespan. Over the years, little monitoring has been performed on these structures, resulting in unexpected failures. Amsterdam is one of the municipalities dealing with problems regarding their quay walls, as in recent years a number of these collapsed: the Entrepotdok (van Belzen, 2017) and the Marnixstraat in 2017 (AT5, 2017), the Nassaukade in 2018 (AT5, 2018) and the Grimburgwal in 2020 NOS (2020). Thus, Amsterdam is in dire need for research into the behaviour and failure mechanisms of their quay walls, and how to adequately monitor them. Of the 600 km of quay wall in the inner-city, it is expected that at least 200 km has to be reassessed, and potentially renovated or renewed, in order to make sure their future lifespan is extended up to sufficient levels. See figure 1.1 for the map of the inner city of Amsterdam and the locations of the aforementioned quay wall collapses (Gemeente Amsterdam, n.d.a; AT5, 2017; Ginopress B.V., 2018; Buurtorganisatie 1018, 2017; Brante, M., 2020).

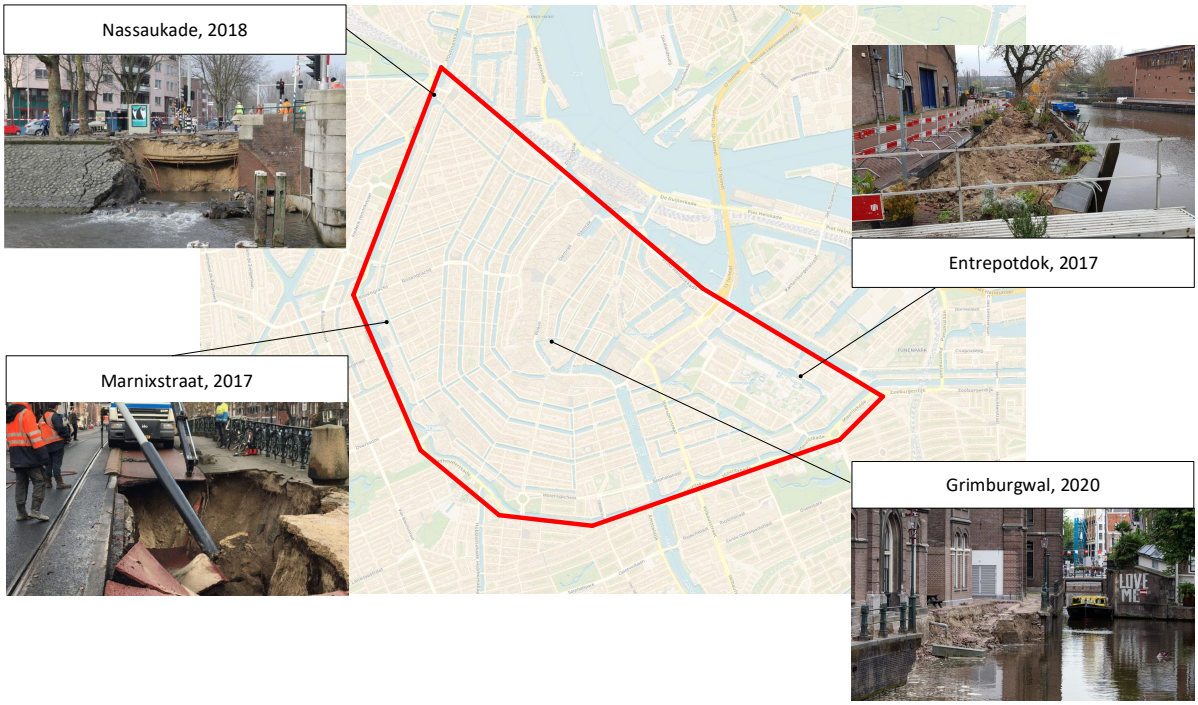

Figure 1.1: Map of the inner city of Amsterdam with locations of quay wall collapses (Gemeente Amsterdam, n.d.a; AT5, 2017; Ginopress B.V., 2018; Buurtorganisatie 1018, 2017; Brante, M., 2020). The study area is highlighted in red.

At least in the case of the quay wall collapses of the Marnixstraat, the Nassaukade, and the Entrepotdok, failure has coincided with leakage of utility lines in their vicinity, i.e. potable water pipes and sewer systems. Therefore, it is reasoned that there is a link between failure of utility lines and failure of quay walls. Utility lines located in the vicinity of quay walls is not a unique situation for the aforementioned collapses, but is almost standard due to the limited available space in inner cities. As of yet, there is a lack of studies linking leakage of utility lines to quay wall failure. Other collapses of infrastructure have been linked via research to utility line leakage, for example a dike along Juliana channel, near Stein (Limburg) (Onderzoeksraad voor Veiligheid, 2005) in 2004. Additionally, due to the existence of standard series NEN 3650 (NEN, 2020a), the importance of understanding the effects of utility line leakage in the vicinity of infrastructure has been highlighted on a governmental level. The mechanisms in which failure of utility lines results in failure of quay walls are expected to be linked to internal erosion and sediment entrainment processes.

In order to find the link between utility line leakage and quay wall failure, the main research question was formulated as follows:

> **How does utility line leakage relate to deformation and failure of Amsterdam's inner-city quay walls and when does this interaction become significant?**

In order to answer the main question, the sub-questions were formulated as follows:

1. **What is the current status of the utility line infrastructure and the quay walls of Amsterdam's inner-city?**
   (a) **What is the typical design of the inner-city quay walls, and what are the characteristics of the environment these are located in?**
   (b) **What types of utility lines are situated in the vicinity of the quay walls and how is leakage instigated in these?**
2. **How is leakage of a utility line linked to failure of a quay wall?**
3. **How is quay wall deformation linked to utility line leakage?**

The research into the influence of utility line leakage on the failure of quay walls mainly follows a qualitative approach, while the influence of quay wall displacements onto deformations of utility line is described using an analytical model. The deformations of utility lines due to quay wall displacements are expected to result in a positive feedback loop. Therefore, the study is mainly focused on how utility line leakages result from quay wall displacements, resulting in a central role for the aforementioned analytical model. The scope of the study is limited to the inner-city of Amsterdam, commonly known by its Dutch name the "Grachtengordel". This is due to the fact that the municipality is in the midst of a huge reassessment and renovation study of both their historic bridges and -quay walls: the "Programma Kademuren en Bruggen" (Program for Quay walls and Bridges). However, it is expected that the findings of this study are relevant for any city with a similar inner-city canal structure as Amsterdam, f.e. Delft, Leiden and Utrecht.

The report is structured according to the order of the sub-questions. First, the design of the inner-city quay walls, loads acting on them, and other relevant factors in their vicinity, are discussed in chapter 2. Next, a similar analysis is provided for the utility lines in the vicinity of the quay walls in chapter 3. The second sub-question is researched in the following chapters. Chapter 4 provides an overview through which utility line leakage is linked to quay wall failure. In the following chapters, the reasoning towards said overview is provided, as the effect of utility line leakage in a soil medium is discussed in chapter 5, while in chapter 6 these effects are specified for utility lines in the vicinity of quay walls. Chapter 7 provides the outline of the analytical model used to research sub-question 3, and the results of this model are provided in chapter 8. In term these results are discussed and linked to the qualitative research in chapter 9, and the conclusion of the report is provided in chapter 10. Recommendations to further studies are provided in chapter 11

2

Analyis: Quay walls of Amsterdam

In this chapter an analysis of the quay walls in the inner city is provided. This analysis is required in order to find an answer to sub-question 1a:

> **What is the typical design of the inner-city quay walls, and what are the characteristics of the environment these are located in?**

Thus, it has to be noted that the provided information in the following sections is primarily focused on the inner-city quay walls of Amsterdam.

The chapter starts with a brief overview of the history of the quay walls in section 2.1. Next, in section 2.2, the quay wall design is discussed. Section 2.3 provides an overview of the most significant loads acting on the quay walls. As quay walls are located at the interface between water and soil, the (ground)water levels and soil profile are discussed in section 2.4 and 2.5 respectively. The chapter closes with observed displacements of the quay walls in section 2.6.

2.1. History

According to de Gijt (2010), transport over water dates back to at least 6000 BC. As initially ships had a very shallow draught, ships could simply sail up to shore and river banks without any limitations. However, as draughts of ships got deeper, quay walls became a necessity in order to load goods from ship to shore and vice versa. Nowadays, ports handling transport of goods between ships and the hinterland are for the majority of the situations located outside of busy city centers. Historically, this is a fairly new trend. For example, the port of Rotterdam only migrated towards the mouth of the New Waterway in the 1950's Port of Rotterdam (n.d.).

The pivotal driver of the development of the characteristic channels in Amsterdam is the foundation of the "Vereenigde Oostindische Compagnie" (VOC) at the start of the 17th century (Geschiedenis Lokaal Amsterdam, n.d.). The channels were used to efficiently transport goods to the various warehouses located along their quays. In Dutch history books this period of time is known as the "Golden Age", as Amsterdam and other VOC cities flourished due to trade with ports all over the world. As the ports moved out of the inner-cities, their function shifted from enabling (un)loading of ships to providing support for the roads constructed on top of them and the traffic using these roads. Especially heavy traffic poses a problem for the quay walls, as they were never designed for loads of this magnitude and direction of acting (Kruyswijk, 2020b).

2.2. Design of quay walls

In the inner-city of Amsterdam, two main designs of bank protection are utilized: a quay wall in the form of a gravity wall on piles and a sloping revetment in combination with sheetpiles. The former can be found all over the inner-city, the latter is mostly situated in the vicinity of bridges along the outer channel, the "Singelgracht". Both bank protection designs are susceptible to failure due to utility lines, as the collapsed Nassaukade was of the form of a sloping revetment with sheetpiles (AT5, 2018). However, as both designs and their failure mechanisms are notably different, only the actual quay walls of the inner city are taken into account. See appendix A for an overview of the design of the sloping wall.

2.2.1. Type of quay wall

Virtually every quay wall in the inner city of Amsterdam utilizes the gravity wall on pile design, the failed quay walls of the Marnixstraat (AT5, 2017) and the Grimburgwal (NOS, 2020) included. In figure 2.1, a typical cross-section of the gravity wall on pile quay wall design is provided (Stadsarchief Amsterdam, 1906). This particular quay wall is located along the "Lijnbaansgracht".

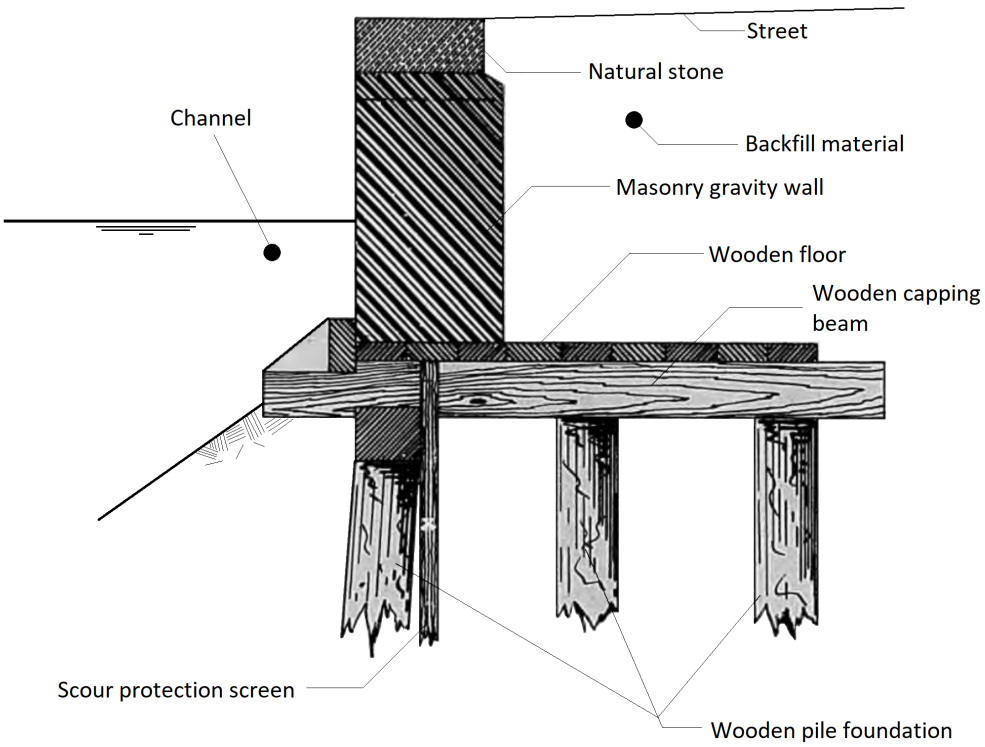

Figure 2.1: Typical cross-section of the quay wall design consisting of a gravity wall on piles (Stadsarchief Amsterdam, 1906).

Although many variants and dimensions are found in the vicinity of quay walls are found, the height of the quay wall from quay wall floor up to surface level is in the order of 3 m, while the length of the quay wall floor is in the order of 4 m. These values are used in the rest of the study. Historically, the foundation piles, the capping beams, the quay wall floor and the scour protection screen were made out of wood. The material was used extensively in quay wall construction up to the 20^{th} century (de Gijt, 2010). Next to vertical transfer of loads, the connection between the capping beam and piles is capable of transferring horizontal loads and even moments, by use of indentations and stability pins.

Masonry is used for the construction of the gravity wall. According to van der Pluijm (1997), the material properties of masonry under tension are comparable to concrete, as in both materials the modulus of elasticity is significantly higher in compression than in tension. After construction of the quay walls, backfill material in the form of a soil body is placed behind the masonry on which the quay itself is constructed. As said before, these quays are nowadays used as roads instead as loading facilities.

Starting in the 1930's, a shift is noticed in the use of materials in the restoration and construction of quay walls in the inner city. Reinforced concreted was introduced, replacing the majority of the masonry of the gravity wall except the visual part. An examples is the restauration of a quay wall section along the "Singel" (Stadsarchief Amsterdam, 1933). However, the majority of the quay walls still consist solely of masonry

2.2.2. Scour protection screen

Virtually all quay walls of the inner city of Amsterdam are installed with a scour protection screen. However, the location of this screens varies. The quay wall represented in figure 2.1 has this feature installed behind the first row of piles as seen from the channel. In other configurations the screen is installed in front of the last row of piles as seen from the channel. The scour protection screen is meant to prevent seepage underneath the structure, and prevent soil from washing away due to f.e. ship actions or currents in the vicinity of the quay walls. The soil profile in front of the quay wall was found not to be dependent on the location of the scour protection screen (Stadsarchief Amsterdam, 1911, 1932). The screen reaches from the quay wall floor down to the impermeable clay layer present underneath the structure as discussed in section 2.5, ensuring a water tight seal.

2.2.3. Deterioration of wooden quay wall elements over time

Over the lifetime of a structure, wood is not very susceptible to decay due to fungi, as long as the material is submerged (de Gijt, 2010). However, according to Klaassen (2007), even wooden foundation piles permanently located in water are susceptible to decay due to bacteria. For part of this study, a total of 1692 foundation piles originating from Amsterdam were examined. A significant number of the pine, spruce and alder piles, species of wood also used for the foundation of the quay walls, were found to have experienced severe bacterial degradation over their full length. In the most severe cases of degradation, the mean depth measured from bark to center was found to be 36 mm in pine trees. The similarly measured mean depth of degradation for alder piles was found to be 81 mm. It has to be noted that it is assumed that in order to enable the bacterial decay in anaerobic conditions, flow has to be present in the water, which is the case for the channels in Amsterdam (Meershoek, 2020). As also the quay wall floor and scour protection screen are made of wood, these are affected by bacterial decay as well, resulting in leakages in these structure elements.

2.3. Loads acting on quay walls

In this section, the major loads inner-city quay walls are subjected to, are discussed. These include loads for which the quay walls were originally designed for, and types of loading which were not taken into account at the time of design and construction but to which quay walls are subjected to. All forces discussed in this section have the ability to result in quay wall displacement, although some to a higher degree than others.

2.3.1. Forces due to retaining of soil and head difference

One of the main functions of any quay wall is the retainment of soil. In both previously discussed designs, the horizontal loading is assumed to be the most relevant parameter, as it not only exerts a force on the structure, but also a turning moment. However, it follows from Rankine's theory that horizontal earth pressure is a function of vertical earth pressure, by means of an active or a passive constant (Verruijt, 2001). As the quay walls were designed with the function of soil retainment in mind, they are well equipped to handle the pressures due to the own weight of the soil. Additionally to an inequality in soil height between both sides of the cross-section of a quay wall, it is possible that a head difference can be observed as well, resulting in a net horizontal pressure acting on the quay wall. The reason for this is the result of a higher or lower groundwater table than the water level in the channel. Note that in order for this type of loading to be relevant, a watertight seal has to be in place between both sides of the quay wall, either natural or artificial.

2.3.2. Berthing- & direct impact forces

As previously stated, another function of the quay walls is to act as a mooring facility. Originally meant the (un)loading of cargo, but nowadays the main goods being transport from shore to ship and vice versa are passengers. When ships are moored, berthing forces are exerted on the mooring facilities along the quay, due to rocking which is initiated by wind and currents (de Gijt, 2004). As these forces act rather locally, these forces can be schematized as point loads. As ships moor to a quay wall, it is not unlikely that they hit the structure due to wind or currents. Due to the nature of the structure, these forces are taken into account in quay wall design. However, after a number of impacts, the structure can start to deteriorate.

2.3.3. Vertical static- and dynamic loading

As previously pointed out, the function of the quays in the inner city have shifted from providing space for cargo storage and (un)loading of ships to functioning as a road with parking spaces. Throughout the years, the weight of the vehicles using these roads has increased, especially the vehicles transporting the goods needed for restocking the growing number of shops in the inner city (Kruyswijk, 2020b). An even more extreme case of traffic loading is the placement of large mobile cranes on the quay, which are used during construction or renovation works of various buildings throughout the inner city (Gemeente Amsterdam, 2019). Another case of large vertical static loads are for example the (temporary) containers used for storage of demolition waste. The vertical static loads act on the quay walls via the soil body, resulting in vertical and horizontal loads and displacements of the quay wall. Additionally to the static traffic loads, the dynamic loads of traffic generate vibrations. In general, these vibrations can travel further through the soil medium in the vicinity of the quay walls than the dimensions of the area of influence of the static loading, proving in some cases even larger problems. Vibrations can also originate from pile-driving activities in the area.

2.3.4. Propeller wash

One of the major tourist attractions of Amsterdam is taking a channel cruise through its inner city. Next to that, during the warmer seasons, privately owned ships fill up the channels as well. In contrast to the row- and sailboats the which were used during construction of the channels of the inner city, propellers are used nowadays to navigate the channels. The maximum velocity ships are allowed to sail at is set at 6 km/h (Gemeente Amsterdam, n.d.b), thus limiting the propeller wash. However, the width of the channels is fairly limited, resulting in an abundance of tight corners in which propellers and (if available) bow thrusters come in close proximity of the quay wall. The turbulence caused by the propellers is able to displace the granular material directly in front of the quay walls, resulting in instability.

2.3.5. Trees along the quay

Throughout the years trees have been planted along a significant part of the quay's in the city of Amsterdam, located almost directly on top of the quay walls(Kruyswijk, 2020a). As these grew older and larger, their roots became intertwined with the quay walls, deforming and even fracturing the masonry of the gravity wall. Although the trees thus pose a significant problem for the structural integrity of the quay walls, there is a lot of sentiment for them among the population. Many have been labeled as monumental trees, preventing them from being automatically cut down when they are proven to pose a problem.

2.4. Surface-, water- & groundwater level

In this section, the surface- and water levels in the vicinity of the quay walls are discussed:

- **Surface level of quay walls**
  According to the Actueel Hoogtebestand Nederland (2019), the surface level in the vicinity of the quay walls ranges from about NAP +0.8 m up to NAP +1.3 m. The average surface level of the quay walls is situated at NAP +1 m. Additional information regarding the surface level is provided in section 2.5.

- **Water level in channels**
  The municipality of Amsterdam aims to keep the water level at NAP -0.40 m (Vaarwijzer Amsterdam, n.d.). The Main board of Waterschap Amstel, Gooi en Vecht (2008), the waterboard of which Amsterdam is a part of, has determined that a fluctuation of 5 cm is allowed, with the exception for periods with ice in the channels. One of the main pumping stations used for the regulation of the water level in the channels is the "Gemaal Zeebrugge", located on the East side of the city and capable of discharging 60 m^3/s Waterschap Amstel, Gooi en Vecht (n.d.).

- **Groundwater level**
  Similarly to large parts of the rest of The Netherlands, the groundwater level in the inner-city of Amsterdam is close to the surface. However, in the vicinity of the quay walls, the groundwater level is predominantly equal to the water level in the channels (Wimmers et al., 2020). However this level is subjected to larger fluctuations during periods of extreme rainfall or drought, more so than the water level in the channels as it is harder to regulate. High intensity precipitation can result in peaks of the groundwater level, although in the recent dry years (2015-2020) the groundwater level was lower than desirable (van Zoelen, 2020).

2.5. Soil profile of inner-city of Amsterdam

This section provides an overview of the soil profile of the inner-city of Amsterdam. The upper- and lower layers are discussed separately in sections 2.5.1 and 2.5.2 respectively. See figure 2.2 for an overview of the soil profile in the inner-city of Amsterdam (de Gans, 2011).

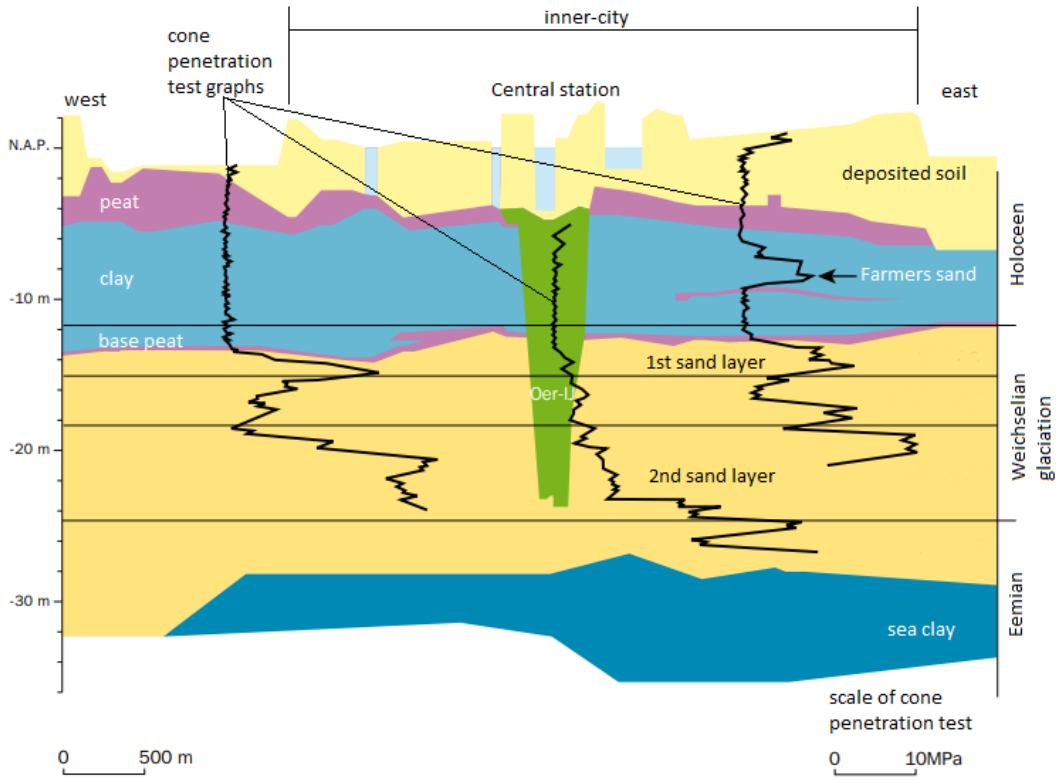

Figure 2.2: Overview of the soil profile in the inner-city of Amsterdam (de Gans, 2011).

2.5.1. Upper layers of soil profile

Originally, the soil medium in the region consisted of a clay layer, topped with a thinner peat layer which was situated at NAP +2 to NAP +3 m (de Gans, 2011). Around 1000 AD, the peat layer had already subsidenced to about the level of NAP. This was for a major part due to land reclamation projects in the surrounding lands of Amsterdam. Peat is characterized as being a very poor soil to use as a base for building, and as being a cause of public health concern. Therefore, it was determined that a sand layer had to be deposited on the existing peat layer. This process started some time during the middle ages and was continued until the late 1800's. Part of the reasoning behind this was that it is much easier to construct utility lines in sand than in peat. The effect of this measure is that nowadays the majority of the city surface is located at about NAP +1 m and that the peat layer is located at around NAP -1 to NAP -2 m. This same sand was used as backfill material for the quay walls. The application of a relatively thick body of sand on the peat layer was not without consequences. A major drawback is that the weight of sand is much higher than peat. As undisturbed peat largely consists of water, vertical loading of a peat layer drains this type of soil, resulting in large settlements of the peat layer. According to the Technische Adviescommissie voor de Waterkeringen (2001), peat has a rather low permeability in the order of 10^{-7} m/s. Sand has a minimal permeability of 10^{-5} m/s for fine grain sizes, but often one or more orders of magnitude higher for larger grains. Although the permeability of peat is rather low, it is expected that the rate of subsidence has declined, as the last sand deposits were carried out over 200 years ago. However nowadays, due to for example new construction projects and other high types of top loading, these settlements are still resulting in problems. One of the main causes for this is the inhomogeneity of both the soil and settlements over the full area of the inner-city, resulting in a positive feedback loop. Shallow founded infrastructure and buildings are directly affected by this phenomenon, a notable example being the utility line network. Contrary to sand, peat is considered a cohesive soil. Its cohesion is similar and in some instances even higher than clay, ranging from 1 up to 15 kN/m^3.

2.5.2. Lower layers of soil profile

Within the aforementioned clay layer, starting at NAP -8 m, a relatively thin sand layer is situated on which most of the buildings utilizing pile foundations constructed during the middle ages are founded on, called the "Farmers Sand" ("Boerenzand" in Dutch). At NAP -12 m, the first actual natural sand layer is situated, originating from the Pleistocene. This sand layer is the basis for most of the piled foundations in the inner city of Amsterdam, including the majority of the quay walls (de Gans, 2011). Relatively new structures, like metro-stations, are founded on deeper sand layers. An extreme case of this is the metro-station connected to the central train station, which is founded on an old river sand layer situated at NAP -60 m. As these layers are not directly linked to the construction and maintenance of quay walls, they are not further discussed in this report.

2.6. Observed displacements of quay walls

As said before, Amsterdam is not the only historic city of The Netherlands in which the state of the quay walls is diminishing. For example, in 2015 an inspection of the quay wall of the Bakenessergracht in Haarlem was carried out (Witteveen+Bos, 2015). The inner-city quay walls of Haarlem are similar to the once found in the inner-city quay walls of Amsterdam, both in design and time of placement. Thus, it is expected that deterioration of the quay walls as found in Haarlem can be seen in both inner-cities.

At first glance, the quay and the connected street show a lot of uneven settlement, indicating settlements of the subsoil. The quay wall bulges towards the channel, resulting in a horizontal deformation of 65 mm at the top of the wall. It was found that the masonry had deteriorated over the full length of the inspected quay wall. Cracks had formed over the full height of the wall and the mortar was washed away, resulting in missing and loose bricks no longer providing support. The piles of the front row are no longer connected to the capping beam, presumably due to wood-decay. Thus these no longer provide any support to the structure. The state of the piles of the other rows is relatively good. See figure 2.3 for both the situation above and below the waterline (Witteveen+Bos, 2015). Appendix C provides a full overview of the visual inspection of the quay wall.

At the water line, large quantities of the mortar has washed away. A number of bricks are no longer connected to the quay wall, other bricks are missing. The pores which were created by the washed away mortar have an average depth of 40 *mm*, with maxima up to 100 *mm*.

At various locations the piles of the front row are no longer connected to the capping beam above it. Wood-decay is deemed as the cause for this. This space ranges from 30 *mm* up to 150 *mm*.

Figure 2.3: Pictures of the inspection at both the water line and below the water line (Witteveen+Bos, 2015).

3

Analysis: Utility lines

In this chapter an analysis of the quay walls in the inner city is provided. This analysis is required in order to find an answer for sub-question 1b:

> **What types of utility lines are situated in the vicinity of the quay walls and how is leakage instigated in these?**

Thus, similarly to chapter 2, the provided information in this chapter is primarily focused on the inner-city utility lines of Amsterdam. Both the potable water pipes and the sewer systems of Amsterdam are regulated and maintained by Waternet, a governmental entity directed by both the municipality of Amsterdam and the Water Board "Amstel, Gooi en Vecht". A meeting with potable water pipe- and sewer system experts of Waternet, in combination with data provided by the Kadaster, resulted in this analysis of the current situation of utility lines in Amsterdam.

The chapter starts with a definition of the term "utility line" in section 3.1. The next sections discus the various aspects of both the potable water pipe network and the sewer system network, in sections 3.2 and 3.3 respectively. The chapter closes in section 3.4 with an explanation of the various factors contributing to utility line leakage.

3.1. Definition of utility line

The term "utility line" is generally used to describe a number of enclosed infrastructural works distributing goods from producer to a number of end users by means of pumping, gravity or conduction. Utility lines include but are not limited to water-, oil-, and gas pipes, electrical grids, telephone- and data cable networks, and sewer systems. This report limits the use of the term "utility line" to describe the utility lines in place in the vicinity of the inner-city quay walls of Amsterdam, potentially capable of causing failure of said quay walls. Therefore, the term in this report is limited to water pipes and sewer systems.

Erosion caused by leakages of gas pipes are placed outside of the scope of research, although gas leakages are known to potentially cause erosion. However, the impact of a utility line on its surrounding is proportional to the pressure at which the medium inside it is transported (Mastbergen, 1991). The high pressure network in the inner-city, transporting gas at about 8 bar, is fairly limited. The low pressure network is covers significantly more area than its high pressure counterpart, which transports gas at about 0.03 bar. Due to the low pressures, soil erosion due to gas line leakage is not part of the scope of this study. Alternatively, a gas explosion in the vicinity of a quay wall is expected to cause significant damage to said quay wall. However, in order to cause an explosion, a significant quantity of gas has to be trapped in an enclosed spaced and a spark has to be introduced causing the explosion. A case can be made for an explosion due to a gas leak leading to the filling of a basement in the vicinity of a quay wall, but this scenario is deemed outside of the scope of the study as well.

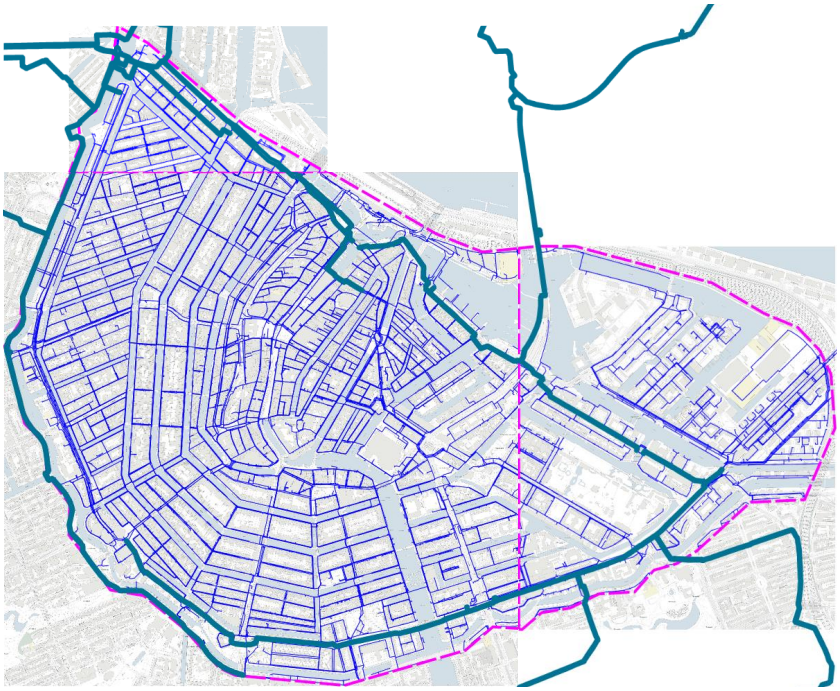

Figure 3.1: Overview of the potable water pipe network of the inner-city of Amsterdam.
The bold blue lines represent the main potable water pipe system.
The thinner blue lines represent the secondary potable water pipe system.

3.2. Potable water pipes

The first potable water pipe of The Netherlands completed construction in 1853, which provided the inner city of Amsterdam with clean dune filtered drinking water (Waternet, n.d.). Water was sold for one cent per per bucket. This water pipe was only replaced in 2017 (Het Parool, 2017), proving the possible relative long lifetime of water pipes.

Potable water pipes are placed using a cut and cover method. This means that for placement first a trench is dug to the required depth. Next the potable water pipe is placed in said trench. In the last step, the dug trench which now includes the potable water pipe is filled with the earlier removed soil up to surface level.
A distinction is made between the various potable water pipes. This distinction is made by their size: main pipes have a diameter of >450 mm, all others are considered secondary pipes. The main potable water pipes are primarily located on the outer perimeter of the inner city. See figure 3.1 for an overview of the potable water pipe network of the inner-city of Amsterdam

3.2.1. Materials

Through the years, a lot of different materials have been used in the distribution network of potable drinking water of the inner city of Amsterdam. In this section, the materials of water pipes mainly used in the vicinity of quay walls is discussed. A more complete overview of the materials of water pipes still in use and water pipes no longer in use but still in place is given in appendix B.

- **Grey cast iron (GCI)**
  The older water pipes of the city, like the oldest pipe discussed in the previous section, were constructed using GCI. The material was used up to the 1940's. According to Saint-Gobain Pipe Systems (2006), GCI is characterized by high compression strength, high resistance to abrasion and high fatigue resistance. The material is also known for its easy castability and workability. Pipes of this material found in the vicinity of the channels have diameters ranging from 76 mm up to 760 mm, although the majority are found in the range 100 mm up to 760 mm.

- **Nodular cast iron (NCI)**
  Nowadays, GCI pipes are no longer placed in Amsterdam. Instead, another type of cast iron is used: NCI. This material is obtained by adding magnesium to GCI, resulting in a different structure of the already present carbon. Compared to GCI, NCI has a higher yield-, compression- and tensile strength Saint-Gobain Pipe Systems (2006). Next to that its resistance to shock, in the form of for example a water hammer, is notably higher as well. Due to the more complex manufacturing process, it is more costly than its grey counterpart. The life expectancy of NCI pipes is at least 50 years. Pipes of this material found in the vicinity of the channels have diameters ranging from 80 mm up to 800 mm, although the majority are found in the range 100 mm to 800 mm.

- **Steel**
  Steel pipes are known for their high yield- and ultimate strength, ductile behaviour and high shock resistance (AWWA, 2004). Mayor drawbacks of these pipes are their high density and susceptibility to corrosion if the protective layer is compromised. Next to that, the life expectancy of these pipes are between 20 and 50 years Mr. Rooter Plumbing (2019). Pipes of this material found in the vicinity of the channels have diameters ranging from 100 mm up to 800 mm.

3.2.2. Placement depth & foundation

The minimum coverage of the potable water pipes of Amsterdam is set at 800 mm. In general, this is the placement depth of all potable water pipes. The value of the minimum cover depth is predominantly determined to be a safeguard against freezing of the water inside the pipe. It has been determined that, at this depth, traffic loads are sufficiently damped by the soil body surrounding the pipe.

Non of the water pipes in the inner city of Amsterdam are founded on piles. Instead, the water pipes are directly placed in the soil body.

3.2.3. Operating pressure

The pressure at which water is transported in the potable water pipes ranges between 25 mwc and 30 mwc. Pipe line pressure is provided relative to a pressure of absolute zero and not relative to atmospheric pressure. The definition of the unit mwc is "meters water column", i.e. the height up to which the water in a pipe would rise if a column was placed perpendicular to the flow direction.1 mwc is equal to 0.1 bar, which in term is equal to 10 kPa. Thus, the operating pressure is equal to 2.5 and up to 3 bar.

3.2.4. Joints

A water pipe is not a continuous system, but is constructed by connecting pipe segments each generally 6 m long (Saint-Gobain Pipe Systems, 2006). In general in Amsterdam, these segments of water pipe are linked to eachother using flexible, non-tensile resistant connections, each allowing an angular deflection of up to 1.5^o. Non-tensile resistant water pipes are preferred in the construction, the exception being water pipes laid in curves and at locations branching of water pipes occurs. Figure 3.2 provides an example of both a tensile resistant- and non-tensile resistant connection for potable water pipes, respectively in the form of a flenge connection and a standard socket-spigot connection ("mof-spie" connection in Dutch) (infoDWI, 2017).

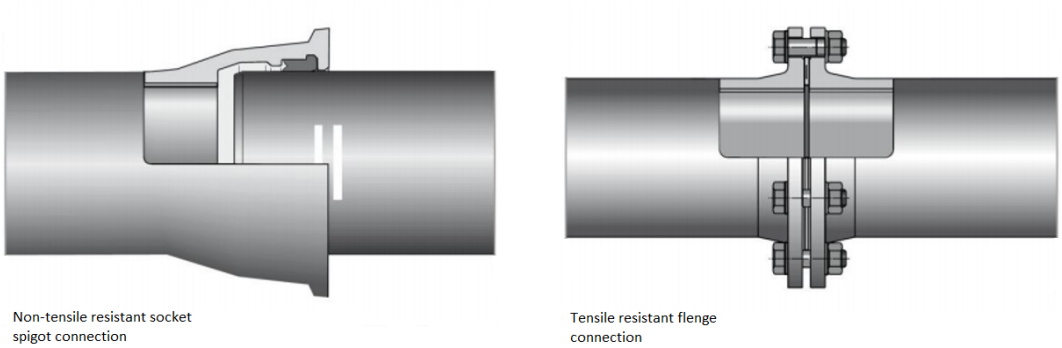

Figure 3.2: Examples of both tensile- and non-tensile resistant pipe segment connections (infoDWI, 2017).

3.2.5. Emergency shutdown systems

In Amsterdam, only one water pipe is outfitted with a system capable of closure in case of a breach. This pipe is located in the "IJtunnel" and is the main supply of potable water for the Northern part of the city. The system consists of a number sensors capable of detecting water on the floor of the tunnel tube the pipe is placed in. When water is detected on the floor, the system automatically closes the valves.

3.3. Sewer System

The sewer system currently in use of the inner city of Amsterdam is one of the youngest of The Netherlands, as it was constructed in the 1970's and 1980's (Riolering en Waterbeheersing, 1985). Prior to the currently in place sewer system, waste water and precipitation was directly discharged to the channels of the inner city. Most buildings were connected to the channels by an inclined masonry pipe, mouthing in the quay wall ("gewelven" in Dutch). Due to the lack of regulations, there is no and has never been a clear picture were these masonry pipes are situated or the status of their constructional integrity. Figure 3.3 provides an example of one of these masonry pipes being excavated, which mouthed in the "Rokin" channel (Bakker, n.d.).

The currently in place sewer system is in essence a mixed system, capable of discharging to the channels during extreme rainfall. However, rain falling on streets and buildings situated next to the channels is directly discharged to the channels, relieving the sewer system.

The sewer system of the inner city is split up into two subsystems: the upper system and the transport system. The upper system consists of finely meshed network of building-sewer connections, situated as the name suggests in the upper parts of the ground. The transport system collects the discharge of the various branches of the upper system and is meant for the transport to sewage collection sites located outside of the system. These collection sites in their turn transport their discharge towards the sewage treatment plant, either under pressure or not. There is a correlation between the placement depth and the diameter of the sewer pipes. The diameters range from a diameter of 200 mm at about NAP -1 m, up to diameters of 3 m at NAP -4.5 m, respectively corresponding to the upper system and the transport system. The specific characteristics of the two aforementioned subsystems are discussed in the sections below.

Figure 3.3: Masonry pipe named the "Oude Spoye" being excavated, which mouthed in the "Rokin" channel (Bakker, n.d.).

3.3.1. Materials

Originally, the sewers of the inner city were constructed using primarily two materials: concrete and GCI. Nowadays, concrete is still being used. For the upper system it is not known if this concrete it reinforced. However, the lower system utilizes reinforced concrete everywhere. GCI is no longer used for the construction of sewer systems. Instead, PVC is used. The material properties of GCI are discussed in section 3.2.1. For PVC the material properties are discussed in appendix B.

(Reinforced) concrete is known for its high strength, -stiffness and durability. When adequately constructed, the life time of these sewers can reach up to 100 years (CPAA, n.d.). The diameters of concrete pipes vary greatly, from 300 mm for the upper system pipes and up to 4 m for large main transport system pipes. In the vicinity of quay walls, generally diameters are found ranging from 300 mm up to 1000 mm.

3.3.2. Placement depth, slope & foundation

The minimum coverage of the sewer system is set at 800 mm, for the same reasons as given for the potable water distribution network given in section 3.2.2. However, in order to instigate transport via gravity, the sewer pipes are placed under a slope, resulting in significantly deeper placed sewers. Due to the relatively low discharge in the upper sewer system, slopes ranging from 1:300 up to 1:500 are required. As the transport sewer system has a higher discharge, less steep slopes ranging from 1:500 up to 1:750 are sufficient. Sewer systems are constructed using the aforementioned cut and cover method, similarly to the construction of potable water pipes

Similarly to the potable water distribution network, the upper sewer system is not founded on piles and instead placed directly in the soil body. However, a significant part of the transport system is founded on piles. The distance between the piles of sewers on these foundations in the inner-city of is generally about 4 m (Stadsarchief Amsterdam, 1955)

3.3.3. Joints

Similarly to the potable water pipes, sewers are constructed using pipe segments. The joints connecting the sewer pipe segments of the upper system are flexible and allow a angular deflection of 1.5^o, again similarly to the connections of the potable water network. The determination if tensile construction is similar to the water pipe system as well: in general not preferred, except for curves and at branching locations. The non-tensile connections of the sewer systems are similar to the socket-spigot connection represented in figure 3.2.

Contrary to the upper system, the transport system is founded on piles. Therefore the connections of the latter system are rigid.

3.4. Factors contributing to utility line leakage

In this section, the main factors contributing to utility line leakage are discussed, focusing on deterioration due to usage in section 3.4.1, deterioration due to the soil environment 3.4.2 and the failure mechanisms of both utility lines itself in section 3.4.3. Finally, the deterioration of joints is discussed in section 3.4.4.

3.4.1. Corrosion and deterioration due to usage

In this section the effects of long term usage on both potable water- and sewer pipes are discussed. Note that the focus of this section is purely on the deterioration effects of the pipes utilization as a transport system of precipitation, potable-, and wastewater. External effects are discussed in the further sections of this chapter. Although corrosion and deterioration are generally not the main cause of leakage, these long term effects are in general the kick-starter and catalyst for other, generally more severe, failure mechanisms. Each material predominantly used in the inner-city of Amsterdam for both potable water pipes and sewer systems, as discussed in sections 3.2.1 and 3.3.1 respectively, is discussed in the sections below.

- **NCI and GCI**
  For both NCI and GCI, Makar and McDonald (2000) state that two types of corrosion can be observed. The first type is called simple erosion, which is similar to corrosion of untreated steel. By itself, additionally to being an aforementioned kick-start of other failure mechanisms, this form of corrosion can cause minor trough holes in the pipes, resulting in minor leakages. The second type of corrosion is a process called graphitisation. During this process, the iron is removed from the affected pipes area, but leaves behind the graphite which is present in the material. For short periods of time, this material can even be strong enough to resist the internal and external pressures exerted on the pipe. Note that graphitisation is less likely to occur in NCI.

- **Steel**
  Without treatment, steel pipes are very susceptible to corrosion. In order to counter corrosion, various other materials are added to the steel in the form of f.e. chromium and copper, or protective layers are applied to the surface, f.e. paint (AWWA, 2004).

- **(Reinforced) concrete**
  According to Millar (2006), corrosion of reinforcement steel is countered by the alkalinity of concrete, as in this environment a very thin layer of of oxide forms on the surface of the steel. A reduction of the concrete's pH value can result in deterioration of said thin layer of oxide, which in term results in corrosion of the reinforcement steel. This reduction of the pH value is caused by a process called carbonation, which is triggered by the reaction between cement paste and carbon dioxide present in either the surrounding soil or the pipe's transported material. It has to be noted that this process can not occur in sound reinforced concrete pipes, even when cracks deemed allowable for the type of concrete are situated over the circumference, as controlled cracking is required for reinforced concrete structures to carry tensile loads via the reinforcement steel. However, in the case of larger cracks, this process can pose an issue as the carbonation can reach further into the concrete. Larger cracks can form f.e. due to extreme loading or placement errors. Additionally, sulfide corrosion is relevant as well, which is caused by the sulfate present in the transported wastewater (Zamanian, 2016). This sulfate is converted to hydrogen sulfide, which condensates on the surrounding concrete. In term, this component reacts with oxygen to form sulfuric acid. This acidic environment partly affects the reinforcement steel in an even more sever manor as the previously explained carbonation process, as the hydrogen sulfide results in even lower pH values. Additionally, due to said low pH value, this process can result in corrosion of the concrete itself.

3.4.2. Soil affecting deterioration of utility lines

In this section, various forms in which soil can enable failure of utility lines are discussed. Note that only aspects deemed relevant for the study are mentioned. A significant part of the literature focuses on pipeline deformation resulting from soil displacement due to earthquakes, but these displacement are generally significantly higher than encountered in the study towards quay walls.

- **Corrosion due to soil environment**
  A three year long study of the potable water pipe network of the city of Toronto concluded that the type of soil in which pipes are placed in can have a significant influence on the state of corrosion and deterioration of the outer layers of said pipes (Seica et al., 2002). In this research, it is stated that the relative alkaline soil due to the present sea salts can generate such a negative environment, particularly for steel, NCI, and GCI pipes. As the deposited upper sand layer of Amsterdam originates from beaches along the North Sea, it can be reasonably assumed that these salts are present in there as well.

- **Influence of saturation degree**
  Research has also been conducted in order to find out the influence of soil saturation to the soil pressures acting on pipeline during lateral soil displacement (Robert and Soga, 2013). This research was carried out with soil conditions similar to the deposited sand in which the inner-city utility lines of Amsterdam are embedded. Robert and Soga concluded that in these conditions, no influence was found relative to soil saturation.

3.4.3. Failure mechanisms of utility lines

In this section, the various failure mechanisms of utility lines are discussed. Although corrosion is not mentioned in this section, all of the failure mechanisms mentioned here are much less likely to occur without it.

- **Failure mechanisms of steel, NCI, and GCI pipes**
  Makar and McDonald (2000) define a number of failure modes for GCI and NCI. It is assumed that steel potable water pipes have similar failure modes. Smaller (<380 mm) diameter pipes have smaller cross-sectional moments of inertia, making them more susceptible to failure regarding longitudinal bending, in the form of f.e. circumferential cracking. Larger (>500 mm) diameter pipes are more likely to fail due to shearing and longitudinal cracking, which is generally the result of crushing- and compressive forces acting on the pipe. For pipes with diameters between the given values, both kind of failure mechanisms can occur. The bell shaped socket of the aforementioned non-tensile resistant socket-spigot connection (see section 3.2.4) is also relatively susceptible to failure. In smaller diameter pipes the socket is more likely to fail due to splitting, resulting from differences of the thermal co-efficient of expansion between the material used for generating a watertight seal and the material itself (originally lead, but later a sulphur based compound called leadite, and rubber). As the minimal prescribed coverage of utility lines in Amsterdam is explicitly determined to counter effects of freezing, it is not likely that this failure mechanism plays a large role. For larger diameter pipes the socket is more likely to fail due to shearing, possibly due to larger compressive forces acting on it originating from the spigot of the adjacent pipe. See figure 3.4 for an overview of the aforementioned failure modes of potable water pipes made of steel, NCI and GCI (Makar and McDonald, 2000). Note that these failures generally do not occur in the same pipe. The leaking potable water pipe resulting in the dike failure along the Julianakanaal at Stein, Limburg, was partly made of steel (see appendix D).

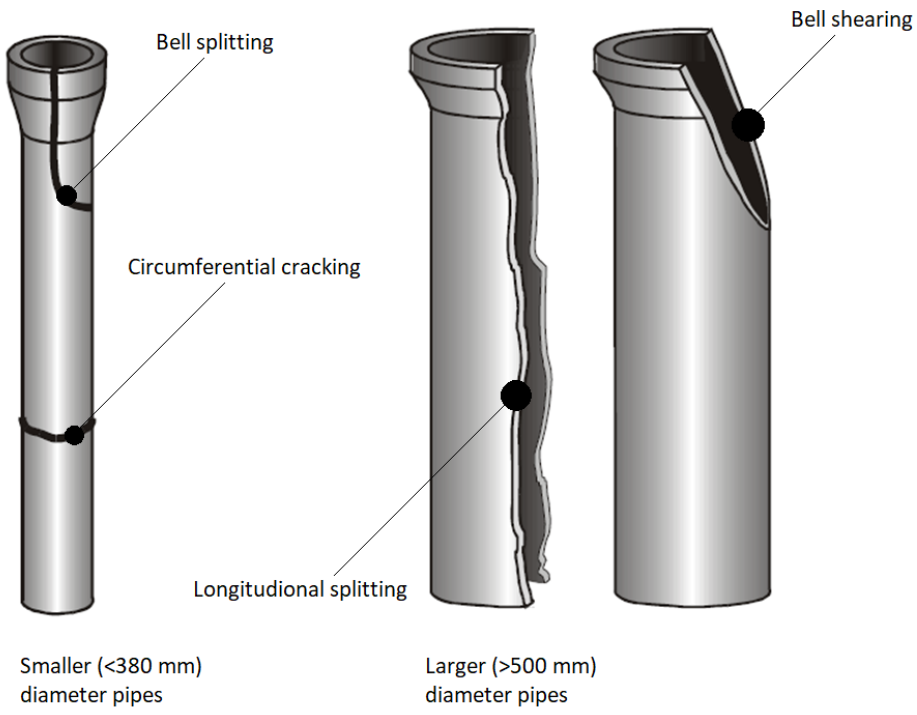

Figure 3.4: Overview of the failure modes of potable water pipes made of steel, NCI, and GCI (extreme cases) (Makar and McDonald, 2000).

- **Failure mechanisms of (reinforced) concrete**
  Zamanian (2016) states that buried concrete pipes are susceptible to two kinds of failure mechanism, namely ring failure and beam failure. The former failure mechanism can be attributed to compressive forces acting on the axial cross-section of the pipe. The latter can be attributed to bending moments acting over the length of the pipe. See figure 3.5 for a schematization of both failure modes (Zamanian, 2016) (extreme cases for both failure mechanisms).

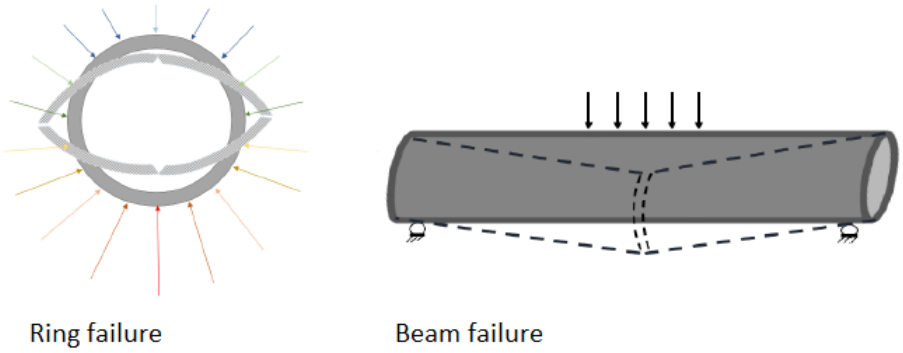

Figure 3.5: Schematization of the failure modes of concrete pipes (extreme cases) (Zamanian, 2016).

According to Millar (2006), in order for the cracks to be of a significant problem for the strength of the steel in sewer pipes made of reinforced concrete, they have to be deeper than 25% of the depth of the coverage. only the resulting circumferential cracks are located closely to eachother, there is a reasonable chance of failure. Generally, such cracks only form due to handling errors during placement.

3.4.4. Deterioration of joints

As said before, generally rubber is used in the socket-spigot joints of utility lines to create a water tight seal between segments. According to standard NEN 3650 NEN (2020a), seals utilizing natural rubber are susceptible to bacterial decay resulting in degradation of said seal. Additionally, it is stated by Renner-Hahn et al. (2014) that deformations of utility lines result in an increase in deterioration and following leakages of rubber seals.

3.5. Overview of utility lines further used in study

In table 3.1, an overview is provided of the parameters for various utility lines as discussed in this chapter. Note that only an overview is provided of the types of utility lines further used in this study.

Table 3.1: Overview of utility line parameters as used in study.

Material	**Type**	**Transport system**	**Placement period**	**Min. outer diameter** $D_o\,[mm]$	**Max. outer diameter** $D_o\,[mm]$	**Coverage** $H\,[mm]$
GCI	Potable water pipes	Pressurized	1850's-1940's	100	800	800
NCI	Potable water pipes	Pressurized	1940's-current	100	800	800
Steel	Potable water pipes	Pressurized	1940's-current	100	800	800
Concrete	Sewer Systems	Gravity	1970's-current	300	1000	800 (minimum value)

4

Overview of the quay wall failure mechanisms caused by utility line leakage

In this chapter, an overview is provided for the possible quay wall failure mechanisms caused by utility line leakage, starting with a flow chart relating these phenomenons to eachother in figure 4.1. Schematizations of these utility line-quay wall interactions are provided in sections 4.1, 4.2, 4.3, and 4.4.

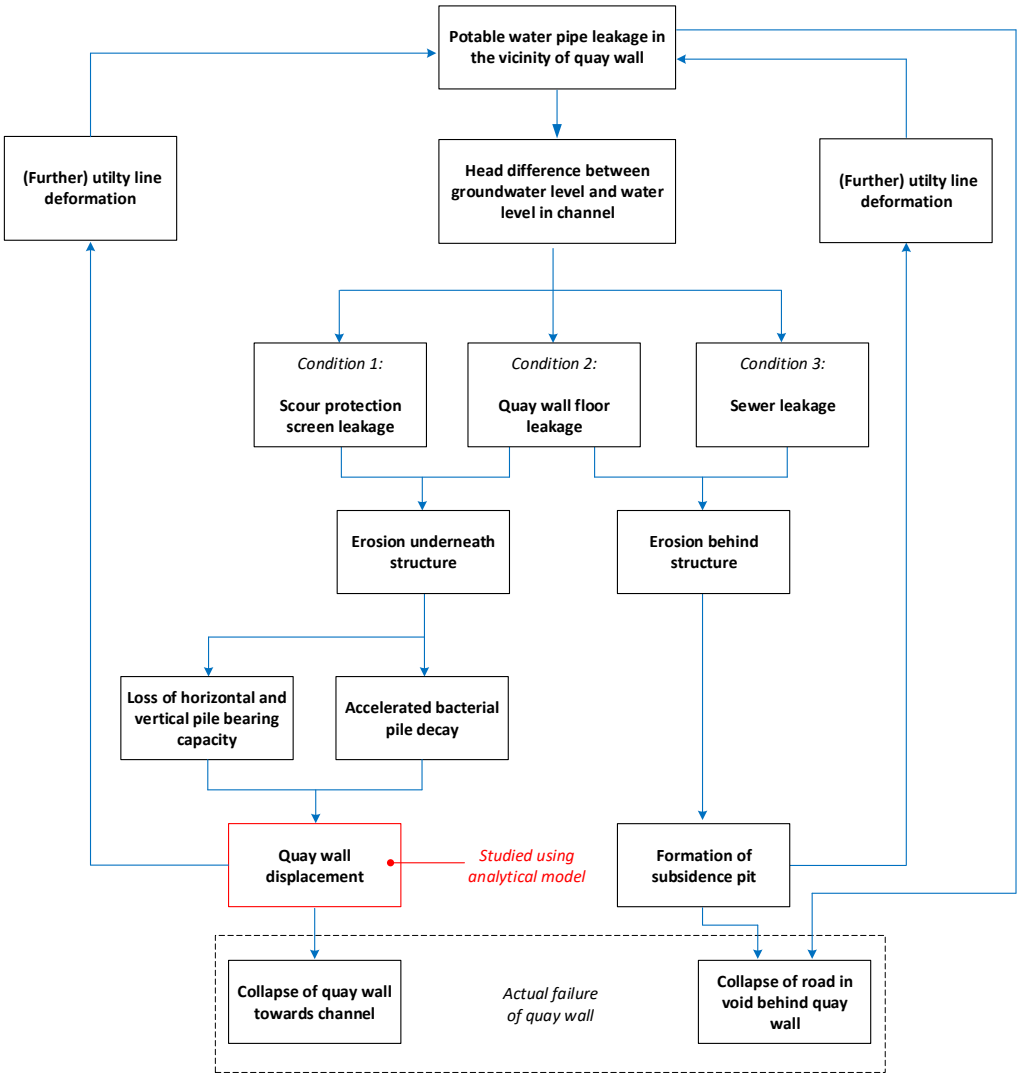

Figure 4.1: Flow chart relating utility line leakage to quay wall failure.

The provided overview shows the possible interactions between utility line's and quay walls, and how leakages of the former are related to failure of the latter. As the overview shows possibilities, it by no means guarantees that a step in the overview is certainly proceeded by the next step. This is highly dependent on the status of both the quay wall and the utility lines in its vicinity.

Note that the starting point of this overview is variable, and is not limited to start at "potable water pipe leakage in the vicinity of quay wall". For example, the initial quay wall displacement can be caused by any of the loads acting on quay walls as discussed in section 2.3, in term instigating utility line deformation. Additionally, utility line leakage is not the sole instigator of the rise in groundwater level, but can be caused by f.e. intense precipitation. In the following sections, the mechanisms through which quay wall failure is related to quay wall failure are schematized. In term, these are discussed in more depth in chapters 5 and 6. The effect of quay wall displacement on utility line deformation and leakage is quantitatively discussed in chapter 7.

4.1. Head difference between groundwater level and water level in channel

As follows from the overview in figure 4.1, potable water pipe leakage can result in rising of the groundwater level in the soil body behind the quay wall. This results in a head difference (ΔH) as represented in figure 4.2. Note that as said before, the head difference is not limited to originate from potable water pipe leakages.

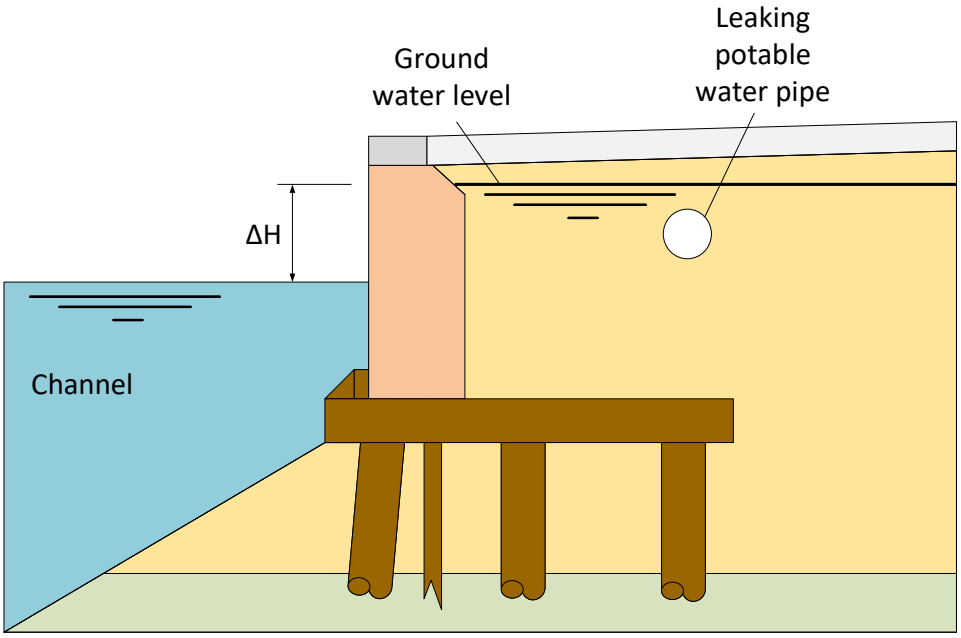

Figure 4.2: Head difference between groundwater level and water level in channel.

4.2. Internal erosion in vicinity of quay wall

The head difference as represented in figure 4.2 has the potential to result in internal erosion, if water and soil are able to flow from the soil body towards the channel. This is explained in more detail in sections 5.2 and 6.1.2. The possible methods in which this flow is enabled are: scour protection screen leakage, quay wall floor leakage, and sewer leakage. These are portrayed in sections 4.2.1, 4.2.2, and 4.2.3 respectively. Note that in these sections, the leakages are represented using cross-sectional 2D views at the location of the leakage. However, the system might still be sound and not contain any leakage over the rest of the length of the quay wall.

4.2.1. Internal erosion due to scour protection screen leakage

Figure 4.3 provides a schematization of internal erosion due to scour protection screen leakage potentially resulting in quay wall displacement and further utility line deformation, as portrayed in the overview of figure 4.1. Erosion underneath the quay wall structure is discussed in section 6.1.3, and its effects are discussed in section 6.1.4.

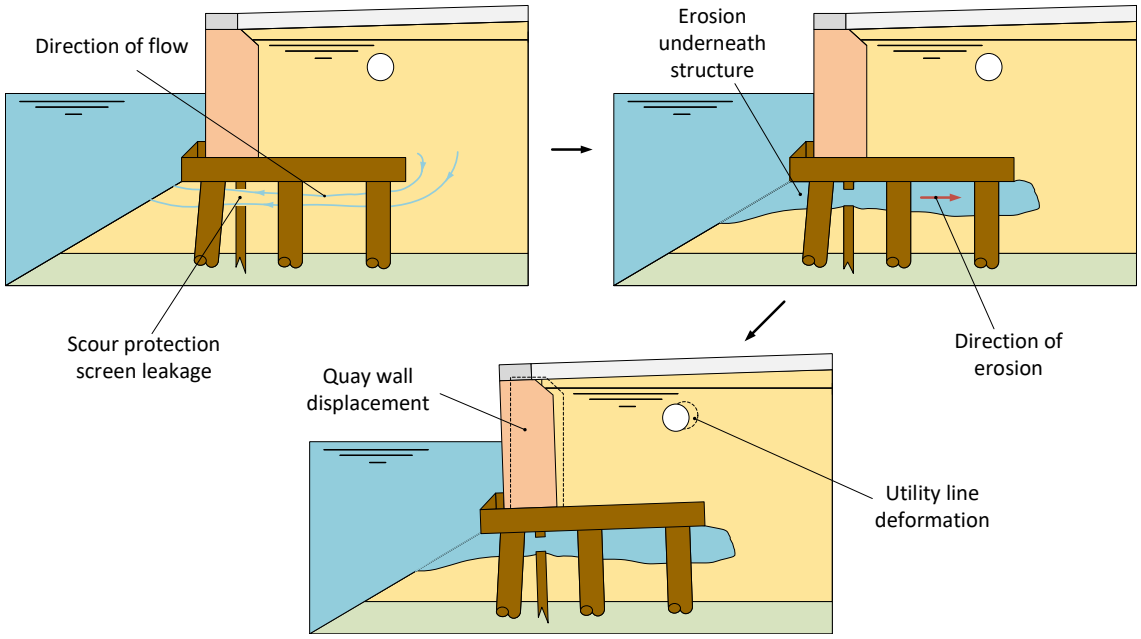

Figure 4.3: Possible effects of internal erosion due to scour protection screen leakage in combination with a head difference (exaggerated portrayal).

4.2.2. Internal erosion due to quay wall floor leakage

Figure 4.3 provides a schematization of internal erosion due to scour protection screen leakage potentially resulting in quay wall displacement, or in the formation of a subsidence pit. Both have the potential to result in further utility line deformation, as portrayed in the overview of figure 4.1. Again, erosion underneath the quay wall structure is discussed in section 6.1.3, and its effects are discussed in section 6.1.4. Erosion behind the structure is discussed in section 6.1.5, and its effects are discussed in section 6.1.5.

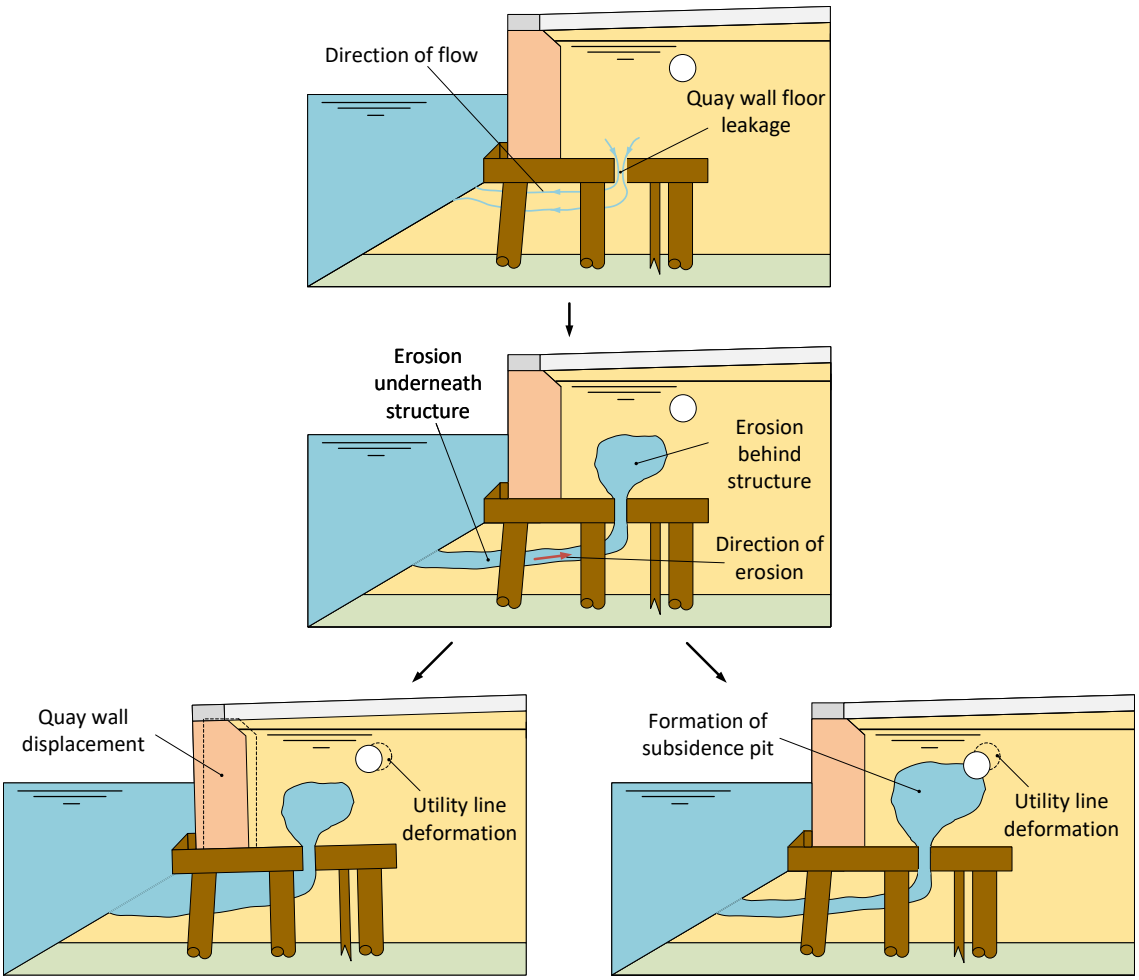

Figure 4.4: Possible effects of internal erosion due to quay wall floor leakage in combination with a head difference (exaggerated portrayal).

4.2.3. Internal erosion due to sewer leakage

Figure 4.5 provides a schematization of internal erosion due to sewer leakage in the vicinity of a quay wall potentially potentially resulting in the formation of a subsidence pit. Again, erosion behind the structure is discussed in section 6.1.5, and its effects are discussed in section 6.1.5. Note that sewer leakage can also be instigated due to quay wall displacement or the formation of a subsidence pit resulting in utility line deformation, resulting from either leakage of the scour protection screen or the quay wall floor.

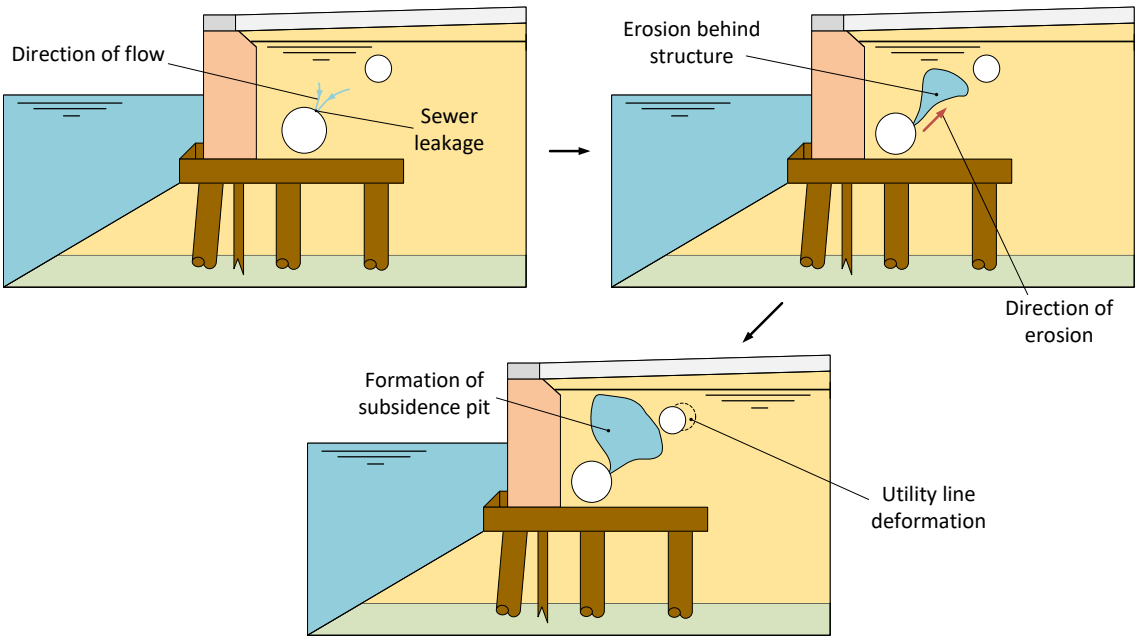

Figure 4.5: Possible effects of internal erosion due to sewer leakage in combination with a head difference (exaggerated portrayal).

4.3. Gaping leak resulting in erosion crater

A gaping leak is defined as a major potable water pipe burst, which is capable to form an erosion crater due to the force generated by the outflow out of the pipe leakage. Note that gaping leaks can result from minor leaks due to (further) utility line deformation and deterioration. This process is explained in more detail in section 5.3. The erosion crater can result in internal erosion due to leakages in the structure (i.e. scour protection screen-, quay wall floor- and sewer leakage), but can result in the collapse of the road in its formed subsidence pit as well. This is explained in more detail in section 6.2. See figure 4.6 for an overview of a gaping leak in the vicinity of a quay wall.

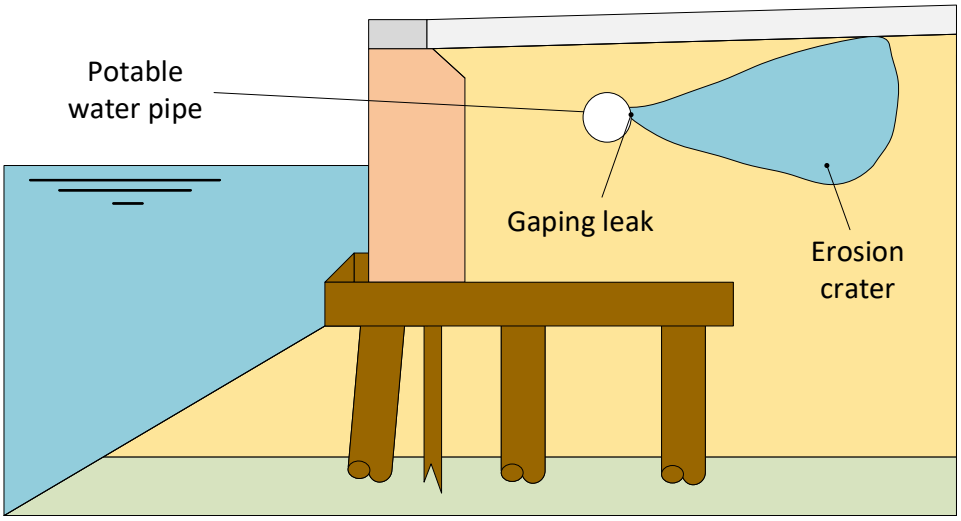

Figure 4.6: Gaping leak in the vicinity of a quay wall.

4.4. Actual failure of quay wall

Actual failure of quay wall due to the internal erosion in its vicinity as presented in section 4.2 can either be in the form of quay wall collapse towards the channel, or in the form of road collapse into the void behind the quay wall generated by the formation of a subsidence pit or an erosion crater due to a gaping leak. These failures of quay walls are represented in figures 4.7a and 4.7b respectively. The failure mechanisms of quay walls are discussed in sections 6.1.4 and 6.1.5 respectively.

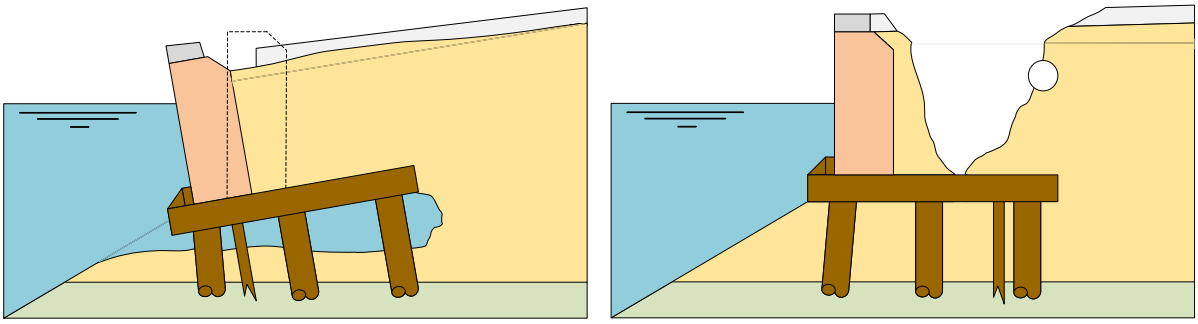

(a) Collapse of quay wall towards channel.

(b) Collapse of road in subsidence pit

Figure 4.7: Actual failure of quay wall due to utility line leakage.

5

Effects of utility line leakage on soil medium

This chapter is meant to provide a basis for answering sub-question 2, which is formulated as follows:

How is leakage of a utility line linked to failure of a quay wall?

In order to get an overview of the effects of utility line leakage on a quay wall, this chapter discusses the various ways such leakages affects the soil body surrounding the utility line. This information is in term used to determine said effects in the vicinity of inner-city quay walls, discussed in chapter 6.

The chapter is split up in three sections. Section 5.1 gives a definition of the various types of utility line leakages. Next, the process of internal erosion due to groundwater flow is discussed in section 5.2. The chapter closes with a discussion regarding erosion craters, in section 5.3.

5.1. Types of utility line leakages

In this section the possible types of leakages of utility lines are discusses, both for potable water pipes as well as sewer systems.

5.1.1. Potable water pipe leakages

It is natural that variations in the characteristics of a utility line (for example its diameter, operational pressure, and material) have a major influence on the kind of occurring leakage. In order to differentiate between these leakages, the framework formulated by Schweckendiek (2018) is utilized in this study. This framework was specifically formulated for the safety of primary dikes regarding utility lines under pressure in their vicinity, but is deemed to applicable for the situation with quay walls as well. The framework defines two kinds of utility line leakages, which for this study thus refer to the potable water pipes:

- **Minor leaks**
  Minor leaks are defined as minor leaks and limited discharges, resulting in minor losses of pressure in the water pipe. The result of these kinds of leaks can result in raised water pressures and saturation in the vicinity of a hydraulic structure like a dike or a quay wall, under the right conditions. The previously mentioned framework by Schweckendiek (2018) does state that full saturation of the soil body surrounding a minor leak is a conservative assumption. However, there are known cases in which this full saturation did occur. One of these was the failure of a dike along the "Julianakanaal" at "Stein, Limburg", during which settlements of said dike resulted in leakage of an older, deteriorated potable water pipe. See appendix D for more details.
- **Gaping leaks**
  Gaping leaks are defined as major water pipe burst, resulting large erosion craters. In case of a gaping leak, there is a possibility that the pipe is completely sheared over its full circumference. In this case, the downstream part of the pipe might start to function as a drain, capable of transporting both water and soil. However, as can be seen in figure 3.1, the potable water pipe network is set up for the main part as a parallel network. Therefore, it is not inherent to this situation of a sheared of pipe that its downstream part acts as a drain, as this pipe is connected to a larger system of pipes which are all under pressure. Gaping leaks can result in erosion craters, as discussed in section 5.3. Note that minor leaks can grow into the gaping leaks, due to (further) utility line deformation and deterioration.

5.1.2. Sewer system leakages

As only sewer systems relying on gravity transport are within the scope of this study, gaping leaks are not able to be formed by this kind of utility line. In case of a sewer leakage, waste water would be able to flow from the sewer. Although this might pose an environmental issue, it is not expected that this results in erosion of the surrounding soil body, due to the relatively low flow velocities. However, in this case the sewer can act as a drain, capable of both transporting water and soil.

Therefore, it is expected that sewer leakage by itself does not cause problems, as an external source of water is required in order to let the sewer function as a drain. This water might originate as groundwater naturally present in the soil medium, or as water resulting from a leaking potable water pipe.

5.2. Internal erosion

According to Verruijt (2001), internal erosion is the collective name of processes causing instability to a soil medium due to seepage forces resulting from ground water flow. The studies to internal erosion processes are mainly centered around water retaining structures, like dams and dikes. However, these processes can be linked to utility lines and quay walls as well, as also in their case the instigation of internal erosion is the flow of groundwater. Again, the origin of the groundwater is not limited to potable water pipe leakage. The time frame of internal erosion from instigation up to failure of the structure is in the same order of the velocity of groundwater flow, thus in the case of a sandy soil in the order of m/day. Of course, slower processes might also occur due to the presence of more cohesive soil layers. In case of gaping leaks, internal erosion is expected to occur as well under the same circumstances, although over a significantly shorter time.

According to Koelewijn and Bridle (2017), four phases can be identified in the process of internal erosion resulting in failure of the structure:

1. Initiation of internal erosion after reaching a critical water gradient, by one of the following mechanisms.
   (a) Concentrated leak erosion, see section 5.2.1
   (b) Contact erosion, see section E.1
   (c) Suffusion, see section E.2
   (d) Backward erosion, see section 5.2.2
   (e) Forward erosion, see section 5.2.3
   (f) Dissolution, see section E.3
2. Continuation, as the eroded particles are able to continue movement after the initiation of erosion.
3. Progression, during which erosion pipes are formed in the soil medium as cracks and openings are connected.
4. Breach, as the structure collapses due to the enlargement of the erosion pipes.

Another term used for internal erosion in the literature is "piping", referring to the erosion pipes which are generated in stage three of the process. In the following sections, the relevant internal erosion mechanisms for utility line leakage in the vicinity of quay walls are discussed. The mechanisms deemed less relevant in this situation are discussed in appendix E.

5.2.1. Concentrated leak erosion

The study by Förster et al. (2012) states that this process is initiated by the presence of a crack in the soil body, leading to a concentration of flow lines, resulting to erosion of soil particles and eventually widening of the crack. The presence of cracks indicates cohesive quantities of the soil, thus this process is not able to occur in a sand layer. However, the aforementioned study also notes that a crack between structure and soil can also instigate this particular process. The situation in which either a leaking sewer, the downstream part of a sheared of potable water pipe, or a through hole in a port of the quay wall's structure acts as a drain can probably also be described as a concentrated leak, as flow lines center around these imperfections in the same way as they would around a crack in the soil body.

5.2.2. Backward erosion

Backward erosion is the internal erosion mechanism occurring in a non-cohesive soil layer like sand, situated underneath either an impermeable cohesive layer or underneath a construction van Beek (2015), in which erosion pipes are generated from the downstream side towards the upstream side. This configuration is key, as a roof has to be in place to keep the formed pipe intact and keep it from collapsing in on itself. Additionally, there has to be an open and unfiltered exit in place at the downstream side of the potential pipe location. If a cohesive top layer is present at the downstream pipe location, hydraulic fracture of this layer (also known as heave) has to occur prior to the instigation of backward erosion, in order to meet the latter requirement. The flow lines then concentrate around this exit, in the same way as they do during the concentrated leak erosion mechanism of section 5.2.1. Next, the pipe grows backwards through the non-cohesive soil layer, up to the point that an open connection is formed from the downstream side to the upstream side, resulting in a positive feedback loop of higher flow velocities and thus an increase in erosion, eventually leading to failure of the structure. Figure 5.1 (van Beek, 2015) provides a step by step overview of the backward erosion process in case of a dike, starting from the indentation up to failure of the structure. The phases match those as defined by Koelewijn and Bridle (2017), given in the beginning of this section (with the addition of a fifth phase representing full failure of the dike).

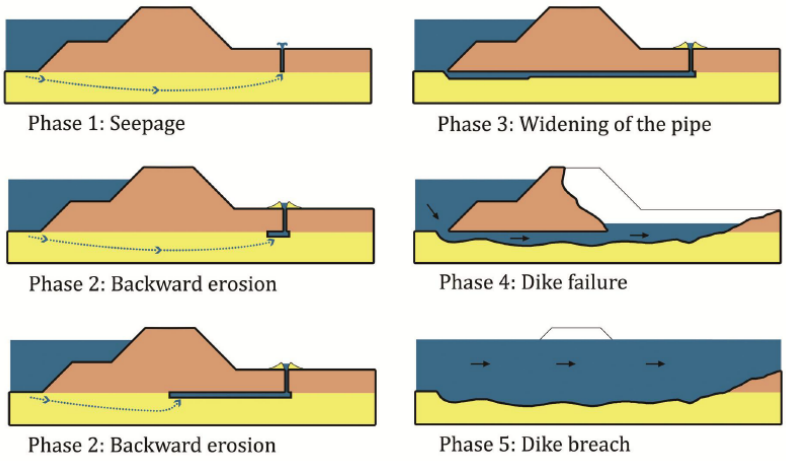

Figure 5.1: Phases of backward erosion (van Beek, 2015).

5.2.3. Forward erosion

During the forward erosion process, the pipe formation starts at the upstream side of the structure and progresses towards the downstream side. The process is enabled if a gap is pressent between a non-cohesive layer and its upper cover (van Beek, 2015). Thus, this process is unlikely to occur if a cohesive soil layer is located above the layer susceptible to internal erosion (f.e. a sand layer underneath a clay layer), as the particles of the cover layer interlock and exert pressure on the layer underneath. However, in case of a rigid structure (like the floor of a quay wall), a gap can be in place between said structure and the layer susceptible to internal erosion. Gaps of less than 1 mm are usually sufficient for instigation of the erosion process and generally lower water gradients are required relative to the instigation of the backward erosion process.

5.3. Erosion craters due to gaping leaks

The Netherlands is known for its hydraulic structures and the land protected by these being densely populated. Due to this combination, it is inevitable that utility lines are found in the vicinity of said structures, the inner-city quay walls of this study being one of many examples. Thus, utility lines are also found in the vicinity of the country's primary flood defenses, in particular the dikes along the North Sea, the IJsselmeer, and the various large rivers. There is a significant possibility that an erosion crater is generate in case of pressurized utility line leakage, which result from a gaping leak as specified in section 5.1.1. As these erosion craters compromise the structural safety, studies have been carried out towards these pits, of which the study regarding potable water pipes is discussed in appendix F.

Due to these studies, standard NEN 3651 was formulated for the placement and maintenance of utility lines in the vicinity of important infrastructure, including primary flood defenses. See section F.3 of appendix F for the relevant parts of this standard regarding the study towards the relation between utility lines and inner-city quay walls.

Using equations for the determination of the width of erosion craters as provided in appendix F, the graphs of figure 5.3 were obtained. In figure 5.3a, the width of the erosion crater is plotted against the diameter of the gaping leak. Note that according to the MEN standard the size of the hole can not be larger than the size of the internal diameter of a potable water pipe (D_i). From the graph it follows that the largest width of erosion craters are found for the largest diameters of water pipes. In figure 5.3b, the length of the erosion crater over the axial direction of the potable water pipe is plotted against the hole size diameter. It has to be noted that for all sizes, the largest erosion crater dimension are found if the size of the internal potable water pipe diameter is equal to the hole size, i.e. a fully sheared of pipe. This also follows from equation F.1, as the width of an erosion crater (R_w) only depends on the diameter of hole in the pipe (d_h). The height of the erosion crater (D_c) only depends on the coverage and outer diameter (D_o) of the potable water pipe. The height of the erosion crater is plotted against the outer diameter in figure 5.3c.See figure 5.2 for an overview of the mentioned parameters.

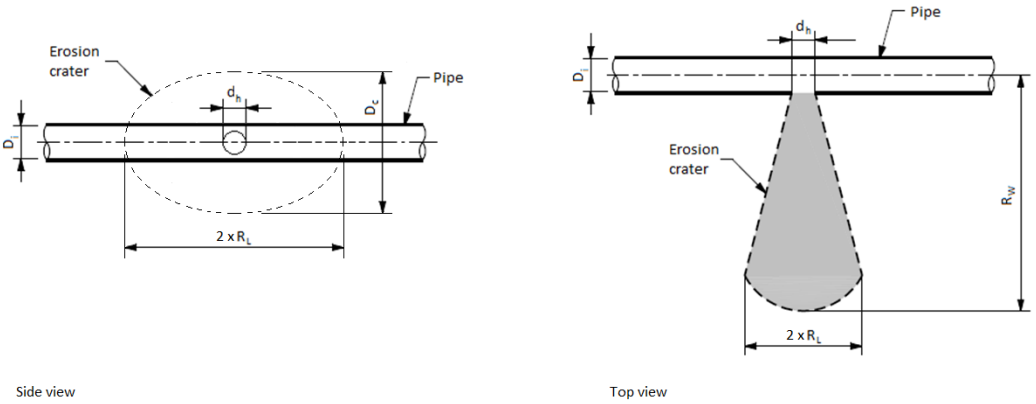

Figure 5.2: Overview of the definitions of erosion crater dimensions (NEN, 2020b).

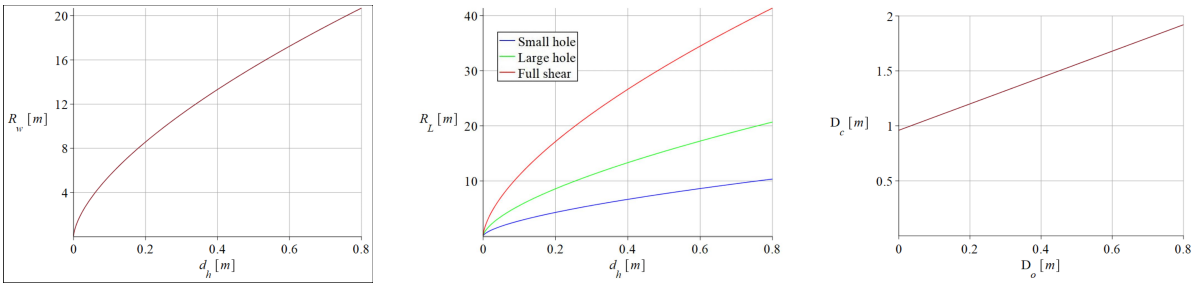

(a) Width of erosion crater (R_W) plotted against the diameter of the gaping leak (d_h).

(b) Length of erosion crater (R_L) plotted against the diameter of the gaping leak (d_h).

(c) Height of erosion crater (D_c) plotted against the outer diameter of the potable water pipe (D_o).

Figure 5.3: Graphs depicting the dimensions of erosion craters. Note: scale of y-axis varies in graphs.

Again, it has to be noted that the dimensions for gaping leaks found using the equations as given in this section result from a NEN standard concerning important infrastructure. Thus, failure of such infrastructure would have catastrophic effects. Therefore, the aforementioned dimensions of gaping leaks as calculated are worst case scenarios. Most likely, the dimensions of a gaping leak of a utility line in the vicinity of a quay wall would be significantly smaller.

6

Effect of utility line leakage in the vicinity of quay walls

This chapter is meant to specify the information provided in chapter 5 for the case of utility line leakage in the vicinity of the typical inner-city quay wall structure of Amsterdam as discussed in section 2.2. Thus, this chapter provides another part of the answer to sub-question 2:

How is leakage of a utility line linked to failure of a quay wall?

The chapter is split up into two sections. First, in section 6.1, the effect of internal erosion in the vicinity of a quay wall structure is discussed. Both the required mechanisms which have to be in place in order to enable internal erosion, as well as its various possible effects are touched upon. Section 6.2 discusses the effects of Gaping leaks.

It is important to note that the various situations discussed in this chapter are schematized in 2D cross-sections. However, it is reasonable to assume that leakage of a utility line can result in failure of part of the quay wall located along the longitudinal direction of the structure in the vicinity of said failed utility line, as a weak spot of the structure might be present at this location (f.e. in the form of a wooden floor or scour protection screen leakage as discussed in section 6.1.2). Additionally, it has to be noted that it is stated by Waternet that although a utility line might be leaking, if the structure of the quay wall is not compromised, leakage of said utility line does not result in failure of the quay wall. Finally, the process described in this section is not limited to be the result of utility line leakage. If the utility line located in the soil body behind the quay wall does not show leakages but the groundwater level in said soil body has risen up to sufficient levels due to f.e. heavy rain, the result are the same.

6.1. Internal erosion in the vicinity of quay walls

As explained in section 5.2, one of the main conditions for the occurrence of internal erosion in a soil medium is the flow of water, which can either be the result of a potable water pipe leakage, or due to any other reason for which the groundwater level has risen. Thus, both a head difference and an open connection are required for the instigation of the process. An open connection is defined as being capable to transport both water and soil, i.e. a connection via which internal erosion processes can occur as explained in section 5.2. Such a connection comes in the form of a combination of a through hole in the structure combined with a non-cohesive soil layer, or a cohesive soil layer subjected to hydraulic fracture. It is assumed that a check for the quay wall structure's susceptibility for backward erosion is sufficient as a check for all internal erosion processes. This is partly because backward erosion is assumed to play a role in most quay wall failures due utility line leakages and partly because the hydraulic gradient (ΔH) required for instigation of backward erosion is higher than the instigation of other internal erosion processes (f.e. forward erosion (van Beek, 2015)). The test if the quay wall structure is susceptible to backward erosion, and thus internal erosion in general, is provided in section 6.1.1.

The various ways in which an open connection is enabled in a typical configuration of an inner-city quay wall in Amsterdam are discussed in section 6.1.2. Pipe formation resulting in erosion underneath structure as well as in the soil body behind the structure is discussed in section 6.1.3. The section closes with the effects of pipe formation underneath the structure and pipe formation in the soil body behind the quay wall in sections 6.1.4 and 6.1.5 respectively. Note that combinations of these locations of pipe formation and thus their effects can occur as well.

6.1.1. Susceptibility to backward erosion

In order to check if the quay wall structure is susceptible to backward erosion, the adapted Sellmeijer model test was applied (Förster et al., 2012). With this model, the critical hydraulic gradient can be determined; if the hydraulic gradient over the structure is higher than this determined critical gradient, the structure is susceptible to backward erosion. van Beek (2015) states that the model over-predicts the critical gradient in more loose- and/or more coarse sand, as well as in 3D situations. Thus in the case of the inner-city quay walls, if the hydraulic gradient over the structure is found to be higher than the critical gradient, it can be said with high probability that the structure is susceptible to internal erosion. Using general parameters valid for the inner city in Amsterdam it was found that in case of full saturation, i.e. groundwater level up to surface level, the susceptibility of the quay wall structure to backward erosion is proven up to a horizontal seepage length of approximately 5 m. In case of saturation only up to the level at which potable water pipes are located (i.e. 0.8 m from surface level), the susceptibility of the quay wall is proven up to a horizontal seepage length of approximately 2 m. Calculations for the seepage lengths are provided in appendix G. These values are of the same order magnitude of inner-city quay wall floors in general, indicating the susceptibility to backward erosion.

6.1.2. Possible open connections enabling internal erosion

In this section the ways in which a head difference with an open connection are generated, is discussed. Three critical points have been determined:

1. **Scour protection screen leakage**
   In theory, a relatively water tight seal is in place between the backfill soil body above the wooden floor of the quay wall and the channel: the wooden scour protection screen. Due to the age of this screen, there is a fair possibility that it has lost its water tightness as a result of deterioration. See figure 6.1, in which the seepage length is depicted with L_s. Note that the figure is a 2D cross-section of a 3D structure, depicting the specific location of the leakage. The rest of the scour protection screen might still be sound.

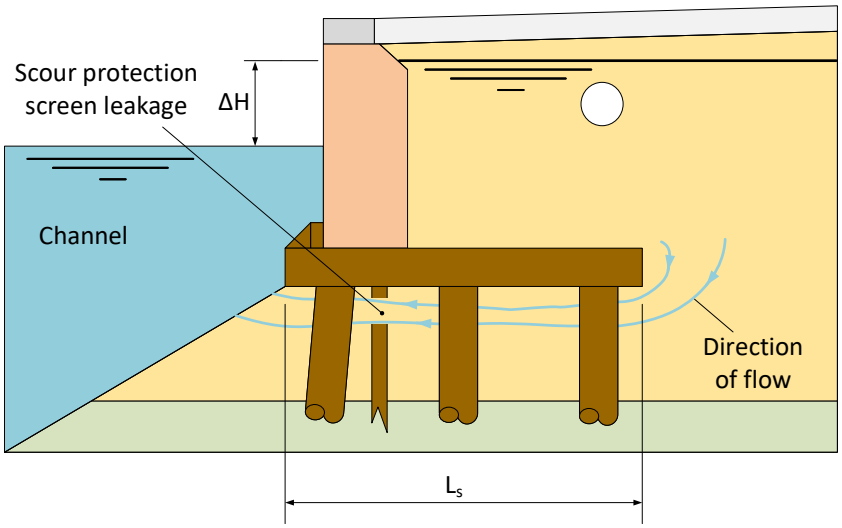

Figure 6.1: Example of a leak in the scour protection screen as an open connection. The seepage length is depicted with L_s.

2. **Quay wall floor leakage**
   Similarly to the scour protection screen, it is possible that in time gapes and leakages have formed in the floor of the quay wall. The location of the scour protection screen plays a high role in the severity of this situation. If the screen is located closer to the channel than the leak in the floor, no head difference with open connection is present, assuming the screen is still functioning properly. However, leakage of the quay wall floor does become relevant if the leak is located between the channel and the screen 6.2, in which the seepage length is depicted with L_s. Again, note that the figure is a 2D cross-section of a 3D structure, depicting the specific location of the leakage. The rest of the quay wall floor might still be sound.

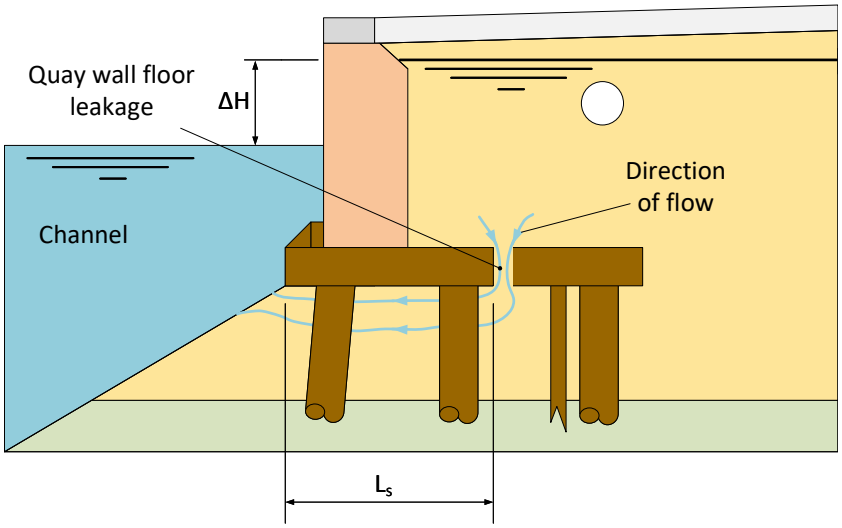

Figure 6.2: Example of leak in the
wooden floor as an open connection. Note that the scour protection screen is located behind the leak. The seepage length is depicted with L_s.

3. **Sewer leakage**
   Contrary to the two previous critical points, sewer leakage is not directly related to the design of the quay wall. As explained before, a leaking sewer can function as a drain for water and soil. It functions as a head difference with an open connection on its own, bypassing the need for an open connection with the channel side of the structure. See figure 6.3. Again, note that the figure is a 2D cross-section of a 3D structure, depicting the specific location of the leakage. The rest of the sewer pipe might still be sound.

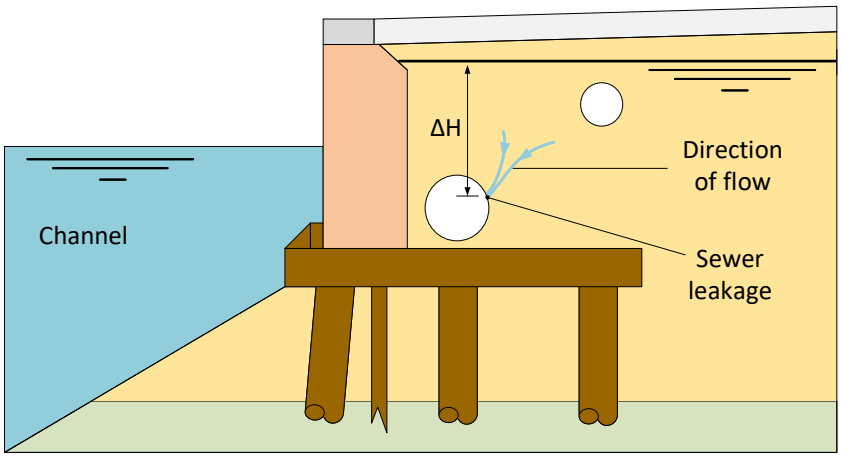

Figure 6.3: Example of a leak in the sewer system as an open connection.

6.1.3. Pipe formation due to internal erosion

For each of the previously listed modes a head difference with open connection can be generated, the ways in which pipes are formed due to internal erosion are discussed in this section.

1. **Pipe formation due to scour protection screen leakage**
   In this case, three internal erosion processes play a role in the formation of the pipe. Starting from the channel side over the full width of the floor, backward erosion takes place as explained in section 5.2.2. Additionally, at the location of the leakage in the screen a concentration of flow lines occurs, thus enabling concentrated leakage erosion as explained in section 5.2.1. Finally, as the wooden floor of the quay wall is a rigid structure, forward erosion can play a role as well (explained in section 5.2.3. Resulting from this kind open connection and pipe formation is erosion underneath the structure. The effects of erosion underneath structures is given

in section 6.1.4. See figure 6.4 for a schematization of the resulting erosion underneath the structure due to scour protection screen leakage.

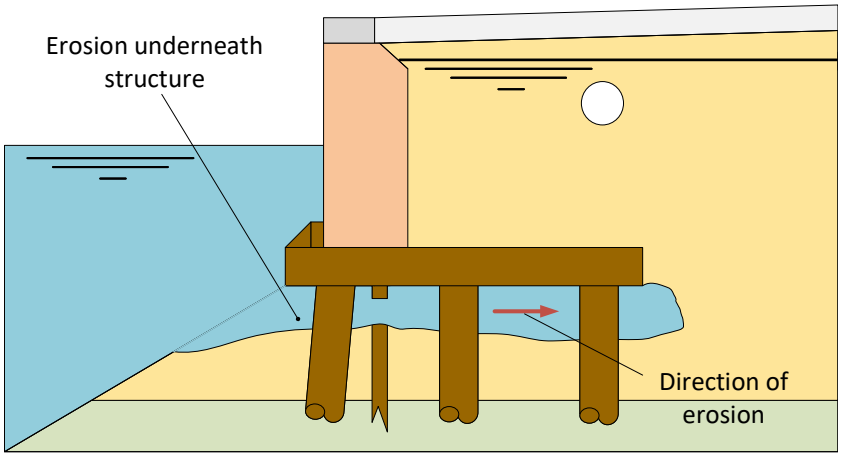

Figure 6.4: Schematization of erosion underneath the structure due to scour protection screen leakage (exaggerated portrayal).

2. **Pipe formation due to quay wall floor leakage**
   Due to quay wall floor leakage, backwards erosion can occur starting from the channel side up to the location of the leak, thus creating a pipe underneath the structure similarly to the previous case of scour protection screen leakage. Also, at the location of the floor leakage, concentrated leakage erosion is likely to occur. The main difference with the previous case is that due to the location of the leak, erosion of the soil directly behind the quay wall is more likely to occur. On the other hand, pipe formation underneath the structure does not extend over the full width of the floor but only up to the floor leakage. Similarly to the previous case of pipe formation due to scour protection screen leakage, the wooden floor acts as a rigid structure, thus forward erosion can play a role in the internal erosion process as well. In this case, similarly to the previous case, the open connection and pipe formation results in erosion underneath the structure. Additionally, the open connection and pipe formation result in erosion of the soil body behind the structure. The effect of the erosion underneath the structure is also similar to the previous case, given in section 6.1.5. The additional effect of erosion in the soil body behind the quay wall is given in section 6.1.5. See figure 6.5 for a schematization of the resulting erosion due to quay wall floor leakage.

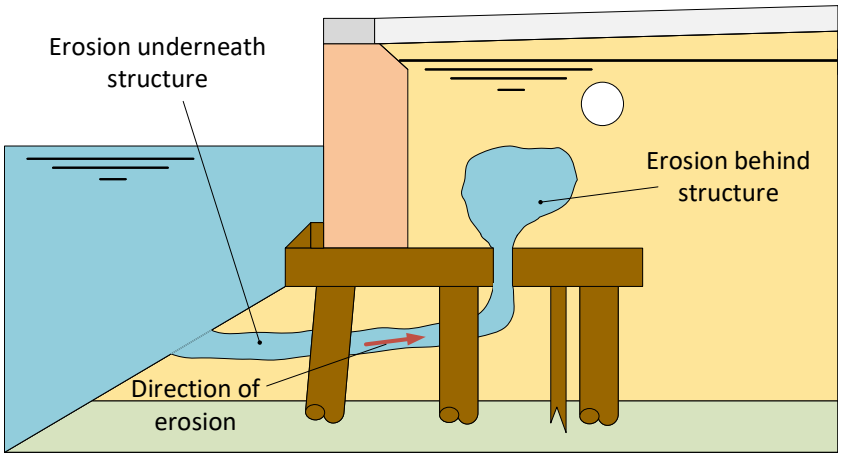

Figure 6.5: Schematization of erosion underneath- as well as behind the structure due to quay wall floor leakage (exaggerated portrayal).

3. **Pipe formation due to sewer leakage**
   Contrary to the previous cases, in this case, non of water tightness properties of the quay wall's components are compromised. Thus, in this case internal erosion does not result in pipe formation underneath the structure. Instead, pipe formation occurs solely in the soil body behind the quay wall, primarily due to concentrated

leakage starting from the location of the leak in the sewer pipe. If the sewer leakage is allowed to continue untreated, the resulting pipe formation can eventually result in erosion in the soil behind the quay wall, of which the effects are given in section 6.1.5. The location of the leak on the pipe has a significant influence on the volume of soil inflow in said pipe (Kamel and Meguid, 2008). If a leak is located at the crown of the pipe, the inflow is about a factor 2-3 higher when compared to a leak located at a 45^o angle with the crown. See figure 6.6 for a schematization of the resulting erosion due to sewer leakage.

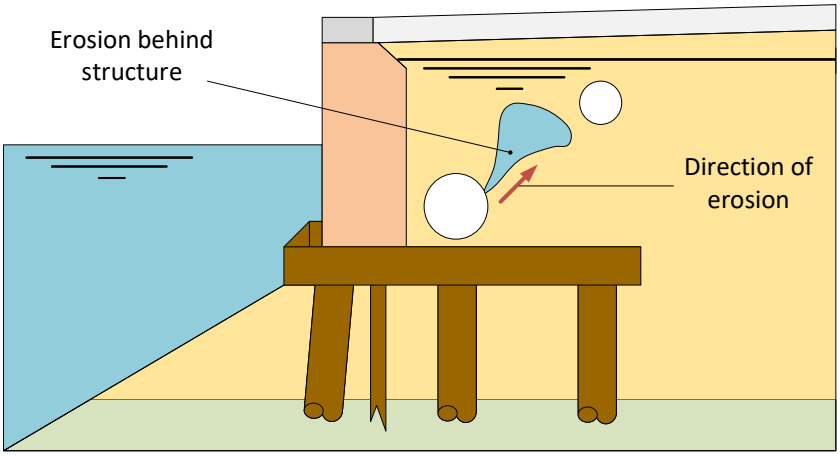

Figure 6.6: Schematization of erosion underneath the structure due to sewer leakage (exaggerated portrayal).

6.1.4. Effects of erosion underneath structure

Pipe formation- and the resulting erosion underneath the quay wall structure primarily affects the pile foundations of the structure. Assuming that the leakage and pipe formation goes unnoticed for a sufficient time, a significant quantity of pipes may have formed underneath the structure, resulting in both a significant loss of material and high number of voids. These voids can affect both the vertical- as well as the horizontal bearing capacity of the pile foundation. In vertical direction, erosion of soil surrounding piles results in a reduction of support via cohesion (Meireman, 2016). In horizontal direction, erosion of this soil results in a reduction of the passive soil resistance acting on the pile shafts (Davisson, n.d.). If in case of quay wall floor leakage the erosion behind the quay wall structure is sufficient, this results in a reduction of soil behind the quay wall, in term resulting in a reduction of horizontal soil loading on the structure and thus on the pile foundation.

Additionally, due to erosion underneath the structure, the amount of water flow surrounding said pile heads increases. This enables and potentially increases the rate of bacterial decay as discussed in section 2.2.3, accelerating the deterioration of the foundation piles.

If the bearing capacity of the pile foundation has been compromised due to any reason, i.e. they are found to be no longer connected to the capping beam as the was the case of the inspected quay wall in Haarlem as explained in section 2.6, the vertical loads originally carried by this pile might then transfer to the soil underneath the structure. Erosion of this soil can then in term result in additional settlements.

Therefore, due to various reasons erosion of soil underneath the structure can result in settlements in different magnitudes over the width and length of the floor, resulting in relative displacements of the quay wall components and thus stresses on the utility line, discussed in more detail in section 7.2. Thus, erosion underneath the structure can trigger a second order effect in the form of additional utility line deformation, instigating a positive feedback loop. See figures 6.7a and 6.7b for the effects of erosion underneath the structure, due to scour protection screen- and quay wall floor leakage respectively.

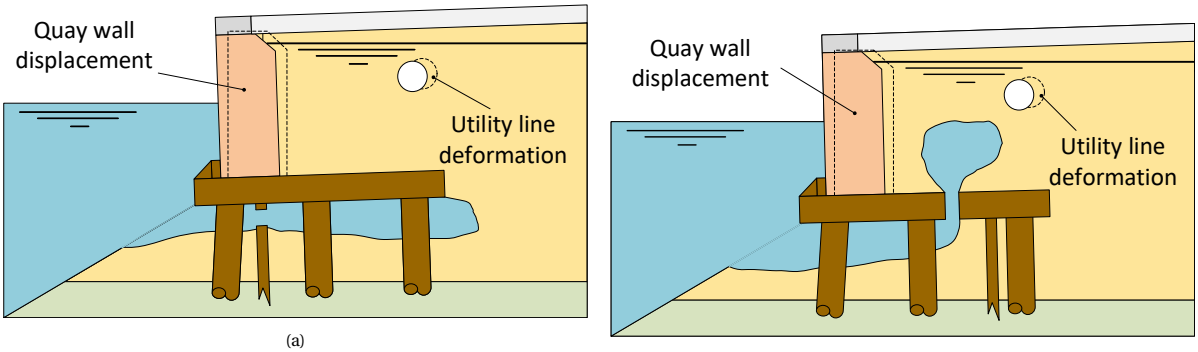

(a)
Effect of erosion underneath structure due to scour protection screen leakage.

(b) Effect of erosion underneath structure due to quay wall floor leakage.

Figure 6.7: Effect of erosion underneath structure.

Eventually, erosion underneath the quay wall structure can result in quay wall collapse towards the channel. One example of this being the collapse of the quay wall along the Entrepotdok in 2017 (van Belzen, 2017). Another example being the of the collapse of the quay wall along the "Bemuurde Weerd Oost" in Utrecht (DUIC, 2013). A leak in either the quay wall floor or the scour protection screen in combination with a high ground water level resulted in the collapse of said quay wall, due to the own weight of the structure. It has to be noted that the masonry on the channel side of the quay wall was directly founded on the sandy soil naturally present. However, research into various other visually similar quay walls made clear that the structure could be classified as a gravity wall on wooden piles, thus the structure is comparable to the quay walls as they are found in the inner-city of Amsterdam. See figure 6.8 for the resulting collapse of the quay wall in Utrecht due to erosion underneath the structure.

Figure 6.8: Collapsed quay wall of the "Bemuurde Weerd Oost" in Utrecht (AD, 2013).

Due to its nature, it is expected that in case of a fully functioning pile foundation, the loads of the quay wall are not transported towards the soil underneath the quay wall structure. Thus, in this case, it can be assumed that erosion underneath the structure does not directly result in quay wall displacement.

6.1.5. Effect of erosion in soil body behind quay wall

As can be seen both in figure 6.5 and 6.6, internal erosion and thus the outflow of soil in the soil behind the quay wall above the foundation floor results in voids in said soil medium. The loss of soil by definition does not result in increased horizontal soil pressures on the masonry of the quay wall, thus the soil retaining properties of the structure are not compromised. However, as the street located on the quay is founded on the soil body behind the quay wall, voids in said soil body results in loss of this foundation, which in term can result in settlements visible at surface level. An example of these settlements were observed during the aforementioned quay wall inspection in Haarlem,

as discussed in section 2.6 and appendix C.

Additionally, as explained in sections 3.2 and 3.3, utility lines are generally rely the soil in which they are embedded in as a foundation. Thus, if this soil is eroded, the utility line's foundation is removed as well, resulting in utility line deformations and leakages. This can be defined as a second order effect, resulting in a positive feedback loop similarly to the effect of erosion underneath the structure. See figures 6.9a and 6.9b for the effect of erosion behind structure, due to both quay wall floor- and sewer leakage respectively.

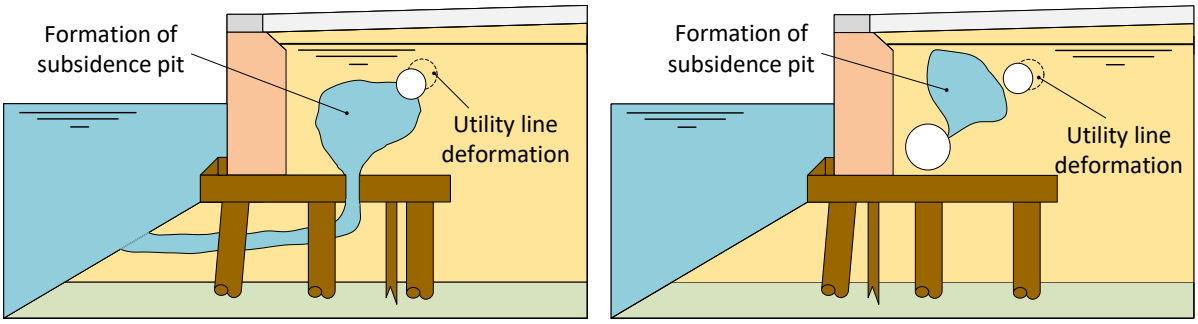

(a) Effect of erosion behind structure due to quay wall floor leakage.

(b) Effect of erosion behind structure due to sewer leakage.

Figure 6.9: Effect of erosion behind structure.

In a more extreme case, the voids in the soil body behind a quay wall created by erosion can lead to collapse of the street founded on said soil body. This phenomenon is called a subsidence pit and has been observed at various locations, for example in 2017 at the "Marnixstraat, Amsterdam" (AT5). Outflow of water was observed at this location, and as the water supply of the buildings in the vicinity was lacking, the subsidence pit was attributed to a potable water pipe leakage. The subsidence pit and the collapsed street can be seen in figure 6.10 (AT5, 2017).

Note that in some literature this phenomenon is described as a sinkhole. However, according to Beck and Balkema (1984) the term sinkhole should only be used to describe "enclosed depressions caused ultimately by dissolution of the underlying rocks, i.e. karst processes". Human induced sinkholes are therefore also limited to cases in which human activities resulted in generation or acceleration of karst processes, i.e. poor groundwater management. As at least the upper 25 m of the subsoil in Amsterdam consists of deposited sediments, karst processes are irrelevant for research into their inner-city quay walls.

Figure 6.10: Subsidence pit as observed in the Marnixstraat, Amsterdam (AT5, 2017).

6.2. Gaping leaks in the vicinity of quay walls

Gaping leaks generate erosion craters, which are in essence voids in the soil body behind the quay wall. Thus, gaping leaks show similarities to the discussed erosion in the soil body behind the quay wall as discussed in section 6.1. Thus, the effects of gaping leaks are generally similar as well, although the timescale of gaping leaks resulting in quay wall failure is much shorter than in case of minor leaks. Again, note that a minor leak can grow to a gaping leak, due to further utility line deterioration and deformation.

As mentioned before, water discharges resulting from gaping leaks are higher than resulting from minor leakages. This results in higher forces capable of displacing soil. Close to the gaping leak these forces might result in rearrangement of the soil structure itself, and in the vicinity of the leakage saturation of the soil will definitely occur. This by itself can generate enough displacement to result in a subsidence pit as represented in figure 6.10 (AT5, 2017). However, in order for a gaping leak to further erode its surrounding soil and generate a sizable erosion crater, it is expected that an open connection as explained in section 6.1.2 has to be in place in order for the water originating from the leakage to be able to transport soil. See figure 6.11 for a schematization of an erosion crater formed due to a gaping leak, and thus the similarities it shows with the schematizations of erosion behind the structure due to either quay wall floor- or sewer leakage, represented in figures 6.5 and 6.6 respectively. In figure 6.11, the width and height of the erosion crater are depicted as R_W and D_c respectively.

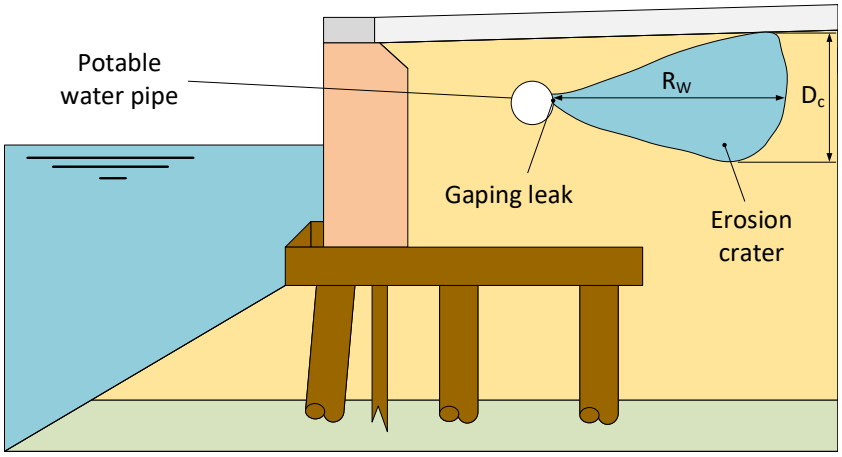

Figure 6.11: Schematization of an erosion crater due to gaping leak.

7

Analytical model of utility line deformation

This chapter revolves around sub-question 3, formulated as follows:

How is quay wall deformation linked to utility line leakage?

In order to answer this research question and to gain more insight in the interaction between a quay wall, its soil body, and the utility line in its vicinity, an analytical model was developed. This chapter provides the outline of said model, while chapter 8 provides the results of the model.

The chapter starts with an overview of the known relevant literature regarding quay wall-soil-utility line interaction in section 7.1. Next, section 7.2 discusses the manner in which quay wall displacements influence soil displacements. The following section (section 7.3) discusses how these soil displacements are implemented in the analytical model. In section 7.4 the general outline of the model is provided, including the equations of motion (EoM) and boundary conditions. The applicability of the model is discussed in section 7.5. Section 7.6 provides an overview of the values for the input parameter of the model. The output parameters are discussed in section 7.7 and the formulation of the leakage criteria is provided in section 7.8. The chapter follows with an outline of the model in two specific situations: quay wall displacement over greater length in section 7.9, and localised quay wall displacement in section 7.10. Finally, an overview of the analytical model and the affected soil areas is provided in section 7.11.

7.1. Previously conducted research into quay wall-soil-utility line interaction

The starting point for the quay wall-soil-utility line interaction is the comparison of quay walls to retaining walls in general, as a significant amount research of research has been conducted on their displacements. Generally in these studies, the quay wall displacement was the researched entity, resulting from external factors. In these studies, a major external factor causing said displacement is the backfill soil. However, research into the displacement of soil due to quay wall displacement, i.e. quay wall displacement switching the roles of cause and effect with soil displacement, is limited. An exception being research conducted by Sarvanis et al. (2017), who conducted research into utility line displacement resulting from soil displacement modeled after what was observed at fault lines. In this experiment, the soil was displaced via partial displacement of a retaining wall, bearing comparisons to quay wall displacement. One major difference was that the soil was displaced trough both push and pull, while in the case of quay wall displacement towards the channel the soil is not pushed.

Most of the previously conducted research into soil-utility line interaction in vertical and lateral direction focuses on large soil movements happening relatively quickly, mostly resulting from earthquakes or unstable slope collapses (f.e. research conducted by Yoshizaki and Sakanoue (2004) and Zhang and Askarinejad (2018) respectively), for which both analytical- as well as numerical models are applied. Soil-pipeline interaction for smaller vertical deformations has been researched by WANG et al. (2011). In their study, an analytical model was set up to research the effect of tunneling-induced soil settlements on utility lines. To model the interaction between soil and utility lines, a Winkler-foundation was used, i.e. an Euler-Bernoulli beam on a distributed spring foundation. The distributed spring was assumed to be linear. The model was compared to a finite element model and showed little variation. If finite element methods are applied, it is stated by Karamanos et al. (2014) that these can be subdivided into two levels. In a level 1 approach the interaction between soil and utility line shows similarities to the aforementioned analytical approach of WANG et al. (2011), in which the soil-utility line interaction is modelled as horizontal-, lateral-

and longitudinal springs. This approach level is "adequate for regular design purposes." Level 2 type approaches are defined as taking into account the utility line's and the soil's inelastic material behaviour, as well as cross-sectional distortions due to the soil-interaction. As expected, level 2 type approaches are more accurate, but require far more computational time, and are therefore only used "in special cases, where increased accuracy is necessary".

7.2. Soil displacement due to quay wall displacement in 2D

Central to the interaction between quay walls and utility line is that the displacement of a quay wall results in displacement of the soil body behind it. The magnitude and reach in lateral direction of this displacement is determined using PLAXIS 2D: a finite element method (FEM) model, widely used in geo-engineering (Bentley, n.d.a). In term, the results of the PLAXIS 2D model are in term implemented into the analytical model. By using the analytical model, the effect of soil-utility line interaction can be studied over the length of the quay wall. Another option might be to use PLAXIS 3D, in which the quay wall-soil-utility line interaction can be studied over the length of the quay wall in a fully numerical manor instead of analytically. However, in order to get adequate results, model-run times would increase significantly if this option is used. As explained in section 7.1, for a more general approach it is sufficient to model the quay wall-soil-utility line interaction using an analytical model. An overview of the used PLAXIS 2D model is provided in section 7.2.1 and the results of said model are provided in section 7.2.2.

7.2.1. PLAXIS 2D model

As the sole reason for the use of a PLAXIS model is to find the magnitude of displacement of the soil body behind the gravity wall and above the quay wall floor, induced by displacements of the quay wall, the model can be fairly simple. The reason for this being that virtually all utility lines influencing the quay wall structure are situated in this area. As this is a 2D model, the cross section of the quay wall is represented. See figure 7.1 for an overview of the model, in which the aforementioned soil body of interest is highlighted as well. Note that the actual model ranges from -15 to 20 m in horizontal direction, and ranges from 0 to -10 m in vertical direction. The model is based on the displacements as seen during the quay wall inspection in Haarlem (Witteveen+Bos, 2015), in which primarily horizontal quay wall displacement was observed. The displacement is assumed to occur over a long period of time, resulting in a slow loading situation.

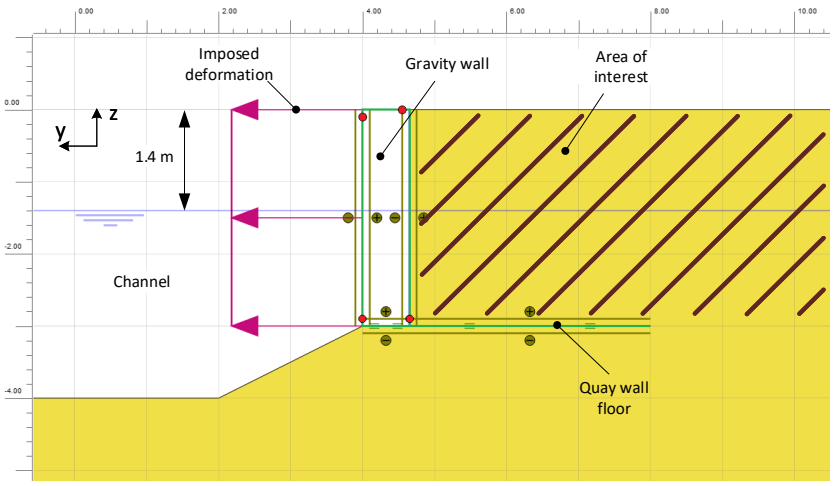

Figure 7.1: Overview of the PLAXIS 2D model. Note that both the positive and negative interfaces of the upper element of the gravity wall has been left out of the figure for simplicity.

The dimensions of the quay wall structures in the model are based on the general dimensions of quay walls in Amsterdam, as it is seen in figure 2.1. Thus, the height of the quay wall is equal to 3 m and the width of the quay wall floor is equal to 4 m (which are outer limits for quay walls, producing the most unfavourable situation). The width of the gravity wall is, including the thickness of the elements, in the order of 1 m, while the thickness of the quay wall floor is equal to 0.35 m. The waterline is located 1.4 m from the top of the quay wall, and it is assumed that the groundwater level is equal to the level in the channel. Although it is more than likely that the soil body in the area of interest is not 100% sand, the model is mainly required to provide inside into the situation and the soil is

thus modelled as being so. The hardening soil model is applied, as this soil model is more advanced than the simpler Mohr-Coulomb model and good at capturing soil properties of sand under slow loading situations (van der Wel, 2018). More details regarding the PLAXIS model and the applied soil parameters are provided in appendix H.

As only the deformation of the soil in the area of interest is sought for in this model, and not the displacement of the quay wall structure itself, the material properties of the quay wall and the quay wall floor and the soil properties underneath the structure are fairly insignificant. For the same reason, the pile foundation is not modelled as well. The pile foundation is represented by prescribing zero displacement to the quay wall floor in the vertical direction, although it is questionable that the pile foundations are not deformed if the quay wall is deformed in the horizontal direction. However, for the displacements of the soil body in the area of interest in either the horizontal or vertical direction, there is no significant difference if this prescribed vertical fixation is in place or not. The displacement of the quay wall is modelled by imposing a deformation on the quay wall in horizontal direction. Due to the assumed rigid connection between the quay wall floor and gravity wall, this results in a similar horizontal displacement of said floor. Note that this behaviour is a fairly exaggerated representation of the real life situation, as piles are likely to be able to resist motion in the horizontal direction. However, if sufficient erosion of soil around the piles has taken place, their capability to resist motion in horizontal direction diminishes.

7.2.2. PLAXIS 2D result

Applying a displacement in the range as was found in Haarlem (Witteveen+Bos, 2015), to the PLAXIS model, results in a displacement behind the quay wall as displayed in figures 7.2, 7.3, 7.4, 7.5 and 7.6. In these figures, horizontal displacements of 20 mm, 40 mm, 60 mm, 80 mm and 100 mm respectively were applied to the quay wall. For all quay wall displacements, both the horizontal- as well as the vertical soil displacement are provided.

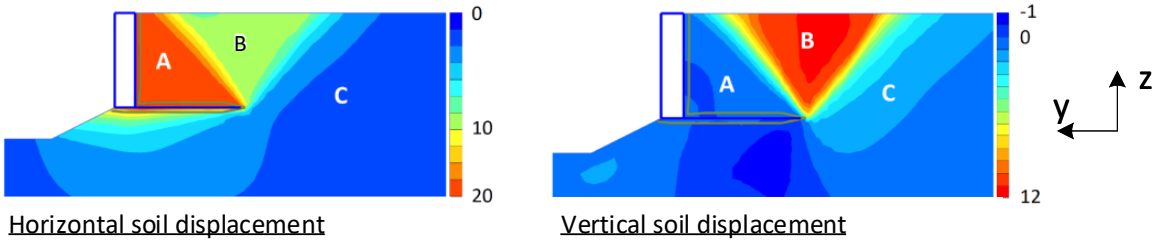

Figure 7.2: Soil displacements resulting from the PLAXIS 2D model with 20 mm horizontal quay wall displacement. Note: legends of the soil displacement are not equal and are presented in mm.

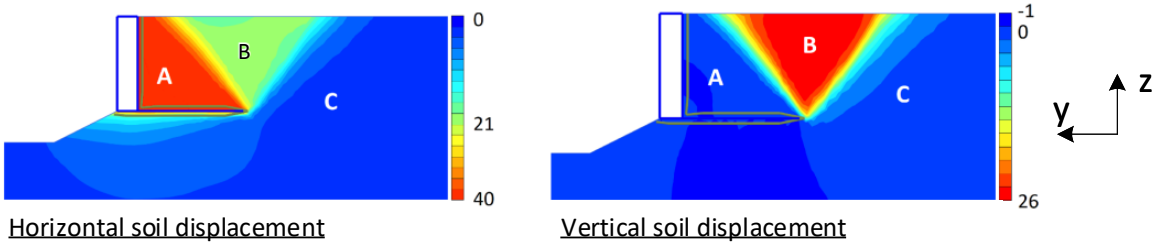

Figure 7.3: Soil displacements resulting from the PLAXIS 2D model with 40 mm horizontal quay wall displacement. Note: legends of the soil displacement are not equal and are presented in mm.

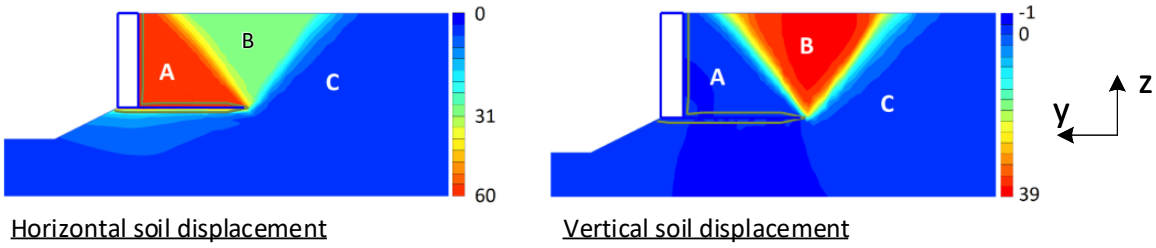

Figure 7.4: Soil displacements resulting from the PLAXIS 2D model with 60 mm horizontal quay wall displacement.
Note: legends of the soil displacement are not equal and are presented in mm.

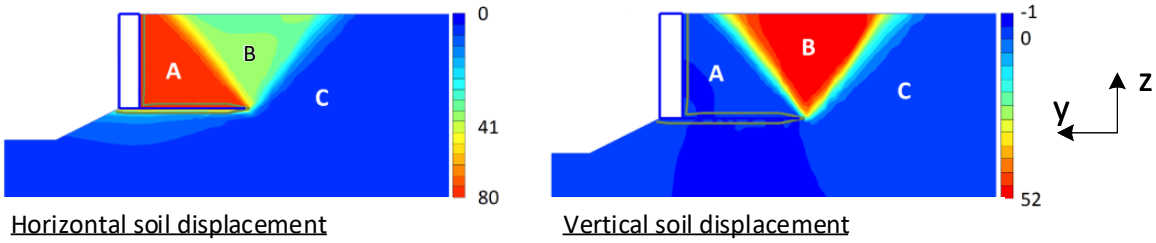

Figure 7.5: Soil displacements resulting from the PLAXIS 2D model with 80 mm horizontal quay wall displacement.
Note: legends of the soil displacement are not equal and are presented in mm.

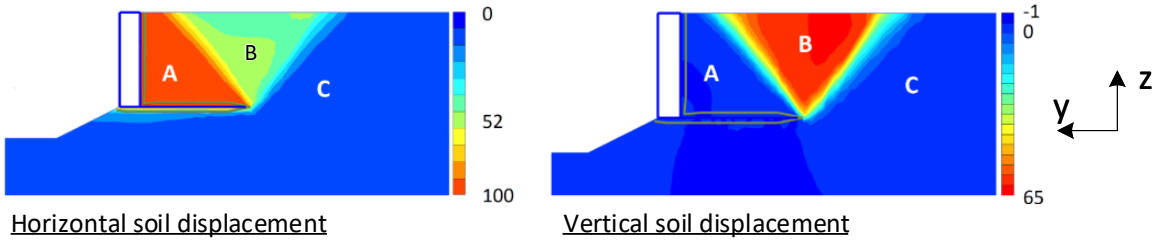

Figure 7.6: Soil displacements resulting from the PLAXIS 2D model with 100 mm horizontal quay wall displacement.
Note: legends of the soil displacement are not equal and are presented in mm.

From figures 7.2 to 7.6, it follows that the soil in the area directly behind the quay wall, is exclusively displaced in horizontal direction. This area is depicted as area A for both directions in all quay wall displacements.

Again for all quay wall displacements and for both the horizontal- and vertical displacement, starting from the outer point of the quay wall floor, a triangular area can be seen behind the aforementioned soil area directly behind the quay wall. This area is depicted as area B for all quay wall displacements in both the horizontal- and vertical soil displacement. This is practically the only area behind the quay wall were both horizontal- and vertical displacement occurs. Using Pythagoras theorem ($c^2 = a^2 + b^2$), the total displacement is calculated for all applied quay wall displacements. The results are provided in table 7.1. This area reaches to about half the length of the quay wall floor in the opposite direction of the quay wall displacement.

Table 7.1: Overview of the horizontal-, vertical- and total displacements of area B for the various quay wall displacements.

Quay wall displacement ($S_{max}[mm]$)	**Hor. displacement Area B** $[mm]$	**Ver. displacement Area B** $[mm]$	**Total displacement Area B** $[mm]$
20	10	12	16
40	21	26	33
60	31	39	50
80	41	52	66
100	52	65	83

Behind these triangular shaped areas occurring in the horizontal- and vertical soil displacements for all quay wall displacements, it can be seen that the soil displacements in both directions are approximately equal to zero. In figures 7.2 to 7.6 this area is depicted as area C.

It follows that directly behind the quay wall the total displacement is equal to the horizontal displacement. Additionally, the soil displacement in the aforementioned triangular area B further away from the quay wall is almost equal in magnitude to the horizontal soil displacement in area A. The soil reaction for motion in downwards direction is not directly equal to the soil reaction in horizontal direction, especially for smaller diameters of utility lines (see section I.2 of appendix I). However, as for every quay wall displacement the maximum vertical displacement is less than the horizontal displacement as seen in area A, in order to simplify the analytical model it is deemed sufficient to only take horizontal quay wall displacements into account. Note that utility lines are found in the area's A, B, and C, depicted in figures 7.2 to 7.6. In section 7.11, a top view is provided of the affected soil areas due to horizontal quay wall displacement.

7.3. Relative soil displacement at location of quay wall displacement

As said before, the analytical model is based on relative displacements of the soil and the utility line. It has to be noted that the quay wall does not directly interact with the utility lines situated behind it, but only through said soil body. The PLAXIS 2D model shows that soil displacements follow the displacement of the quay wall, discussed in section 7.2. Thus, If the quay wall is displaced over its full length, the soil body behind it would displace along with it. As utility lines are embedded in said soil body, displacement of this soil body does not automatically lead to additional stresses or relative deformations of the utility line. However, said soil body does experience relative displacement over the length of the quay wall at locations were the quay wall has displaced from its original state.

One of major assumptions made in this analytical model is that the only the soil body located directly behind a displaced part of a quay wall is affected by said deformation. By applying this assumption, it automatically follows that the soil body behind a non-displaced part of the quay wall does not deform as well. It follows from experiments by Sarvanis et al. (2017) into the effects of fault lines on soil bodies with utility lines embedded in them that this assumption is roughly valid. Additionally, the quay wall displacement is modelled to occur abruptly over its length. This assumption is validated in section 7.5.

The relative displacement of the utility line and the soil body is visualized in figures 7.7 and 7.8, providing a top- and cross-sectional view respectively. At this location the left side of the quay wall structure remains at rest while the right side has displaced over a length S_{max}. Following from the previous, the corresponding soil body behind the structure follows the displacement of said quay wall sections. Due to this soil displacement the utility line embedded in this soil body follows these motions. However, as the utility line has a bending stiffness, the utility line is unable to follow the motion of the soil body directly, but the line requires a certain length to adapt to this new soil location. This results in the aforementioned relative utility line displacements and thus stresses in the line, with a net soil pressure q_h (as given in equation 7.1) acting against this relative displacement. This net soil pressure is equal to the summation of passive and active soil pressures. These soil pressures are in term responsible for the utility line deformations and leakages.

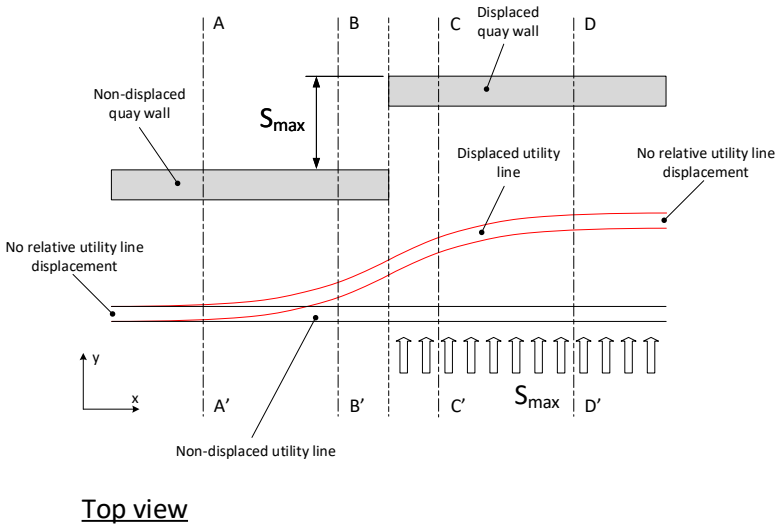

Figure 7.7: Relative displacement of utility line at the location of abrupt quay wall displacement, top view.

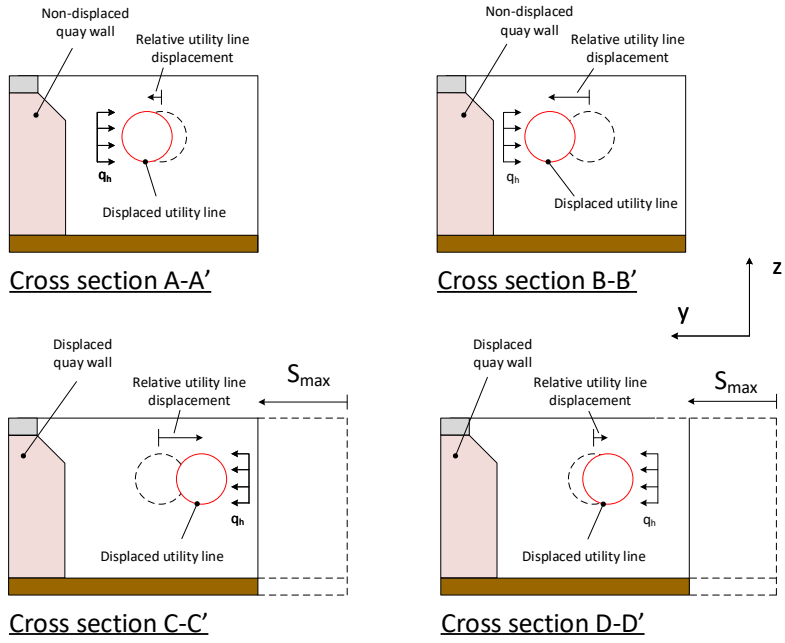

Figure 7.8: Relative displacement of utility line at the location of abrupt quay wall displacement, cross-sectional view.

7.4. Analytical model for utility line deformation

As said before in section 7.1, according to WANG et al. (2011) the interaction between a utility line and its surrounding soil can be modelled as a beam founded on a distributed spring with spring stiffness K_h, which is known as a Winkler foundation. This method of modelling shows similarities to the way longitudinal effects of tunnels are analytically modelled, in which these effects are distinguished as the "beam effect" (Reinders, 2019). The assumption of soil acting as a distributed spring is valid up to a certain maximum soil deformation, dependent on the characteristics of soil. If the horizontal deflection of the utility line ($y(x)$) is higher than said maximum equilibrium soil bearing capacity, the soil is not able to provide support in this form of a distributed spring, and the beam acts as a general Euler-Bernoulli beam. See figure 7.9 for an overview of both a Winkler foundation and a general Euler-Bernoulli beam. As explained in section 7.2.2, only the horizontal deformation of the soil, and thus the utility line, is mod-

elled. Note that although the relative displacements as discussed in section 7.3 are responsible for the stresses and thus possible failure of utility lines, the model uses absolute displacements for calculations. The analytical model is executed using a Maple script.

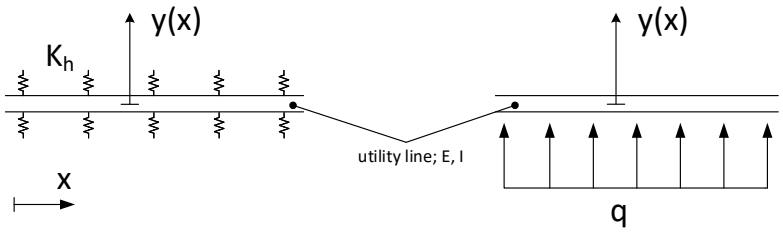

Figure 7.9: Left side: beam on a Winkler foundation. Right side: Euler-Bernoulli beam.

In section 7.4.1, the nature of these characteristics and the resulting stiffness of the aforementioned horizontal distributed spring are explained. Section 7.4.2 provides the EoM for both ways the utility lines are modelled as shown in figure 7.9. The boundary- and interface conditions are discussed in section 7.4.3.

7.4.1. Horizontal distributed spring stiffness

The horizontal distributed spring stiffness is based on the general relation for horizontal soil deformation, given in equation 7.1 (NEN, 2020a).

$$\frac{q_h}{q_{he}} = \frac{y_s / y_{s,max}}{\alpha + (1-\alpha) \cdot y_s / y_{s,max}} \tag{7.1}$$

In which:

y_s	Horizontal soil deformation ($y_s < y_{s,max}$);
q_h	Horizontal soil pressure corresponding to a soil deformation y_s ($q_h < q_{he}$);
q_{he}	Horizontal equilibrium bearing capacity, i.e. the maximal horizontal soil pressure;
$y_{s,max}$	Maximum allowable horizontal soil deformation. At this soil deformation, the horizontal equilibrium bearing capacity is reached;
α	Empirical stiffness constant. For sand and clay in a slowly loaded, drained situation (corresponding to the situation of quay wall deformation): $\alpha = 0.145$.

The equilibrium bearing capacity is also described as the net pressure resulting from the difference between active- an passive soil pressures. Plotting the relation for soil deformation as given in equation 7.1 results in the graph as given in figure 7.10 (NEN, 2020a).

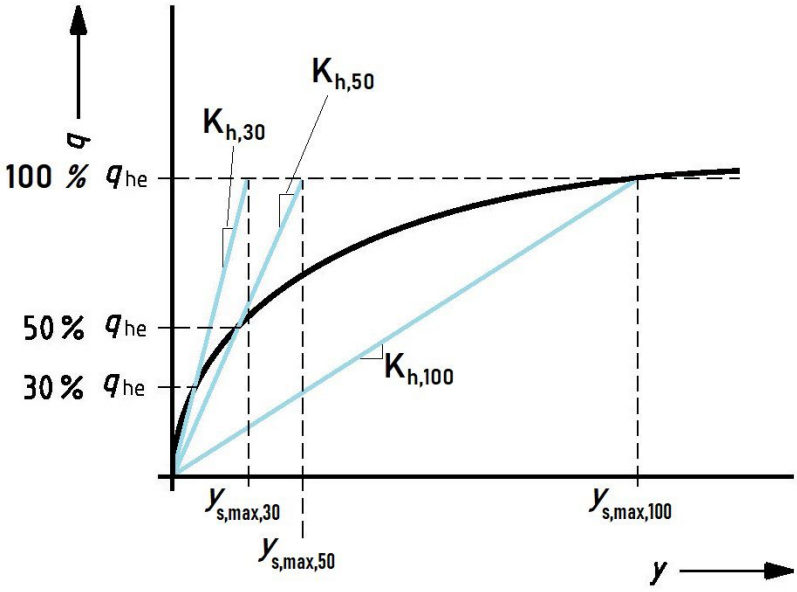

Figure 7.10: Graph of the relation between horizontal soil deformation and pressure in black (NEN, 2020a). The relation between the horizontal soil pressure and deformation used in the analytical model is represented in cyan.

The distributed horizontal spring stiffness is defined as the first derivative to the displacement of 7.1. As can be seen in figure 7.10, contrary to a regular spring, the spring stiffness is not constant. Up to the maximum soil deformation, the soil reaction can be described as elastic behaviour, which is represented by a distributed spring. If the horizontal soil deformation is larger than the maximum allowable soil deformation, the soil shows plastic behaviour. At this plastic limit the soil starts to breach. See equation I.2 for the determination of the horizontal equilibrium soil pressure and equation I.1 for its corresponding maximum horizontal displacement, both in appendix I.

In order to limit computation time, the spring stiffness is assumed to be bi-linear. The cutoff for the soil acting as a linear elastic material is determined by said maximum allowable soil deformation. If the soil deformation is larger than this value, the soil is modelled as acting on the utility line with a distributed load acting equal to the horizontal equilibrium bearing capacity. For this system, the spring stiffness is determined by drawing a line trough a point on the original q_{he} curve, corresponding to a percentage of q_{he}, up to 100% q_{he} and determining the corresponding maximum allowable soil deformation for this percentage of q_{he}. The spring stiffness is equal to the slope of said drawn line. See figure 7.10 for a visualization. The determination of the bi-linear spring is represented equation 7.2.

$$K_{h,\%} = \begin{cases} \frac{q_{he}}{y_{s,max,\%}} & y_s < y_{s,max,\%} \\ 0 & y_s \geq y_{s,max,\%} \end{cases} \tag{7.2}$$

From this relation it follows that a greater spring stiffness corresponds to a smaller maximum allowable soil deformation and vice versa. The influence of the magnitude of the spring stiffness and its corresponding maximum soil deflection are determined in a sensitivity analysis given in chapter 8

7.4.2. Equations of motion (EoM)

As previously mentioned, for sections of utility line of which the deflection is less than the maximum soil deflection, as defined in section 7.4.1, a Winkler foundation is assumed. The equation of motion (EoM) for a Winkler foundation is given as in equation 7.3.

$$E \cdot I \cdot \frac{d^4}{dx^4} y(x) + K_h \cdot y(x) = q \tag{7.3}$$

In which:

E	Utility line's material modulus of elasticity;
I	Cross-sectional moment of inertia of the utility line, given in equation I.6 of appendix I.

The solution to the EoM of the Winkler foundation can be found in the form provided as in equation 7.4

$$y(x) = \overbrace{e^{-\beta \cdot x}(C_1 \cdot cos(\beta \cdot x) + C_2 \cdot sin(\beta \cdot x)) + e^{\beta \cdot x}(C_3 \cdot cos(\beta \cdot x) + C_4 \cdot sin(\beta \cdot x))}^{\text{gen. solution}} + \overbrace{y^*}^{\text{part. solution}} \tag{7.4}$$

$$\beta = \sqrt[4]{\frac{K_h}{4 \cdot E \cdot I}}$$

For sections of utility line of which the deflection is greater than the maximum soil deflection, the general Euler-Bernoulli beam equation is used as the EoM, as represented in equation 7.5. Note that in order to apply q_{he} as a distributed load, it has to be multiplied with the outer diameter of the utility line $Q_{he} = q_{he} \cdot D_o$.

$$E \cdot I \cdot \frac{d^4}{dx^4} y(x) = Q_{he} \tag{7.5}$$

The solution to the EoM of the general Euler-Bernoulli beam as given in equation 7.5 can be found in the form provided as in equation 7.6.

$$y(x) = \overbrace{\frac{1}{24} \cdot \frac{Q_{he}}{E \cdot I}}^{\text{part. solution}} + \overbrace{\frac{1}{6} \cdot C_1 \cdot x^3 + \frac{1}{2} \cdot C_2 \cdot x^2 + C_3 \cdot x + C_4}^{\text{gen. sol}} \tag{7.6}$$

7.4.3. Boundary- and interface conditions

The basis for the analytical model is that, at a sufficiently long length away from the quay wall displacement, the relative displacement between the utility line and the soil body behind quay wall is equal to zero and that no stresses act on the utility line due to quay wall displacement. Additionally, the utility line can be assumed to be sufficiently long to model it as infinitely long. Thus, by definition, in every model the outer most ends of the utility line are modelled as beams on a Winkler foundation. Knowing these characteristics, the boundary conditions can be formulated. Substitution of $x = -\infty$ into the solution for the EoM of the Winkler spring (equation 7.4) results in equation 7.7. Note that due to the aforementioned reasons the particular solution y^* has to be constant and by definition: $\beta > 0$.

$$\begin{gathered} e^{-\beta \cdot -\infty}(C_1 \cdot cos(\beta \cdot -\infty) + C_2 \cdot sin(\beta \cdot -\infty)) + e^{\beta \cdot -\infty}(C_3 \cdot cos(\beta \cdot -\infty) + C_4 \cdot sin(\beta \cdot -\infty)) + y^* = constant \\ e^{\beta \cdot \infty}(C_1 \cdot cos(-\beta \cdot \infty) + C_2 \cdot sin(-\beta \cdot \infty)) + y^* = constant \\ C_1 = 0 \qquad C_2 = 0 \end{gathered} \tag{7.7}$$

Substitution of $x = \infty$ into the same solution as at the other end results in equation 7.8.

$$\begin{gathered} e^{-\beta \cdot \infty}(C_1 \cdot cos(\beta \cdot \infty) + C_2 \cdot sin(\beta \cdot \infty)) + e^{\beta \cdot \infty}(C_3 \cdot cos(\beta \cdot \infty) + C_4 \cdot sin(\beta \cdot \infty)) + y^* = constant \\ e^{\beta \cdot \infty}(C_3 \cdot cos(-\beta \cdot \infty) + C_4 \cdot sin(-\beta \cdot \infty)) + y^* = constant \\ C_3 = 0 \qquad C_4 = 0 \end{gathered} \tag{7.8}$$

At all interfaces (i.e. the x-coordinates at which the utility line modelling switches from a Winkler foundation to an Euler-Bernoulli beam and vice-versa) the displacement, angular deflection, bending moment, and shear force of the utility line have to be equal on both sides of said interface. Thus, at each interface, the interface conditions as defined in equation 7.9 are valid. In this equation, the subscripts l and r represent the displacement of the utility line left and right of the interface respectively. x_{ic} represents the x-coordinate of the interface condition.

$$\begin{aligned} y_l(x_{ic}) &= y_r(x_{ic}) \\ \frac{d}{dx} y_l(x_{ic}) &= \frac{d}{dx} y_r(x_{ic}) \\ \frac{d^2}{dx^2} y_l(x_{ic}) &= \frac{d^2}{dx^2} y_r(x_{ic}) \\ \frac{d^3}{dx^3} y_l(x_{ic}) &= \frac{d^3}{dx^3} y_r(x_{ic}) \end{aligned} \tag{7.9}$$

7.5. Applicability of the analytical model

In this section, the major factors determining the applicability of the analytical model are discussed, and in what way these affect the outcome of the model.

7.5.1. Representation of utility lines as continuous systems

In the analytical model, the utility lines are represented as a continuous beam. This means that, over their length, material properties and dimensions do not vary and that deformations, bending moments, normal- and shear stresses are transported. Thus, only external factors like the applied soil deformations are capable of inducing variations in the line's deformation, bending moments and shear forces over its length. However, as said in section 3.2.4 and 3.3.3, utility lines are made up of multiple line segments, which in term are connected to eachother via joints. In these aforementioned sections, it is explained that for straight sections of utility lines, non-tensile resistant socket-spigot joints are applied. Contrary to the aforementioned assumption of a continuous system, these joints prevent the full transfer of normal stresses and bending moments over the full length of a utility line.

According to Hetényi (1946), a certain length of influence (L_{infl}) can be defined for a boundary condition, given in equation 7.10.

$$\begin{aligned} L_{infl} &= \frac{\pi}{\beta} \\ L_{infl} &= \pi \cdot \sqrt[4]{\frac{4 \cdot E \cdot I}{K_h}} \end{aligned} \tag{7.10}$$

It follows from this definition of the influence length that it is independent of the magnitude of the boundary condition itself, i.e. the magnitude soil displacement following from the quay wall displacement's. In general, utility line segments have a length of 6 m (Saint-Gobain Pipe Systems, 2006). If it is assumed that the quay wall displacements location corresponds to the location of the utility line's center point, full deformation of the utility line has to occur within a distance of 3 m on either side of the displacement (equal to half of the pipe segment's length). Thus, in order for the continuum assumption of the analytical to be valid, the influence length has to be less than 3 m. For utility lines for which the influence is less the predetermined value of 3 m, the maximum angular deflections, -bending moments, and -shear forces found using the analytical model are expected to be valid. For utility lines with larger influence lengths, it is expected that only the maximum angular deflections found using the analytical model are deemed valid. It follows from equation I.9 and the graph in figure I.2 of appendix I that the influence length is proportional to the outer diameter of an utility line.

7.5.2. Applicability of Euler-Bernoulli beam model

As said before, the utility line is modelled as an Euler-Bernoulli beam, either with or without a Winkler foundation (distributed spring). The applicability of this beam model is limited to small displacements, i.e. angular deflections up to 5^o, and relatively slender structures (Erochko, 2020). For utility lines, the slenderness is defined by the line's ratio of the segment length ($L_{segment}$) over their outer diameter (D_o) as given in equation 7.11.

$$\frac{L_{segment}}{D_o} > 10 \tag{7.11}$$

Thus, if this aforementioned ratio is larger than 10, the utility line can be regarded as slender. As in general utility line segments are equal to 6 m, for $D_{outer} < 600\ mm$ the assumption of an Euler-Bernoulli beam model is valid. It follows from section 3.2 In the inner city, diameters of utility lines up to 800 mm are found, thus their representation as an Euler-Bernoulli beam is less valid. For these less slender utility lines, a more accurate but also more complex model would be a Timoshenko beam. In this beam model, shear forces are taken into account as well, additionally to bending forces (Labuschagne et al., 2009).

7.5.3. Applicability of the Winkler model

The representation of the soil-utility line interaction as a distributed spring, i.e. the Winkler foundation, can be considered to be a relatively simple model. According to A (2009), the main shortcoming of the Winkler foundation is the negligence of soil shear stresses in this model, as he says: "The model implies that a point undergoes vertical deformation independently of other adjoining points". Note that his research considered vertical displacements, although the same quote applies to horizontal displacement. However, the use of the Winkler foundation has been widely accepted in the engineering world, especially in first order analytical models. An examples being the research done by Rajani et al. (1996), regarding potable water pipe-soil interaction in Canadian cities. Thus, the use of the Winkler model is deemed valid for this study as well.

7.5.4. Displacement over length of quay wall

From figure 7.7 it follows that the quay wall displacement is modelled to occur abruptly over its length. In reality, quay wall displacement can occur more gently over the length of the quay wall, instead of in the binary manor as represented in the aforementioned figure. Said gentle quay wall displacement is represented in figures 7.11 and 7.12, providing a top- and cross-sectional view respectively. By doing so, the effect of a more gentle displacement over the length of the quay wall is discarded.

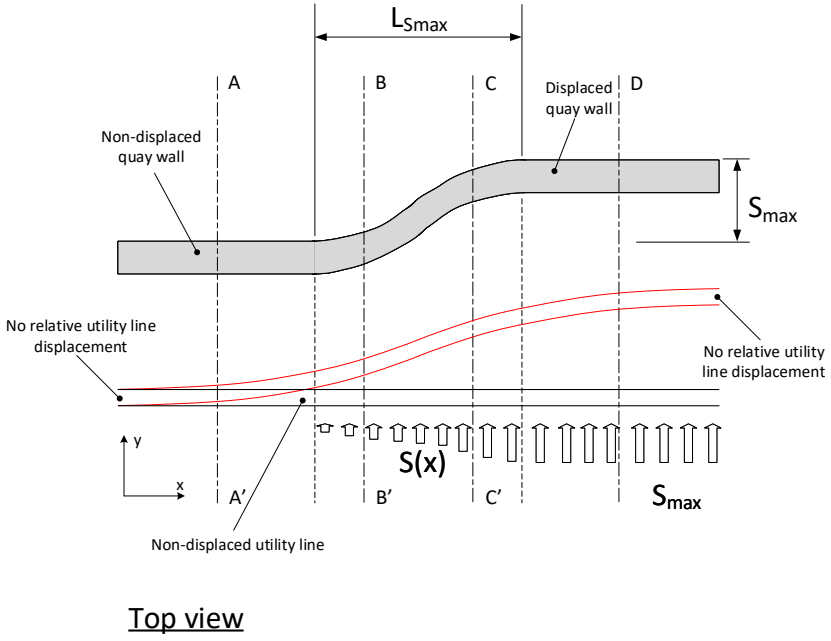

Figure 7.11: Relative displacement of utility line at the location of gentle quay wall displacement, top view.

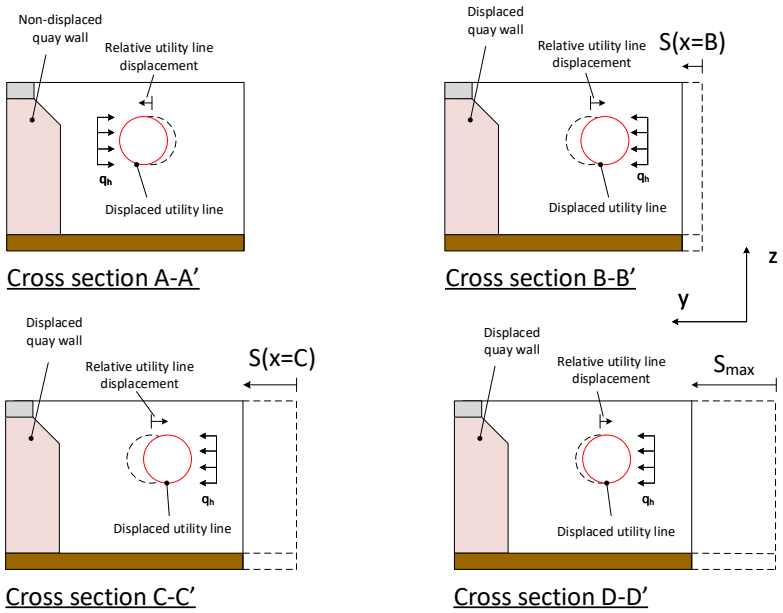

Figure 7.12: Relative displacement of utility line at the location of gentle quay wall displacement, cross-sectional view.

As can be seen by comparing the figures representing abrupt quay wall displacement (figures 7.7 and 7.8) and the figures representing gentle quay wall displacement (figures 7.11 and 7.12), gentle displacements result in a lower relative displacement between utility line and soil, over the length of the quay wall. As explained in section 7.3, its this relative displacement which results in soil stresses acting on utility lines, capable of resulting in leakages. An increase of the length over which the gentle increase of quay wall displacement occurs (L_{Smax} in figure 7.11), leads to a reduction of the relative displacement between utility line and soil body. Thus gentle quay wall displacement over its length results in a more favorable situation than abrupt quay wall displacements.

In order to determine the validity of the assumption of abrupt quay wall displacement, a discretized model was implemented. In this model, the quay wall was split up over the length L_{Smax}. In term, each section was subjected to a portion of S_{max}, mimicking the effect of a more gentle, continuous quay wall displacement. Various GCI potable water pipes were tested for lengths L_{Smax} ranging from 0.5 up to 2.5 m, and the results of this model were compared to the regular model with abrupt quay wall displacement. See appendix J for a full discussion of said test of this assumption of abrupt quay wall displacement. In table 7.2, the reduction of the maximum angular deflection is provided for various outer diameters and lengths L_{Smax}, compared to the regular model containing abrupt quay wall displacement.

Table 7.2: Reduction of maximum angular deflection compared to assumption of abrupt quay wall displacement, for GCI pipes.

	D_o $[mm]$				
L_{Smax} $[m]$	100	200	300	400	500
0.5	8%	3%	2%	1%	1%
1.0	22%	9%	6%	3%	3%
1.5	36%	16 %	10%	5 %	4%
2.0	47%	24%	14%	10%	7%
2.5	55%	31%	20%	14%	10%

From table 7.2 it follows that utility lines with higher bending stiffnesses are relatively accurately represented by abrupt quay wall displacement. This can concluded from the fact that the reduction of angular deflection of GCI pipes with an outer diameter of 500 mm is only 10% for an L_{Smax} equal to 2.5 m, while for this same L_{Smax} the 100 mm pipe shows a reduction of 55%. GCI potable water pipes have the lowest bending stiffness in general of all utility lines tested in this study, thus for similar utility line diameters of other materials, the reduction will be less for all output values.

The angular deflection is a significant factor in determining if a utility line is susceptible to leakages. Thus the fact that for increasing quay wall displacement (L_{Smax}) over a length of 1 m the reduction of the smallest tested utility line (100 mm), the reduction of the angular deflection is only 22%, it is deemed sufficient to assume the abrupt quay wall displacement instead of discretized quay wall displacement. However, if L_{smax} surpasses about 2 m, it has to be noted that the assumption of abrupt quay wall displacement is less valid, especially for smaller utility lines.

7.6. Input parameter values for analytical model

In this section, the various values of the parameters used in the analytical model are listed. For each parameter, it is discussed how this value and its variations are determined. These listed parameters are used in both model cases, i.e. quay wall deformation over longer length and localized quay wall displacement.

- **Percentage of equilibrium horizontal bearing capacity**
  Due to the assumption of a bi-lineal spring stiffness as explained in section 7.4.1, each run of the model is carried out using various percentages of the soil's equilibrium horizontal bearing capacity, starting at 20% q_{he} and ranging up to 100% q_{he}, with increasing steps of 20%. As explained before, this also has an effect on the maximum allowable soil deformation and thus the elastic and plastic behaviour of the soil in the model.

- **Coverage of utility line** (H)

  - **Coverage of potable water pipes**
    As told in section 3.2.2, the coverage for potable water pipes is set by Waternet at 0.8 m, and thus this value is used for all runs of the model for potable water pipes.

  - **Coverage of sewer system**
    It follows from the data of the kadaster that the sewer systems in the vicinity of quay walls are located at a depth ranging from about NAP +0 m to NAP −4 m. Following from all available sewer systems in the vicinity quay walls, the mean value of the depth was calculated to be equal to NAP −1.03 m. As in general the top of structure of inner-city quay walls in Amsterdam are located at NAP +1 m, the coverage of the sewer system is set at 2.03 m. By doing so, the lowest point of the sewer pipe is almost equal to the quay wall floor used in the model (which is located at a depth of 3 m relative to surface level), as the largest diameter tested for concrete sewer pipes has an outer diameter of 1000 mm.

- **Utility line's material modulus of elasticity** (E)
  As discussed in section 3.2, three materials are mainly used for the construction of potable water pipes. For each of which the modulus of elasticity is discussed below:

  - **Modulus of elasticity of potable water pipes**

    - **GCI**
      The modulus of elasticity depends on the type of GCI used for potable water pipes in the inner-city of Amsterdam. As these exact material properties are unknown, a mean value is used, which is set at 110 GPa (SN Cast Iron, 2018a). GCI is known for brittle failure, as the yield strength of the material is close to its ultimate strength.

    - **NCI**
      Similarly to GCI, the material properties of NCI used for the potable water pipes in Amsterdam are not well known. However, the modulus of elasticity is fairly constant for all types of NCI, and is set at 170 GPa (SN Cast Iron, 2018b). NCI shows a much more ductile kind of failure than GCI. Thus, it has to be noted that loading up to failure of NCI is not perfectly represented in the analytical model, as the model is based on elastic deformation.

    - **Steel**
      The modulus of elasticity of steel is fairly constant, regardless of the type of steel, equal to 210 GPa (MachineMFG, n.d.). Like NCI, steel shows a ductile kind of failure.

  - **Modulus of elasticity of concrete sewer pipes**
    As said in section 3.3.1, mainly concrete is used for the upper- and lower sewer system. It is assumed that the sewer pipes located in the backfill soil behind the quay wall are not founded on piles, but use the surrounding soil as a foundation. Therefore, it is assumed that these concrete sewer pipes are not

reinforced. Additionally, it is assumed that lower grades of concrete are used for the construction of sewer pipes, i.e. concrete grades of C20/25 up to C35/45. According to standard EN 1992, the modulus of elasticity for these grades of concrete is in the range of 30 GPa (CEN, 2004).

- **Outer diameter of utility line** (D_o)
  See figure 7.13 for the definition of the outer diameter of a utility line.
  - **Potable water pipes**
    It follows from data obtained via the Kadaster that the outer diameters of potable water pipes in the vicinity of the quay walls inner-city of Amsterdam range from about 100 mm up to 800 mm. Thus, for all materials, these diameters are all used as input for the model, with steps of 100 mm.
  - **Concrete sewer system**
    From the same data obtained via the Kadaster, it follows that the outer diameters of the majority concrete sewer systems in the vicinity of the quay walls of the inner-city of Amsterdam range from 300 mm up to 1000 mm

- **Thickness of utility line** (t)
  The pipe thickness corresponding to the diameters of potable water pipes are determined using known thicknesses of the corresponding material type (Walraven, 2015). For the concrete sewer pipes these are determined using data obtained via De Hamer (n.d.). The dimensions of all utility line materials are given in table 7.3. See figure 7.13 for the definition of the thickness of a utility line.

Table 7.3: Thickness of utility lines corresponding to the material type.

D_o $[mm]$	$t[mm]$		
	GCI and NCI	**Steel**	**Concrete**
100	3.13	3.33	-
200	4.88	5.71	-
300	5.88	6.82	41.18
400	7.55	8.70	49.46
500	8.77	10.87	57.74
600	9.68	12.50	66.02
700	10.61	14.00	74.30
800	11.76	15.38	82.58
900	-	-	90.86
1000	-	-	100

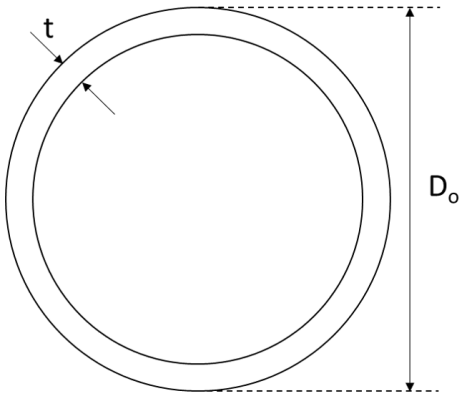

Figure 7.13: Cross-section of a utility line, depicting its outer diameter and thickness.

- **Effective weight of the soil** (γ')
  As defined in appendix H, the effective weight of the soil is set at 16 kPa

- **Angle of internal friction of the soil** (ϕ)
  Again, as defined in appendix H, the angel of internal friction of the soil is set at 30^o.

- **Quay wall displacement** (S_{max})
  The input of the quay wall displacement ranges from 20 mm up to 100 mm, increasing with steps of 20 mm. This deformation is based on the displacements as seen in Haarlem during the quay wall inspection as explained in appendix C (Witteveen+Bos, 2015). It follows from the PLAXIS 2D model that soil displacements follow the displacement of the quay wall, discussed in section 7.2.

- **Length over which quay wall displacement occurs** (l)
  The length over which quay wall displacement occurs varies from local displacement to displacement over an assumed infinite length. Based on these types of displacement, two distinct models have been formulated: quay wall displacement over longer length and localized quay wall displacement, discussed in sections 7.9 and 7.10 respectively. As follows, for the first model the length over which quay wall displacement occurs is not an input parameter. For the second model, the utility line deformation is tested for quay wall displacements over a length of 1, 3, and 7 m.

7.7. Model output

The model produces three outputs which are used to determine if a utility line is susceptible to leakage, in accordance with the discussion of failure mechanisms (provided in section 3.4). These three outputs are as follows:

- **Angular deflection of the utility line**
  In the model, the angular deflections of the utility line ($\theta(x)$) are found by taking the derivative of the deformation relative to the length. For both cases of the model, the magnitude of the maximum angular deflection is extracted. See equation 7.12 for this relation.
- **Bending moments acting on the utility line**
  In term, the bending moments acting on the utility line ($M(x)$) are found by taking the derivative of the angular deflection relative to the length, i.e. the second derivative of the deformation, and multiplying it by the materials model of elasticity and cross-sectional moment of inertia, i.e. the utility line's stiffness. See equation 7.13 for this relation.
- **Shear force acting on the utility line**
  The final output of the model are the shear forces acting on the utility line ($V(x)$), found by taking the derivative of the bending moment relative to the length, i.e. the third derivative of the deformation. See equation 7.14

$$\theta(x) = \frac{d}{dx} y(x) \tag{7.12}$$

$$M(x) = -E \cdot I \cdot \frac{d^2}{dx^2} y(x) \tag{7.13}$$

$$V(x) = -E \cdot I \cdot \frac{d^3}{dx^3} y(x) \tag{7.14}$$

7.8. Formulation of criteria for utility line leakage

In this section, the criteria for potable water pipe leakage are formulated for the various ranges of input parameters parameters as these were discussed in section 7.6. Section 7.2 provides the basis for the assumption of binary soil body displacement behind quay wall displacement. Therefore, the distance in lateral direction between the utility line and quay wall does not impact the utility line displacement, either the soil body in which the utility line is embedded deforms or does not deform. It follows from the limitations given in section 7.5 that the reliability of the analytical model's output mainly depends on two the outer diameter of the utility lines. Additionally, as discussed in section 7.6, the material properties and the failure modes of the most common potable water pipes in the inner-city of Amsterdam (GCI, NCI, and steel) and sewer systems (concrete) vary. Thus, the criteria for leakage are defined as resulting from utility line diameters and material properties. Note that the leakage criteria of utility lines are dependent on utility line deformation or derivatives of said deformation. Naturally, an increase of the deformation results in an increase of leakage, as larger leakages are able to form.

7.8.1. Smaller utility lines

Smaller utility lines are defined as lines for which the influence length is less than half the length of a typical utility line segment, i.e. $L_{infl} < 3\ m$. The definition of utility lines is given in section 7.5. Note that the influence length depends on most of the parameters used in the model. However, for utility lines in equal circumstances, the influence length is proportional to the outer diameter. The criteria for utility line leakage of smaller utility lines are discussed below:

- **Leakage due to exceedance of allowable angular deflection**
  As mentioned in section 3.2.4 and 3.3.3, the non-tensile resistant socket-spigot joints used for utility lines are able to cope with angular deflections up to 1.5^o. Therefore, a utility line is deemed susceptible to leakage if this value is this threshold is surpassed, regardless of its material.
- **Leakage due to exceedance of maximum bending moment**
  To determine if the maximum bending moment is surpassed for each combination of quay wall deformation, utility line material and -diameter, a unity check (UC_{moment}) is executed as represented in equation 7.15. If the UC is larger than 100%, the occuring maximum bending moment surpasses the allowable bending moment of the utility line.

$$UC_{moment} = \frac{\sigma_M}{\sigma_{max,mat}} \tag{7.15}$$
$$\sigma_M = \frac{M \cdot z}{I}$$

In which:

σ_M	Maximum compression- and tension stress occurring in the utility line's cross-section due to the maximum moment;
$\sigma_{max,mat}$	Maximum allowable tensile stress of a material;
M	Maximum bending moment occurring in the utility line due to quay wall deformation;
z	Distance from the neutral axis to the outer fibre of the utility line, i.e. equal to half of the outer diameter;
I	Cross-sectional moment of inertia of the utility line.

- **Potable water pipes**
  It follows from the failure mechanisms of potable water pipes of steel, NCI and GCI given in section 3.4.3, that due to the relatively smaller cross-sectional moment of inertia of smaller diameter pipes, circumferential cracking is the most likely failure mechanism of these metallic pipes, and thus the most likely cause of leakage due to exceedance of the maximum allowable bending moment of said pipes. For the various materials of potable water pipes, the maximum allowable stress due to bending moment is defined as the stress at which plastic deformation occurs, i.e. the ultimate tensile strength. In reality, deformations might occur before reaching said ultimate tensile strength.
  - **GCI**
    The maximum allowable tensile stress of GCI ($\sigma_{max,GCI}$) is set at 360 MPa (SN Cast Iron, 2018a). Note that this value is a mean value for the material in general, in reality this depends on the actual type of GCI used in the inner-city of Amsterdam. As said in section 7.6, of all metallic materials used for potable water pipes, GCI shows the most brittle failure. The compression strength of GCI is higher than the tensile strength, with a mean value of 840 MPa. Thus failure due to compression before tension following from bending moments is highly unlikely.
  - **NCI**
    The maximum allowable tensile stress of NCI ($\sigma_{max,NCI}$) is noticeably higher than GCI, and set at 575 MPa (SN Cast Iron, 2018b). Similarly to the material properties of pipes made of GCI, the exact material properties of NCI potable water pipes used in the inner-city of Amsterdam are unknown. Again, the compression strength of this material is significantly higher than its tensile strength, with a mean value of 925 MPa. As said in section 7.6, NCI follows a ductile failure path.
  - **Steel**
    The maximum allowable tensile stress of steel ($\sigma_{max,steel}$) is again heavily dependable of the type of steel used for the potable water pipe. However, it is assumed that not the highest grades of steel are used for this application. According to Walraven (2015), ST37 is generally used for the construction of pipelines, which has a mean maximum tensile strength 435 MPa (ANSON STEEL, n.d.). For compression, the maximum allowable stress is of the same magnitude. Steel follows a ductile failure path, as said in section 7.6.
- **Concrete sewer systems**
  From the model of case 1 it follows that the influence length of all tested concrete sewer systems, the influence length is larger than half the typical length of a utility line segment, i.e. $L_{infl} > 3\ m$. Therefore, no maximum allowable stress is provided resulting from bending moments.

- **Leakage due to exceedance of maximum shear force**
  Similarly to the check for exceedance of maximum allowable bending moment, a unity check (UC_{shear}) is defined in equation 7.16, which determines that utility line leakage due to shear force occurs if it surpasses 100%.

$$UC_{shear} = \frac{\tau_V}{\tau_{max,mat}} \tag{7.16}$$
$$\tau_V = 2 \cdot \frac{V_{max}}{A}$$

In which:

τ_V	Maximum shear stress occurring in the utility line's cross-section due to the maximum shear force (approximation for thin-walled elements, i.e. $D_o >> t$);
$\tau_{max,mat}$	Maximum allowable shear stress of the material;
V_{max}	Maximum shear force occurring in the utility line due to quay wall deformation;
A	Cross-sectional area of the utility line.

– **Potable water pipes**
Although it is stated in 3.4.3 that for smaller diameters failure due to shear force is less likely than a bending moment, the potential for leakage due to this is still checked. For the various materials of potable water pipes, the maximum allowable shear stress is given as follows:

◇ **GCI**
Similarly to the maximum allowable tensile stress, due to the actual material properties of the potable water pipes in the inner-city of Amsterdam being unknown, a mean value of the maximum allowable shear stress ($\tau_{max,GCI}$) is used and set at 285 MPa (SN Cast Iron, 2018a).

◇ **NCI**
For the same aforementioned reasoning as for GCI potable water pipes, a mean value of the maximum allowable shear stress ($\tau_{max,NCI}$) is used and set at 518 MPa (SN Cast Iron, 2018b).

◇ **Steel**
The mean value of the shear stress of ST37 steel ($\tau_{max,steel}$) used for potable water pipes is set at 345 MPa (MachineMFG, n.d.).

- **Concrete sewer systems**
Similary to the leakage due to exceedance of maximum bending moment, from the model of case 1 it follows that the influence length of all tested concrete sewer systems, the influence length is larger than half the typical length of a utility line segment, i.e. $L_{infl} > 3\ m$. Therefore, no additional maximum shear stress is provided.

7.8.2. Larger utility lines

Following for the reasoning of the definition of smaller utility lines, larger utility lines are defined as lines with influences greater than half the typical length of a line segment, i.e. $L_{infl} > 3\ m$. The criteria for failure of said larger utility lines are given below.

- **Leakage due to exceedance of maximum angular deflection**
For the similar reason as given in section 7.8.1, the criteria for leakage is set at a maximum angular deflection of 1.5^o.

- **Leakage due to exceedance of maximum bending moment and -shear force**
In section 3.4.3, it is formulated that the failure mechanisms for larger diameters are more linked to shear forces than bending moments, although both can cause leakages. However, as discussed in section 7.5, one of the limitations of the analytical model is the length of influence of the quay wall displacement being proportional to the outer diameter of potable water pipes. Thus, for these larger diameters, the outputs of the model regarding bending moments and shear forces are deemed too unreliable and not further taken into account as criteria for utility line leakage.

7.9. Case 1: quay wall displacement over greater length

In this model, it is assumed that a large section of a quay wall deforms in the direction of the channel, while the other section remains stationary. A real life example might be the connection between two types of quay walls, with one of these two being more susceptible to displacement than the other. First, in section 7.9.1, the model is explained

for the case if the deformation at any point of the utility line is larger than the maximum allowable soil deformation. It is found that this situation occurs if the quay wall displacement is larger than 2 times the maximum allowable soil deformation ($S_{max} > 2 \cdot y_{s,max}$). Next, in section 7.9.2, the opposite case is discussed: thus if $S_{max} \leq 2 \cdot y_{s,max}$.

7.9.1. Quay wall displacement over greater length: utility line deformation larger than maximum allowable soil deformation

This case is modelled using 4 differential equations, separated by the interfaces located at $x = a$, $x = 0$, and $x = b$. See figure 7.14 for an overview of the model. The utility line is modelled using a Winkler foundation ranging from negative infinity up to $x = a$. Up to this interface, the displacement of the utility line is less than the maximum allowable soil deformation. From x ranging from a up to 0, the utility line's displacement is greater than the maximum allowable soil deformation, resulting in the soil acting on the utility line in the form of the horizontal equilibrium bearing capacity, as that is the maximum force the soil is able to act on the utility line. On this domain, the utility line is modelled as an Euler-Bernoulli beam.

The model shows a double mirrored symmetry at the interface location $x = 0$. Starting from this interface up to positive infinity, the soil is modelled as to have displaced an S_{max} amount. Ranging from interface $x = 0$ up to interface $x = b$, the absolute utility line's displacement is greater than the soil displacement S_{max}, and from interface $x = b$ up to positive infinity, the absolute utility line's displacement is less than said soil displacement. Similarly to the domain from minus infinity up to interface $x = 0$, the utility line is modelled using an Euler-Bernoulli beam and a Winkler foundation respectively. The location of $x = a$ (and thus, due to the symmetry, also $x = -b$) is found using iteration. For all domains, an overview of the model parameters, their EoM's and their solutions are provided in equations I.10, I.11, and I.12 respectively.

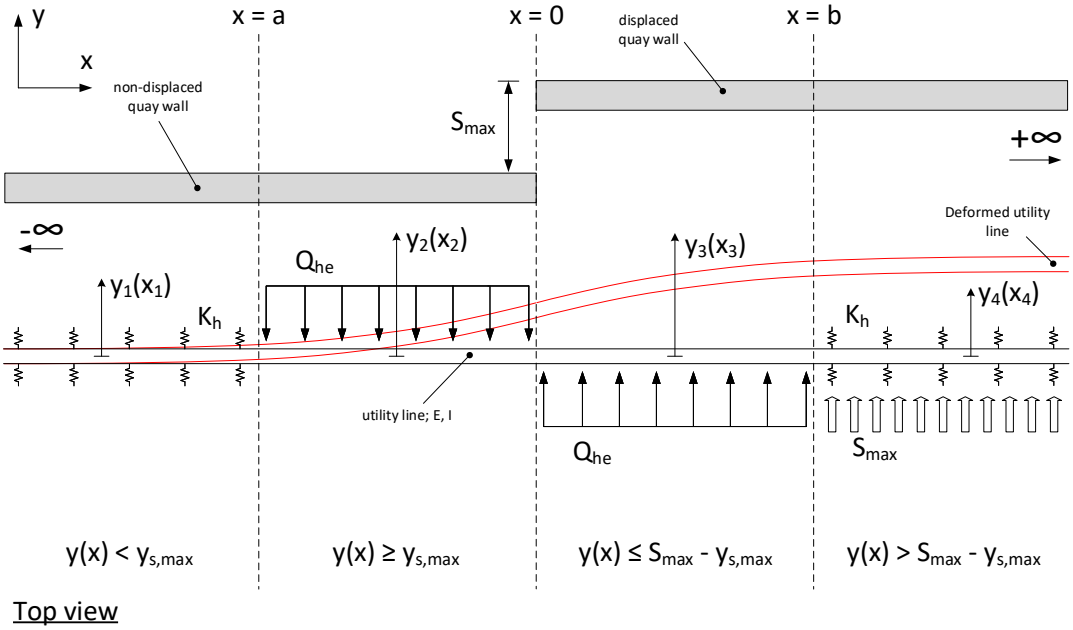

Figure 7.14: Model of the case: quay wall displacement over greater length, utility line displacement larger than maximum allowable soil deformation.

7.9.2. Quay wall displacement over greater length: utility line displacement smaller than maximum allowable soil deformation

In this model case the limit of the elastic foundation by which the soil-utility interaction is modelled is never reached, as the displacement of the utility line never surpasses the maximum allowable soil deformation. Therefore, both on the domain ranging from negative- as well as from positive infinity towards $x = 0$, the utility line can be modelled as a Winkler foundation. As only the soil is displaced on the right domain ranging from $x = 0$ towards positive infinity, the model contains two differential equations with an interface at $x = 0$. See figure 7.15 for an overview of the model.

For all domains, an overview of the model parameters, their EoM's and their solutions are provided in equations I.13, I.14, and I.15 respectively.

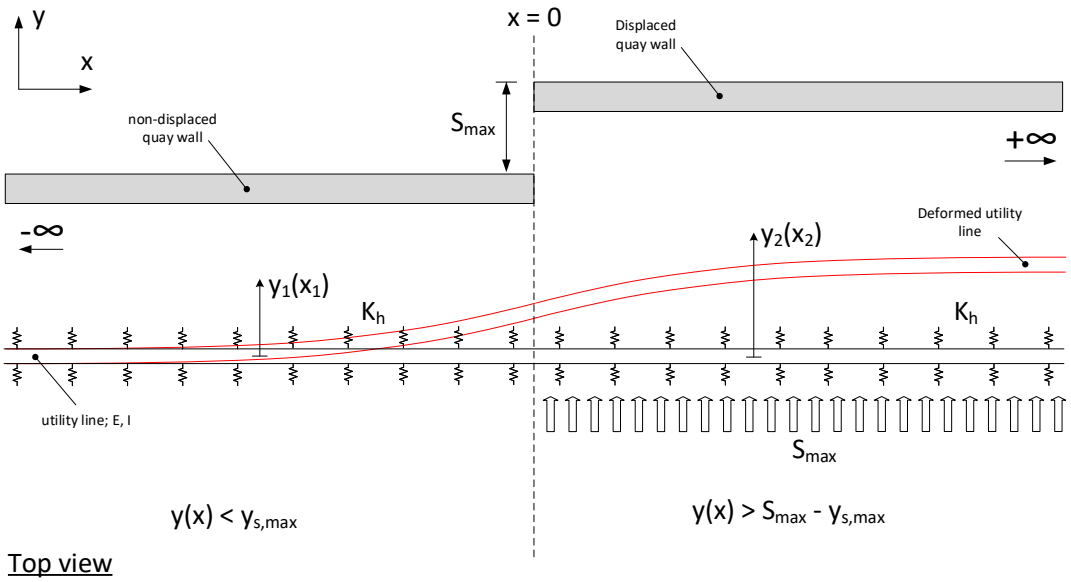

Figure 7.15: Model of the case: quay wall displacement over greater length utility line displacement smaller than maximum allowable soil deformation.

7.10. Case 2: localised quay wall displacement

Contrary to the case of quay wall displacement over a greater length as explained in section 7.9, in this case a clear localised quay wall displacement is modelled. A real life case for this situation is the quay wall displacement as seen during the quay wall inspection in Haarlem (Witteveen+Bos, 2015). Four variants of this model are discussed in sections 7.10.1, 7.10.3, 7.10.2 and 7.10.4, for all of which their validity depend on the magnitude of utility line displacement relative to the maximum allowable soil deformation.

7.10.1. Loc. quay wall displ: utility line displacement smaller than maximum allowable soil deformation over full length

This model case describes utility line displacement due to localized quay wall displacement for the situation in which the relative displacement of the utility line never surpasses the maximum allowable soil deformation (see figure 7.16). Thus, this model bears a resemblance with the model as discussed in section 7.9.2 and therefore the utility line is modelled soley as a Winkler foundation using 3 differential equations with 2 interface conditions at $x = a$ and $x = b$. However, the length over which the quay wall displacement occurs might not be sufficient to deform the section of the utility line between coordinates $x = a$ and $x = b$ up to the quay wall displacement S_{max}. If the length over which the quay wall displaces becomes sufficiently large ,this model is equal to the aforementioned model for quay wall displacement over greater length with relative utility line displacements less than the maximum allowable soil deformation. For all domains, an overview of the model parameters, their EoM's and their solutions are provided in equations I.16, I.17, and I.18 of appendix I respectively.

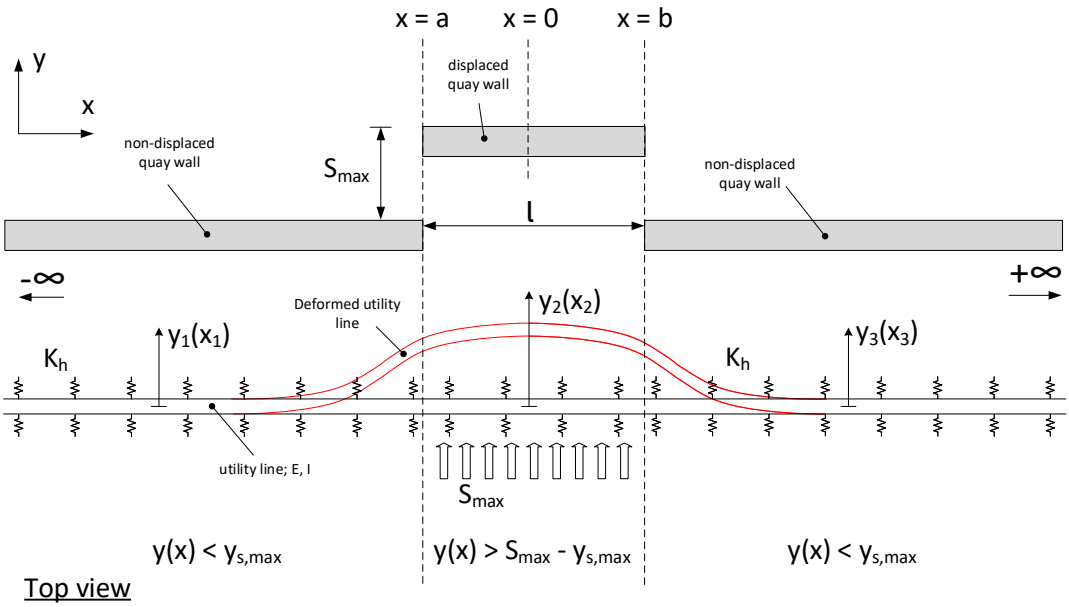

Figure 7.16: Model of the case: localized quay wall displacement, utility line displacement smaller than maximum allowable soil deformation over full length

7.10.2. Loc. quay wall displ: utility line displacement only larger than maximum allowable quay wall displacement in displaced soil section

This model is valid if, for the domains ranging from negative- and positive infinity up to the local deformation of the quay wall, the deformation of the utility line is less than the maximum allowable soil deformation, while the contrary is valid in the utility line section located behind the deformed quay wall. This results in a model consisting of 3 differential equations, with interfaces at $x = a$ and $x = b$. The outer most domains are modelled as Winkler foundations. As the relative displacement of the utility line in the domain ranging from $a \leq x < b$ is larger than the maximum allowable soil deformation, this domain is modelled as an Euler-Bernoulli beam. See figure 7.17 for an overview of the model. For all domains, an overview of the model parameters, their EoM's and their solutions are provided in equations I.19, I.20, and I.21 of appendix I respectively.

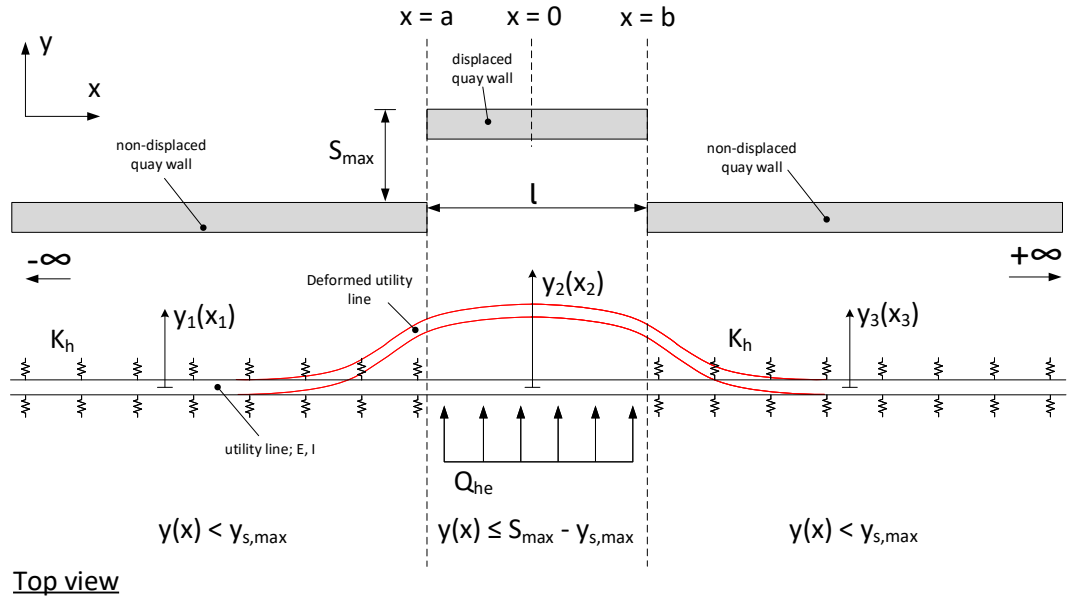

Figure 7.17: Model of the case: localized quay wall displacement, utility line displacement only larger than maximum allowable soil deformation in displaced soil section

7.10.3. Loc. quay wall displ: utility line displacement greater than maximum allowable soil deformation both in displaced soil section as right next to displacement

This case is modelled using 5 differential equations, separated by interfaces at $x = a$, $x = b$, $x = c$ and $x = d$. The localized deformation has a width equal to l. Note that if l becomes sufficiently large, the model is better represented using the model as discussed in section 7.9, thus as a quay wall displacement over greater length. As discussed before, the most outer domains (ranging from negative infinity up to $x < a$ and ranging from $x > d$ up to positive infinity) are modelled using Winkler beams. As the basis for this model is that for a sufficient length from the localized quay wall displacement the quay walls are not deformed, it is assumed that no external forces or displacements acts on these domains. Due to the nature of the case of localized deformation, the model shows a symmetry in $x = 0$. This model is valid if on the domains $a \leq x < b$ and $c \leq x < d$ the utility line displacement is greater than the maximum allowable soil deformation. The location of $x = a$ (and thus, due to the symmetry, also $x = -d$) is found using iteration. See figure 7.18 for an overview of the model. For all domains, an overview of the model parameters, their EoM's and their solutions are provided in equations I.22, I.23, and I.24 of appendix I respectively.

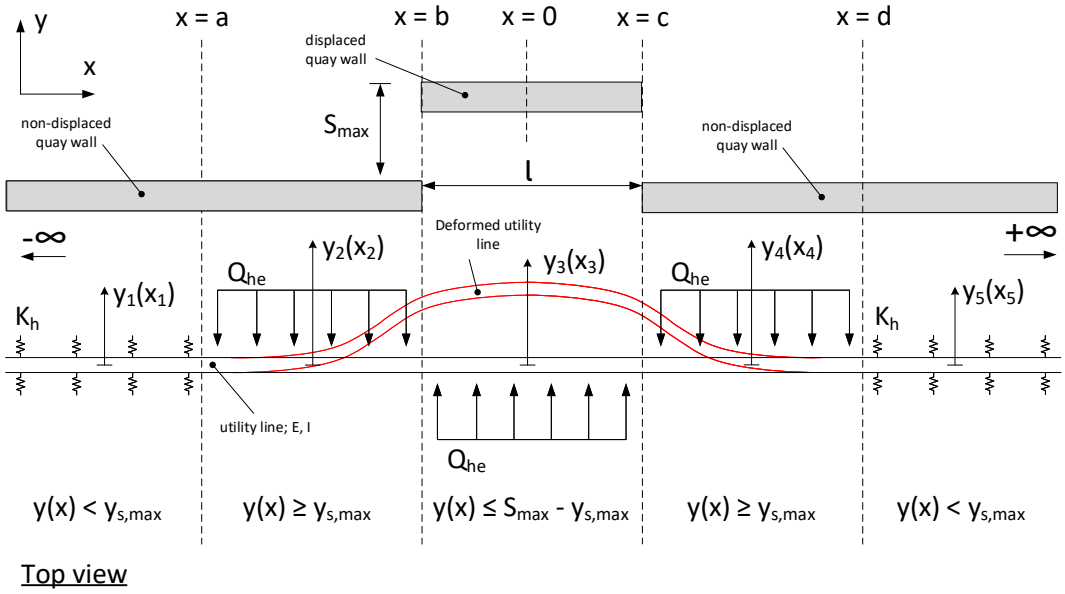

Figure 7.18: Model of the case: localized quay wall displacement, utility line displacement greater than maximum allowable soil deformation both in displaced soil section as right next to displacement

7.10.4. Loc. quay wall displ: utility line displacement partially smaller than maximum allowable soil deformation in displaced soil section

In this model, the combination of the length over which the quay wall displaces and the magnitude of said displacement result in a section of soil behind the displaced quay wall for which its deformation is smaller than the maximum allowable soil deformation (see figure 7.19). Therefore, for this section of utility line (located between the coordinates $x = c$ and $x = d$), a Winkler foundation can be assumed. The model bears a resemblance to the model of quay wall displacement over longer length, with relative utility line displacements larger than the maximum allowable soil deformation, as discussed in section 7.9.1. Similarly the first model case of localized quay wall displacement as discussed in section 7.10.1, if the length over which the quay wall displaces becomes sufficiently large, these models of localized quay wall displacement and quay wall displacement over longer length are similar. However, the length over which quay wall displacement occurs might not be sufficiently large to displace the utility line up to the displacement of the quay wall (S_{max}). Therefore, the distance between coordinate $x = a$ and $x = b$ is not by definition equal to the distance between coordinate $x = b$ and $x = c$, contrary to the model for quay wall displacement over greater length. The locations of these coordinates are both found using iteration. Due to the symmetry in $x = 0$, this model is represented using 4 differential equations, with the additional boundary conditions at $x = 0$ that both the angular deflection and shear force are equal to zero, which follows from the rules for symmetry in structures as presented by Hartsuijker and Welleman (2004)). For all domains, an overview of the model parameters, their EoM's and their solutions are provided in equations I.25, I.26, and I.27 of appendix I respectively.

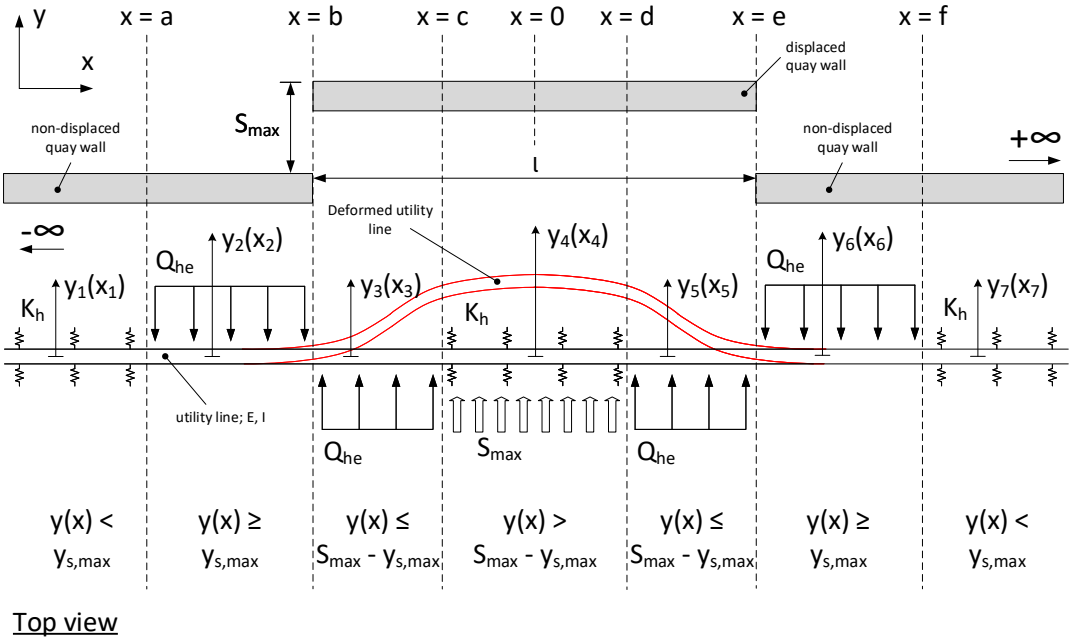

Figure 7.19: Model of the case: localized quay wall displacement, utility line displacement partially smaller than maximum allowable soil deformation in displaced soil section

7.11. Overview of critical soil areas

In this section, an overview of the critical area's according to the analytical model are graphically depicted. First, the cross-sectional view is provided in figure 7.20. Next for both quay wall displacement over longer length and localized quay wall displacement, these areas are depicted as a top view in figures 7.21 and 7.22 respectively.

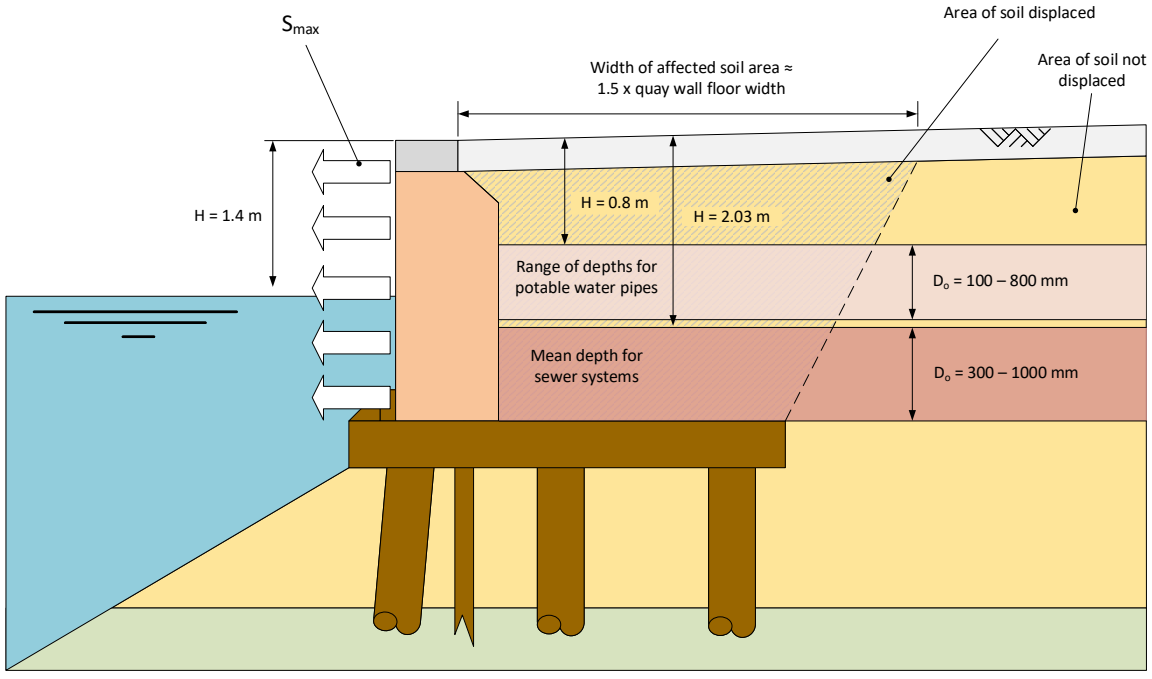

Figure 7.20: Cross section of critical area's for both analytical models.

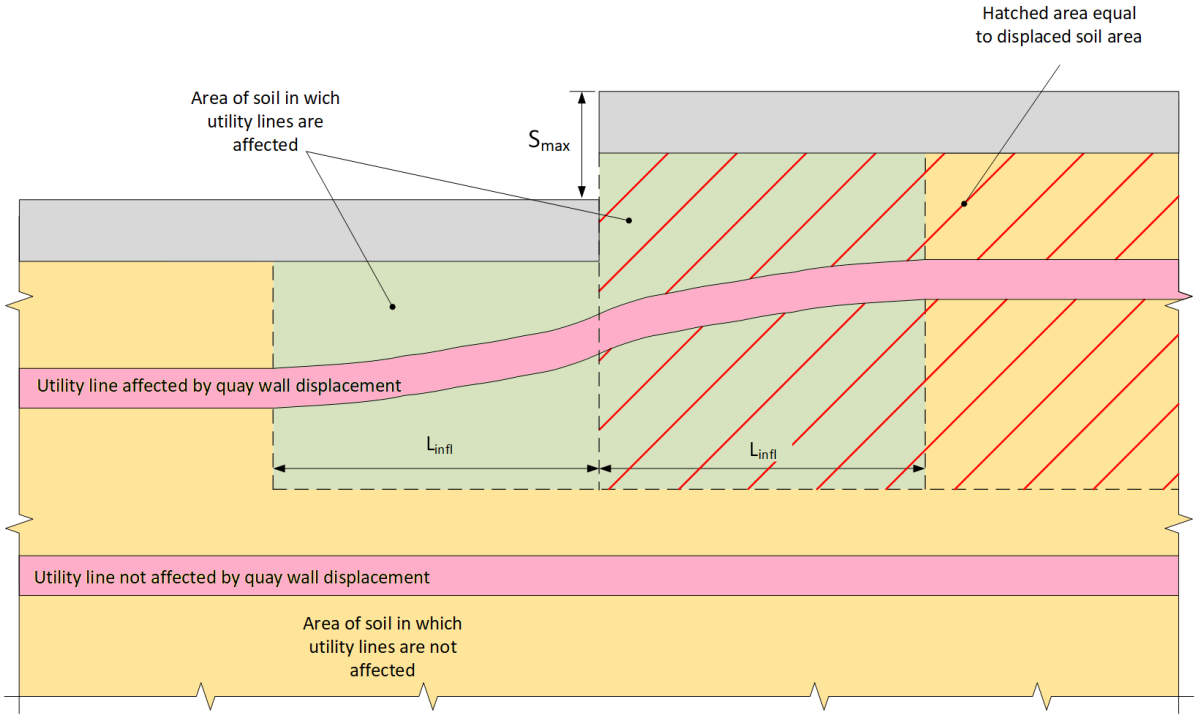

Figure 7.21: Top view of critical areas for quay wall displacement over greater length.

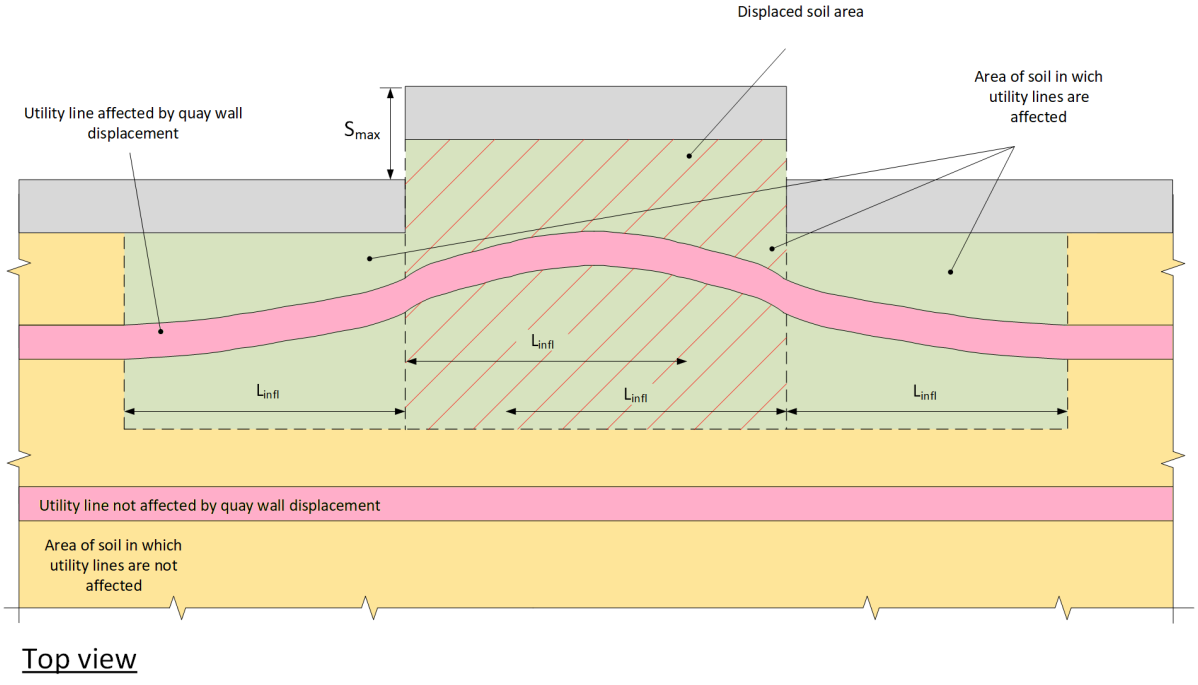

Figure 7.22: Top view of critical areas for localized quay wall displacement.

8

Results analytical model

In this chapter the results of the analytical model are discussed. First, the model result regarding exceedance of maximum allowable angular deflection, -bending moment, and -shear force are discussed in sections 8.1, 8.2, and 8.3 respectively. These concern both the results of the model for quay wall displacement over greater length as well as the model for localized quay wall displacement. Next, the influence of variation in horizontal distributed spring stiffness to the analytical model is discussed in section 8.4. A sensitivity analysis of the model to all parameters is provided in section 8.5. The chapter closes with an overview of the results of the analytical model in section 8.6.

8.1. Utility line leakage due to exceedance of allowable angular deflection

For both the model cases (i.e. the quay wall displacement over greater length and the localized quay wall displacement) the results of the analytical model are provided in this section, in sections 8.1.1 and 8.1.2 respectively.

8.1.1. Model results regarding angular deflection for quay wall deformation over greater length

For each of the utility line types, the mean maximum angular deflection is plotted for the previously discussed range of quay wall deformation. This mean value follows from the previously discussed applied variation of the horizontal distributed spring stiffness in section 7.4.1, which in terms follows from the variation in the percentage of the soil's equilibrium horizontal bearing capacity. The justification for using this mean value is discussed in section 8.4. In every case, the maximum angular deflection occurs at location $x = 0$ in the models represented in figures 7.14 and 7.15.

In figures 8.1a, 8.1b, 8.2a and 8.2b the angular deflection is plotted against the quay wall deformation for the aforementioned outer diameters of GCI, NCI, steel and concrete utility lines respectively. The maximum allowable angular deflection of 1.5^o is highlighted in each graph. In table 8.1, for each material and utility line diameter, the range of quay wall displacement in which said maximum allowable angular deflection is exceeded, is given. As the model is run using discrete values, an exact magnitude of quay wall displacement for which the utility line is susceptible to leakage can not be provided.

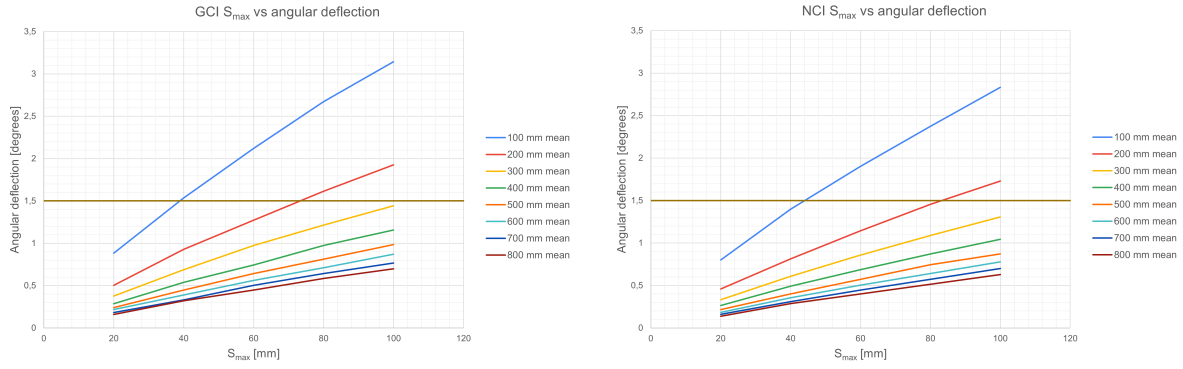

(a) (b)

Figure 8.1: Quay wall deformation plotted against the mean maximum angular deformation of multiple diameters of GCI and NCI utility lines, for quay wall deformation over greater length.

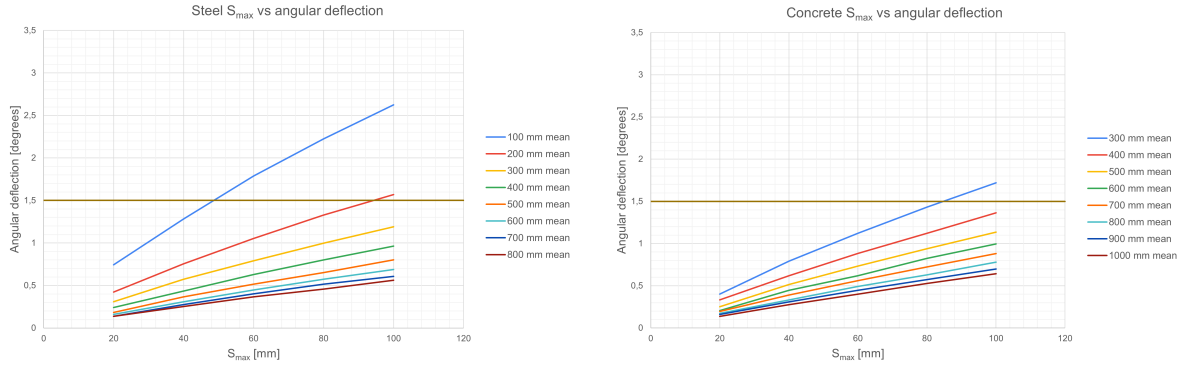

(a) (b)

Figure 8.2: Quay wall deformation plotted against the mean maximum angular deformation of multiple diameters of steel and concrete utility lines, for quay wall deformation over longer length.

Table 8.1: Range of horizontal quay wall displacement in which maximum allowable angular deflection (1.5^o) is surpassed for quay wall displacement over greater length.

D_o $[mm]$	**GCI range** $[mm]$	**NCI range** $[mm]$	**steel range** $[mm]$	**concrete range** $[mm]$
100	$20 < S_{max} < 40$	$40 < S_{max} < 60$	$40 < S_{max} < 60$	-
200	$60 < S_{max} < 80$	$80 < S_{max} < 100$	$80 < S_{max} < 100$	-
300	not surpassed	not surpassed	not surpassed	$80 < S_{max} < 100$
≥ 400	not surpassed	not surpassed	not surpassed	not surpassed

8.1.2. Model results regarding angular deflection for localized quay wall deformation

In figures 8.3, 8.4, 8.5 and 8.6 respectively, the angular deflection of GCI, NCI, steel and concrete utility lines are plotted against the magnitude of quay wall displacement over a length of 1, 3 and 7 m. The maximum allowable angular deflection of 1.5^o is highlighted in each graph, as far as this is relevant. Similary to table 8.1, in table 8.2, for each material and utility line diameter, the range of quay wall displacement in which said maximum allowable angular deflection is exceeded, is given. As also this model is run using discrete values, an exact magnitude of quay wall displacement for which the utility line is susceptible to leakage can not be provided. Additionally, for all materials, runs have been executed for utility line diameters up to the highest utility line diameter for which the maximum value no longer surpassed the 1.5^o threshold. This results in diameters of GCI, NCI and steel potable water pipes ranging up to 400 mm, and concrete sewer pipes ranging up to 500 mm.

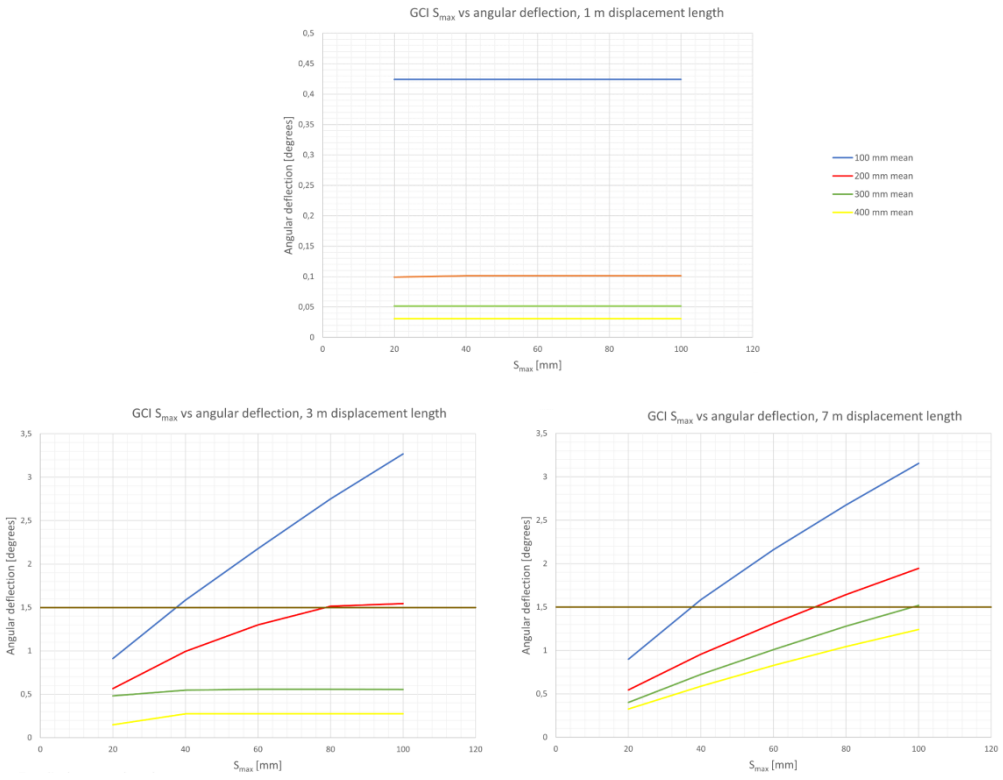

Figure 8.3: Quay wall deformation plotted against the mean maximum angular deformation of multiple diameters of GCI pipes, for localized quay wall displacement over a length of 1, 3 and 7 m.
Note: y-axis is not equal for all graphs.

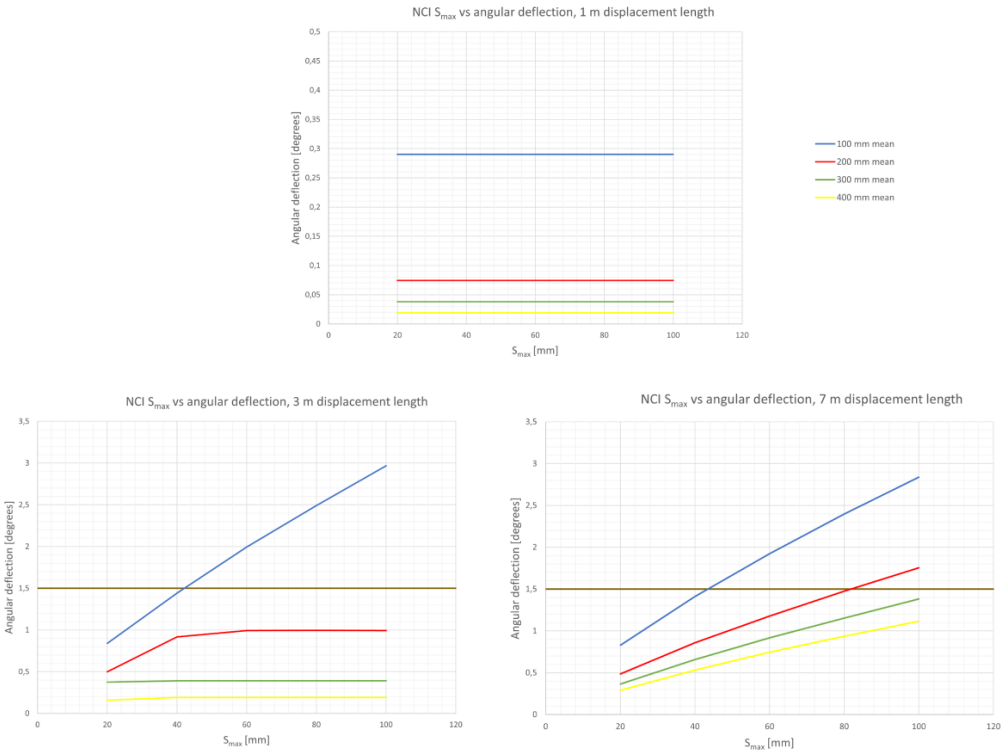

Figure 8.4: Quay wall deformation plotted against the mean maximum angular deformation of multiple diameters of NCI pipes, for localized quay wall displacement over a length of 1, 3 and 7 m.
Note: y-axis is not equal for all graphs.

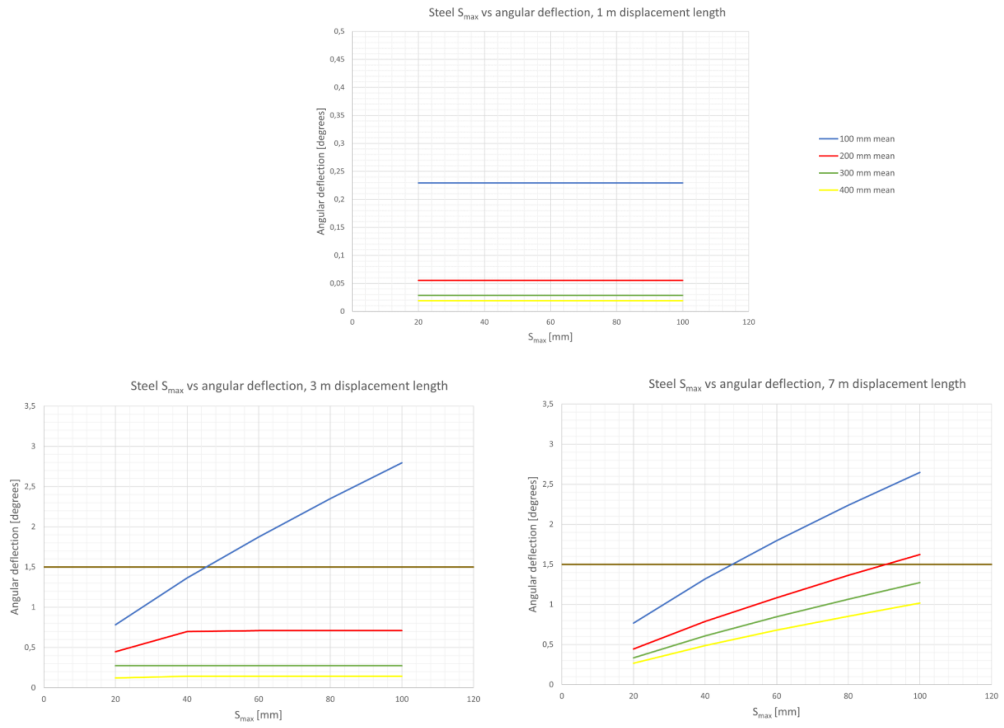

Figure 8.5: Quay wall deformation plotted against the mean maximum angular deformation of multiple diameters of steel pipes, for localized quay wall displacement over a length of 1, 3 and 7 m.
Note: y-axis is not equal for all graphs.

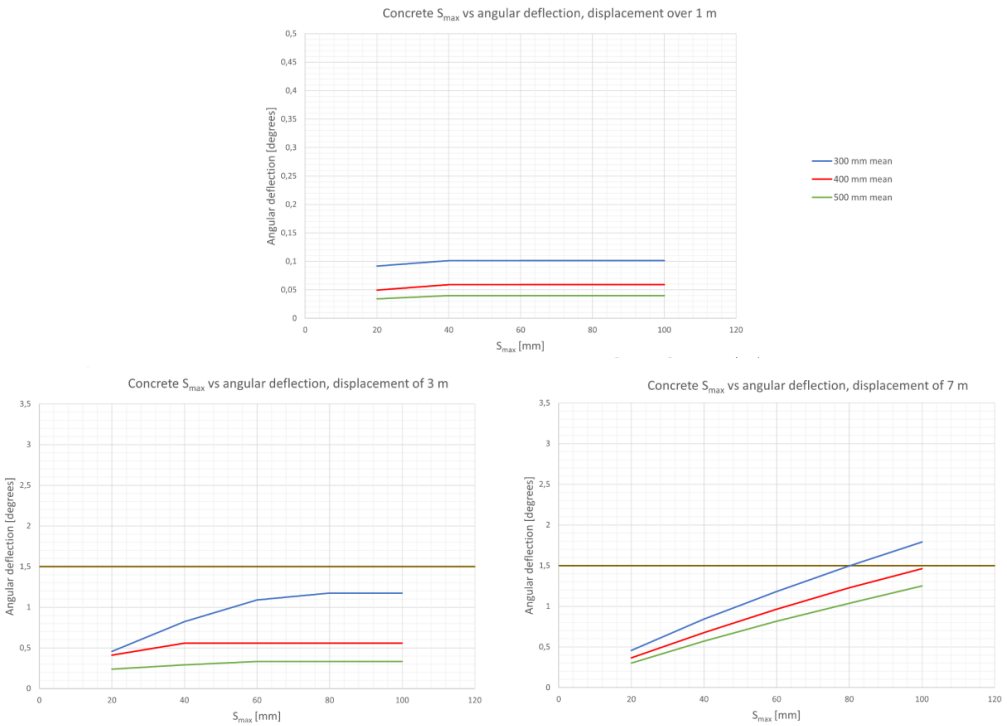

Figure 8.6: Quay wall deformation plotted against the mean maximum angular deformation of multiple diameters of concrete pipes, for localized quay wall displacement over a length of 1, 3 and 7 m.
Note: y-axis is not equal for all graphs.

Table 8.2: Range of horizontal quay wall displacement in which maximum allowable deflection (1.5^o) is surpassed for quay wall displacement over greater length.

D_o $[mm]$	**GCI range** $[mm]$	**NCI range** $[mm]$	**steel range** $[mm]$	**concrete range** $[mm]$
	Quay wall displacement over length of 1 m			
≥ 100	not surpassed	not surpassed	not surpassed	-
	Quay wall displacement over length of 3 m			
100	$20 < S_{max} < 40$	$40 < S_{max} < 60$	$40 < S_{max} < 60$	-
200	$60 < S_{max} < 80$	not surpassed	not surpassed	-
300	not surpassed	not surpassed	not surpassed	not surpassed
≥ 400	not surpassed	not surpassed	not surpassed	not surpassed
	Quay wall displacement over length of 7 m			
100	$20 < S_{max} < 40$	$40 < S_{max} < 60$	$40 < S_{max} < 60$	-
200	$60 < S_{max} < 80$	$80 < S_{max} < 100$	$80 < S_{max} < 100$	-
300	$80 < S_{max} < 100$	not surpassed	not surpassed	$80 < S_{max} < 100$
≥ 400	not surpassed	not surpassed	not surpassed	not surpassed

8.2. Utility line leakage due to exceedance of maximum bending moment

Similarly to the check for exceedance of the maximum allowable angular deflection discussed in section 8.1, for both the model cases the results of the analytical model are provided in this section regarding the exceedance of maximum bending moment. These results are discussed in sections 8.2.1 and 8.2.2 respectively. As discussed, only the

outputs with influence lengths less than half the aforementioned typical length of utility line segments are deemed representative and only these outcomes are presented in the following figures. For both models, only GCI, NCI and steel utility lines with outer diameters of 100 mm meet this requirement. Additionally, for GCI pipes, the influence length is less for an outer diameter of 200 mm, but only for lower applied percentages of horizontal equilibrium bearing capacity, namely 20% and 40%. Note that it follows from the determination of the influence length as given in 7.10, that said influence length is independent of both the magnitude of quay wall deformation as well as the length over which said deformation occurs. The influence length for all diameters of concrete sewer pipes is larger than 3 m, therefore no results are provided for this material type.

8.2.1. Model results regarding the maximum bending moment for quay wall deformation over greater length

In figures 8.7, 8.8a and 8.8b, the unity check for maximum bending moment is plotted against the applied quay wall deformation, for GCI, NCI and steel potable water pipes respectively. In the aforementioned figures, the minimum and maximum values of the unity check are also displayed for utility lines with diameters of 100 mm of all materials, resulting from the variance in horizontal equilibrium bearing capacity. Note that the 100% unity check for maximum bending moment is not surpassed for any tested and valid utility line subjected to horizontal quay wall displacement up to 100 mm.

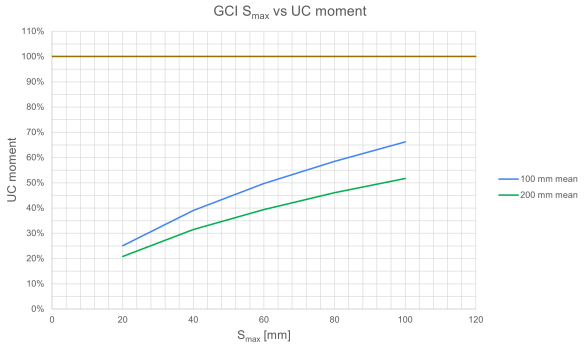

Figure 8.7: Quay wall deformation plotted against the mean unity check regarding the maximum bending moment of multiple diameters of GCI pipes, for quay wall deformation over longer length.

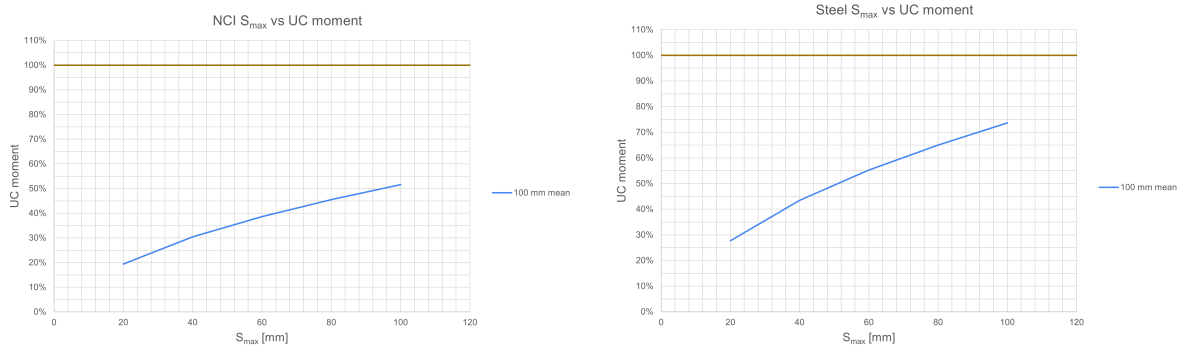

(a) (b)

Figure 8.8: Quay wall deformation plotted against the mean, minimum, and maximum unity check regarding the maximum bending moment of NCI and steel pipes with outer diameters of 100 mm, for quay wall deformation over longer length.

8.2.2. Model results regarding the maximum bending moment for localized quay wall deformation

The model results regarding the maximum bending moments of section 8.2.1, figures 8.9, 8.10 and 8.11 the unity checks for maximum bending moment are plotted against the applied quay wall displacement over a length of 1,3

and 7 m for GCI, NCI and steel potable water pipes respectively. As the magnitude of the mean, minimum and maximum values for all various tested quay wall displacements, length of quay wall displacements and materials are virtually the same, only the mean values are given in said figures. Note that the 100% unity check for maximum bending moment is not surpassed for any tested and valid utility line subjected to horizontal quay wall displacement up to 100 mm over any length of quay wall displacement, except for steel potable water pipes with an outer diameter of 100 mm at quay wall displacement over a length equal to 3 m.

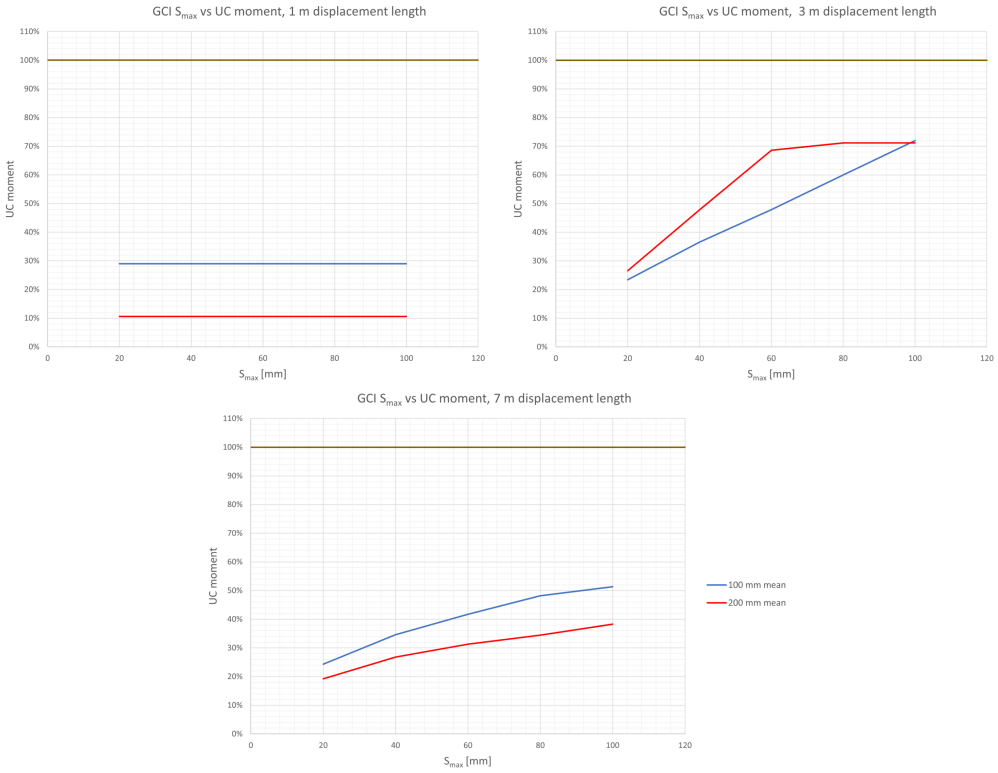

Figure 8.9: Quay wall displacement plotted against the mean unity check regarding the maximum bending moment of multiple diameters of GCI pipes, for localized quay wall deformation of 1, 3 and 7 m.

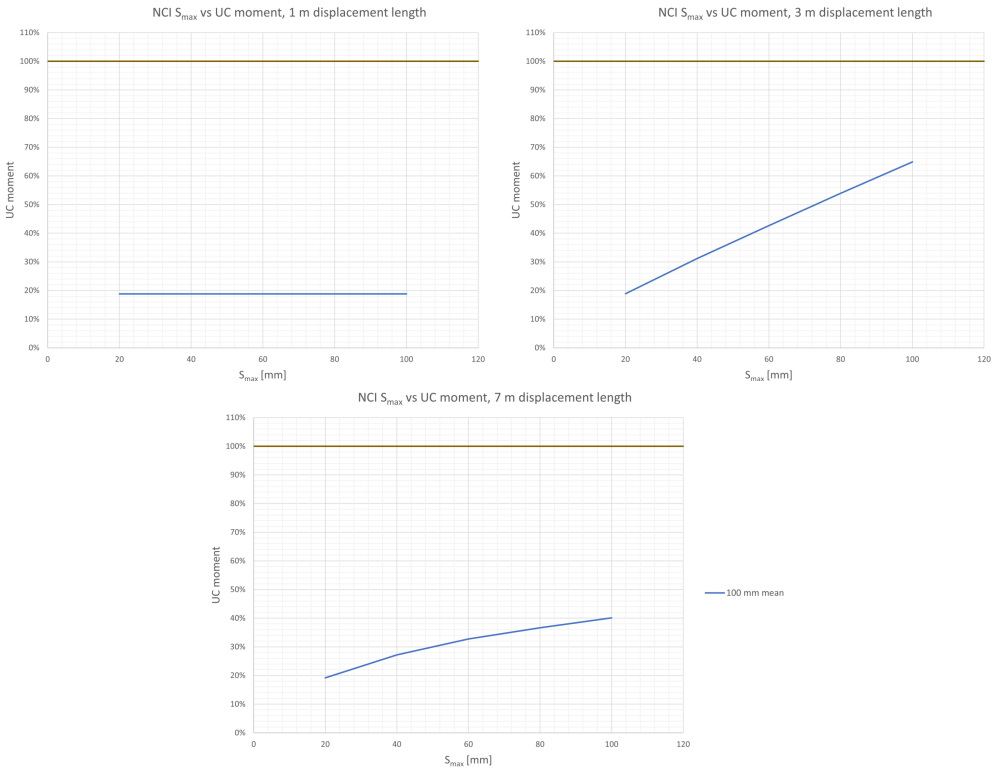

Figure 8.10: Quay wall displacement plotted against the mean unity check regarding the maximum bending moment of 100 mm diameter NCI pipes, for localized quay wall deformation of 1, 3 and 7 m.

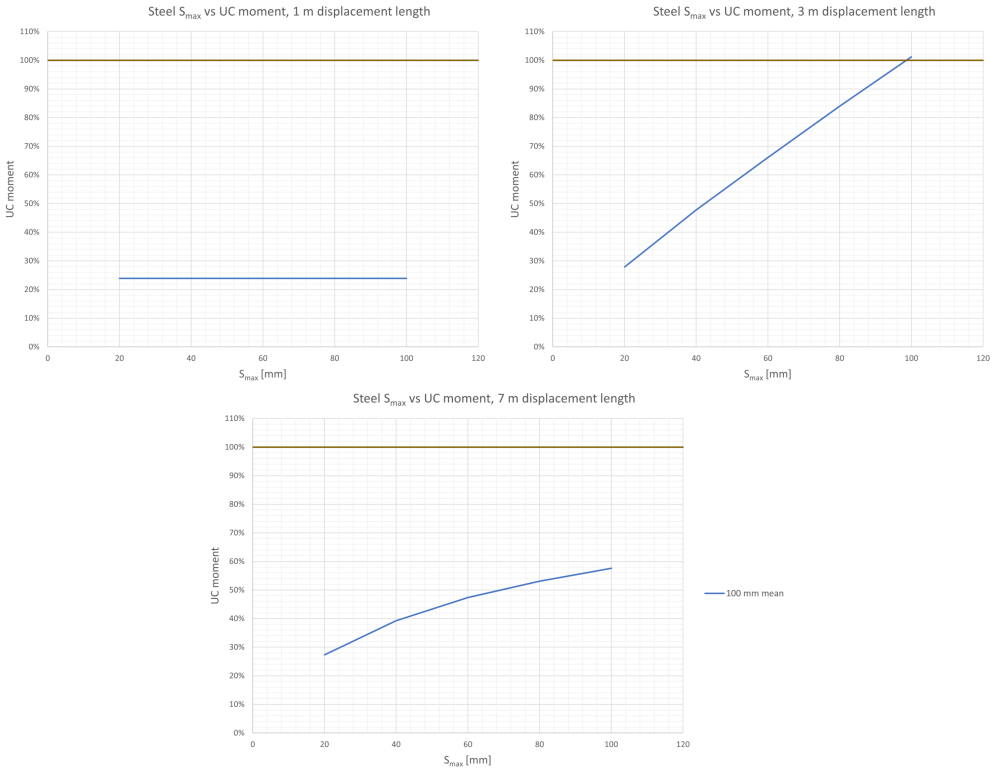

Figure 8.11: Quay wall displacements plotted against the mean unity check regarding the maximum bending moment of 100 mm diameter steel pipes, for localized quay wall deformation of 1, 3 and 7 m.

8.3. Utility line leakage due to exceedance of maximum shear force

The check for the exceedance of the maximum shear force resulting in utility line leakage follows a similar pattern as the check for their exceedance of maximum bending moment in section 8.2.1. Sections 8.3.1 and 8.3.2 present the model results regarding maximum shear force for quay wall deformation over greater length and localized quay wall deformation respectively. As discussed in section 7.5.1, only results of the model with an influence less than 3 m are taken into account. Additionally, only GCI, NCI and steel utility lines with outer diameters of 100 mm and GCI lines with an outer diameter of 200 mm are represented in the figures of both models. This follows from the same reasoning concerning the surpassing of the influence length for larger utility line diameters as explained in section 8.2.

8.3.1. Model results regarding the maximum shear force for quay wall deformation over greater length

Similarly the model results regarding the maximum bending moments given in section 8.2.1, the unity check for maximum shear force is plotted against the applied quay wall deformation for GCI, NCI and steel potable water pipes in figures 8.12, 8.13a and 8.13b respectively. In the aforementioned figures, the minimum and maximum values of the unity check are also displayed for utility lines with diameters of 100 mm of all materials, resulting from the variance in horizontal equilibrium bearing capacity. Note that the 100% unity check for maximum shear force is not surpassed for any tested and valid utility line subjected to horizontal quay wall displacement up to 100 mm.

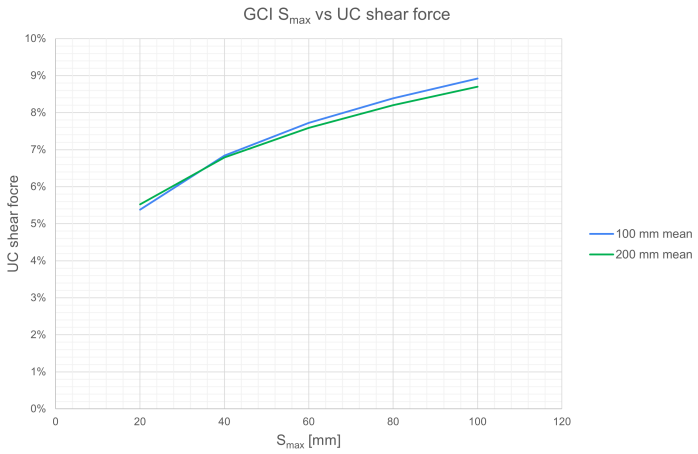

Figure 8.12: Quay wall deformation plotted against the mean unity check regarding the maximum shear force of multiple diameters of GCI pipes, for quay wall deformation over longer length.

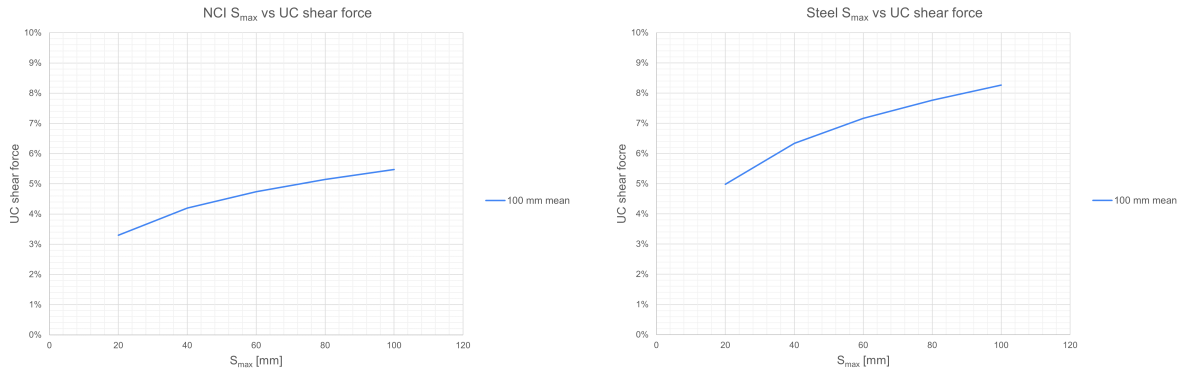

(a) (b)

Figure 8.13: Quay wall deformation plotted against the mean, minimum, and maximum unity check regarding the maximum shear force of NCI and steel utility lines with outer diameters of 100 mm, for quay wall deformation over longer length.

8.3.2. Model results regarding the maximum shear force for localized quay wall deformation

Similarly to the model results regarding the maximum bending moments of section 8.2.2, figures 8.14, 8.15 and 8.16 the unity checks for maximum shear force is plotted against the applied quay wall displacement over a length of 1,3 and 7 m for GCI, NCI and steel potable water pipes respectively. As the magnitude of the mean, minimum and maximum values for all various tested quay wall displacements, length of quay wall displacements and materials are virtually the same, only the mean values are given in said figures. Note that the 100% unity check for maximum shear force is not surpassed for any tested and valid utility line subjected to horizontal quay wall displacement up to 100 mm over any length of quay wall displacement.

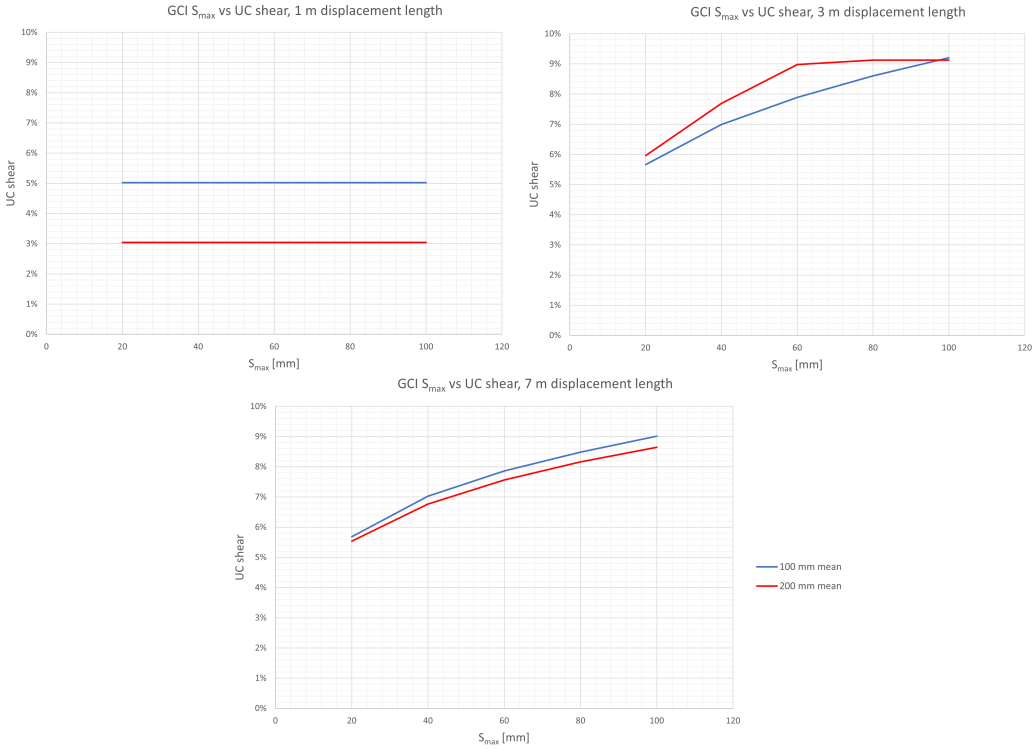

Figure 8.14: Quay wall deformation plotted against the mean unity check regarding the maximum shear force of multiple diameters of GCI pipes, for localized quay wall deformation of 1, 3 and 7 m.

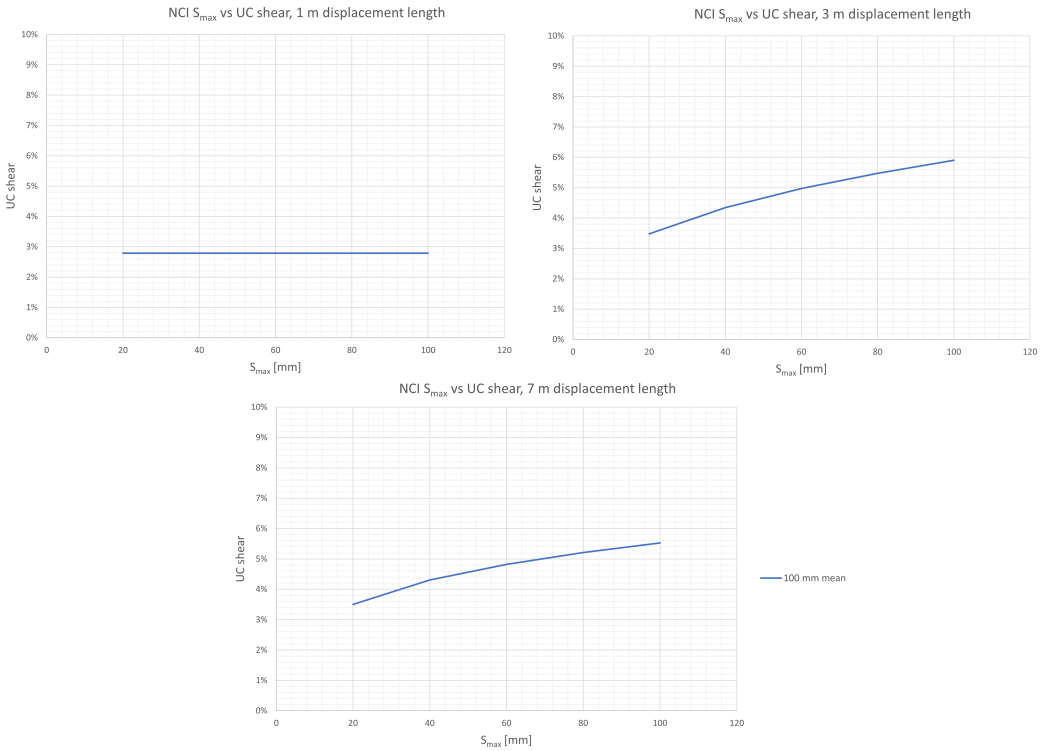

Figure 8.15: Quay wall deformation plotted against the mean unity check regarding the maximum shear force of 100 mm diameter NCI pipes, for localized quay wall deformation of 1, 3 and 7 m.

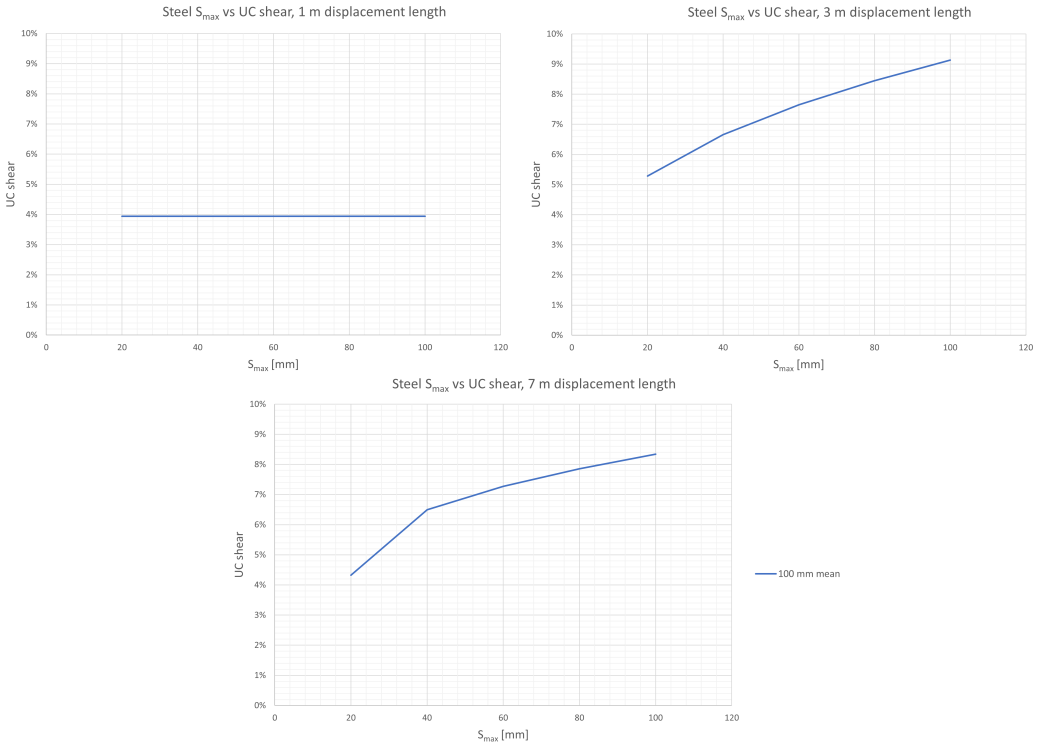

Figure 8.16: Quay wall deformation plotted against the mean unity check regarding the maximum shear force of 100 mm diameter steel pipes, for localized quay wall deformation of 1, 3 and 7 m.

8.4. Influence of variation in horizontal distributed spring stiffness to analytical model

As mentioned before, for each run of the model the horizontal distributed spring stiffness was varied by assuming various percentages of the horizontal equilibrium bearing capacity, ranging from 20% up to 100%. In order to determine the impact of this variation, the maximum angular deflection outputted by the analytical model is used, for each combination of quay wall deformation, utility line diameter and material. This is because the influence length is of less importance for the reliance of this particular model output. The sensitivity of the analytical model to the variation in horizontal distributed spring stiffness was checked using the model for quay wall displacement over greater length. Due to the fact that the soil behaviour is modelled using the same principles in this model as well as in the model for localized quay wall displacement, a separate similar analysis for localized quay wall displacement is deemed unnecessary.

In figures 8.17a, 8.17b, 8.18a, 8.18b (for GCI, NCI, steel and concrete utilty lines respectively), the maximum angular deflection is plotted against the quay wall deformation, for both the material's smallest and largest utility line diameter. As said before, a mean value of the angular deflection for each utility line diameter resulting from a particular quay wall deformation is calculated resulting from the aforementioned variation in percentage of horizontal equilibrium bearing capacity. In each figure, the blue graph depicts the mean value for the maximum angular deflection of the utility line's smallest diameter, while the green graph depicts the mean value for the maximum angular deflection of the utility line's largest diameter. In all figures, for both utility line diameters the red graph depicts the maximum value resulting from the variation of equilibrium bearing capacity, while the yellow graph depicts the minimum value obtained in the similar manor. For simplicity, only the utility material's smallest and largest diameters are depicted, as for all materials the rest of the diameters follow a similar pattern. It has to be noted that for all utility line diameters, materials and quay wall displacements, all minimum values for all outputs were found at 100% horizontal bearing capacity, while all maximum values of the same output were found at 20% horizontal bearing capacity.

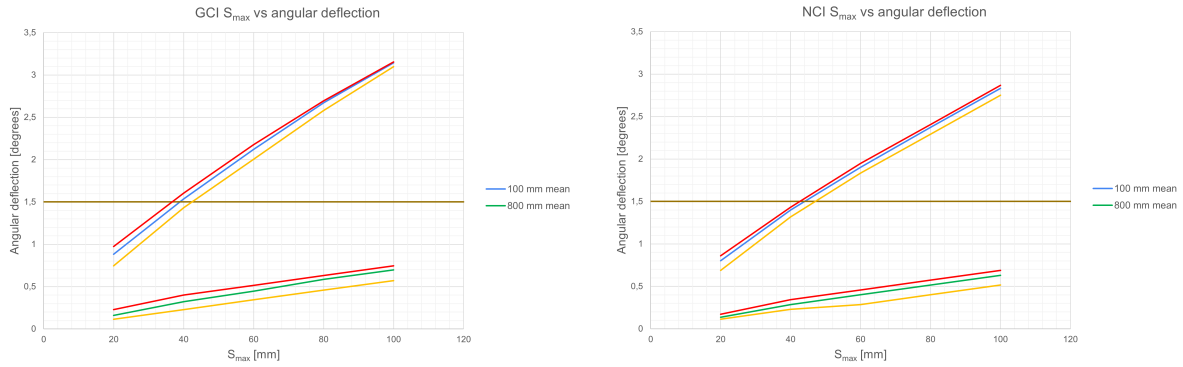

(a) Mean, maximum and minimum angular deflection plotted against the quay wall deformation for GCI utility lines

(b) Mean, maximum and minimum angular deflection plotted against the quay wall deformation for NCI utility lines

Figure 8.17: For both materials, the blue graph is equal to the mean value for an outer diameter of 100 mm, the green graph is equal to the mean value for an outer diameter of 800 mm. For both diameters of both materials, the red graph depicts the maximum value, while the yellow graph depicts the minimum value

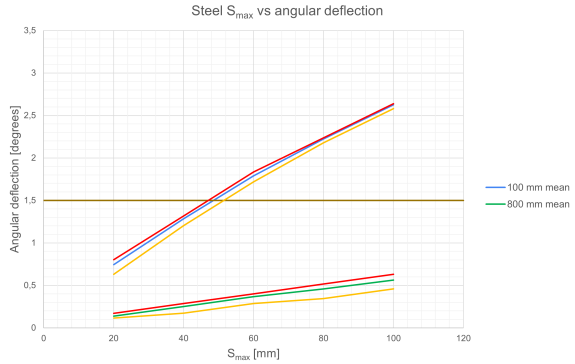

(a) Mean, maximum and minimum angular deflection plotted against the quay wall deformation for steel utility lines

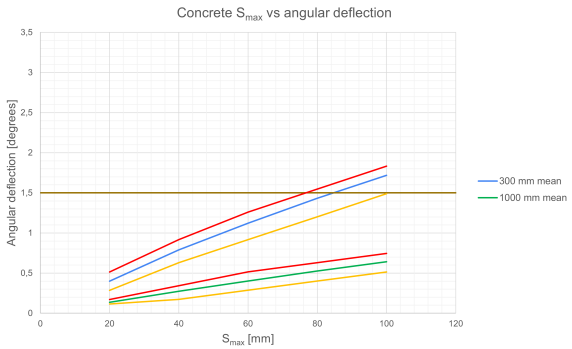

(b) Mean, maximum and minimum angular deflection plotted against the quay wall deformation for concrete utility lines

Figure 8.18: For both materials, the blue graph is equal to the mean value corresponding to the smallest utility line diameter, while the green graph is equal to the mean value for the largest utility line diameter. For both diameters of both materials, the red graph depicts the maximum value, while the yellow graph depicts the minimum value

From the previous figures a number of observations can be made:

- For all materials and diameters, the mean value is significantly closer to the maximum than to the minimum.
- The variation between minimum and maximum values is significantly larger for concrete than for the metal utility lines.
- The difference of this variation between GCI, NCI and steel utility lines is negligible.
- Smaller utility line diameters result in smaller variatons for GCI, NCI and steel pipes. This variation is less pronounced for concrete sewers.

From the aforementioned observations it follows that increase in placement depth (H) is proportional to increase in variation, as all potable water pipes (i.e. metal utility lines) were tested using a placement depth of 0.8 m, while the concrete sewer systems were all tested using a placement depth of 2.3 m. It can be concluded that the assumed magnitude of the horizontal bearing capacity is of less importance at shallower placement depths than at lower placement depths.

8.5. Sensitivity analysis of analytical model input parameters

In this section a sensitivity analysis is provided for both cases of the model to the various input parameters. In order to determine the sensitivity to the various parameters, the mean values of the input parameters, which are discussed in section 7.6, are used to determine the mean model outputs. Additionally, the mean influence length is determined. Next, each mean value of the input parameters is in term both increased and decreased by 25%, while keeping the rest of the input parameters equal to its mean value. One exception being the length over which quay wall displacement occur, which is increased and decreased significantly more in order to enforce the various types of this model. Finally, for each aforementioned increase and decrease, the output values are compared to the mean output values. Although the increased and decreased values may be not representative to values found in the inner-city of Amsterdam, they are nevertheless still realistic.

In table 8.4 and 8.5, the sensitivity analysis are given for the model for quay wall displacement over greater length and localised quay wall displacement respectively. Additionally, for both models the mean values of the output parameters are given in tables 8.3a and 8.3b.

Table 8.3: Output parameters resulting from mean values for both model cases.

(a) Output parameters resulting from mean values found using model regarding quay wall displacement over greater length.

Output parameter	Value	Unit
Max angular defl.	0.43	^{o}
Max bending moment	453.6	kNm
Max shear force	345.7	kN
Influence length	10.6	m

(b) Output parameters resulting from mean values found using model regarding localized quay wall displacement.

Output parameter	Value	Unit
Max angular defl.	0.5	^{o}
Max bending moment	320.9	kNm
Max shear force	197.6	kN
Influence length	10.6	m

Table 8.4: Overview of sensitivity of the input parameters for model regarding quay wall displacement over greater length.

	γ' $[kPa]$	E $[GPa]$	S_{max} $[mm]$	H $[m]$	D_o $[mm]$	% of q_{he}	t $[mm]$	ϕ $[dgr]$
Mean value	16	120	50	1.55	550	50	51.8	30
+25% of mean	20	150	63	1.94	688	63	64.5	38
-25% of mean	12	90	38	1.16	413	38	38.7	23
Output for mean values +25%								
Max angular defl.	+5%	-5%	+21%	+5%	-15%	-5%	-4%	+16%
Max bending moment	+12%	+12%	+19%	+11%	+50%	-12%	+8%	+36%
Max shear force	+18%	+6%	+9%	+22%	+35%	-6%	+4%	+58%
Influence length	-5%	+6%	+0%	-5%	+19%	+5%	+4%	-14%
Output for mean values -25%								
Max angular defl.	-7%	+8%	-23%	-7%	+23%	+4%	+5%	-16%
Max bending moment	-13%	-13%	-22%	-12%	-41%	+10%	-10%	-29%
Max shear force	-19%	-7%	-12%	-20%	-32%	+5%	-5%	-40%
Influence length	+7%	-7%	+0%	+5%	-21%	-4%	-5%	+19%

Table 8.5: Overview of sensitivity of the input parameters for localized quay wall displacement.

	γ' $[kPa]$	E $[GPa]$	S_{max} $[mm]$	H $[m]$	D_o $[mm]$	% of q_{he}	t $[mm]$	ϕ $[dgr]$	l $[m]$
Mean value	16	120	50	1.55	550	50	51.8	30	3
+25% of mean	20	150	63	1.94	688	63	64.5	38	5
-25% of mean	12	90	38	1.16	413	38	38.7	23	1
Output for mean values +25%									
Max angular defl.	+20%	-13%	0%	+27%	-27%	-7%	+7%	+53%	+167%
Max bending moment	+18%	+8%	0%	+27%	+53%	+5%	+14%	+56%	+86%
Max shear force	+25%	0%	0%	+33%	+19%	0%	0%	+83%	+67%
Influence length	-5%	+6%	0%	-4%	+19%	+4%	+5%	-14%	0%
Output for mean values -25%									
Max angular defl.	-20%	+27%	0%	-20%	+53%	+20%	-13%	-40%	-87%
Max bending moment	-17%	-8%	0%	-22%	-37%	-6%	-13%	-34%	-65%
Max shear force	-25%	0%	0%	-27%	-21%	0%	0%	-48%	-67%
Influence length	+8%	-7%	0%	+5%	-21%	-5%	-4%	+17%	0%

From the sensitivity analysis in table 8.4, it can be concluded that the quay wall displacement (S_{max}), the outer diameter of the pipe (D_o) and the soil's angle of internal friction (ϕ) have the highest influence on the outcome of the model for quay wall displacement over greater length. The influence of the effective weight (γ') is limited. As said before in section 2.5, the soil used as backfill most probably sand, thus the angle of internal friction is kept at 30^o, as

it is assumed that the angle of internal friction does not vary significantly from this value. The bending stiffness of the utility line, i.e. the product of modulus of elasticity and the cross-sectional moment of inertia ($E \cdot I$), shows to be one of the major factors influencing the outcome of the model.

The sensitivity analysis of the model for localised quay wall displacement given in table 8.5 determines that again the outer diameter of the pipe and soil internal friction also have a major effect on said model. Contrary, the influence of the effective weight is more pronounced than in the other model, although this effect is only visible for the maximum angular deflection. The influence of the quay wall displacement is equal to zero at this length over which quay wall displacement occurs, which follows from the fact that for the mean values, the relative displacement of the utility line is larger than the maximum allowable soil deformation. As expected, the length over which quay wall displacement occurs (l) has a high influence on the outcome of the model. Similarly to the other model, the bending stiffness is a major factor for the outcomes of this model as well.

8.6. Overview of results analytical model

In this section, an overview is provided regarding the results obtained of the analytical model. First, in section 8.6.1, an overview is provided of the types of utility lines susceptible to leakages at various combinations of quay wall displacement and length over which said displacement occurs. Next, in section 8.6.2, the obtained relation between utility line leakage and the dimensionless parameter resulting from the ratio of the utility line's outer diameter and quay wall displacement (D_o / S_{max}) is discussed.

8.6.1. Overview of utility line leakage due to quay wall displacement

In table 8.6, an overview is provided of the types of utility lines susceptible to leakage at a given combination of magnitude of quay wall displacement and length over which said quay wall displacement occurs. The overview follows from the results of the analytical model as provided in this chapter and is meant to be independent of the mechanism resulting into leakage. However, it has to be noted that of each case provided in the overview, the mechanism resulting into leakage is exceedance of the maximum allowable angular deflection of the joints.
Similarly to all input variables, the magnitude of horizontal quay wall displacement (S_{max}) and the utility line outer diameter (D_o) are discrete values. Thus in the overview, the magnitude of horizontal quay wall displacement has been divided in ranges of 20 mm. Additionally, for each utility line material, the outer diameter was tested in increasing steps of 100 mm. Thus, for each combination of magnitude of quay wall displacement and length over which said displacement occurs, the overview provides the minimum value of the outer diameter of each utility line material which is not susceptible to leakage. Utility lines of the same material with diameters smaller than this given minimum value may be susceptible to leakages. This follows from the fact that it has been found that under the same circumstances, a utility line of the same material with an outer diameter of 100 mm less than the provided minimum value was susceptible to leakage. Note that this minimum value is determined using the results of the analytical model. The minimum value of the outer diameter for GCI, NCI and steel potable water pipes is set at 100 mm, as smaller diameters of these types of utility lines have not been tested. For similar reasons, the minimum value of outer diameter for concrete sewer pipes has been set at 300 mm.

Table 8.6: Overview of minimum outer diameters of utility lines which are not susceptible to leakage, for all tested materials, according to the analytical model.

Magnitude of horizontal quay wall displacement (S_{max}) [mm]	Length over which quay wall displacement occurs (L_s)			
	1 m	3 m	7 m	Greater length
$0 < S_{max} \leq 20$	100 300	100 300	100 300	100 300
$20 < S_{max} \leq 40$	100 300	200 100 300	200 100 300	200 100 300
$40 < S_{max} \leq 60$	100 300	200 300	200 300	200 300
$60 < S_{max} \leq 80$	100 300	200 300	200 300	200 300
$80 < S_{max} \leq 100$	100 300	200 300	400 200 400	300 400

[value]	D_o [mm] of GCI potable water pipe
[value]	D_o [mm] of NCI potable water pipe
[value]	D_o [mm] of steel potable water pipe
[value]	D_o [mm] of concrete sewer pipe

The given outer diameter in each cell is a minimum value of the corresponding utility line for which it is not susceptible to leakage, under the corresponding circumstances. Utility lines of similar material under the same circumstances with smaller outer diameters may be susceptible to leakages.

8.6.2. Dimensionless parameter of utility line diameter and quay wall displacement in relation to leakage

As the analytical model produces discrete results for discrete values of utility line diameters and magnitude of quay wall displacement, it is valuable to provide a continue relation between utility line diameter, quay wall displacement and susceptibility to leakage. This continue relation has been found through the ratio between the outer diameter of a utility line and the magnitude of quay wall displacement, i.e. D_o/S_{max}. It is found that when this ratio for each tested outer diameter is plotted against the maximum angular deflection, a seemingly continue relation is obtained. As this relation is dimensionless, it can be used for any combination of quay wall displacement and utility line diameter, within reasonable limits. The described relation is found for every material, however it is only valid if the quay wall displacement can be modelled to be acting over a greater length. See figure 8.19 for said continue relation. Appendix K provides similar relations for NCI, steel and concrete utility lines.

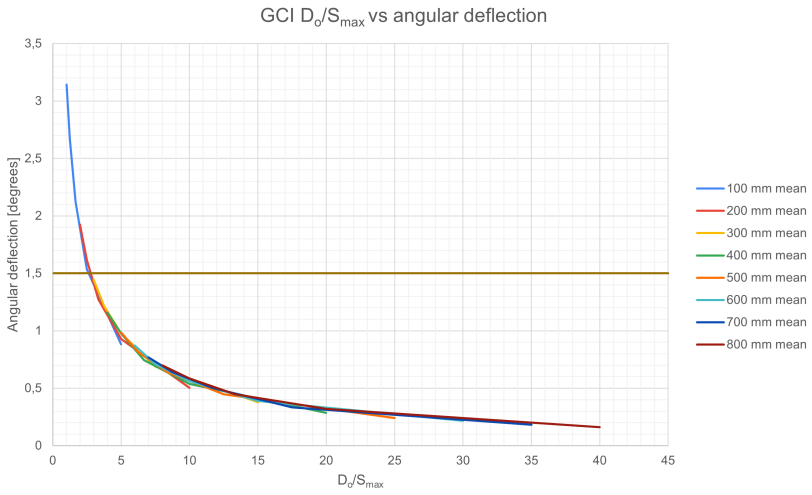

Figure 8.19: D_o/S_{max} plotted against the mean maximum angular deflection for all diameters of GCI utility lines, for quay wall displacement over greater length.

As exceedance of angular deflection is found to be the governing instigator of leakage for each utility line material and diameter, the ratio D_o/S_{max} at which the threshold of 1.5^o angular deflection is reached is appointed as a maximum value. Table 8.7 provides this maximum value of D_o/S_{max} for each tested utility line material. If in real life smaller values of this ratio are found, the utility line is susceptible to leakage.

Table 8.7: Maximum value of D_o/S_{max} at which utility line is susceptible to leakage at quay wall displacement over greater length, for each tested material

Utility line Material	**Maximum value of** D_o/S_{max}
GCI	2.6
NCI	2.3
Steel	2.0
Concrete	3.5

9

Discussion

In this chapter, the obtained results are discussed and linked to the conducted research into utility line leakage resulting in quay wall failure, in sections 9.1 and 9.2 respectively. The chapter closes with a discussion of the limitations of the study in section 9.3.

9.1. Discussion of results of the analytical model

In this section, the results of the analytical model regarding the angular deflection, the maximum moment, and the maximum shear force are discussed in sections 9.1.1, 9.1.2 and 9.1.3 respectively.

9.1.1. Discussion of analytical model results: angular deflection

In this section, the results of the analytical model regarding angular deflection are discussed, which are presented in section 8.1. As expected from the sensitivity analyses of both models for quay wall displacement over greater length and localised quay wall displacement, given in section 8.5, utilty lines with higher bending stiffness (i.e. utilty lines with higher values of $E \cdot I$) result in smaller angular deflections. This follows from all results of both models. Although from these same sensitivity analyses is follows that the placement depth has a significant positive influence on the magnitude of maximum angular deflection, the bending stiffness of the concrete sewer systems is large enough that up to a quay wall displacement of 100 mm. This follows from the fact that only tested sewers pipes with outer diameters of 300 mm surpass the threshold of 1.5^o, whereas tested sewer pipes of 400 mm and larger stay below this threshold.

It follows that for quay wall displacement over a length of 1 m, for all diameters and materials, the angular deflection is constant, but not equal to zero. Thus it appears that virtually for all tested diameters, materials and magnitudes of quay wall deformation, the deflection of the utility line's section behind the quay wall deformation, is relatively larger than the maximum soil deformation, resulting in a constant equilibrium soil pressure.

Looking at the utility line's angular deflections at quay wall displacement over a length of 3 m for all diameters and materials, at higher magnitudes of quay wall displacement and larger outer diameters of utility lines, the influence of the magnitude of the quay wall displacement is similar to the behaviour of the utility lines at aforementioned quay wall displacements over a length of 1 m. However, for smaller diameter pipes the behaviour is comparable to the behaviour of utility lines subjected to quay wall displacement over longer length. This corresponds to the fact that less stiffer utility lines result in smaller influence lengths (as given in equation 7.10), i.e. the length required for the utility line to form towards the soil deformation is shorter for less stiff utility lines.

It follows from comparison of the results for angular deflection at quay wall displacement over a length of 7 m and the results for angular deflection of quay wall displacement over greater length, that these results are almost equal. This can also be seen by comparing the results in the tables for these lengths over which quay wall displacement occurs, i.e. tables 8.2 and 8.1 respectively. The largest deviation between these models appears to occur for concrete, although the magnitude of quay wall displacement at which the threshold of $1.5\ ^o$ is surpassed is almost equal for pipes of this material with an outer diameter of 300 mm .

The results show that at very localized quay wall displacements of 1 m, leakage due to angular deflection does not play a role, regardless of the magnitude of said displacement. For a quay wall displacements over a length of 3 m, potable water pipes with lower bending stiffnesses start to become susceptible to joint leakage. For checking the angular deflection of utility lines, especially for potable water pipes, a length of 7 m over which quay wall displacement occurs is sufficiently large to model the quay wall displacement using the model for said displacement over greater length, as for both models the relevant utility lines act similar. At this length over which quay wall deformation occurs, for multiple tested smaller diameters of potable water pipes and the smallest tested concrete sewer pipes the threshold of 1.5^o is reached for quay wall displacements with magnitudes less than 100 mm.

Concluding from these results, it follows that bending stiffness of utility lines has the most pronounced effect on the angular deflection. Especially at the typical placement depth of potable water pipes (i.e. 0.8 m), the effect of soil is less pronounced. This follows from the linear relation between the horizontal equilibrium bearing capacity of the soil and the depth. The effect of soil does become a larger player at greater depths, the depths at which sewer sewer systems are typically found. However, although the modulus of elasticity of the concrete sewer systems which are generally in place in the vicinity of quay walls is small compared to the GCI, NCI and steel potable water pipes, their higher thickness and generally larger diameters result in relatively higher bending stiffnesses, diminishing the aforementioned effects of greater placement depths

9.1.2. Discussion of analytical model results: maximum bending moment

In this section, the results of the analytical model regarding the maximum bending moment are discussed, which are presented in section 8.2. As for all materials and corresponding utility line diameters the angular deflection is constant for all quay wall displacements over a length of 1 m, it follows that the maximum moment and following unity checks are independent of quay wall displacement above a certain magnitude as well. At this length over which quay wall displacement occurs, for all relevant diameters and materials, the maximum allowable bending moment is never surpassed. It appears that this length over which quay wall displacement occurs is too narrow to let the relative soil displacement acting on the utility line generate a significant bending moment. Note that for GCI, NCI and steel potable water pipes, of all tested diameters only 100 and 200 mm were deemed valid for checking the occurring maximum bending moment. due to their influence length.

The highest unity checks regarding bending moments are found for every material and diameter at quay wall displacements over a length of 3 m. Although the unity checks regarding the maximum bending moment for both GCI and NCI are still less than 100% at the maximum quay wall displacement of 100 mm, this unity check is surpassed by steel utility lines at a quay wall displacement in the range of $80 < S_{max} < 100$ mm. This means that leakage due to exceedance of maximum allowable bending moments does become likely, contrary to every other case. The reason for this being that this length over which quay wall displacement occurs is narrow enough for the bending moment generated at either side of the quay wall displacement to play a role over the whole length of said displacement, while being wide enough to let the relative soil displacement generate a significant bending moment. As all unity checks of utility lines with diameters of 100 mm for all materials increase with increasing quay wall displacement, these are all fully dependent on said displacement. Contrary, for smaller magnitudes of quay wall displacements, the unity check regarding maximum bending moment for GCI utility line of 200 mm diameter is larger than its 100 mm diameter counterpart. However, starting at a quay wall displacement equal to 60 mm, the unity check stays constant, thus indicating that the maximum bending moment is independent of the quay wall displacement starting from this magnitude.

Contrary to the angular deflections found in section 8.1.2, the unity checks regarding maximum bending moment at quay wall displacement over a length of 7 m for all materials are lower than the found similar unity checks for quay wall displacement over greater length as given in section 8.2.1. The largest difference is found at the largest quay wall displacement (100 mm), for which the difference between the two models in every material is equal to about 10%. As the results in this model of quay wall displacement over a length of 7 m are lower than its counterpart over greater length, the unity check never surpasses 100% for any material.

For quay wall deformation over greater length and localized quay wall deformation over a length of 7 m, the unity check never surpasses 100%. This means that, according to the models, for all tested and valid utility line diameters and materials, failure due to exceedance of maximum bending moment resulting from quay wall displacement up to a magnitude 100 mm is highly unlikely.

Again, an increase in bending stiffness results in larger maximum bending moments. However, increase in bending stiffness also results in lower unity checks, due to the precedence of the cross-sectional moment of inertia in the corresponding equation 7.15. Due to the higher maximum allowable tensile stress of NCI compared to both steel and GCI, the unity check for this material is lower for all magnitudes of quay wall deformation compared to the other two materials of potable water pipes.

It can be concluded that for diameters providing valid results, utility line leakage due to exceedance of maximum bending moment is generally unlikely for all materials and lengths over which quay wall deformation occurs, if the unity check for exceedance of maximum bending moment is taken as the criterion. Note that the unity check concerns utility line leakage due to exceedance of the material's ultimate tensile stress, i.e. the stress at which a material breaks. However, lower bending moments could instigate stresses in the utility line material which, in collaboration with for example internal water pressure, could result in micro fractions as explained in section 3.4.3. These have the potential to grow to larger fractions, resulting in higher leakage discharges.

9.1.3. Discussion of analytical model results: maximum shear force

In this section, the results of the analytical model regarding angular deflection are discussed, which are presented in section 8.3. Similarly to the angular deflection and the UC for bending moments, the UC for shear force in this model is constant for a quay wall displacement over a length of 1 m for all valid utility line diameters and materials. Note that for GCI, NCI and steel potable water pipes, of all tested diameters only 100 and 200 mm were deemed valid for checking the occurring maximum shear force, due to their influence length.

For quay wall displacements over a length of 3 m, shear force increase with said displacement. Again, for the 200 mm GCI potable water pipe, 2 distinct sections can be seen at this length of 3 m over which quay wall displacement occurs, i.e. starting from a magnitude of quay wall displacement of 60 mm. Up to this displacement, the unity check increases even faster than for a 100 mm GCI utility line. At greater displacements, the GCI utility line of 200 mm is no longer dependent of the quay wall displacement, as the unity check is constant for higher magnitudes of quay wall displacements. At this length over which quay wall displacement occurs, the utility lines of the other two materials follow the same pattern as displacement over greater length.

At quay wall displacements over a length of 7 m, all pipe diameters of materials are similar to the results found for quay wall displacement over greater length, as expected when looking at the results for angular deflection.

It follows from the results of all models that the effect of shear force is negligible, as the maximum found unity check for shear is less than 10%. This is in line with what was discussed in section 3.4.3, in which it was discussed that smaller utility lines are less susceptible to leakage due to exceedance of maximum shear force. Thus, utility line leakage due to exceedance of the maximum shear force is highly unlikely.

9.2. Relation between qualitative and quantitative studies

In this section outcomes of the qualitative study and quantitative study are linked. First, the influence of utility line deterioration on the results is discussed in section 9.2.1. Next, the effects of utility line leakage on quay wall failure as discussed chapter 6 are linked to the obtained results of the analytical model 9.2.2.

9.2.1. Influence of utility line deterioration

As explained in section 9.2.1, age and usage of utility lines both contribute to their deterioration. This deterioration has an effect on various input parameters of the analytical model, listed below:

- **Thickness of utility line (t)**
  Due to the various forms of corrosion, the (effective) thickness of utility lines is reduced. This results in lowering of bending stiffness, which according to the sensitivity analyses of section 8.5 results in higher angular deflections but lower bending moments and shear forces. However, alteration of the thickness indirectly also influences the outer diameter (D_o). This is due to corrosion on the outside of the utility line, which again according to the sensitivity analyses result in higher angular deflections but lower bending moments, due to its

effect on the bending stiffness. Although both the occurring maximum bending moment and -shear force are reduced due to reduction of the utility line's thickness, its cross-sectional area (A) and -moment of inertia (I) are negatively affected by this reduction as well. This results in a reduction of the maximum allowable bending moment and shear force, due to the reduction of the maximum allowable tensile stress and -shear stress.

- **Maximum allowable angular deflection**
  Due to deterioration of joints, the maximum allowable angular deflection is negatively influenced. If this is the case, the required magnitude of quay wall displacement at which the allowable angular deflection is reached is lowered.

- **Maximum allowable tensile stress ($\sigma_{max,material}$) and -shear stress ($\tau_{max,material}$)**
  As said before, the deterioration of utility lines does not only affect its cross-section, it can also influence the material properties itself. This is most pronounced GCI (and to a degree also in NCI) utility lines, as graphitisation can occur, resulting in a decrease in the maximum allowable tensile and -shear stress of a material. This has a direct effect on the unity check regarding both maximum allowable bending moment and -shear force.

As expected, it follows from the aforementioned list of affected parameters and their effects that deterioration has a major influence on the susceptibility of a utility line to leakage.

9.2.2. Relation between utility line leakage effects quay walls and analytical model

In this section, the effects of utility line leakage to quay walls are linked to the analytical model of quay wall displacement resulting in said utility line leakage. To recap, three possible open connections enabling both flow of water and soil were appointed, each capable to result in internal erosion and possibly failure of said quay wall: leakage of the quay wall floor, leakage of the scour protection screen, and sewer leakage. It is shown in the schematizations of chapter 4 how utility line leakage is linked to quay wall failure and vice versa via these aforementioned open connections.

Although according to the analytical model quay wall displacement plays a role in the deformation (and therefore leakage) of utility lines, said displacement first has to be instigated. One instigator being that the pile foundation is no longer capable of bearing the quay wall, due to bacterial deterioration, washing away of soil surrounding said piles, or excessive loads for which it was not originally designed for acting on the quay wall (f.e. heavy traffic loads, both static and dynamic). It has to be noted that if the pile foundation has been deteriorated over time, chances are the quay wall floor and scour protection screen are as well, as all three are constructed at the same time from the same material.

Another instigator can be in the form of a high groundwater levels in the soil body behind the quay wall. This can be the result of deteriorated potable water pipe leakage, but also the result of other processes like heavy rainfall. Although the cause of high ground water levels might be different, the effect on a quay wall is similar. If said high groundwater level is in place, an open connection has to be in place as well. In the form of a leak in the quay wall floor or the scour protection screen this can result in internal erosion underneath the structure, which as explained can trigger quay wall displacement. In the form of a sewer- or quay wall floor leakage via which erosion in the soil body behind the structure is eroded, this can result in loss of foundation of the utility line, resulting in deformations and leakages. Both options create a positive feedback loop.

As follows from the results regarding angular deflection of section 8.1 , the displacement of a quay wall can result in potable water pipe- as well as sewer leakage. This way, both a source of water and an open connection are in place, capable of forming a subsidence pit in the soil body behind the quay wall. As stated before, note that this combination of potable water pipe and sewer leakage can occur in combination with aforementioned quay wall floor- and/or scour protection screen leakage.

From the previous, it follows that utility line leakage due to deformation is mainly a second order effect to the displacement of a quay wall. However, if instigated, utility line leakage has the potential to result in a positive feedback loop with quay wall failure, in term potentially resulting in failure of a quay wall. Using the analytical model, it has been quantitatively shown to what extend quay wall displacement affects utility line leakage. However, the study has only qualitatively shown in what way utility line leakage results in quay wall failure. There are two notable unknown factors: a critical diameter of a sneaking leak capable of resulting in localized saturation of the soil body, and

the reach of said localized saturation relative to the quay wall structure. It is stated by various research institutes, Deltares and POV-K&L among them, that determination of a critical leakage diameter is vital (Kruse and Schelfhout, 2019). However, these same institutes acknowledge that research in this field is lacking. Additionally, it is stated by them that the shift from sneaking leak to gaping leak in a utility line has to be more clearly defined, and taken into account into the NEN 3650 standard series. There is a direct correlation between leak size and the reach over the axial dimension of the utility line. This can be seen in the graph of figure 5.3b, in which the length of an erosion crater due to a gaping leak is plotted against the size of the hole. Even at small leak diameters, the length of the erosion crater is in the order of meters. Note that in general, a higher degree of leakage parameters (angular deflection, bending moment, and shear force), results in a higher degree of leakage. Thus, sneaking leaks can grow into gaping leaks under increased quay wall displacement.

Although at this moment the critical leakage diameter is undetermined, the interaction between quay walls and utility lines has been acknowledged. Therefore, if it is found that a quay wall is displaced, it is advised to check which utility lines are in place in its vicinity. Depending on the magnitude of said displacement, the length over which said displacement has occured, the location of the utility lines relative to the structure and the characteristics of the utility line, the utility line can be susceptible to leakage. Characteristics of utility lines include its function, material and status regarding deterioration. The overview provided in section 8.6.1 provides the susceptibility of utility line leakage due to quay wall displacement, following from the tested leakage parameters. Additionally, the dimensionless parameter D_o/S_{max} as explained in section 8.6.2 can be used to determine if utility line leakage occurs according to the analytical model, as a relatively clear relation is found of this ratio versus all tested leakage parameters.

9.3. Limitations of the study

A number of limitations in the research have been identified, in both the qualitative as well as the quantitative studies. These are listed and further explained below. Note that chapter 7 already provides a number of limitations directly affecting the output of the analytical model.

- **Soil displacement in multiple directions**
  It follows from the PLAXIS 2D model that even if only horizontal displacement is applied to the quay wall, a smaller but still significant vertical soil deformation occurs in the area further away from the quay wall displacement. In the analytical model, it is assumed that the total soil body displaces with the same magnitude in horizontal direction, due to the fact that the vertical displacement is significantly smaller. However, in order for the model be more exact, the vertical equilibrium bearing capacity should be taken into account as well. From section 8.4, it follows that at the depth at which potable water pipes are generally located, the effect of the assumed magnitude of the spring stiffness is limited. Thus it can be reasoned that the additional effects of soil in vertical direction are limited at this depth. At greater depths, i.e. at the depths at which sewers are generally located, the effects of soil on utility lines is more pronounced. However, from the PLAXIS 2D model provided in section 7.2, it follows that the soil displacement behind the quay wall at these depth is primarily in the horizontal direction, thereby justifying the assumption of horizontal displacement.

- **Bi-linear horizontal spring stiffness**
  Although the horizontal distributed spring stiffness is modelled to be bi-linear, in reality this stiffness is fully dependent on the relative utility line deformation, i.e. a varying stiffness for each longitudinal coordinate of the utility line for which the relative displacement varies (displayed in figure 7.10). However, the influence of the magnitude of spring stiffness is relatively low for the depth at which potable water pipes are located (see section 8.4). For deeper utility lines like sewers, it is expected that this is is of a higher importance, due to the higher degree of dependence on the magnitude of the spring stiffness.

- **Incorrect modelling of joints: lack of hinge**
  As said before, the utility line is treated as a continuous model, while in reality the line is made up of separate pipe segments, connected by non-tensile resistant flexible joints. To accurately represent these joints, hinges would be a suitable model. However, the influence length (L_{infl}) plays a major role in the validity of the model, as it is explained in section 7.5 that only utility lines with influence lengths less than 3 m are deemed to be represented adequately. As it turns out, utility lines with higher bending stiffnesses, i.e. utility lines with larger diameters, are less susceptible to leakage due to either angular deflection or exceedance of bending moments. As only for these larger utility lines the influence length is too large to guarantee the validity of the model, the

model is still usable. However, utility line leakage of larger utility lines due to higher magnitudes of quay wall displacement are less accurately described using this model.

- **Incorrect modelling of joints: effect of normal stresses**
  The analytical model focuses on bending moments and shear forces, while in reality normal forces play a role the model as well. According to the the Euler-Bernoulli beam model, which is used in the analytical model, bending moments result in elongation of the affected beam, linearly increasing from center towards the outer fibre. As elongation is proportionate to normal stress, all elements of the utility line within the influence length of the quay wall displacement have to be able to cope with said normal stresses. As the joints of utility lines are generally non-tensile resistant, if these are located within the influence length, the socket and spigot of the joint might slide off of eachother, resulting in utility line leakage.

  It has to be noted that the friction between utility line and soil in axial direction does provide some capability to absorb the normal stresses resulting from the bending moments to a certain degree Rajani et al. (1996); NEN (2020a). As results from section I.11 in appendix I, this friction force is proportional to the outer diameter of a utility line and is in the order of 8 kN for a utility line with an outer diameter of 100 mm. However, as explained in section I.11, this effect is not enough to counter the utility line sliding out the socket-spigot joint. However, even in the most extreme case tested, the length over which sliding occurs in the socket spigot joints is deemed within limits. Te effect of the lacking of normal stress is more pronounced in utility lines with lower bending stiffness, resulting in an additional susceptibility to leakage. However, as said before, the utility lines with higher bending stiffness are in term affected to a higher degree by the lack of hinges in the model.

- **Use of NEN standards**
  For various parts of the study, NEN standards have been used. Although theses standards are based on extensive research and practical experience, these standards have a high degree of inherent safety build into them. Thus, in order to more accurately represent the various parts of the research based on NEN standards, tests specifically meant for these situations have to be conducted.

10

Conclusion

To recap, the main aim of this research was to answer the following question:

> **"How does utility line leakage relate to deformation and failure of Amsterdam's inner-city quay walls and when does this interaction become significant?"**

The interaction between utility lines and quay walls works in both ways. Qualitatively, it has been determined utility line leakage can result in displacement and eventual failure of a quay wall trough a number of mechanisms, all related to internal erosion. However, this is highly dependent on the status of the quay wall in question, as there has to be an open connection in place to enable the flow of soil due to flow of water. A number of these open connections have been identified and explored: quay wall floor leakage, scour protection screen leakage, and sewer leakage. Note that in the latter, the head difference is not required. This is because the direction of flow is not towards the channel, but towards the sewer leakage, given that the sewer pipe is located below the groundwater level. Depending on the type of open connection, this results in erosion underneath the structure or in the soil body behind the quay wall. Erosion underneath the structure can result in quay wall displacement towards the channel, while erosion in the soil body behind the structure can result in the formation of a subsidence pit. Actual failure of the quay wall due to utility line leakage can come in two forms: either due to collapse of the road on top of the structure into the generated subsidence pit, or due to collapse of the quay wall towards the channel.

An analytical model was developed to study the effects of quay wall displacements on utility lines. In this model, the interaction between utility line and surrounding soil was represented using a beam on a Winkler foundation, i.e. a beam supported by a distributed spring. The stiffness of the spring was represented as bi-linear, resulting from the equilibrium bearing capacity of the soil. Quay wall displacements ranging from 20 up to 100 mm were applied to the most common types and outer diameters of utility lines found in the vicinity of quay walls. Utility line leakage was deemed to occur if a predetermined threshold is passed of either maximum angular deflection, maximum allowable bending moment or maximum allowable shear force, each resulting from the utility line displacement. Using the analytical model, it has been determined that quay wall displacement can result in utility line leakage. Note that the instigation of quay wall displacement is not limited to be the result of utility line leakage, but can also be the result of increased horizontal soil pressures due to f.e. heavy traffic. It is found that the quay wall displacement transfers via the soil body onto the utility line located in its vicinity, resulting in relative displacements of said utility line. Qualitatively, it has been determined that the formation of a subsidence pit can result in relative displacement of utility lines as well, due to loss of the soil in which the utility line is embedded. Thus, both quay wall displacement and subsidence formation have the potential to result in a positive feedback loop triggering further utility line leakages, in term resulting in further internal erosion. It has to be noted that the displacement of a quay wall is not limited to occur due to utility line leakage, but can be triggered due to other loads as well. Additionally, the required local head difference between the channel and groundwater in soil body behind the gravity wall is not limited to originate from potable water pipe leakage, but can also be the effect of f.e. intense rainfall. Due to the dependence on external factors, quay wall failure resulting from utility line leakage can be described as a second order effect.

From the analytical model, it followed that localized quay wall displacement over a length of 1 m does not result in failure for any of the tested utility line types and corresponding outer diameters. At localized quay wall displacement over a length of 3 m, the results of tested utility lines with lower bending stiffness (i.e. the product of the

modulus of elasticity and the cross-sectional moment of inertia) are equal to the results of utility lines with the same bending stiffness subjected to quay wall displacement over greater length. Contrary, utility lines of higher bending stiffness react in the same manor as being subjected to quay wall displacement over a length of 1 m. At quay wall displacement over a length of 7 m, the results are virtually equal for all tested utility lines subjected to quay wall displacement over greater length. In all tested cases for which the analytical model was valid, exceedance of the angular deflection threshold for the utility line joints is the cause of failure in all types of utility lines and corresponding outer diameters. The influence of the maximum bending moment on utility line leakage is found to be relatively high as well, although almost never enough to instigate leakages. In contrast, the influence of the maximum shear force is found to be insignificant in all tested cases. It can be concluded that higher bending stiffness results in higher resistance to leakage.

An overview of the results is provided in table 10.1. In this table, the outer diameters are provided of the tested utility line materials, for which no leakage was found for the corresponding combination of horizontal quay wall displacement and length over which said displacement occurs. If utility lines of the same material but smaller diameters are found in the vicinity of a quay wall, at the given combination of quay wall displacement and length over which said displacement occurs, it is advised to carry out more in depth monitoring of these utility lines and check them for leakages, deformations and status of deterioration.

Table 10.1: Overview of minimum outer diameters of utility lines (D_o) which are not susceptible to leakage, for all tested materials, according to the analytical model.

Magnitude of horizontal quay wall displacement (S_{max}) [mm]	Length over which quay wall displacement occurs (L_s)			
	1 m	3 m	7 m	Greater length
$0 < S_{max} \leq 20$	100 300	100 300	100 300	100 300
$20 < S_{max} \leq 40$	100 300	200 100 300	200 100 300	200 100 300
$40 < S_{max} \leq 60$	100 300	200 300	200 300	200 300
$60 < S_{max} \leq 80$	100 300	200 300	200 300	200 300
$80 < S_{max} \leq 100$	100 300	200 300	400 200 400	300 400

[value]	D_o [mm] of GCI potable water pipe
[value]	D_o [mm] of NCI potable water pipe
[value]	D_o [mm] of steel potable water pipe
[value]	D_o [mm] of concrete sewer pipe

The given outer diameter in each cell is a minimum value of the corresponding utility line for which it is not susceptible to leakage, under the corresponding circumstances. Utility lines of similar material under the same circumstances with smaller outer diameters may be susceptible to leakages.

11

Recommendations

A number of recommendations for further research can be distilled from the conducted research. These are listed below:

- **Quantitative analysis of the effect of utility line leakage on quay wall deformation**
  It is natural to assume that leakages of larger utility lines at similar operating pressures can result in higher rates of internal erosion. Additionally, the size of said leak plays a major role in this phenomenon as well. At the moment, a quantitative study linking leakage size to the amount of internal erosion is lacking. One study which comes close to this is the study towards gaping leaks conducted by Mastbergen (1991). However, in the case of sneaking leaks, research is lacking. Therefore, to fully comprehend the relation between utility line leakage and failure of a quay wall, more in depth study towards this quantitative relation has to be conducted.

- **Use of a more advanced method to model soil-utility line interaction**
  The interaction between soil and utility line has been modelled using an analytical model. Such a model does provide more insight into their behaviour, but is always a simplification of reality. In a further study, it is advised to apply a more advanced numerical model to better model this interaction, as this interaction is key in understanding how displacements of quay walls result into utility line leakage. Additionally, the model should include a more exact representation of the joints in place between the various segments of a utility line, f.e. in the form of a hinge.

- **Research towards the ratio D_o/S_{max}**
  In the research, one of the findings was the apparent relation between ratio of the outer diameter over the quay wall displacement (D_o/S_{max}) and the occurring maximum angular deflection, maximum bending moment, and maximum shear force in the utility line. For now, the value has been determined of this ratio at which the angular deflection no longer surpasses the 1.5^o threshold. However, it is advised to conduct more in depth research towards this aforementioned relation, by means of more variance of utility line diameter and quay wall displacement. By doing so, an even more reliable check can be generated for determining the angular deflection of a utility line due to quay wall displacement.

- **Monitoring of utility lines**
  As explained in various parts of the research, utility line deterioration in combination with deformation results in leakage. Under ideal circumstances, it is recommended to monitor all utility lines in the vicinity of quay walls in order to find leakages. However, due to limited time and budget, it is advised to prioritize monitoring of utility lines in the vicinity of quay walls which have displaced towards the channel, or which have visible settlements of the road on top of the structure. In order to determine if there are leakages present, the same method can be applied as in the study towards the dike failure at Stein, Limburg (see appendix D). In this study, a camera was placed in the potable water pipe to check for the leakage, which was determined to be the cause for dike failure. Regardless of the method of monitoring, it will generate nuisance. This is due to the fact that utility lines, and especially potable water pipes, are generally sealed of from the outside world, only reachable by opening the road, temporary limiting its use.

Bibliography

Worku. A, 2009. Winkler's single-parameter subgrade model from the perspective of an improved approach of continuum-based subgrade modeling. Department of Civil Engineering, Addis Ababa University. Journal of EEA, Vol. 26, 2009.

Actueel Hoogtebestand Nederland, 2019. Ahn viewer.

AD, October 15 2013. Deel kademuur van Utrechtse gracht ingestort. URL https://www.ad.nl/utrecht/deel-kademuur-van-utrechtse-gracht-ingestort~aa5f82c7/.

ANSON STEEL, n.d. Steel Plate DIN 17100. URL http://www.steelplatesforsale.com/useful-links/steel-plate-din-17100.html.

AT5, November 1 2017. Deel Jordaan zonder water door enorm sinkhole Marnixstraat. URL https://www.at5.nl/artikelen/174805/tramverkeer-plat-door-sinkhole-aan-marnixstraat.

AT5, March 3 2018. Kademuur bij Nassaukade ingestort; lek waterleiding weer gedicht. URL https://www.at5.nl/artikelen/179152/kademuur-bij-nassaukade-ingestort.

AWWA, 2004. History, Uses, and Physical Characteristics of Steel Pipe.

T. Bakker, n.d. sluizen, keringen en duikers in Amsterdam. URL https://www.theobakker.net/pdf/sluizen.pdf.

R. J. Barrett, September 1966. Use of Plastic Filters in Coastal Structures. Proceedings from the 16th International Conference Coastal Engineers, Tokyo, pp. 1048–1067.

B.F. Beck and A.A. Balkema. Sinkholes: their geology, engineering and environmental impact. Proceedings of the First Multidisciplinary Conference on Sinkholes/Orlando/Florida, 117, 1984.

Bentley, 2020a. PLAXIS: Material Models Manual.

Bentley, 2020b. PLAXIS 2D - Tutorial Manual. CONNECT Edition V20.04 PLAXIS 2D.

Bentley, n.d.a. PLAXIS 2D Geotechnical Finite Element Software. URL https://www.bentley.com/en/products/product-line/geotechnical-engineering-software/plaxis-2d.

Bentley, n.d.b. PLAXIS Geotechnical Finite Element Analysis Software. URL https://bentley.com/en/products/brands/plaxis.

Brante, M., September 1 2020. Kade ingestort in centrum Amsterdam, situatie 'stabiel'. URL https://www.parool.nl/amsterdam/kade-ingestort-in-centrum-amsterdam-situatie-stabiel~b2f44086/.

Buurtorganisatie 1018, December 15 2017. Kade Entrepotdok ingestort; woonschip zwaar beschadigd.

CEN, December 2004. Eurocode 2: Design of concrete structures - Part 1-1: General rules and rules for buildings.

Charter Plastics, 2020. Advantages of Polyethylene Pipe. URL https://www.charterplastics.com/advantages-of-polyethylene-pipe.

CPAA, n.d. Concrete Pipe Facts. URL https://www.cpaa.asn.au/General/concrete-pipe-facts.html#durability.

M.T. Davisson, n.d. Lateral Load Capacity of Piles. Department of Civil Engineering, University of Illinois, Urbana.

W. de Gans, 2011. De bodem onder Amsterdam, een geologische stadswandeling. TNO.

J.G. de Gijt, November 2004. Structures in hydraulic engineering, Lecture notes on Port Infrastructure - CT 5313. TU Delft.

J.G. de Gijt, 2010. A History of Quay walls: Techniques, types, costs and future. TU Delft.

De Hamer, n.d. Ronde Buizen. URL https://www.dehamer.nl/producten/buizen/ronde-buizen/.

DUIC, November 21 2013. Opeenstapeling van factoren oorzaak inzakken kademuur Bemuurde Weerd. URL https://tinyurl.com/fpjjs38x.

J. Erochko, October 12 2020. An Introduction to Structural Analysis. ISBN: 978-1777411909.

Facility Management, n.d. Using the Right Piping Material for Your Plumbing Application. URL http://facilitymanagement.com/piping-material-plumbing/#:~:text=Unfortunately%2C%20most%20PVC%20is%20not,it%20unsafe%20for%20drinking%20water.

U. Förster, G. van den Ham, E. Calle, and G. Kruse, March 2012. Onderzoeksrapport Zandmeevoerende Wellen. Deltares.

Gemeente Amsterdam, July 2 2019. Actieplan bruggen en kademuren Amsterdam.

Gemeente Amsterdam, n.d.a. Hoe groot is Amsterdam? URL https://maps.amsterdam.nl/hoegroot/?LANG=nl.

Gemeente Amsterdam, n.d.b. Regels op het water. URL https://www.amsterdam.nl/parkeren-verkeer/varen-amsterdam/regels-varen/#h1d7b8f5b-eb64-482b-a854-57163ef977dd.

Georg Fischer Piping Systems, n.d. Polyvinyl chloride chlorinated (PVC-C). URL https://www.peterss.lv/en/products/pvc-c-c3#:~:text=Mechanical%20properties,particularly%20prevalent%20at%20higher%20temperatures.

Geschiedenis Lokaal Amsterdam, n.d. De aanleg van de Grachtengordel. URL https://www.geschiedenislokaalamsterdam.nl/bronnen/de-aanleg-van-de-grachtengordel/.

Ginopress B.V., March 3 2018. Kademuur Nassaukade in Amsterdam ingestort. URL https://www.telegraaf.nl/nieuws/1744208/kademuur-nassaukade-in-amsterdam-ingestort.

C. Hartsuijker and J.W. Welleman, 2004. Mechanica; Statisch onbepaalde constructies en bezwijkanalyse. Academic Service, ISBN: 97809039527528.

Het Parool, Oktober 25 2017. Oudste waterleiding van Amsterdam wordt vervangen. URL https://www.parool.nl/nieuws/oudste-waterleiding-van-amsterdam-wordt-vervangen~b4e3bf8a/.

M. Hetényi, 1946. Beams on Elastic Foundations. Michigan: The University of Michigan Press.

infoDWI, January 2017. LEIDINGMATERIALEN: Gietijzeren buizen/nodulair, hulpstukken en verbindingen. Waterwerkblad, WB 2.2 F.

S. Kamel and A. M. Meguid, 2008. An experimental study of soil erosion around leaking pipes. North American Society for Trenchless Technology 2008 No-Dig Conference & Exhibition.

S.A. Karamanos, B. Keil, and R.J. Card, 2014. Seismic design of buried steel water pipelines. Pipelines 2014: From Underground to the Forefront of Innovation and Sustainability 1005 © ASCE 2014.

R.K.W.M. Klaassen, July 9 2007. Bacterial decay in wooden foundation piles—Patterns and causes: A study of historical pile foundations in the Netherlands. International Biodeterioration & Biodegradation 61 (2008) 45–60.

A.R. Koelewijn and R. Bridle, September 2017. Internal erosion in dams and dikes: a comparison. 25th Meeting of th European Working Group on Internal Erosion.

H. Kruse and H. Schelfhout, February 26 2019. Memo: Lekkage proeven ter simulatie van het falen van waterleidingen. Deltares & POV-K&L.

M. Kruyswijk, April 16 2020a. Bomen langs grachten gaan massaal sneuvelen. Het Parool.

M. Kruyswijk, September 2 2020b. Architect: 'Zwaar verkeer moet Amsterdam uit om kades te beschermen'. URL https://www.ad.nl/binnenland/architect-zwaar-verkeer-moet-amsterdam-uit-om-kades-te-beschermen~a7491460/. AD.

A. Labuschagne, N.F.J. van Rensburg, and A.J. van der Merwe, January 2009. Comparison of linear beam theories. Elsevier, Volume 49, Issues 1-2, Pages 20-30.

MachineMFG, n.d. Metal Mechanical Properties Chart: Shear Strength, Tensile Strenght, Yield Strength. URL https://www.machinemfg.com/metal-mechanical-properties-chart/.

Main board of Waterschap Amstel, Gooi en Vecht, October 2 2008. PEILBESLUIT STADSBOEZEM. (AB 08/xxx-II).

J.M. Makar and S.E. McDonald, 2000. Failure Modes and Mechanisms in Gray Cast Iron Pipes. Institute for Research in Construction, National Research Council Canada, Ottawa, Ontario, Canada.

D.R. Mastbergen, 1991. Ontgronding bij persleidingbreuk, herinterpretatie M1007. Waterloopkundig Laboratorium, Delft.

P. Meershoek, May 23 2020. Het water in de grachten was nog nooit zo helder. URL https://www.parool.nl/nieuws/het-water-in-de-grachten-was-nog-nooit-zo-helder~b1649688/.

P. Meireman, December 7 2016. Draagvermogen van paalfunderingen. Expertgroep Grondmechanica & Funderingstechniek, Ingenieurshuis, Antwerpen.

D. Millar, February 2006. Durability of reinforced concrete pipe – the hard facts! CPAA Seminar 'Stormwater Drainage Pipe - The Long Life Asset'.

Mr. Rooter Plumbing, July 15 2019. The Pros and Cons of Different Types of Plumbing Pipes. URL https://www.mrrooter.com/greater-syracuse/about-us/blog/2019/july/the-pros-and-cons-of-different-types-of-plumbing/.

NEN, January 2020a. NEN 3650-1:2020, Eisen voor buisleidingsystemen – Deel 1: Algemene eisen. ICS 23.040.10.

NEN, January 2020b. NEN 3651:2020, Aanvullende eisen voor buisleidingen in of nabij belangrijke waterstaatswerken. ICS 23.040.10; 93.010.

NOS, September 1 2020. Kademuur in centrum Amsterdam deels ingestort. URL https://nos.nl/artikel/2346286-kademuur-in-centrum-amsterdam-deels-ingestort.html.

Oasen, September 3 2018. Werken met asbestcement leidingen. URL https://www.oasen.nl/drinkwater/leidingen/werken-met-asbestcement-leidingen.

Onderzoeksraad voor Veiligheid, 2005. Leidingbreuk veroorzaakt dijkverzakking op 27 januari 2004 te Stein. reference: CB-9-04-010.

Port of Rotterdam, n.d. Geschiedenis van de haven. URL https://www.portofrotterdam.com/nl/onze-haven/zien-doen-en-beleven/zien/geschiedenis-van-de-haven.

B. Rajani, C. Zhan, and S. Kuraoka, 1996. Pipe-soil interaction analysis of jointed water mains. Can. Geotech. J. 33: 393-404.

K. Reinders, 2019. Lecture notes CIE5305: Bored and Immersed Tunnels. TU Delft.

S. Renner-Hahn, Y. Liu, and T Christen, 2014. Investigation of Rubber Ring Seal Failures of Water Mains. CEED Seminar Proceedings 2014.

Riolering en Waterbeheersing, 1985. De riolering en waterhuishouding van Amsterdam. Dienst Openbare Werken, Amsterdam.

D. Robert and K Soga, 2013. Mechanics of Unsaturated Geomaterials, 13, 303–325.

Saint-Gobain Pipe Systems, 2006. Leidingen voor drinkwatertoepassing; nodulair gietijzer, PE, koper.

G.C. Sarvanis, S.A. Karamanos, P. Vazouras, E. Mecozzi, A. Lucci, and P. Dakoulas, October 21 2017. Permanent earthquake-induced actions in buried pipelines: Numerical modeling and experimental verification. DOI: 10.1002/eqe.3001.

T. Schweckendiek, 2018. WBI Veiligheidsraamwerk Kabels en Leidingen. Deltares, report number: 11202225-005-GEO-0001.

M. V. Seica, J. A. Packer, M.W.F. Grabinsky, and B. J. Adams, 2002. Evaluation of the properties of Toronto iron water mains and surrounding soils. Canadian Journal of Civil Engineering 29 (2), 222–237. DOI: 10.1139/l01-090.

L. Sibille, D. Marot, and Y. Sail, 2015. A description of internal erosion by suffusion and induced settlements on cohesionless granular matter. Acta Geotechnica, Springer Verlag, 10 (6), pp.735-748. ff10.1007/s11440-015-0388-6ff. ffhal-01299663f.

SN Cast Iron, 2018a. Lamellair gietijzer (GG). URL https://www.sn-castiron.nl/nl/materialen/lamellair-gietijzer-gg/.

SN Cast Iron, 2018b. Nodulair gietijzer (GGG). URL https://www.sn-castiron.nl/nl/materialen/nodulair-gietijzer-ggg/.

Stadsarchief Amsterdam, 1906. 17502 Kademuur. Maken kademuur langs Lijnbaansgracht, tussen Palmgracht en perceel no. 14.

Stadsarchief Amsterdam, 1911. 21200 Kademuur. Maken van een kademuur langs de Huddekade.

Stadsarchief Amsterdam, 1932. 25720 Kademuur Weesperplein E.A. Het maken van een walmuur langs de Singelgracht en Weesperplein bij Brug 263.

Stadsarchief Amsterdam, 1933. 32583 Vernieuwen Walmuur Singel. Het vernieuwen van een gedeelte walmuur langs Singel tegenover percelen 371 t/m 381.

Stadsarchief Amsterdam, 1955. 35094 Maken van een zinker met aansluitende riolen door Burgemeester Cramergracht en het leggen van een riool in Louis Couperusstraat.

Stadsarchief Amsterdam, 1968. 46194 Glooiing Enz. Singelgracht. Maken gedeelte glooiing langs Nassaukade bij Nassauplein en een gedeelte walmuur langs korte Marnixkade ten behoeve van zinker aardgasleiding.

Technische Adviescommissie voor de Waterkeringen, Juni 2001. Technisch Rapport Waterkerende Grondconstructies.

Vaarwijzer Amsterdam, n.d. Bruggen en Doorvaarhoogte. URL https://www.vaarwijzeramsterdam.nl/bruggen.html.

V. M. van Beek, 2015. Backward Erosion Piping, Initiation and Progression. TU Delft.

T. van Belzen, December 13 2017. Amsterdamse kademuur ingestort. URL https://www.cobouw.nl/infra/nieuws/2017/12/amsterdamse-kademuur-ingestort-101256053. Cobouw.

R. van der Pluijm, 1997. Non-linear Behaviour of Masonry under Tension. Heron, 42(1), 25-54.

T.J. van der Wel, 2018. Reliability based Assessment of Quay Walls. Master thesis, TU Delft and Witteveen + Bos.

R. van Eijk, 2014. BTO rapport, Betonnen leidingen: inventarisatie,conditiebepaling en onderhoud. KWR. Order number: B222031-005.

B van Zoelen, August 9 2020. De stad heeft dorst: droogte gaat Amsterdam miljarden kosten. Het Parool.

A. Verruijt, 2001. Soil Mechanics. TU Delft.

Walraven, July 2015. Datasheet, Buisafmetingen en -gewichten.

Y. WANG, Q. WANG, and K.Y. ZHANG, 2011. An Analytical Model for Pipe-Soil-Tunneling Interaction. The Twelfth East Asia-Pacific Conference on Structural Engineering and Construction.

Waterloopkundig Laboratorium, September 1969. Veiligheid Persleidingen bij Dijken. Rapport No: M1007.

Waternet, November 1 2017. Geen water groot gedeelte #Jordaan ivm leidingbreuk #sinkhole #Marnixstraat Voor updates blijf ons volgen of check: https://www.waternet.nl/nieuws/2017/oktober/geen-water/. URL https://twitter.com/Waternet/status/925647217985191936/photo/1.

Waternet, n.d. Geschiedenis. URL https://awd.waternet.nl/beleef/geschiedenis/.

Waterschap Amstel, Gooi en Vecht, n.d. Gemaal Zeeburg. URL https://www.agv.nl/recreatie/watererfgoed/gemalen/gemaal-zeeburg/.

R. Wimmers, T. Sweijen, R. Brugman, G. Meinhardt, and J. Maljaars, March 6 2020. Stedelijk grondwater in Amsterdam; hoe gaan we om met infiltratie, barrièrewerking en klimaatverandering? URL https://www.h2owaternetwerk.nl/vakartikelen/.

Witteveen+Bos, August 18 2015. Onderzoek en inspectie kademuur Bakenessergracht te Haarlem. Reference: HLM524-1/15-013.392.

K. Yoshizaki and T. Sakanoue, August 2004. Analytical study on soil-pipeline interaction due to large ground deformation. 13th World Conference on Earthquake Engineering, vancouver, B.C., Canada. Paper No. 1402.

S. Zamanian, 2016. Probabilistic Performance Assessment of Deteriorating Buried Concrete Sewer Pipes. Master thesis, The Ohio State University.

W. Zhang and A Askarinejad, September 25 2018. Behaviour of buried pipes in unstable sandy slopes.

A

Sloping revetment with sheetpiles

The sloping revetment with sheetpiles bank protection design is used along the outer channels of the inner city, the "Singelgracht". They are mainly found in the vicinity of bridges. Note that this is not a quay wall, as the sloping design prevents utilization of the original function of a quay wall, namely the (un)loading of ships.

The quay wall of the Nassaukade utilizes this design, one of the quay walls of which the failure was attributed to failure due to leakage of a potable water pipe (AT5, 2018). See figure A.1 for a typical cross-section of this kind of quay wall design (Stadsarchief Amsterdam, 1968). The location of this particular example is at the location of the aforementioned quay wall collapse.

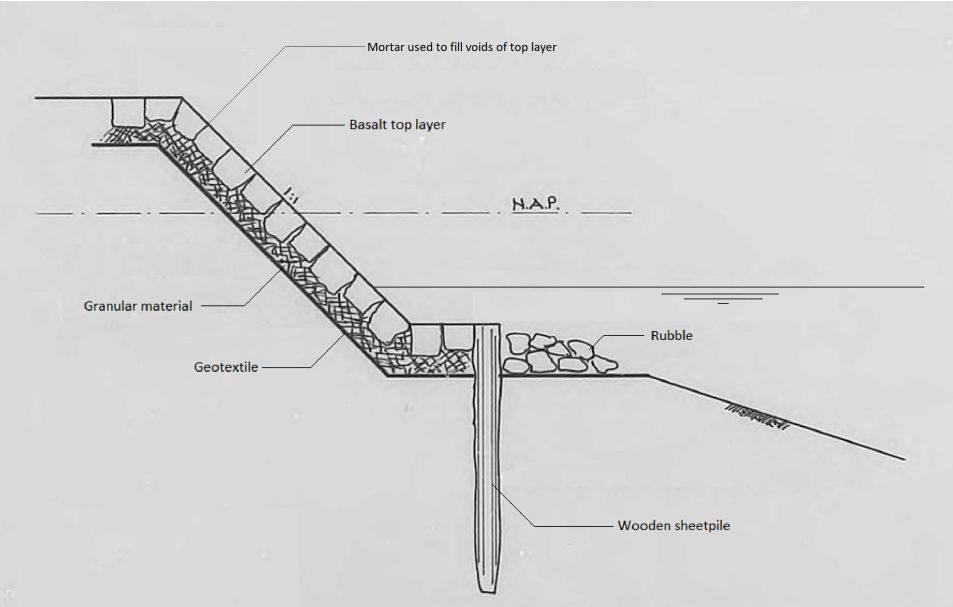

Figure A.1: Typical cross-section of a quay wall design consisting of a sheetpile with sloping gravity wall (Stadsarchief Amsterdam, 1968).

Similarly to the piles of the typical quay wall design found in the inner city of Amsterdam, the gravity wall on piles, the sheetpiles used in this design are mainly constructed of wood (note that in Dutch, a wooden pile like this is called a "perkoenpaal". However, this word is lost in translation and therefore the term "sheetpile" is deemed a suitable alternative.). The example of figure A.1 originates from a renovation project and utilizes a filter layer consisting of granular material and a plastic geotextile. The use of geotextiles as a filter layer started in the 1950's (Barrett, 1966), thus it is expected that previously fully granular filters were applied. It is expected that there are still numerous sections of these type of quay wall not utilizing a geotextile filter. In order to limit the movement of the top layer, mortar is applied to the voids of the basalt stones. The mortar does increase the strength of the slope, however it does not create a water tight seal between both sides of the bank protection.

B

Materials used for utility lines

This appendix gives an overview of the additional materials used in the vicinity of quay walls.

B.1. Copper

Copper pipes are known for their durability, temperature tolerance and inherent safety, as bacteria can not survive in a copper environment and the material does not pollute the drinking water. The life expectancy of copper pipes is at least 50 years. The main drawback of copper is the relatively high costs of the material (Mr. Rooter Plumbing, 2019). Pipes of this material found in the vicinity of the channels have diameters ranging from 150 mm up to 540 mm. They are predominantly installed perpendicular to channels and connecting the drinking water network to domestic connections.

B.2. Polyethylene (PE)

PE is known for its high resistance to fatigue. The material, and especially the high density variant, is a flexible and ductile material. As PE is a thermoplastic, pipe sections can be joined with heat fusion, leading to leak free joints (Charter Plastics, 2020). In Amsterdam, both the regular and the high density variant of PE pipes are implemented and in the vicinity of the channels pipes of this material are found with diameters ranging from 25 mm up to 315 mm.

B.3. Asbestos cement

Asbestos was previously widely used in a variety of constructions, but due to public health concerns its application has been terminated. However, its application in potable water pipes poses no health risks, as only asbestos particles floating in the air are dangerous. Asbestos cement is known for its relatively high life expectancy and its high resistance to abrasion and corrosion. It is a brittle material, with a high resistance to tensile stress (Oasen, 2018). Pipes of this material found in the vicinity of the channels have a diameter of 500 mm. They are no longer in use, but are still present.

B.4. Polyvinylchloride (PVC)

There are multiple varieties of PVC available, each with their own characteristics (Facility Management, n.d.). In Amsterdam, the variety PVC-C is used. The material is characterized by a relatively high tensile strength, high stiffness and high shock resistance (Georg Fischer Piping Systems, n.d.). These material properties are hardly influenced by high temperatures. Sewer pipes of this material are only used in the upper sewer network.

C

Inspection Haarlem

Figure C.1 up to C.6 provide an overview of the visual inspection of the Bakenessegracht in Haarlem. All figures are obtained from the report of the inspection formulated by Witteveen+Bos (2015).

Figure C.1: Settlements are observed at multiple locations on the upper side of the quay and the street connected to it, indicating settlements of the subsoil.

Figure C.2: The front side of the quay wall has settled more than the quay and street, resulting in a small inclination. At the location of this picture the horizontal displacement is 65 mm.

Figure C.3: Over the full length the quay wall bulges towards the channel.

Figure C.4: The masonry of the quay wall has deteriorate over its full length. At various locations the mortar has been washed away and cracks have formed over the height of the wall. The bricks are cracked as well.

Figure C.5: At the water line large quantities of the mortar has washed away. A number of bricks are no longer connected to the quay wall, other bricks are missing. The pores which were created by the washed away mortar have an average depth of 40 mm, with maxima up to 100 mm.

Figure C.6: At various locations the piles of the front row are no longer connected to the capping beam on top of it. Wood-decay is deemed as the cause for this. This space ranges from 30 mm up to 150 mm.

D

Dike failure at Stein, Limburg

The report of the Onderzoeksraad voor Veiligheid (2005) describes the case of failure of a dike located on the eastern bank of the Julina channel, at Stein (Limburg, The Netherlands) on January 27th, 2004. Due to a leaking water pipe which crossed underneath the flood defence, the macro stabilty of the levee's inner slope was compromised. The water pipe in question had a diameter of 100 mm and was made of 5 mm thick steel. The part crossing the levee was cast in reinforced concrete and the different sections of the water pipe were connected by a rigid connection using lead and "striktouw" (van Eijk, 2014). It was found that the combination of settlements in the first decades after construction of the levee and corrosion of the pipe were the cause of the breach in the pipe. Although the outer layer of the levee was made of an impermeable layer of clay, the filling consisted of a mixture of locally available materials like sand, clay and a silty material called loess.

After camera inspection of the water pipe a corrosion leak was found over the full circumference at the location of water extrusion out of the levee. Note that at this location, water and sediment were found to be flowing into the pipe, but this was not deemed as the main cause of failure. After research, GeoDelft provided the most likely cause and effect of the fracture of the water pipe:

- **Cause**
  The concrete cover of the water pipe provided a relatively high axial stiffness. The water pipe was therefore unable to follow differences in settlements of the subsoil over the width of the levee, resulting in high proportions of the loads acting on the pipe, causing axial tensions high enough to result in material failure. Although the mechanism of levee settlement is as said before generally completed after a few decades, failure of the water pipe only occured after 70 years. It was assumed that corrosion, either from inside or outside of the pipe, played a major role. At the location of the leak, both the steel pipe and the rebars of the outer concrete casting were very deteriorated.

- **Effect**
  Relatively short before the failure of the dike, the water pipe eventually breached at the location were the highest settlements occur (the central part of the levee). The water escaping the pipe flowed through the covering soils up to the surface and saturated the sand layers of the levee's core packed between the various impermeable clay layers. Due to the lack of drainage, water pressures build up significantly, leading to micro-instability and failure of the inner side of the levee. See figure D.1 for the resulting failure (Onderzoeksraad voor Veiligheid, 2005).

Figure D.1: Resulting failure of the water pipe leakage at Stein. (Onderzoeksraad voor Veiligheid, 2005)

From these findings, it can be concluded that the deformations and consistency of the subsoil, the used material and type of connection, and the age of the water pipe in the vicinity of the infrastructure are all major parameters regarding the potential of breaching.

E

Additional internal erosion mechanisms

In this appendix, a number of additional internal erosion mechanisms are discussed which are deemed less relevant for the situation of utility line leakage in the vicinity of quay walls.

E.1. Contact erosion

Contact erosion occurs at the interface of a coarse- and a fine soil layer, if the velocity of the water flowing through the voids of the coarser layer is sufficiently high to erode the particles of the fine soil layer (Koelewijn and Bridle, 2017). However, as said in section 2.5, both peat and clay are cohesive material, limiting the occurrence of this form of internal erosion. Some erosion might occur at the interface of the two layers, but this is not significant.

E.2. Suffusion

According to Sibille et al. (2015), suffusion is the process of internal erosion in which the finest particles of the soil matrix are eroded in a cohesionless soil, followed by its larger particles. The research of Sibille et al. concluded that the suffusion process can be split up in two parts. The first part is characterized by the migration of fine soil particles over a long time period. The second part of the process consists of a strong migration of particles in a short time period, resulting in large settlements. The process can only occur in soils with a large gradient, as the fine particles have to be able to migrate between the voids of the larger particles. Förster et al. (2012) states that the sand found in The Netherlands, and thus the upper sand layer of the inner-city in Amsterdam (see section 2.5), is relatively uniform. The uniformity of this sand (d_{60}/d_{10}) is between 1.5 and 3. Therefore, suffusion is not a process likely to occur in the vicinity of quay walls.

E.3. Dissolution

According to Förster et al. (2012), dissolution is the internal erosion process in which a type of soil or rock is dissolved due to contact with water, resulting in a void in the subsurface. An example of this is the dissolution of a limestone layer due to seepage. As the relevant upper layers in The Netherlands virtually only consist of clay, sand and peat, dissolution is not an issue in this area.

F

Study into erosion craters

In order to validate the safety of the countries flood defenses in regards to the presence of pressurized utility lines (thus potable water pipes but also gas pipes), the "Waterloopkundig Laboratorium " was commissioned by "Rijkswaterstaat" in the 1960's to carry out research towards erosion crater (Mastbergen, 1991). The study given in report M1007 specifically deals with gaping leaks of potable water pipes resulting in erosion crater (Waterloopkundig Laboratorium, 1969).In order to find this relation, both scaled down and on scale experiments were carried out, each discussed below.

F.1. Scaled down experiments

The tests of the scaled down experiments were carried out with two sets of pipes of unknown material, having internal diameters of $D_{in} = 46.4\ mm$ and $D_{in} = 93\ mm$. All pipes were placed in a tank containing sand originating from Dutch dunes ($d_{50} = 0.22\ mm$). Dune sand is generally smaller than sand originating from the coast, i.e. the sand deposited in the inner-city of Amsterdam as explained in section 2.5. The reason of this difference in size being that dune sand is eroded by wind, whereas coastal sand is eroded by water. The gaping leaks were simulated in two ways: first as a hole in the pipe with a diameter $d = 0.25 \cdot D_{in}$, $d = 0.50 \cdot D_{in}$, and $d = D_{in}$, second as a pipe cut over the full axis of the pipe (thus $d = D_{in}$). The latter simulating a fully sheared of pipe. For all tests it was found that an equilibrium state was reached after about 5 minutes, independent of the size of the hole and exit velocity of the water from the pipe. The size of the erosion crater was found to be proportional to the exit velocity and the size of the hole and the ratio of the hole size over pipe diameter (d/D_{in}), but inversely proportional to the coverage. A reinterpretation of study M1007 carried out by Mastbergen (1991) determined that the depth of the erosion crater is virtually independent of the jet parameters exiting the pipe and can be determined using the inner diameter and the coverage. Figure F.1 provides pictures taken of the experiment setup after erosion pits were generated by both the pipe with a hole and a pipe cut off over its axis (Waterloopkundig Laboratorium, 1969).

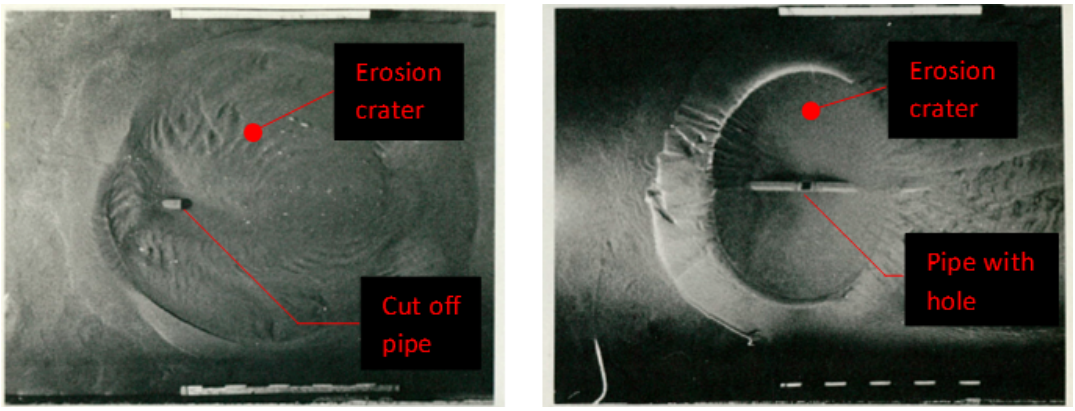

Figure F.1: Pictures of the experiment set up after the generation of erosion pits due to gaping leaks(Waterloopkundig Laboratorium, 1969).

F.2. On scale experiments

Additionally to a variety of scaled down experiments, two on scale experiments were carried out. Both were carried out using pipes of internal diameter $D_{in} = 600\ mm$, in a container with a coverage of $1.2\ m$ also using sand originating from the Dutch coast. The only difference was the simulation of the gaping leak, which was similar to the scaled down experiments: in one experiment a hole with a diameter $d_h = 0.5 \cdot D_{in}$, in the other the pipe was cut over the full axis of the pipe (thus $d_h = 1 \cdot D_{in}$). From these experiments it is known that the pressure in the pipes was of the same order as the operational pressures found in the potable water pipes of Amsterdam's inner-city ($25\ mwc$ as a maximum pressure in the experiment). In general, the findings of the on scale experiments were similar to the findings of their scaled down counterparts, with the exception being that the increase of erosion crater dimensions relative to the exit velocity of the water from the pipe was more substantial in the case of the on scale experiments.

F.3. Standard NEN 3651

Standard NEN 3651 is a derivative of the NEN 3650 series, the series formulated for pressurized utility lines in general. NEN 3651 provides additional measures for utility lines in the vicinity of important infrastructure, including primary flood defences (NEN, 2020b). Strictly speaking, inner-city quay walls are not part of this definition. However, due to lack of a standard formulated for inner-city quay walls (not to mention the lack of a standard formulated for utility lines in their vicinity), parts of this standard are applied.

Based on the experiments discussed in section F.1 (Waterloopkundig Laboratorium, 1969) and the reinterpretation of this study by Mastbergen (1991), analytical expressions were generated to determine the dimensions of erosion craters, which were added to standard NEN 3651. Due to the inherently conservative nature of NEN standards, the dimensions which result from these expressions are fairly high (i.e. 95% of the erosion craters generated by a gaping leak have smaller dimensions). The standard states that the width of the erosion crater (R_W), the dimension in direction of hole's axis, determines the length of the crater (R_L), the dimension over the length of the pipe. Of these parameters the expressions are given in equations F.1 and F.2 respectively. See figure F.2 for an overview of the definitions of these dimensions (NEN, 2020b). The definitions of these dimensions were formulated assuming a horizontal pipe and surface level with a hole located on a plane perpendicular to the surface level.

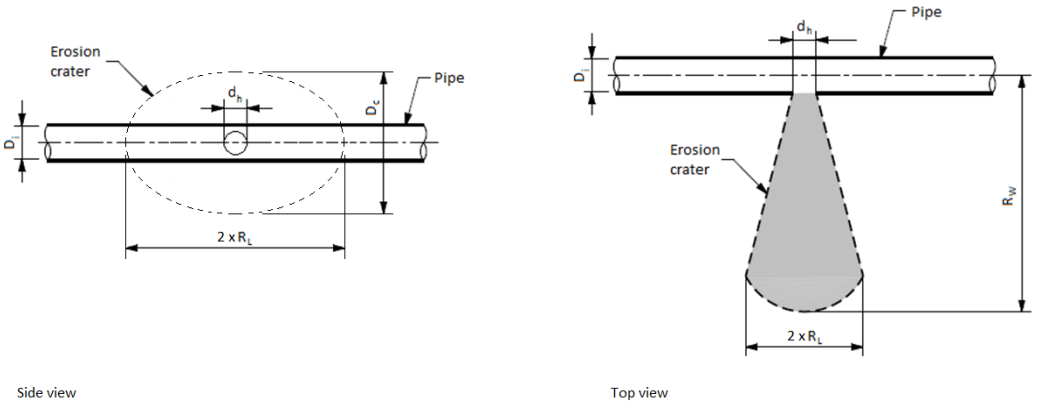

Figure F.2: Overview of the definitions of erosion crater dimensions (NEN, 2020b).

$$R_W = 7.8 \cdot d_h \cdot \left(\frac{P}{\rho_w \cdot g^{1.5} \cdot \mu \cdot d_h^{3.5}} \right)^{0.243} \tag{F.1}$$

In which:

d_h	Diameter of hole in pipe, for $0 < d_h \leq D_i$;
ρ_w	Density of water (1000 kg/m^3);
g	Gravitational acceleration (9.81 m/s^2);
μ	Discharge coefficient of hole. According to the standard, $\mu = 0.0002 \cdot h^2 - 0.02 \cdot h + 1$;
P	Hydraulic power of the outflow ($P = \rho \cdot g \cdot Q \cdot h$);
h	Pressure head at the location of the hole;
Q	Discharge through hole, which is calculated as follows: $Q = \mu \cdot A_h \cdot \sqrt{2 \cdot g \cdot h}$;
A_h	Area of hole in pipe. This hole is assumed to be circular, thus $A_h = \frac{1}{4} \cdot \pi \cdot d_h$.

$$\begin{aligned} &For\ a\ small\ hole: && R_L = 0.5 \cdot R_W \\ &For\ a\ large\ hole: && R_L = R_W \\ &For\ a\ fully\ sheared\ off\ pipe: && R_L = 2 \cdot R_W \end{aligned} \tag{F.2}$$

The height of the erosion crater (D_c) is virtually not dependent of the flow parameters, thus it is calculated using equation F.3.

$$D_c = 1.2 \cdot (D_o + H) \tag{F.3}$$

In which:

D_o	Outer diameter of the pipe;
H	Coverage of the pipe, set at 0.8 m.

The width of the erosion crater is plotted against the diameter of the gaping leak in figure F.3. The length of the erosion crater is plotted against the diameter of the gaping leak as well in figure F.4. The height of the erosion crater is plotted against the outer diameter of the potable water pipe in figure F.5.

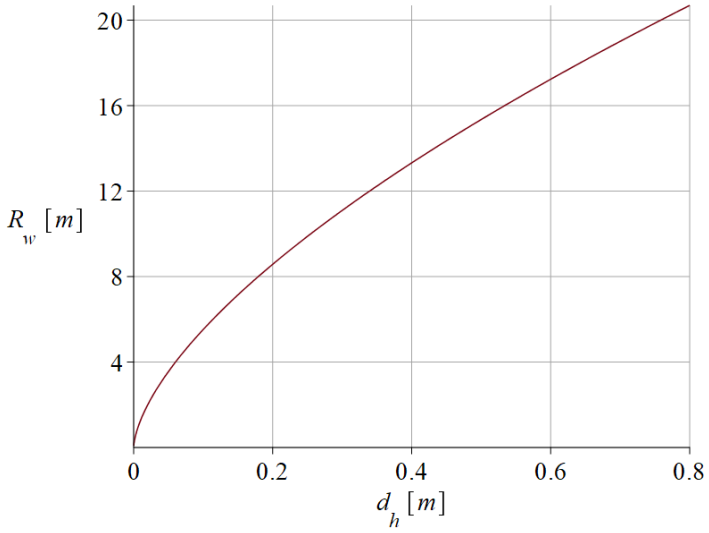

Figure F.3: Width of erosion crater (R_W) plotted against the diameter of the gaping leak (d_h).

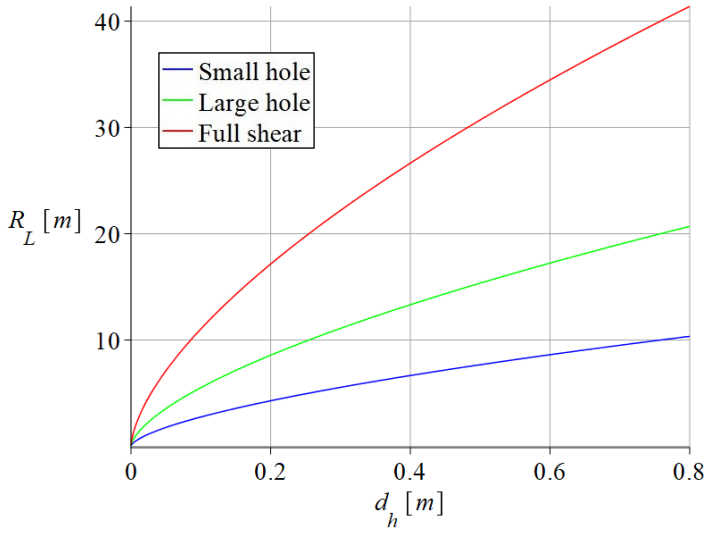

Figure F.4: Length of erosion crater (R_L) plotted against the diameter of the gaping leak (d_h).

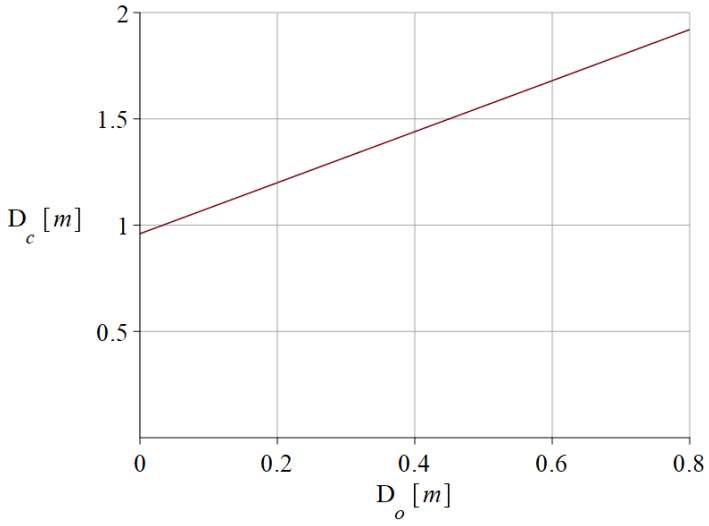

Figure F.5: Height of erosion crater (D_c) plotted against the outer diameter of the potable water pipe (D_o).

G

Adapted Sellmeijer model

To check if a structure is susceptible to erosion, the adapted Sellmeijer model test can be applied. This model produces a critical hydraulic gradient. If the hydraulic gradient over the structure is larger than the calculated critical gradient, the structure is susceptible to backward erosion. Previously, the more simple calculation method developed by Bligh was applied in order to check if a structure was susceptible to backward erosion. The consensus was that this method by Bligh was more conservative. However it was found that in various situations this simple method was even less conservative than the more complex Sellmeijer model, resulting in the adaption of the latter into various Dutch standards. Note that this model only takes a horizontal seepage path into account, thus in case of a fully functioning scour protection screen located behind the first pile row relative to the channel this test is invalid. This situation is discussed more in detail in section 6.1.2.

The experiments conducted by Sellmeijer were originally conducted in fine, compact sands. The model is fine tuned for a standard Dutch dike configuration of a homogeneous sand layer situated underneath an impervious soil layer. Although this situation differs from the situation of the quay walls, the situations are deemed similar enough to be used as a check for susceptibility of the structure to backward erosion. This is because in both situations, a layer with a high permeability (sand) which is susceptible to backward erosion is located underneath a impervious layer, namely clay for the dike and the wooden floor for the quay wall.

By following the Sellmeijer model test the critical hydraulic gradient was found as represented in figure G.1. As discussed in section 2.4, the channel is located at NAP -0.40 m. From section 2.5 it follows that the average surface level of the inner-city is located at NAP +1 m. If it is assumed that a water pipe leakage results in full saturation of the soil body surrounding the water pipe up to the surface level, this results in a hydraulic gradient over the structure ΔH of 1.4 m. From the graph in figure G.1 it follows that the structure is susceptible to backward erosion with high certainty for a horizontal seepage length L_s of up to about 5 m. In this determination the presence of a potential impervious soil layer at the downstream side of the structure is taken into account. As previously explained, the Sellmeijer model slightly over-predicts the critical hydraulic gradient in the situation of the quay walls, thus it can be said with high probability that the structure is susceptible to backward erosion for even larger seepage lengths.
The check for the structure's susceptibility to backward erosion according to the "Adapted Sellmeijer model" is given in equation G.1.

$$\frac{\Delta H_c}{\gamma_n \cdot \gamma_b} < (\Delta H - 0.3 \cdot d_s) \tag{G.1}$$

In which:

ΔH_c	Critical water gradient;
γ_n	Safety factor relating to the allowed exceedance frequency, set to 1.2;
γ_b	Safety factor due to schematization of the problem, set to 1.2;
ΔH	Water gradient present over the structure;
d_s	Thickness of the impervious soil layer covering the sand layer at channel side of the structure in m. Due to the uncertainty of the presence and thickness of this layer, this is set at 0.1 m.

The critical water gradient in the adapted Sellmeijer model is determined by three factors and the horizontal seepage length, as calculated in equation G.2.

$$\Delta H_c = L_s \cdot F_{resistance} \cdot F_{scale} \cdot F_{geometry} \tag{G.2}$$

In which:

L_s	Characteristic horizontal seepage length;
$F_{resistance}$	Relates to the equilibrium of sand particle on the bottom of the pipe formed by backward erosion, calculated in equation G.3;
F_{scale}	Relates to the difference of scale between the experiments and the situation in real life, calculated in equation G.4;
$F_{geometry}$	Relates to the geometry of the subsoil in regards to groundwater flow, calculated in equation G.5.

$$F_{resistance} = \frac{\gamma_p - \gamma_w}{\gamma_w} \cdot \eta \cdot tan\,\theta_r \tag{G.3}$$

$$F_{scale} = \frac{d_{70m}}{\sqrt[3]{\kappa \cdot L_s}} \left(\frac{d_{70}}{d_{70m}} \right)^{0.4} \tag{G.4}$$

$$F_{geometry} = 0.91 \cdot \left(\frac{D_{sand}}{L_s} \right)^{\frac{0.28}{(D_{sand}/L_s)^{2.8}-1}+0.04} \tag{G.5}$$

In which:

γ_p	Volumetric weight of sand particles, equal to 26 kN/m^3;
γ_w	Volumetric weight of water, equal to 9.81 kN/m^3;
η	White's coefficient, equal to 0.25;
θ_r	Roling resistance of sand particles, equal to 37^o;
d_{70m}	Mean value of the 70th percentile of the grain size distribution for which this formula is fitted, equal to $2.08 \cdot 10^{-4}$ m;
d_{70}	70th percentile of the grain size distribution of the sand layer susceptible to backwards erosion. Due to the uncertainty of its grainsize distribution of the sand layer, this is set at $7 \cdot 10^{-4}$ m;
κ	Intrinsic permeability of the sand layer susceptible to backwards erosion ($\kappa = 1.35 \cdot 10^{-7} \cdot k$);
k	Permeability of the sand layer susceptible to backwards erosion, set at 10^{-4} m/s which follows from the experiments conducted by van Beek (2015);
D_{sand}	Characteristic thickness of the sand layer susceptible to backwards erosion in m; Due to the uncertainty of the soil medium and settlements, this is set at 0.5 m.

Substitution of the previously explained parameters in the aforementioned equations and plotting the resulting critical water gradient of equation G.2 results in the graph represented in figure G.1. As said in section 2.4, the channel is located at NAP -0.40 m. From section 2.5 it follows that the average surface level of the inner-city is located at NAP +1 m. If it is assumed that a water pipe leakage results in full saturation of the soil body surrounding the water pipe up to the surface level, this results in a water gradient over the structure ΔH equal to 1.4 m. From the graph in figure G.1 it follows that the structure is susceptible to backward erosion with high certainty for a horizontal seepage length L_s of up to about 5 m.

Additionally, it is checked if saturation up to the level of potable water pipes results in susceptibility of backward erosion. As the coverage of potable water pipes is generally equal to 0.8 m, this results in a gradient ΔH equal to 0.6 m. At this gradient, a horizontal seepage length of about 2 m is found. Thus it can be concluded that also at saturation up to the level of potable water pipe, the structure is susceptible to backward erosion.

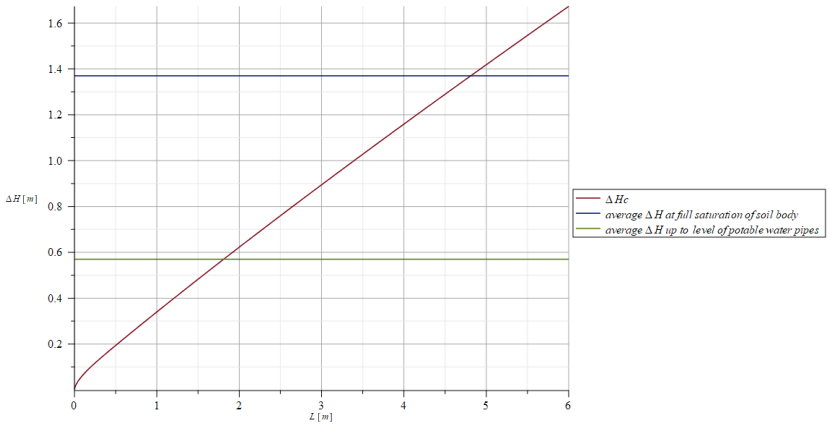

Figure G.1: Graph of the critical hydraulic gradient for which backward erosion is an issue according to the adapted Sellmeijer model.

H

PLAXIS 2D model

In this appendix, the PLAXIS 2D model used to determine the influence of horizontal quay wall displacement on displacement of the soil body behind the quay wall structure is explained. PLAXIS 2D is a FEM package meant for geotechnical analysis, especially appropriate for modelling soil structure interaction and soil deformation, including time-dependent deformations (Bentley, n.d.b). The package consists of a number of models, each specialising in a particular part of geotechnical engineering. First the soil properties are discussed, next the structure used to represent the quay wall is explained, followed by an overview of the the overall composition of the model and the phases the model runs trough used to mimic the displacement. It has to be noted that the model described in this appendix is fairly simple, solely meant to provide insight in the behaviour of the soil behind the quay wall.

H.1. Soil properties

In this section, the soil parameters used in the PLAXIS 2D model are discussed. First the assumption of the sole presence of sand is discussed in section H.1.1. Next the type of material model is explained in section H.1.2. A list of the relevant soil parameters is provided last in section H.1.3

H.1.1. Assumption of sole presence of sand in model

As discussed in section 2.5, the soil profile in the upper layers in the vicinity of quay walls mostly consists of deposited sand originating from both dunes and beaches along the coast of The Netherlands. Although it might be reasonable to assume that other soil types are located in the soil body behind the quay wall, it is chosen only to use sand in the PLAXIS 2D model. This is partly due to the uncertainty of the other soil types present in said soil body, but also partly due to the fact that of all possible soil types present, i.e. most likely sand, peat and clay, sand is the most susceptible to internal erosion (Verruijt, 2001). Additionally, it is assumed that utility line leakages in f.e. a sufficiently thick clay layer can result in the clay layer forming a water tight seal at the leakage location, limiting its effect on quay wall failure.

H.1.2. Material model

PLAXIS 2D has a large number of models available to represent the behaviour of soil. According the the PLAXIS Material Models Manual (Bentley, 2020a) both the Mohr-Coulomb model and the Hardening Soil model represent soils in drained situation subjected to slow and not too extreme deformations relatively well. The main trade-off is found in the fact that the "Mohr-Coulomb" model assumes that after loading, the soil returns to its original state, which in reality is not the case. In the "Hardening Soil" model, this effect called "shear hardening" is taken into account, resulting in a much stiffer soil after the first loading-unloading cycle. Although the model is more advanced, little computational time is added. Therefore, the "Hardening Soil" model is chosen to represent the soil body.

H.1.3. Overview of soil parameters

In this section, a number of relevant soil parameters are provided. Note that due to the uncertainty of all parameters, most of them were kept at the default value provided by PLAXIS itself (Bentley, 2020b).

- **Weight of the soil**
  The dry weight of soil was set at 16 kPa, while the saturated weight of the soil was set at 20 kPa, based on data provided by NEN standard 3650-1 (NEN, 2020a).

- **Secant stiffness in standard drained triaxial test**
  The secant stiffness in standard drained triaxial test is asssumed to be in the order of magnitude as the assumed modulus of elasticity as provided by Reinders (2019), which is equal to 30 MPa. Note that the tangent stiffness for primary oedometer loading is assumed to be equal to 30 MPa as well.

- **Angle of internal erosion ϕ**
  According to NEN 3650 (NEN, 2020a), it is reasonably to assume an angle of internal erosion of the soil equal to 30^o.

- **Groundwater flow**
  Although of less importance in the model, a "Van Genuchten" groundwater flow model is chosen. For the grain size distribution, the soil type "sand" is chosen.

- **Interfaces**
  As the model is not meant to model the effect of soil on the structure, the interface between soil and structure is set to 1, i.e. a rigid interface.

H.2. Quay wall structure

The quay wall structure is modelled as concrete. Mainly due to the fact that masonry behaves similar in tension to concrete, as explained in section 2.2. It has to be noted that the material properties of the quay wall were of a low significance, due to the fact that the model is used to find the behaviour of the soil body located behind the quay wall. The gravity wall is modelled as two vertical concrete elements with a height equal to 3 m, connected by two horizontal elements equal to 0.65 m. As all elements have a thickness equal to 0.35 m, this results in a gravity wall with a width in the order of 1 m. The quay wall floor is modelled as a horizontal concrete element with a width equal to 4 m and a thickness of 0.35 m. The motion of the quay wall floor is fixed in vertical direction, mimicking the effect of a pile foundation situated underneath the floor. The modulus of elasticity of the concrete is set at 30 GPa (Reinders, 2019). The connection between the quay wall floor and gravity wall is assumed to be rigid, which results in an equal horizontal displacement of floor to the wall. This is a fairly exaggerated representation of the real life situation, as piles are likely to be able to resist motion in the horizontal direction. However, if sufficient erosion around the piles has taken place, their capability to resist motion in horizontal direction diminishes.

H.3. Model composition and staged construction

In order to limit potential effects due to too closely situated borders, the grid size is set at 35 m horizontally by 10 m vertically. The groundwater level is set at 1.4 m from surface level, equal to the level of the channels as discussed in section 2.5. The soil body is extruded left of the quay wall structure in order to mimic the channel. The depth of the channel is assumed to be equal to be located 4 m from surface level. Note that in order to limit numerical issues, a slope is applied from the bottom of the channel up to the quay wall. As said before, only the soil body located behind the quay wall is of interest. Therefore, only one soil type is assumed for the total model. See figure H.1 for an overview of the model over the full width, and figure H.2 for a more detailed view at the location of interest of the model. As a boundary condition, free flow of groundwater is imposed in the model. To execute the PLAXIS model, a medium mesh is generated. The imposed deformation is applied to the gravity wall as showed in figure H.2, with increasing steps of 20 mm each in a separate phase, up to a deformation of 100 mm.

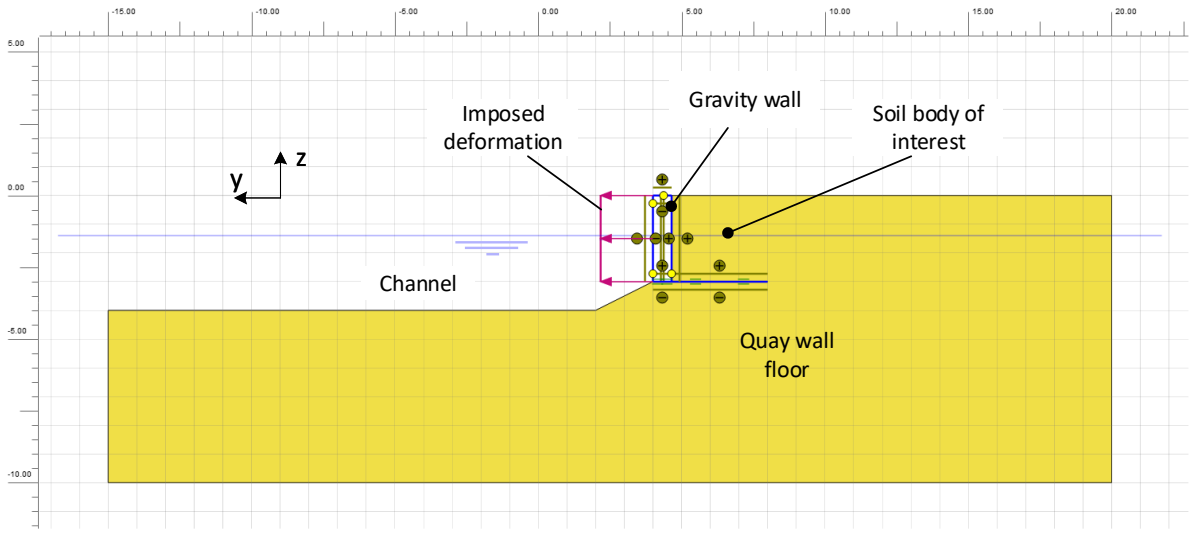

Figure H.1: Overview of the PLAXIS 2D model over full width.

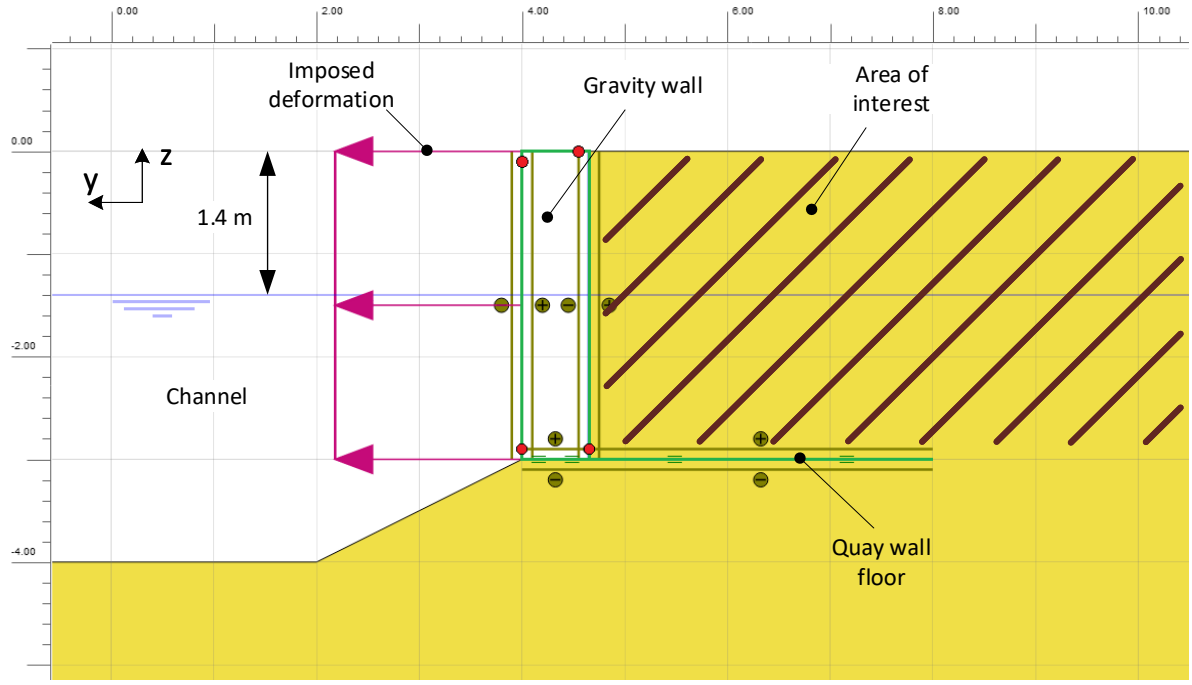

Figure H.2: Detailed overview of the PLAXIS 2D model. Note that both the positive and negative interfaces of the upper element of the gravity wall has been left out of the figure for simplicity.

I

Analytical model

In this appendix a number of additional equations used in the analytical model are provided.

I.1. Horizontal soil spring stiffness

The equations used in the determination of the horizontal soil spring stiffness are provided as given in NEN3650-1 (NEN, 2020a).

I.1.1. Soil spring stiffness: maximum allowable soil deformation

The maximum allowable soil deformation is determined using equation I.1

$$y_{s,max} = D_o \cdot \left(0.05 + 0.03 \cdot \left(\frac{Z}{D_o + 0.5}\right)\right) \tag{I.1}$$

In which:

$y_{s,max}$	Maximum allowable soil deformation;
D_o	Outer diameter of the utility line;
H	Soil coverage of the utility line;
Z	Soil depth up to the utility line's longitudinal axis ($Z = H + D_o/2$).

I.1.2. Soil spring stiffness: horizontal equilibrium bearing capacity

The horizontal equilibrium bearing capacity is determined using equation I.2. This equation is valid for sand in a slowly loaded, drained situation.

$$q_{he} = K_q \cdot \sigma' \tag{I.2}$$

In which:

q_{he}	Horizontal equilibrium bearing capacity;
K_q	Loading coefficient according to the theory of Brinch Hansen, determined using the graph in figure I.1;
σ'	Effective vertical soil pressure at the level of the utility line's longitudinal axis, calculated using equation I.3.

$$\sigma' = \gamma' \cdot Z \tag{I.3}$$

In which:

γ'	Effective weight of the soil, i.e. its dry weight.

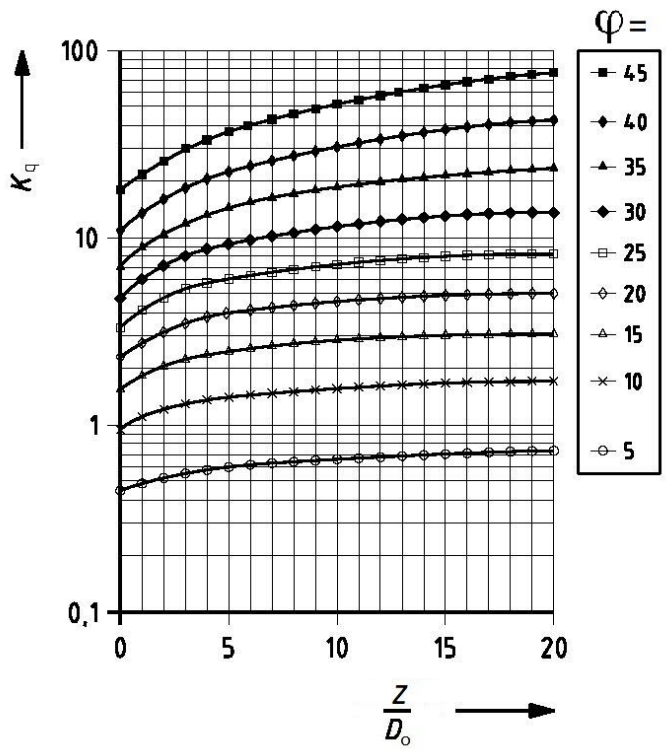

Figure I.1: Graph used to determine the loading coefficient K_q NEN (2020a). Note that ϕ is equal to the internal angle of friction of the soil.

I.2. Vertical soil spring stiffness

Similarly to the horizontal spring stiffness, its vertical counterpart (K_v) is determined using standard NEN 3650-1 (NEN, 2020a). For downward motion, equation I.4 provides the determination of the vertical spring stiffness for sand.

$$K_{v,1} = 0.5 \cdot E_s \cdot \frac{P_{we}}{D_o} \qquad for\ 0 \cdot P_{we} < P_w \leq \frac{2}{3} \cdot P_{we} \tag{I.4}$$
$$K_{v,2} = 0.1 \cdot E_s \cdot \frac{P_{we}}{D_o} \qquad for\ P_w > \frac{2}{3} \cdot P_{we}$$

In which:

E_s Modulus of elasticity of the soil. According to Reinders (2019), for sand this is in the order of magnitude of 30 MPa;

P_{we} Vertical equilibrium bearing capacity, determined using the Brinch-Hansen formula for a drained situation, given in equation I.5;

$$p_{we} = 0.95 \cdot (0.5 \cdot \gamma'_{mean} \cdot D_o \cdot N_\gamma \cdot S_\gamma + S_q \cdot N_q \cdot d_q \cdot q_n) \tag{I.5}$$

In which:

γ'_{mean}	Mean effective volumetric weight ranging from surface level to the level of the utility line axis;
N_γ	Auxiliary factor, $N_\gamma = 1.5 \cdot (N_q - 1) \cdot tan\phi$;
ϕ	Angle of internal erosion of the soil;
S_γ	Auxiliary factor, $S_\gamma = 1 - 0.4 \cdot D_o / L_{sup}$;
L_{sup}	Minimal support length, here $D_o / L_{sup} = 0.1$;
S_q	Shape factor for utility lines, $S_q = 1 + sin\phi \cdot D_o / L_{sup}$;
N_q	Auxiliary factor, $N_q = e^{\pi \cdot tan\phi} \cdot tan^2(45 + \phi/2)$;
d_q	Auxiliary factor, $d_q = 1 + 2 \cdot tan\phi \cdot (1 - sin\phi)^2 \cdot arctan(Z/D_o)$;
Z	Soil depth up to the utility line's longitudinal axis ($Z = H + D_o/2$);
H	Coverage of the utility line;
q_n	Neutral soil pressure, $q_n = \gamma' \cdot H$.

For the input parameters as given in section 7.6, both the horizontal- and vertical spring stiffness are determined. See tables I.1 and I.2 for the horizontal- and vertical spring stiffness at a coverage of 0.8 m and 2.03 m respectively. The horizontal bearing capacity is calculated at both 66% and 100% of horizontal equilibrium bearing capacity, coinciding to the values of vertical equilibrium bearing capacity of $K_{v,1}$ and $K_{v,2}$ respectively.

Table I.1: Horizontal- and vertical spring stiffness for typical utility line outer diameters at a coverage of 0.8 m.

D_o $[mm]$	$K_{v,1}$ $[kN/m/m]$	$K_{v,2}$ $[kN/m/m]$	$K_{h,66\%}$ $[kN/m/m]$	$K_{h,100\%}$ $[kN/m/m]$
100	51680	10336	4462	1485
200	26148	5229	4397	1463
300	17686	3537	4374	1456
400	13487	2697	4327	1440
500	10989	2198	4398	1464
600	9340	1868	4561	1518
700	8172	1634	4634	1542
800	7304	1461	4827	1606

Table I.2: Horizontal- and vertical spring stiffness for typical utility line outer diameters at a coverage of 2.03 m.

D_o $[mm]$	$K_{v,1}$ $[kN/m/m]$	$K_{v,2}$ $[kN/m/m]$	$K_{h,66\%}$ $[kN/m/m]$	$K_{h,100\%}$ $[kN/m/m]$
300	43798	8759	8114	2700
400	32998	6600	8407	2798
500	26530	5306	8332	2773
600	22228	4446	8484	2824
700	19162	3832	8778	2921
800	16870	3374	8811	2932
900	15093	3019	8901	2962
1000	13675	2735	9068	3018

From the previous tables it follows that the difference between the vertical- and horizontal spring stiffness is the most pronounced for smaller diameters of utility lines. However, it follows from the sensitivity analysis in section 8.4 that the influence of the magnitude of the spring stiffness is limited on the output of the analytical model. Additionally, as vertical soil displacements are in smaller than the horizontal soil displacements in case of horizontal quay wall displacement, the assumption is made that the horizontal soil displacement and horizontal distributed horizontal springs are governing for the model.

I.3. Cross-sectional moment of inertia for hollow circular cross-sections

The cross-sectional moment of inertia for hollow circular cross-sections as used in the EoM's is given in equation I.6.

$$I = \frac{\pi}{64} \cdot (D_o^4 - (D_o - 2 \cdot t)^4) \tag{I.6}$$

In which:
t is equal to the thickness of the utility line.

I.4. Relation influence length and utility line dimension

Equation I.7 represents the calculation of the influence length, i.e. the length over which a boundary condition has influence in a Winkler foundation, according to Hetényi (1946).

$$L_{infl} = \pi \cdot \sqrt[4]{\frac{4 \cdot E \cdot I}{K_h}} \tag{I.7}$$

In order to determine the influence length's relation to the dimension of an utility line, the horizontal spring stiffness in case of 100% equilibrium bearing capacity is determined by combining equations I.1, I.2, and I.3 (see equation I.8)

$$K_h = \frac{5 \cdot (2 \cdot D_o + 1)(2 \cdot H + D_o) \cdot \gamma' \cdot K_q}{(1.3 \cdot D_o + 0.5 + 0.6 \cdot H) \cdot D_o} \tag{I.8}$$

By definition, the thickness of a utility line is smaller than its outer diameter (thus $D_o > t$). In this determination, a thickness equal to 5% of the outer diameter is assumed (fairly thick for utility lines). For utility lines located on the same placement depth, parameters H, γ' and E do not vary. According to equation I.1 and figure I.1, parameter K_q is inversely proportional to D_o. However, for phi equal to 30^o, its value has a minimal magnitude of about 6. Substitution of the aforementioned values and equation I.8 into equation I.7 results in equation I.9.

$$L_{infl} = \frac{\pi}{2} \cdot \left(\frac{\pi (D_o^4 - (D_o - 2 \cdot 0.05 \cdot D_o)^4) \cdot (1.3 \cdot D_o^2 + 1.1 \cdot D_o)}{960 + 960 \cdot D_o^2 + 2400 D_o} \right)^{0.25} \tag{I.9}$$

Plotting of the previous equation for of utility line diameters up to 1000 mm results in the graph represented in figure I.2. From this graph it follows that larger outer diameters result in greater lengths of influence.

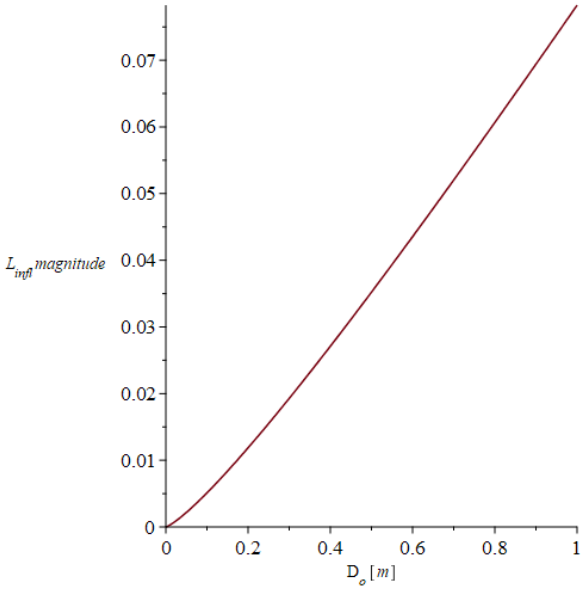

Figure I.2: Graph plotting the outer diameter of an utility line in relation to the magnitude of influence length.

I.5. Overview of case 1: utility line displacement larger than maximum allowable soil deformation

In this section, an overview is provided for the analytical model for quay wall displacement over greater length, with relative utility line displacements larger than the maximum allowable soil deformation. The overview for all sections

of utility line is provided in equation I.10. Next, the EoM's are provided in section I.11. The solutions to the EoM are provided in section I.12. An overview of the model is first provided in figure I.3.

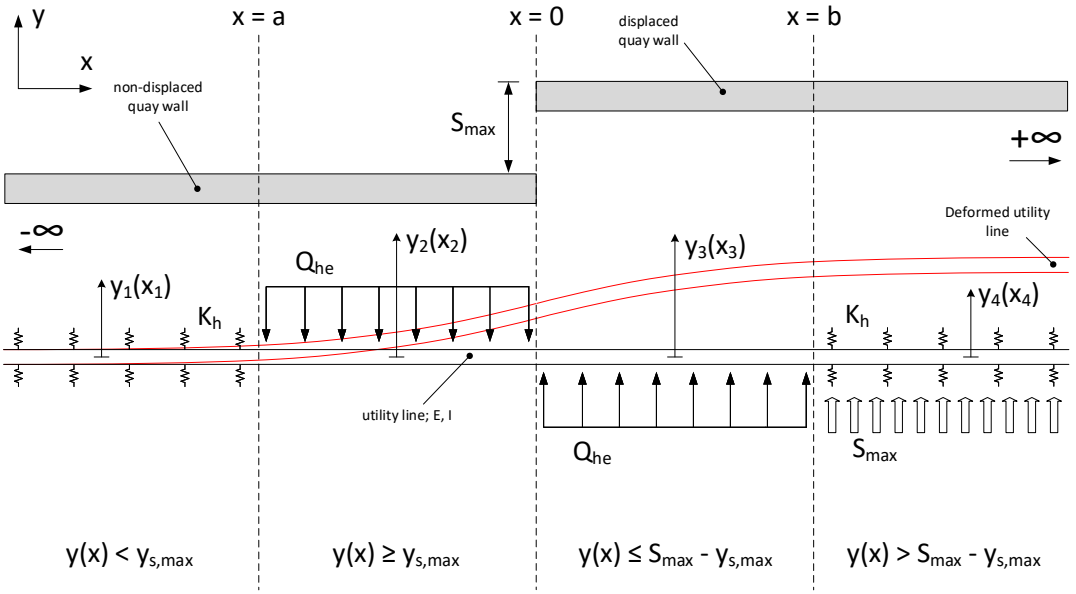

Figure I.3: Model of the case: quay wall deformation over greater length, utility line displacement larger than maximum allowable soil deformation.

$$
\begin{aligned}
&y(x)=y_1(x_1) && for\ x<a && if\ x<a && \rightarrow\ y(x)<y_{s,max}\\
&y(x)=y_2(x_2) && for\ a\le x\le 0 && if\ a\le x\le 0 && \rightarrow\ y(x)\ge y_{s,max}\\
&y(x)=y_3(x_3) && for\ 0\le x\le b && if\ 0\le x\le b && \rightarrow\ y(x)\le S_{max}-y_{s,max}\\
&y(x)=y_4(x_4) && for\ x>b && if\ x>b && \rightarrow\ y(x)>S_{max}-y_{s,max}
\end{aligned}
\tag{I.10}
$$

$$
\begin{aligned}
&E\cdot I\cdot\frac{d^4}{dx_1^4}y_1(x_1)+K_h\cdot y_1(x_1)=0\\
&E\cdot I\cdot\frac{d^4}{dx_2^4}y_2(x_2)=-q_{he}\\
&E\cdot I\cdot\frac{d^4}{dx_3^4}y_3(x_3)=q_{he}\\
&E\cdot I\cdot\frac{d^4}{dx_4^4}y_4(x_4)+K_h\cdot y_4(x_4)=K_h\cdot S_{max}
\end{aligned}
\tag{I.11}
$$

$$
\begin{aligned}
&y_1(x_1)=e^{\beta\cdot x_1}(C_{13}\cdot cos(\beta\cdot x_1)+C_{14}\cdot sin(\beta\cdot x_1))\\
&y_2(x_2)=-\frac{1}{24}\cdot\frac{q_{he}}{E\cdot I}+\frac{1}{6}\cdot C_{21}\cdot x_2^3+\frac{1}{2}\cdot C_{22}\cdot x_2^2+C_{23}\cdot x_2+C_{24}\\
&y_3(x_3)=\frac{1}{24}\cdot\frac{q_{he}}{E\cdot I}+\frac{1}{6}\cdot C_{31}\cdot x_3^3+\frac{1}{2}\cdot C_{32}\cdot x_3^2+C_{33}\cdot x_3+C_{34}\\
&y_4(x_4)=e^{-\beta\cdot x_4}(C_{41}\cdot cos(\beta\cdot x_4)+C_{42}\cdot sin(\beta\cdot x_4))+S_{max}
\end{aligned}
\tag{I.12}
$$

$$
\beta=\sqrt[4]{\frac{K_h}{4\cdot E\cdot I}}
$$

I.6. Overview of case 1: utility line displacement smaller than maximum allowable soil deformation

In this section, an overview is provided for the analytical model for quay wall displacement over greater length, with relative utility line displacements smaller than the maximum allowable soil deformation. The overview for all sections of utility line is provided in equation I.13. Next, the EoM's are provided in section I.14. The solutions to the EoM are provided in section I.15. An overview of the model is first provided in figure I.4.

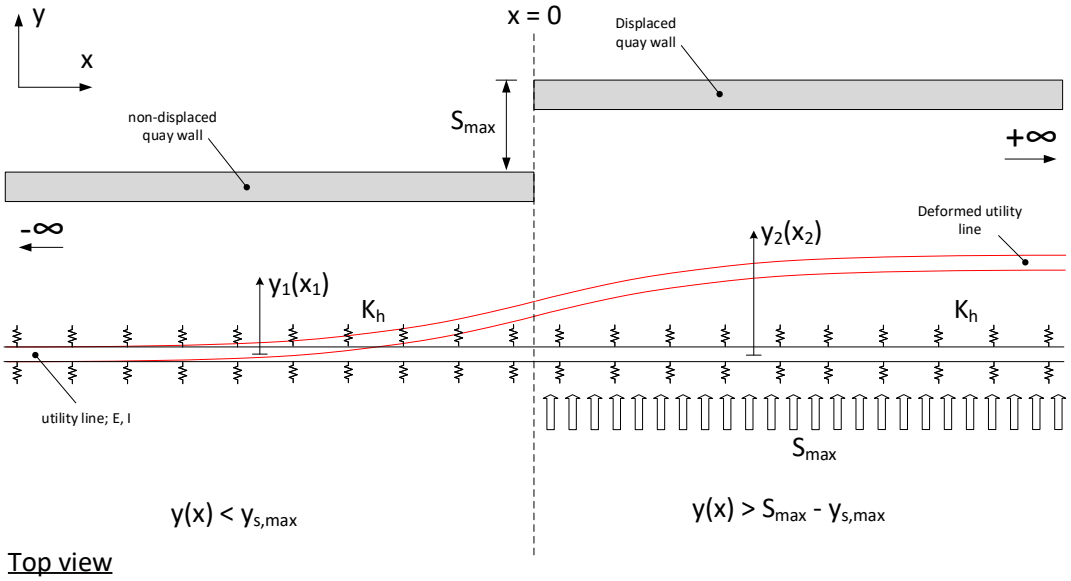

Figure I.4: Model of the case: quay wall displacement over greater length, utility line deformation smaller than maximum allowable soil deformation.

$$\begin{aligned} y(x) &= y_1(x_1) \quad for\ x<0 \quad if\ x<0 \quad \rightarrow\ y(x)<y_{s,max} \\ y(x) &= y_2(x_2) \quad for\ x\geq 0 \quad if\ x\geq 0 \quad \rightarrow\ y(x)>S_{max}-y_{s,max} \end{aligned} \tag{I.13}$$

$$\begin{aligned} E\cdot I\cdot\frac{d^4}{dx_1^4}y_1(x_1)+K_h\cdot y_1(x_1)&=0 \\ E\cdot I\cdot\frac{d^4}{dx_2^4}y_2(x_2)+K_h\cdot y_2(x_2)&=K_h\cdot S_{max} \end{aligned} \tag{I.14}$$

$$\begin{aligned} y_1(x_1)&=e^{\beta\cdot x_1}(C_{13}\cdot cos(\beta\cdot x_1)+C_{14}\cdot sin(\beta\cdot x_1)) \\ y_2(x_2)&=e^{-\beta\cdot x_2}(C_{21}\cdot cos(\beta\cdot x_2)+C_{22}\cdot sin(\beta\cdot x_2))+S_{max} \end{aligned} \tag{I.15}$$

$$\beta=\sqrt[4]{\frac{K_h}{4\cdot E\cdot I}}$$

I.7. Overview of case 2: utility line displacement smaller than maximum allowable soil deformation over full length

In this section, an overview is provided for the analytical model for quay wall displacement over greater length, with relative utility line displacements smaller than the maximum allowable soil deformation. The overview for all sections of utility line is provided in equation I.16. Next, the EoM's are provided in section I.17. The solutions to the EoM are provided in section I.18. An overview of the model is first provided in figure .. I.5.

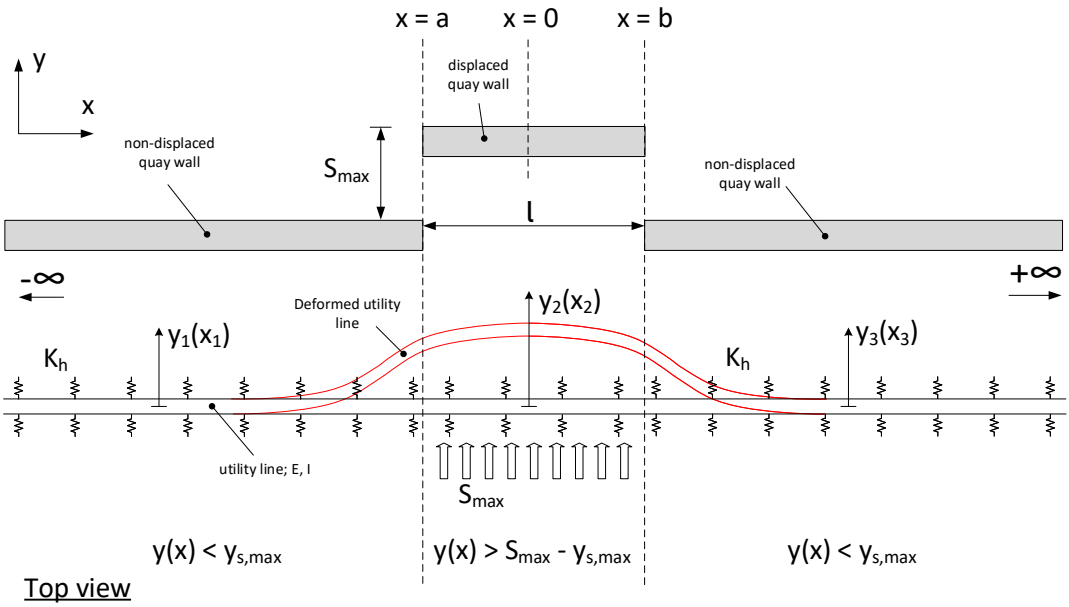

Figure I.5: Model of the case: Localized quay wall displacement, utility line displacement smaller than maximum allowable soil deformation over full length

$$\begin{aligned} &y(x) = y_1(x_1) && for\ x < b && if\ x < b && \rightarrow\ y(x) < y_{s,max} \\ &y(x) = y_2(x_2) && for\ b \le x \le c && if\ b \le x \le c && \rightarrow\ y(x) > S_{max} - y_{s,max} \\ &y(x) = y_3(x_3) && for\ x > c && if\ x > c && \rightarrow\ y(x) < y_{s,max} \end{aligned} \tag{I.16}$$

$$\begin{aligned} E \cdot I \cdot \frac{d^4}{dx_1^4} y_1(x_1) + K_h \cdot y_1(x_1) &= 0 \\ E \cdot I \cdot \frac{d^4}{dx_1^4} y_2(x_2) + K_h \cdot y_2(x_2) &= K_h \cdot S_{max} \\ E \cdot I \cdot \frac{d^4}{dx_3^4} y_3(x_3) + K_h \cdot y_1(x_3) &= 0 \end{aligned} \tag{I.17}$$

$$\begin{aligned} y_1(x_1) &= e^{\beta \cdot x_1} (C_{13} \cdot cos(\beta \cdot x_1) + C_{14} \cdot sin(\beta \cdot x_1)) \\ y_2(x_2) &= e^{-\beta \cdot x_2} (C_{21} \cdot cos(\beta \cdot x_2) + C_{22} \cdot sin(\beta \cdot x_2)) + \\ &\quad e^{\beta \cdot x_2} (C_{23} \cdot cos(\beta \cdot x_2) + C_{24} \cdot sin(\beta \cdot x_1)) + S_{max} \\ y_3(x_3) &= e^{-\beta \cdot x_3} (C_{31} \cdot cos(\beta \cdot x_3) + C_{32} \cdot sin(\beta \cdot x_3)) \end{aligned} \tag{I.18}$$

$$\beta = \sqrt[4]{\frac{K_h}{4 \cdot E \cdot I}}$$

I.8. Overview of case 2: utility line displacement only greater than maximum allowable soil deformation in displaced soil section

In this section, an overview is provided for the analytical model for quay wall displacement over greater length, with relative utility line displacements smaller than the maximum allowable soil deformation. The overview for all sections of utility line is provided in equation I.19. Next, the EoM's are provided in section I.20. The solutions to the EoM are provided in section I.21. An overview of the model is first provided in figure I.6.

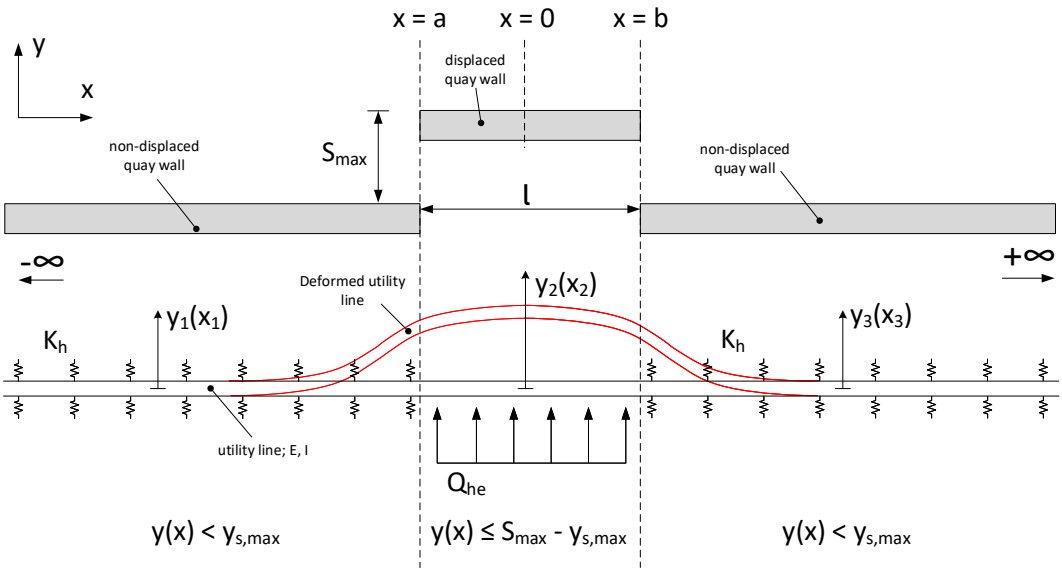

Figure I.6: Model of the case: localized quay wall displacement, utility line displacement only greater than maximum allowable soil deformation in displaced soil section.

$$\begin{aligned} y(x) &= y_1(x_1) \quad for\ x<b \quad if\ x<b \quad \rightarrow\ y(x)<y_{s,max} \\ y(x) &= y_2(x_2) \quad for\ b\leq x\leq c \quad if\ b\leq x\leq c \quad \rightarrow\ y(x)\leq S_{max}-y_{s,max} \\ y(x) &= y_3(x_3) \quad for\ x>c \quad if\ x>c \quad \rightarrow\ y(x)<y_{s,max} \end{aligned} \tag{I.19}$$

$$\begin{aligned} E\cdot I\cdot\frac{d^4}{dx_1^4}y_1(x_1)+K_h\cdot y_1(x_1)&=0 \\ E\cdot I\cdot\frac{d^4}{dx_2^4}y_2(x_2)&=q_{he} \\ E\cdot I\cdot\frac{d^4}{dx_3^4}y_3(x_3)+K_h\cdot y_1(x_3)&=0 \end{aligned} \tag{I.20}$$

$$\begin{aligned} y_1(x_1)&=e^{\beta\cdot x_1}(C_{13}\cdot cos(\beta\cdot x_1)+C_{14}\cdot sin(\beta\cdot x_1)) \\ y_2(x_2)&=\frac{1}{24}\cdot\frac{q_{he}}{E\cdot I}+\frac{1}{6}\cdot C_{21}\cdot x_2^3+\frac{1}{2}\cdot C_{22}\cdot x_2^2+C_{23}\cdot x_2+C_{24} \\ y_3(x_3)&=e^{-\beta\cdot x_3}(C_{31}\cdot cos(\beta\cdot x_3)+C_{32}\cdot sin(\beta\cdot x_3)) \end{aligned} \tag{I.21}$$

$$\beta=\sqrt[4]{\frac{K_h}{4\cdot E\cdot I}}$$

I.9. Overview of case 2: utility line displacement greater than maximum allowable soil deformation both in displaced soil section as right next to displacement

In this section, an overview is provided for the analytical model for quay wall displacement over greater length, with relative utility line displacements smaller than the maximum allowable soil deformation. The overview for all sections of utility line is provided in equation I.22. Next, the EoM's are provided in section I.23. The solutions to the EoM are provided in section I.24. An overview of the model is first provided in figure I.7.

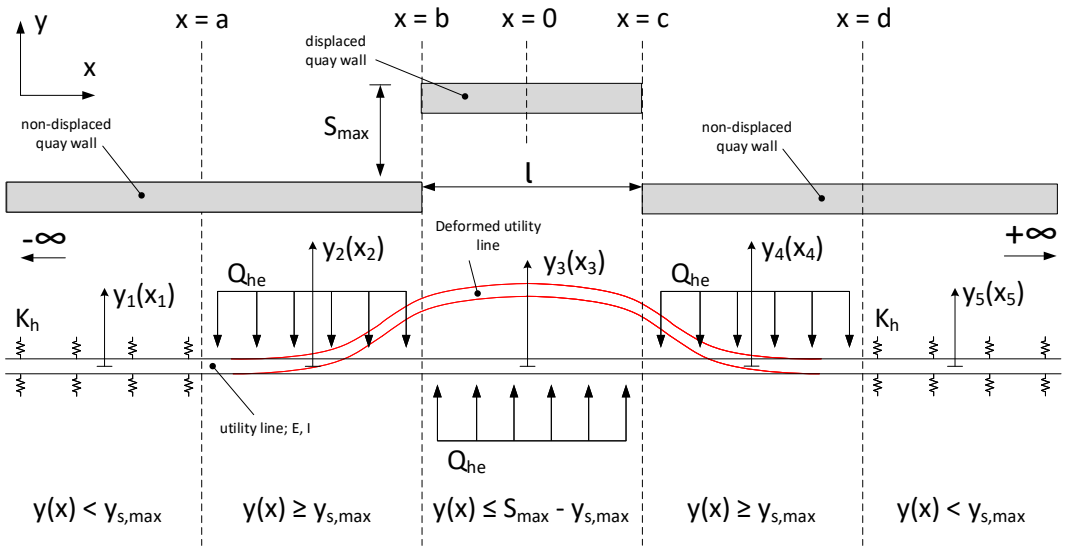

Figure I.7: Analytical model of the case: localised quay wall deformation, utility line displacement partially greater than maximum allowable soil deformation

$$
\begin{aligned}
&y(x)=y_1(x_1) && for\ x<a && if\ x<a && \rightarrow\ y(x)<y_{s,max}\\
&y(x)=y_2(x_2) && for\ a\le x\le b && if\ a\le x\le b && \rightarrow\ y(x)\ge y_{s,max}\\
&y(x)=y_3(x_3) && for\ b\le x\le c && if\ b\le x\le c && \rightarrow\ y(x)\le S_{max}-y_{s,max}\\
&y(x)=y_4(x_4) && for\ c\le x\le d && if\ c\le x\le d && \rightarrow\ y(x)\ge y_{s,max}\\
&y(x)=y_5(x_5) && for\ x>d && if\ x>d && \rightarrow\ y(x)<y_{s,max}
\end{aligned}
\tag{I.22}
$$

$$
\begin{aligned}
E\cdot I\cdot\frac{d^4}{dx_1^4}y_1(x_1)+K_h\cdot y_1(x_1)&=0\\
E\cdot I\cdot\frac{d^4}{dx_2^4}y_2(x_2)&=-q_{he}\\
E\cdot I\cdot\frac{d^4}{dx_3^4}y_3(x_3)&=q_{he}\\
E\cdot I\cdot\frac{d^4}{dx_4^4}y_4(x_4)&=-q_{he}\\
E\cdot I\cdot\frac{d^4}{dx_5^4}y_5(x_5)+K_h\cdot y_5(x_5)&=0
\end{aligned}
\tag{I.23}
$$

$$
\begin{aligned}
y_1(x_1)&=e^{\beta\cdot x_1}(C_{13}\cdot cos(\beta\cdot x_1)+C_{14}\cdot sin(\beta\cdot x_1))\\
y_2(x_2)&=-\frac{1}{24}\cdot\frac{q_{he}}{E\cdot I}+\frac{1}{6}\cdot C_{21}\cdot x_2^3+\frac{1}{2}\cdot C_{22}\cdot x_2^2+C_{23}\cdot x_2+C_{24}\\
y_3(x_3)&=\frac{1}{24}\cdot\frac{q_{he}}{E\cdot I}+\frac{1}{6}\cdot C_{31}\cdot x_3^3+\frac{1}{2}\cdot C_{32}\cdot x_3^2+C_{33}\cdot x_3+C_{34}\\
y_4(x_4)&=-\frac{1}{24}\cdot\frac{q_{he}}{E\cdot I}+\frac{1}{6}\cdot C_{41}\cdot x_4^3+\frac{1}{2}\cdot C_{42}\cdot x_4^2+C_{43}\cdot x_4+C_{44}\\
y_5(x_5)&=e^{-\beta\cdot x_5}(C_{51}\cdot cos(\beta\cdot x_5)+C_{52}\cdot sin(\beta\cdot x_5))
\end{aligned}
\tag{I.24}
$$

$$\beta=\sqrt[4]{\frac{K_h}{4\cdot E\cdot I}}$$

I.10. Overview of case 2: utility line displacement partially smaller than maximum allowable soil deformation in displaced soil section

In this section, an overview is provided for the analytical model for quay wall displacement over greater length, with relative utility line displacements smaller than the maximum allowable soil deformation. The overview for all sections of utility line is provided in equation I.25. Next, the EoM's are provided in section I.26. The solutions to the EoM are provided in section I.27. An overview of the model is first provided in figure I.8.

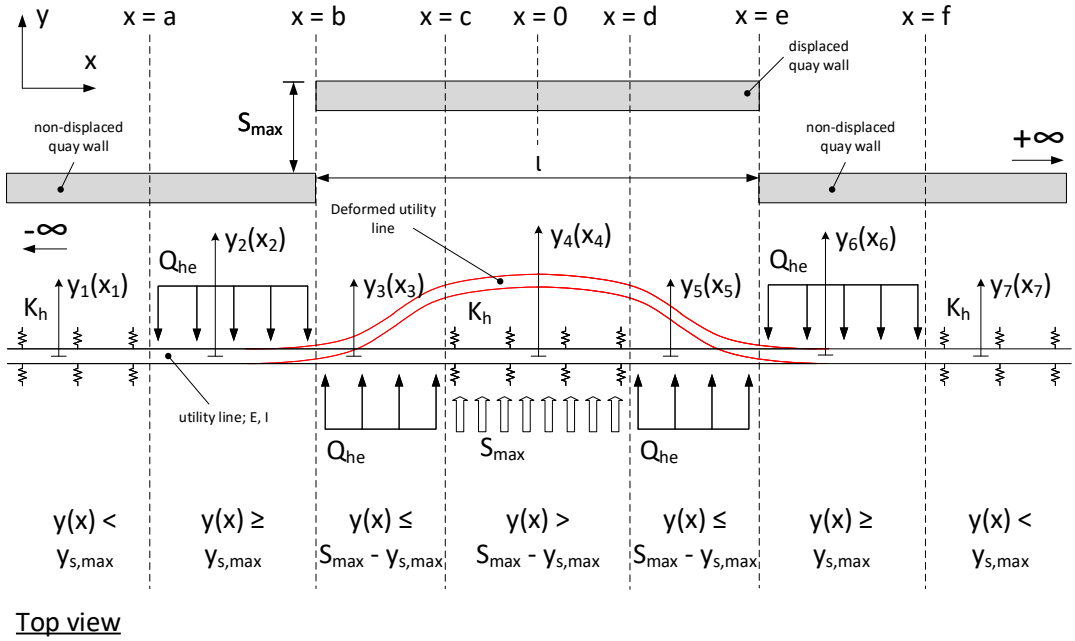

Figure I.8: Model of the case: localised quay wall displacement, utility line displacement partially smaller than maximum allowable soil deformation in displaced soil section.

$$
\begin{aligned}
&y(x)=y_1(x_1) && for\ x<a && if\ x<a && \rightarrow\ y(x)<y_{s,max}\\
&y(x)=y_2(x_2) && for\ a\le x\le b && if\ a\le x\le b && \rightarrow\ y(x)\ge y_{s,max}\\
&y(x)=y_3(x_3) && for\ b\le x\le c && if\ b\le x\le c && \rightarrow\ y(x)\le S_{max}-y_{s,max}\\
&y(x)=y_4(x_4) && for\ c\le x\le 0 && if\ c\le x\le 0 && \rightarrow\ y(x)>S_{max}-y_{s,max}
\end{aligned}
\tag{I.25}
$$

$$
\begin{aligned}
&E\cdot I\cdot\frac{d^4}{dx_1^4}y_1(x_1)+K_h\cdot y_1(x_1)=0\\
&E\cdot I\cdot\frac{d^4}{dx_2^4}y_2(x_2)=-q_{he}\\
&E\cdot I\cdot\frac{d^4}{dx_3^4}y_3(x_3)=q_{he}\\
&E\cdot I\cdot\frac{d^4}{dx_4^4}y_4(x_4)+K_h\cdot y_4(x_4)=K_h\cdot S_{max}
\end{aligned}
\tag{I.26}
$$

$$
\begin{aligned}
y_1(x_1) &= e^{-\beta \cdot x_1}(C_{11} \cdot cos(\beta \cdot x_1) + C_{12} \cdot sin(\beta \cdot x_1)) \\
&\quad e^{\beta \cdot x_1}(C_{13} \cdot cos(\beta \cdot x_1) + C_{14} \cdot sin(\beta \cdot x_1)) \\
y_2(x_2) &= -\frac{1}{24} \cdot \frac{q_{he}}{E \cdot I} + \frac{1}{6} \cdot C_{21} \cdot x_2^3 + \frac{1}{2} \cdot C_{22} \cdot x_2^2 + C_{23} \cdot x_2 + C_{24} \\
y_3(x_3) &= \frac{1}{24} \cdot \frac{q_{he}}{E \cdot I} + \frac{1}{6} \cdot C_{31} \cdot x_3^3 + \frac{1}{2} \cdot C_{32} \cdot x_3^2 + C_{33} \cdot x_3 + C_{34} \\
y_4(x_4) &= e^{-\beta \cdot x_4}(C_{41} \cdot cos(\beta \cdot x_4) + C_{42} \cdot sin(\beta \cdot x_4)) \\
&\quad e^{\beta \cdot x_4}(C_{43} \cdot cos(\beta \cdot x_4) + C_{44} \cdot sin(\beta \cdot x_4))
\end{aligned}
\tag{I.27}
$$

(I.28)

$$
\beta = \sqrt[4]{\frac{K_h}{4 \cdot E \cdot I}}
$$

Additional boundary conditions due to use of symmetry are given in equation I.29. In theory, the left bound is located at $x = -\infty$. In practice, it is found that a distance of 2 times the influence length is sufficient to set as boundary.

$$
\begin{aligned}
&Boundary\ conditions\ at\ x = -\infty \\
&\quad y_1(x = (b - 2 \cdot L_{infl})) = 0 \\
&\quad \frac{d^2}{dx_1^2} y_1(x = (b - 2 \cdot L_{infl})) = 0
\end{aligned}
\tag{I.29}
$$

$$
\begin{aligned}
&Boundary\ conditions\ at\ x = 0 \\
&\quad \frac{d}{dx_4} y_4(x = 0) = 0 \\
&\quad \frac{d^3}{dx_4^3} y_4(x = 0) = 0
\end{aligned}
$$

I.11. Normal forces in utility line

As the utility line displaces in horizontal direction, a frictional force resulting from the interaction between the utility line and soil occurs in axial direction of the utility line. This frictional force acts in opposite direction of the utility line displacement in axial direction. Standard NEN 3650-1 (NEN, 2020a) provides the determination of the maximum frictional force. Up to this maximum frictional force, the soil resistance can be modelled to act linearly proportional relative to the utility line displacement in axial direction. If this maximum frictional force is surpassed, the soil resistance decreases significantly, and no additional resistance to deformation is provided. The determination of this maximum frictional force for sand per unit of utility line length (W) is provided in equation I.30.

$$
W = \pi \cdot D_o \left(\frac{1 + K}{2} \cdot \sigma' \cdot tan(\delta) \right) \tag{I.30}
$$

In which:

$\pi \cdot D_o$	Outer perimeter of utilty line;
K	Ratio of horizontal/vertical soil stresses, at neutral horizontal pressure: $K = 1 - sin(\phi)$;
σ'	Effective vertical soil pressure at utility line axis, at depth of potable water pipe: $\sigma' = H \cdot \gamma$;
δ	Angle of external friction between utility line and soil, $\delta \approx 2/3 \cdot \phi$

As the coverage H is in the order of 1 m, and the effective weight of the soil is in the order of 16 kPa, this results in an effective vertical soil pressure equal to 16 kN/m^2. The angle of internal friction used in this study is equal to 30^o. If a utility line with an outer diameter is taken equal to 100 mm, and applying the aforementioned values for the other parameters, this results in a maximum friction force W in the order of 1.4 kN/m. Knowing

that a typical utility line segment is equal to 6 m, this results in a maximum axial friction force in the order of 8 kN.

As is explained in section 7.5.1, the displacement of the utility line occurs within the influence length (L_{infl}). In case of utility line deformation over greater length, it can be assumed that the relative displacement of the utility line is equal to zero. In absolute terms, this results in a displacement equal to the quay wall displacement S_{max}. Thus, elongation of the utility line has to occur. Due to the assumed abrupt quay wall displacement in the analytical model, said displacement occurs over a length two times equal to L_{infl}. The length of the deformed utility line is approximately equal to L', as represented in figure I.9. In reality, the length of this displaced part of the utility is longer, as the deformation of the utility line itself does not linearly increase.

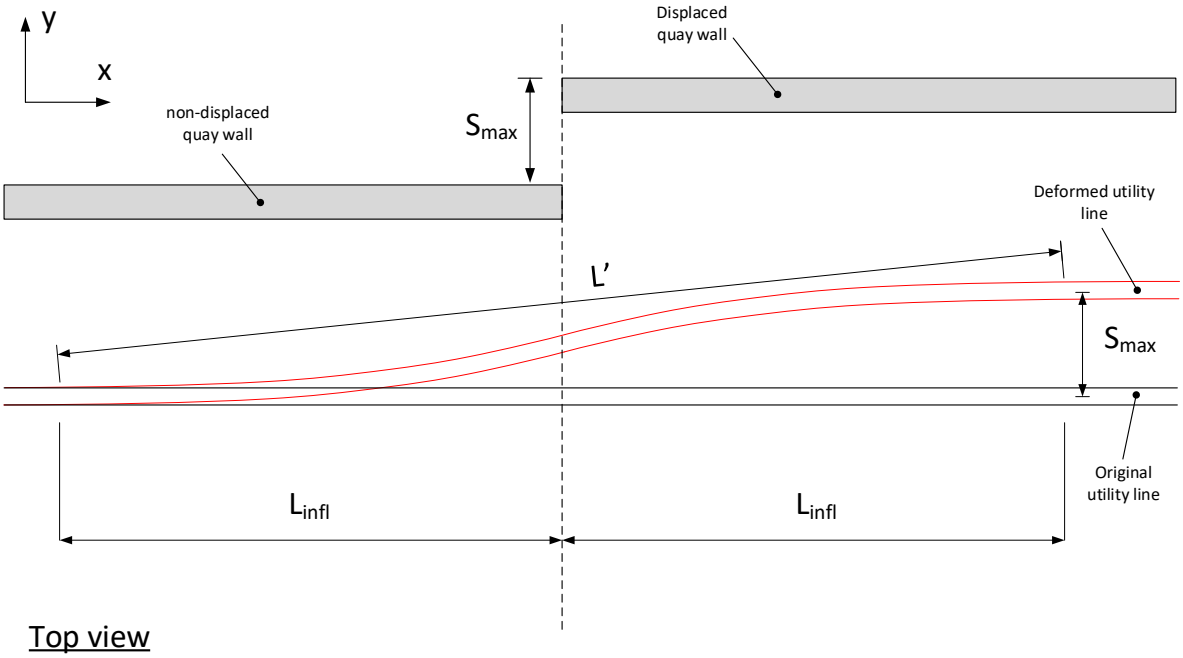

Figure I.9: Elongation of utility line due to displacement.

The assumed length of the deformed part of the utility line is calculated using Pythagoras, i.e. $L' = \sqrt{(2 \cdot L_{infl})^2 + S_{max}^2}$. Knowing the length of the deformed utility line, the elongation (ϵ) is calculated using equation I.31

$$\epsilon = \frac{L' - 2 \cdot L_{infl}}{2 \cdot L_{infl}} \tag{I.31}$$

Notice that the maximum value for S_{max} is equal to 100 mm. By plotting the elongation to the influence length at this value for S_{max}, it is found that larger influence lengths result in lower elongations. Therefore the assumed abrupt quay wall displacement results in the highest elongation, as more gentle quay wall displacement as discussed in appendix J would only elongate the length over which the maximum quay wall displacement S_{max} is reached. This is due to the fact that this length is added to the influence length. See figure I.10 for said relation.

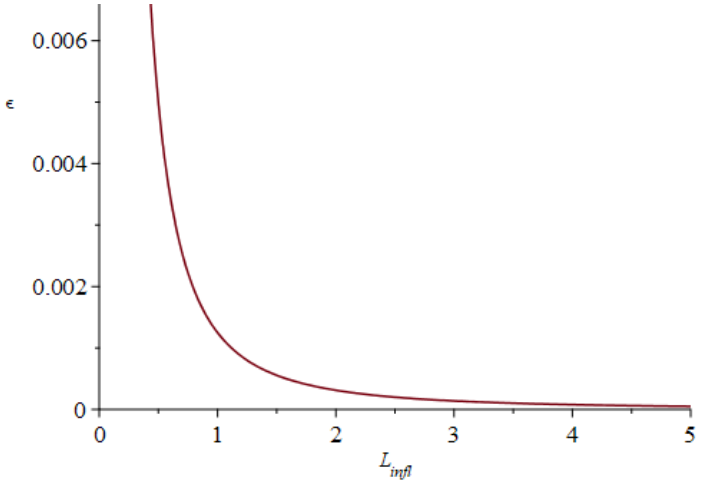

Figure I.10: Influence length L_{infl} plotted against the elongation ϵ.

Assuming elastic utility line deformations, the normal stress- and force corresponding to the elongation (respectively σ and N) are calculated using equations I.32 I.33 respectively, according to Hooke's law.

$$\sigma = E \cdot \epsilon \tag{I.32}$$

$$N = \sigma \cdot A \tag{I.33}$$

According to the analytical model for quay wall displacement over greater length, subjecting a GCI utility line with an outer diameter of 100 mm to 100 mm quay wall displacement results in an influence length equal to 1.50 m (for $K_{h,20\%}$). Plotting the known values for this type of utility line into equations I.31 to I.33, results in a normal force equal to 55 kN. In other words, in order to axially elongate this utility line over the length L', a total of 55 kN as to act in axial direction on this utility line. If it is recounted that the soil is only capable to provide 8 kN due to friction, the utility line does not axially elongate and is pulled out the socket-spigot joint, resulting in leakages. Note that due to the substantial decrease of elongation at higher influence lengths (see figure I.10), this effect is less pronounced for utility lines with higher bending stiffnesses.

Knowing that the utility line slides out of the socket-joint, next it has to be determined how much sliding occurs in said joint. Following the same reasoning as before, the additional length ΔL of the utility line, i.e. the length over which sliding occurs in the socket spigot connection is calculated in equation I.34.

$$\Delta L = L' - 2 \cdot L_{infl} \tag{I.34}$$

Plotting the additional length ΔL against the influence length results in the graph provided in figure I.11.

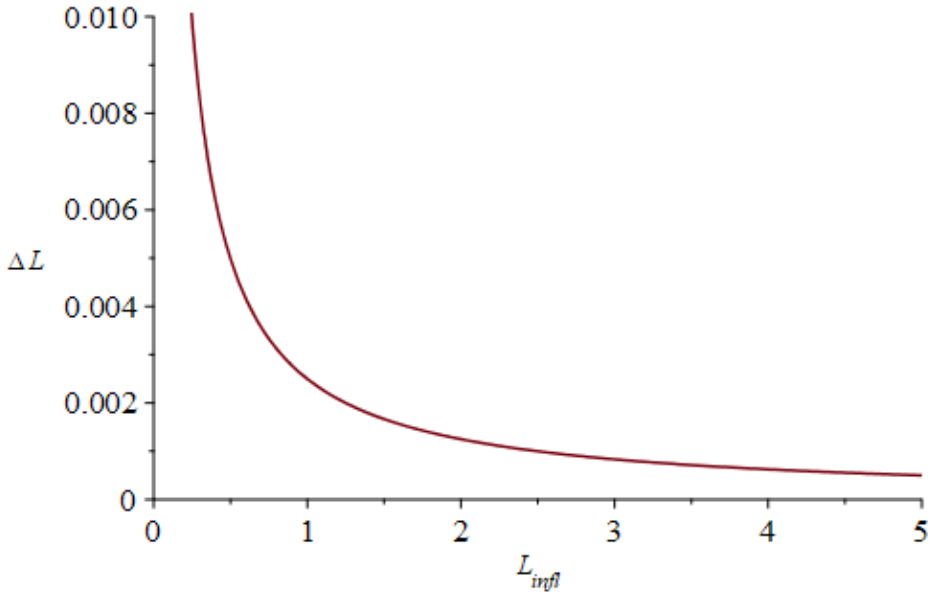

Figure I.11: Additional length of utility line ΔL plotted against the influence length.

Thus, it follows that higher influence lengths result in lower additional lengths. Again, if a more gentle displacement would be applied as discussed in appendix *J*, this would result in a lower additional length.

In a worst case scenario, only one socket-spigot connection is located directly behind the quay wall displacement, soley taking up all the elongation of the utility line. If again the influence length of the GCI potable water pipe of 100 mm is used, it follows from equation I.34 that ΔL is equal to 1.62 mm. Note that this value in reality might be slightly higher, due to the simplified measurement of the deformed utility line length L'. However, this value is deemed reasonable and assumed within limits, as there is always a safety margin build in for sliding in the joints. Due to the inverse relation between ΔL and the influence length, utility lines with higher bending stiffness result in lower values of ΔL.

Note that for localized quay wall displacement, i.e. the model discussed in section 7.10, the maximum deflection of utility lines occurs over a shorter horizontal distance. If the influence length is larger than half the length over which quay wall displacement occurs, the maximum deflection of the utility line is found in the middle of the localized quay wall displacement. Thus, it follows that the length over which the utility line deflection occurs is in this case equal to the influence length plus half the length over which quay wall If half the length over which quay wall displacement occurs is larger than the influence length, the influence of localized quay wall displacement has faded out, and the additional length is again calculated solely using the influence length. See equation I.35 for an overview of the determination of the deformed utility line length L' in case of localized quay wall displacement.

$$for\ L_{infl} > 0.5 \cdot l$$

$$L' = \sqrt{(L_{infl} + 0.5 \cdot l)^2 + S_{max}^2} \tag{I.35}$$

$$for\ L_{infl} \leq 0.5 \cdot l$$

$$L' = \sqrt{(2 \cdot L_{infl})^2 + S_{max}^2}$$

For the GCI potable water pipe with an outer diameter of 100 mm subjected to a quay wall displacement S_{max} equal to 100 mm over a length l equal to 1 m, the maximum deflection is found to be equal to 5.8 mm. The influence length is still equal to 1.5 m, resulting in a horizontal length over which utility line deformation occurs equal to 2 m. Using equations I.34 and I.35, this results in an additional utility line length ΔL equal to only 0.01 mm. Subjecting the same utility line to the same quay wall displacement over a length of 3 m, results in an additional utility line length equal to

1.62 *mm* as well. This is equal to what was found for quay wall displacement over greater length. Thus, for the tested lengths over which quay wall displacement occurs, no variance in magnitude of socket-spigot sliding is found.

J

Continuous quay wall displacement

In the analytical model as discussed in chapter 7, the quay wall displacement is modelled to occur abruptly over its length. However, as discussed in section 7.5.4, this assumption of abrupt quay wall displacement disregards the effect of a more gentle and continuous displacement, i.e. a reduction of maximum output values. In this appendix, the validity of the assumption this abrupt quay wall displacement is determined. The model used for this determination is an adaptation of the analytical model for quay wall displacement over greater length as discussed in section 7.9.2, and thus follows the same principles.

J.1. Discretization of quay wall displacement over its length

As can be seen in figure J.1, the quay wall displacement used in the analytical model is assumed to occur abruptly over its length.

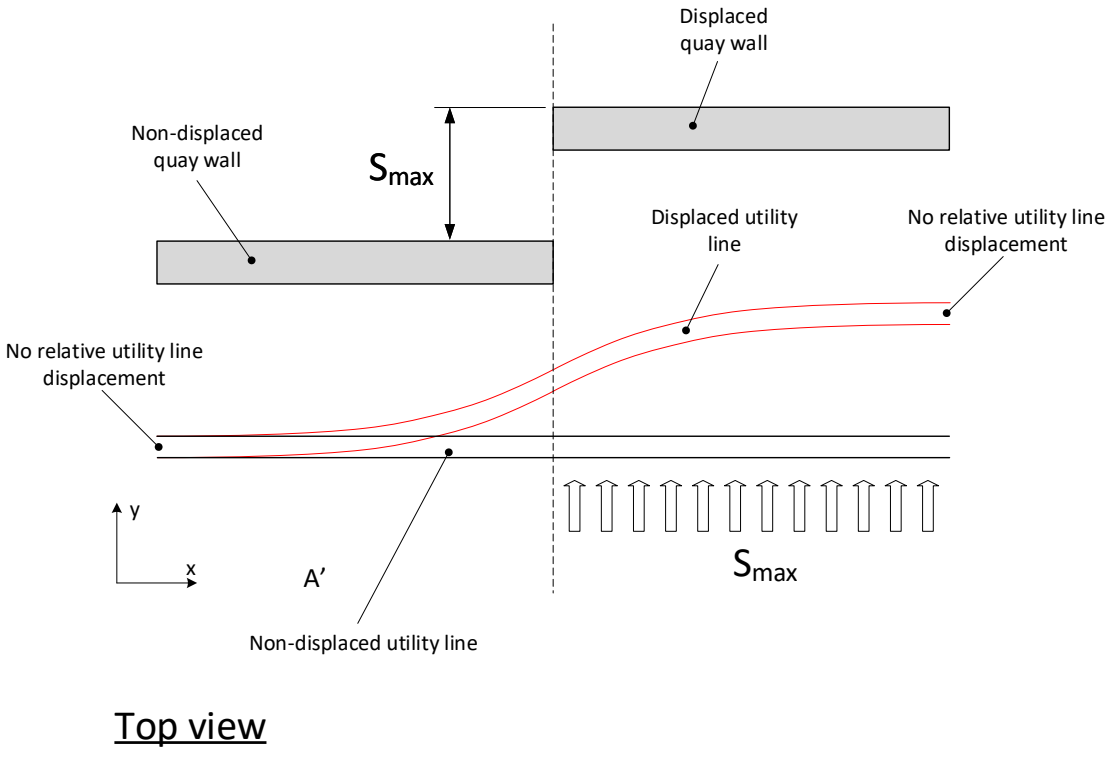

Figure J.1: Abrupt displacement of quay wall as used in analytical model

In figure J.2, a more gentle and continuous quay wall displacement is displayed, instead of the abrupt quay wall displacement as assumed in the analytical model. In this figure, the length L_{Smax} is equal to the length over which said

continuous quay wall displacement occurs. Note that if this length L_{Smax} approaches 0, abrupt quay wall displacement is modelled. As follows from section 7.2.1, it is assumed that the soil body directly located behind a quay wall follows the displacement of said quay wall. Thus, the soil body within the length L_{Smax} is displaced with a magnitude variable over the length of the quay wall, i.e. $S(x)$. In the figure, the quay wall left of the length L_{Smax} has displaced a magnitude S_{max} over its full length, thus the soil displacement is constant and equal to S_{max} as well.

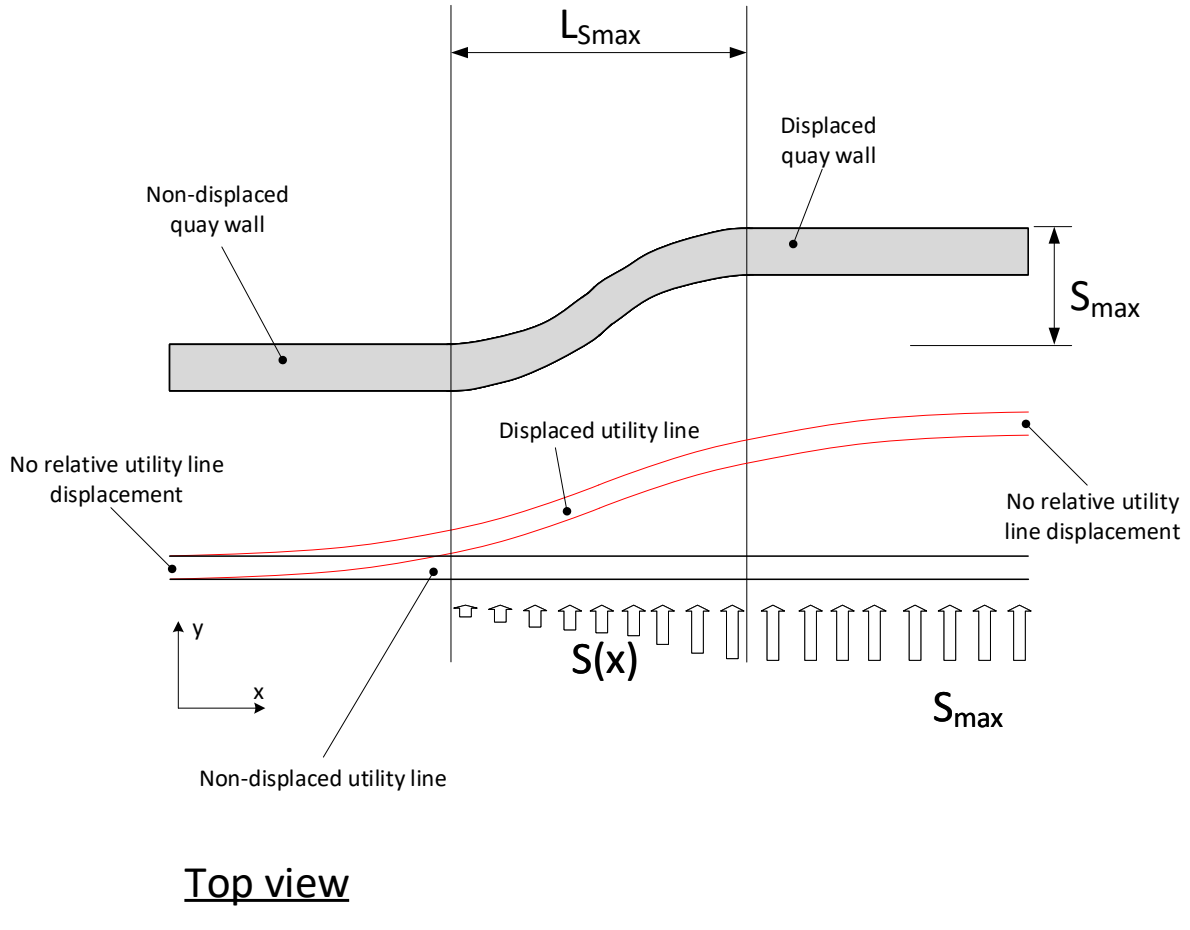

Figure J.2: Gentle displacement of quay wall, continuous displacement

In order to model the continuous displacement of the quay wall, the quay wall displacement can be discretized into sections, each displaced with a constant portion of S_{max}. Applying this principle on the continuous gentle displacement of figure J.2 results in figure J.3. In this case, the quay wall displacement increases in steps equal to 1/4 times S_{max}, resulting in the quay wall being split up in 3 equal sections over a length of L_{smax}. Increasing the number of sections would more accurately display the quay wall displacement as continuous, however this also significantly increases run-time of the model. Additionally, as the effect of increasing L_{smax} is only checked up to 2.5 m, with S_{max} equal to 20 and 100 mm, it is deemed sufficient to keep the number of sections to three.

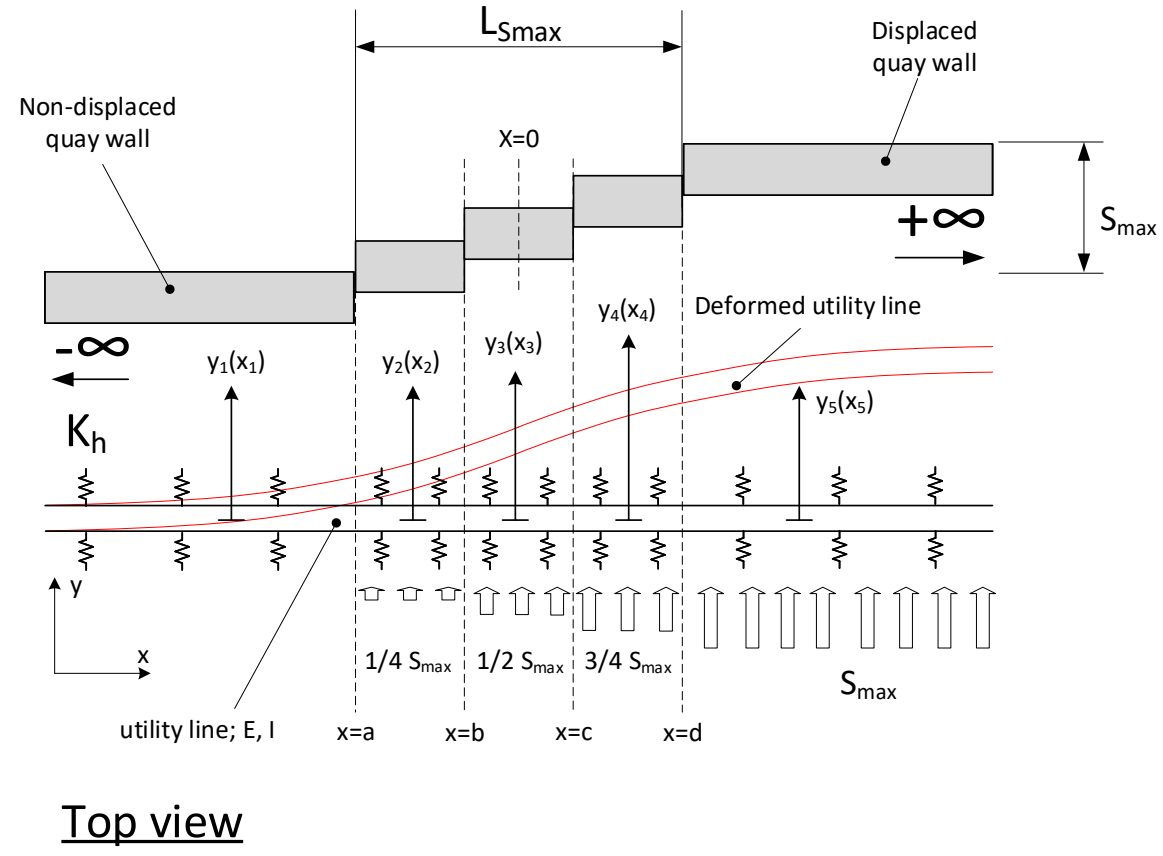

Figure J.3: Gentle displacement of quay wall, discretized displacement

J.2. oM, boundary- and interface conditions

As said before, the model is based on quay wall displacement over a greater length. For simplicity, the interaction between soil and utility line is assumed to be elastic. Thus, each section of utility line is represented as a Winkler foundation with equal distributed spring stiffness K_h. See equation J.1 for an overview of the various sections of utility line. In equation J.2, the EoM's of the model are provided, and their solutions are provided in equation J.3.

$$\begin{aligned} y(x) &= y_1(x_1) && for\ x < a \\ y(x) &= y_2(x_2) && for\ a \le x \le b \\ y(x) &= y_3(x_3) && for\ b \le x \le c \\ y(x) &= y_4(x_4) && for\ c \le x \le d \\ y(x) &= y_5(x_5) && for\ x > d \end{aligned} \tag{J.1}$$

$$
\begin{aligned}
&E\cdot I\cdot\frac{d^4}{dx_1^4}y_1(x_1)+K_h\cdot y_1(x_1)=0\\
&E\cdot I\cdot\frac{d^4}{dx_2^4}y_2(x_2)+K_h\cdot y_2(x_2)=K_h\cdot 0.25\cdot S_{max}\\
&E\cdot I\cdot\frac{d^4}{dx_3^4}y_3(x_3)+K_h\cdot y_3(x_3)=K_h\cdot 0.50\cdot S_{max}\\
&E\cdot I\cdot\frac{d^4}{dx_4^4}y_4(x_4)+K_h\cdot y_4(x_4)=K_h\cdot 0.75\cdot S_{max}\\
&E\cdot I\cdot\frac{d^4}{dx_5^4}y_5(x_5)+K_h\cdot y_5(x_5)=K_h\cdot S_{max}
\end{aligned}
\tag{J.2}
$$

$$
\begin{aligned}
y_1(x_1)&=e^{\beta\cdot x_1}(C_{13}\cdot cos(\beta\cdot x_1)+C_{14}\cdot sin(\beta\cdot x_1))\\
y_2(x_2)&=e^{-\beta\cdot x_2}(C_{21}\cdot cos(\beta\cdot x_2)+C_{22}\cdot sin(\beta\cdot x_2))\\
&\quad+e^{\beta\cdot x_2}(C_{23}\cdot cos(\beta\cdot x_2)+C_{24}\cdot sin(\beta\cdot x_2))+0.25\cdot S_{max}\\
y_3(x_3)&=e^{-\beta\cdot x_3}(C_{31}\cdot cos(\beta\cdot x_3)+C_{32}\cdot sin(\beta\cdot x_3))\\
&\quad+e^{\beta\cdot x_3}(C_{33}\cdot cos(\beta\cdot x_3)+C_{34}\cdot sin(\beta\cdot x_3))+0.50\cdot S_{max}\\
y_4(x_4)&=e^{-\beta\cdot x_4}(C_{41}\cdot cos(\beta\cdot x_4)+C_{42}\cdot sin(\beta\cdot x_4))\\
&\quad+e^{\beta\cdot x_4}(C_{43}\cdot cos(\beta\cdot x_4)+C_{44}\cdot sin(\beta\cdot x_4))+0.75\cdot S_{max}\\
y_5(x_5)&=e^{-\beta\cdot x_5}(C_{51}\cdot cos(\beta\cdot x_5)+C_{52}\cdot sin(\beta\cdot x_5))+S_{max}
\end{aligned}
\tag{J.3}
$$

$$
\beta=\sqrt[4]{\frac{K_h}{4\cdot E\cdot I}}
$$

The interfaces $x=a$, $x=b$, $x=c$ and $x=d$ are located at, $x=-1/2\cdot L_{Smax}$, $x=-1/6\cdot L_{Smax}$, $x=1/6\cdot L_{Smax}$, and $x=1/2\cdot L_{Smax}$ respectively (see figure J.3). Note that these interfaces are chosen such that three equal sections of displaced quay wall are generated within length L_{Smax}. The boundary- and interface conditions are the same as explained as in 7.4.3, i.e. no angular deflection or bending moments on either end of the utility line and continuation of displacement, angular deflection, moment and shear force at the interfaces.

J.3. Validity of assumption of abrupt quay wall displacement

In order to determine to what extend the assumption of abrupt quay wall displacement is valid, the model is run for GCI potable water pipes with outer diameters (D_o) ranging from 100 up to 500 mm. First, the outcomes of the model with abrupt quay wall displacement were obtained. Next, the outcomes of the model with incrementally increasing quay wall displacement as discussed in section J.2 are obtained, with L_{Smax} ranging from 0.5 up to 2.5 m in increasing steps of 0.5 m. The outcomes of both models, i.e. the maximum angular deflection, maximum moment, and maximum shear force, are compared to eachother. In table J.1, the reduction of maximum angular deflection for increasing steps of L_{Smax} compared to the abrupt quay wall deflection is provided. Similarly, this is done for the maximum moment and -shear force in tables J.2 and J.3 respectively. Note that the applied horizontal quay wall displacement S_{max} was varied between 20 and 100 mm, but for every case this resulted in the same reduction of maximum output value.

Table J.1: Reduction of maximum angular deflection compared to assumption of abrupt quay wall displacement, for GCI pipes.

	$D_o\ [mm]$				
$L_{Smax}\ [m]$	100	200	300	400	500
0.5	8%	3%	2%	1%	1%
1.0	22%	9%	6%	3%	3%
1.5	36%	16 %	10%	5 %	4%
2.0	47%	24%	14%	10%	7%
2.5	55%	31%	20%	14%	10%

Table J.2: Reduction of maximum moment compared to assumption of abrupt quay wall displacement, for GCI pipes.

	$D_o\ [mm]$				
$L_{Smax}\ [m]$	100	200	300	400	500
0.5	10%	3%	1%	1%	1%
1.0	29%	11%	6%	3%	2%
1.5	46%	21 %	12%	7%	5%
2.0	57%	31%	19%	12%	8%
2.5	63%	40%	26%	17%	12%

Table J.3: Reduction of maximum shear force compared to assumption of abrupt quay wall displacement, for GCI pipes.

	$D_o\ [mm]$				
$L_{Smax}\ [m]$	100	200	300	400	500
0.5	31%	17%	12%	9%	8%
1.0	51%	32%	23%	18%	16%
1.5	62%	44 %	33%	26%	22%
2.0	68%	53%	42%	34%	28%
2.5	71%	59%	49%	28%	34%

From the previous tables it follows that utility lines with higher bending stiffnesses are relatively accurately represented by abrupt quay wall displacement. This can concluded from the fact that the reduction of angular deflection of GCI pipes with an outer diameter of 500 mm is only 10% for an L_{Smax} equal to 2.5 m, while for this same L_{Smax} the 100 mm pipe shows a reduction of 55%.

The reduction of the maximum moment and maximum shear force is larger for every outer diameter. This follows from the fact that these are related to respectively the second and third derivation of the utility line displacement. GCI potable water pipes have the lowest bending stiffness in general of all utility lines tested in this study, thus for similar utility line diameters of other materials, the reduction will be less for all output values.

The angular deflection is a significant factor in determining if a utility line is susceptible to leakages. Thus the fact that for increasing quay wall displacement (L_{Smax}) over a length of 1 m the reduction of the smallest tested utility line (100 mm), the reduction of the angular deflection is only 22%, it is deemed sufficient to assume the abrupt quay wall displacement instead of discretized quay wall displacement. However, if L_{smax} surpasses about 2 m, it has to be noted that the assumption of abrupt quay wall displacement is less valid, especially for smaller utility lines.

K

Graphs depicting relation between dimensionless ratio and angular deflection

In this appendix the graphs are provided of the relation between angular deflection and the ratio between the utility line's outer diameter and the quay wall displacement, as discussed in section 8.6.2. The graphs relate to NCI, steel, and concrete utility lines in figures K.1, K.2, and K.3 respectively.

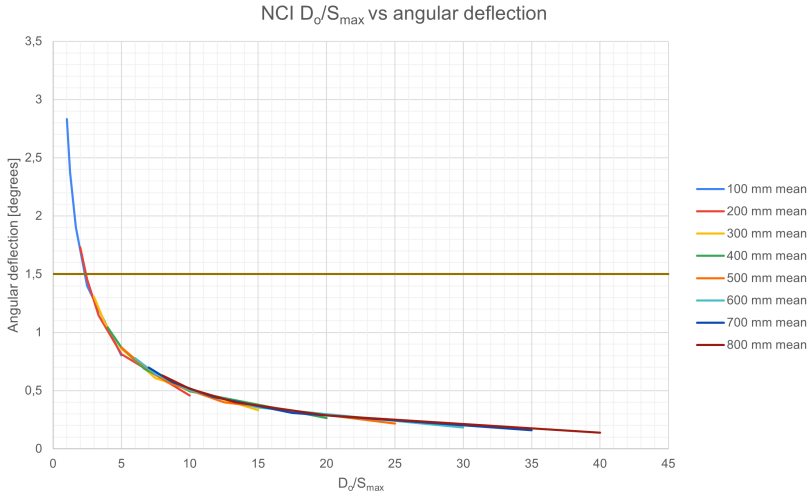

Figure K.1: D_o/S_{max} plotted against the mean maximum angular deflection for all diameters of NCI utility lines, for quay wall displacement over greater length.

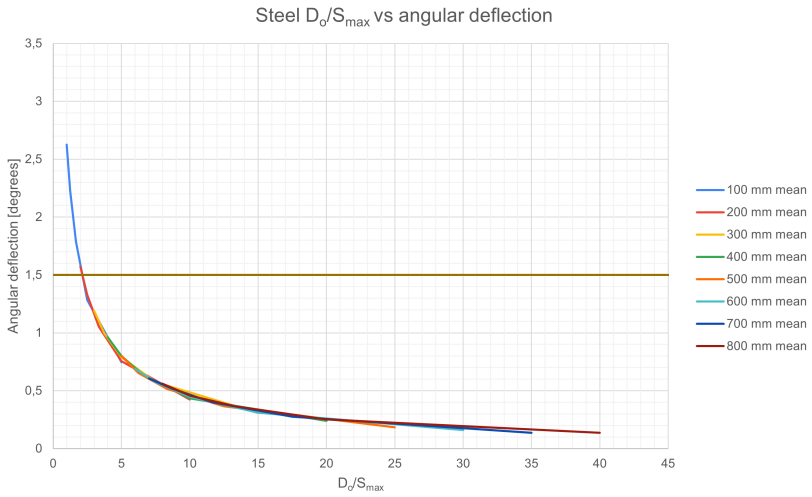

Figure K.2: D_o/S_{max} plotted against the mean maximum angular deflection for all diameters of steel utility lines, for quay wall displacement over greater length.

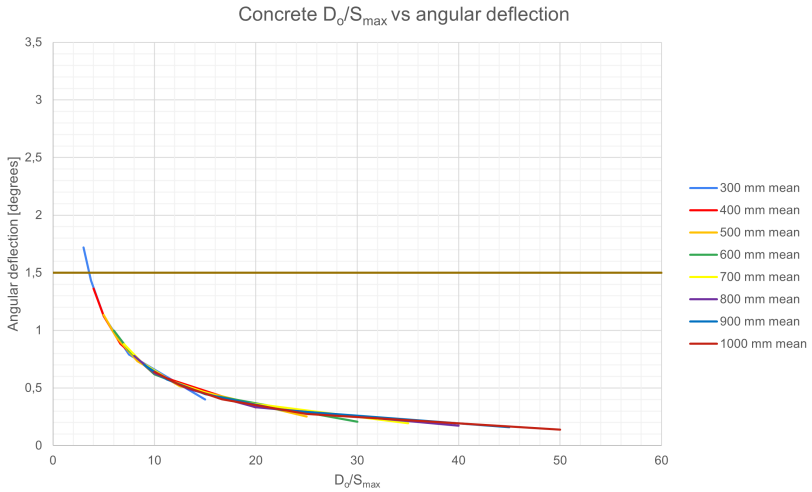

Figure K.3: D_o/S_{max} plotted against the mean maximum angular deflection for all diameters of concrete utility lines, for quay wall displacement over greater length.